ELASTOHYDRODYNAMIC STUDIES USING THIN FILM TRANSDUCERS

MALIK MOHAMMAD ABU SAFA
B.Sc., M.Sc.

A Thesis submitted in partial fulfilment of the requirements for the degree of Doctor of Philosophy of the University of London, and for the Diploma of Imperial College.

Department of Electrical Engineering
Imperial College of Science and Technology

April, 1982

ABSTRACT

Thin film micro-transducers have been developed for application to the study of the variation of pressure, temperature and oil film thickness in an elastohydrodynamically lubricated, nominal line contact. Fabrication techniques for such devices have been improved to enhance the useful life. Techniques have also been developed to achieve higher resolution by reducing sensor size and improving the signal monitoring circuitry. Material properties in thin film form used in fabricating the sensors have been examined. Possible sources of errors in interpreting the results obtained from these devices were studied. Results obtained from these devices, under various operating conditions, have been analysed and compared with the published theoretical and experimental results and reasonably good agreement was found throughout.

ACKNOWLEDGEMENTS

I am greatly indebted to Professor J.C. Anderson and Dr. J.A. Leather for their many excellent ideas, supervision and advice.

It is a pleasure to thank Dr. P.B. Macpherson for his encouragement, recommendations and interest in each stage of the work.

I would like to thank the Ministry of Defence for their financial support.

I would also like to thank Mrs. Wright for typing part of the thesis.

Finally, thanks to all members in the Materials Science Section for providing a stimulating academic environment, and many productive discussions.

CONTENTS

LIST OF FIGURES

INTRODUCTION

The process of elastohydrodynamic lubrication (EHL) occurs in machine elements like gears and roller bearings where the load transmitted is sufficiently high to cause local elastic deformation of the load bearing surfaces. The essential features of this process may be reproduced in a disc machine, where two discs are loaded together and rotated in either a rolling or a sliding mode. Direct measurement of pressure, temperature and oil film thickness in such a contact is complicated by the fact that both the contact width and the oil film that separates the two machine elements are very small. Any sensing devices must not significantly disturb the formation of this very thin oil film. Thin film transducers fabricated on the disc itself provide a way of monitoring these parameters.

Thin film transducers have been used by various researchers to study EHL contact conditions in disc machines. However, the disc machines used were of the dead load type, where the discs could be made to rotate at fairly high speed before applying any appreciable load, so that a fairly thick oil film developed in the contact zone, helping to protect the thin film devices when the discs were loaded. This process drastically reduces the severity of the starting condition. One of the objectives in this project was to improve thin film devices to such a stage that they could be applied to real machine elements where the operating conditions are more severe. The hydrostatic disc machine chosen for this project requires a reasonably high load to start, giving severe starting conditions. Thus existing and alternative techniques of fabricating thin film devices were explored in order to extend the operating range of the

devices in an EHL contact condition.

The bulk properties of the materials used in fabricting these thin film devices are well established, but very little is known about them in their thin film form. It is possible that substantial differences exist between bulk and thin film properties depending on the deposition method. Thus the thin film properties of materials, used in fabricating transducers, were examined in order to ascertain the suitability of these materials as sensing devices.

The temperature rise within an EHL contact zone under a pure rolling condition is generally low, whereas the pressure that develops is extremely high. This makes it difficult to remove pressure effects from the temperature sensors. Thus the possibility of an alternative type of temperature sensor which has negligible pressure sensitivity was also examined.

The presence of secondary pressure peak followed by a large negative pressure gradient at the exit side of an EHL contact zone predicted by theory has already been demonstrated by some researchers, although the magnitudes found experimentally were much less than predicted. Part of this discrepency may be caused by the limited resolution of sensing devices. The possible effects of the transducer geometry on the signal generated by these devices have been studied.

Multiple devices such as pressure/temperature and pressure/film thickness transducers have been fabricated on the same disc with high degree of alignment to study the relative variation of these paramenters within an EHL contact.

Finally, the results produced by these devices are compared with the hitherto published theoretical and experimental results

CHAPTER 1

1.1 A SURVEY OF EHL - THEORETICAL DEVELOPMENTS

Elastohydrodynamic lubrication is that regime of the lubrication in which elastic distortions of the load bearing components has a significant influence on the lubrication process. This influence is most marked when the load carrying members have a high elastic modulus. The high pressures generated can considerably increase the viscosity of a lubricating oil.

The theoretical study of EHL requires the simultaneous solution of three equations,

(i) Reynolds equation,

(ii) the elasticity equation,

(iii) the constitutive equation relating lubricant viscosity to pressure (and any other influencing factors).

The Reynolds equation, in three dimensional form, states that for an incompressible fluid between two moving surfaces

$$\frac{\partial}{\partial x}\left(\frac{h^3}{\eta}\cdot\frac{\partial p}{\partial x}\right) + \frac{\partial}{\partial y}\left(\frac{h^3}{\eta}\cdot\frac{\partial p}{\partial y}\right) = 12U\frac{\partial h}{\partial x}$$

where U is the mean surface velocity in the x direction and p is the pressure generated in a film of thickness h and viscosity η. The derivation of this equation relied on several simplifying assumptions, as described, for instance, by Cameron (1). In the case of infinitely long surfaces with no thickness variation in the y direction, all derivatives with respect to y disappear, and an integration of the remaining equation yields

$$\frac{dp}{dx} = 12U\eta\left(\frac{h-\bar{h}}{h^3}\right)$$

where $\bar{h}$ is the local film thickness at the point of maximum pressure.

The pressure viscosity relation, generally used, is of the form

$$\eta = \eta_o e^{\alpha p}$$

where α is the pressure viscosity co-efficient of the fluid and by substitution of a "reduced pressure" q, where

$$q = \frac{1 - e^{-\alpha p}}{\alpha}$$

the Reynolds equation is simplified.

1.1.1 Development of the Theory

In an attempt to confirm the general belief that a hydrodynamic film exists between gear teeth, Martin (2) in 1916 solved the hydrodynamic equation for the equivalent geometry of a cylinder on a plane. The film thickness formula he derived indicated a film thickness less than the height of the machining marks on the gear teeth, which was clearly impractical. This, in turn, suggested that a hydrodynamic film could not exist between the gear teeth.

The effects of elastic distortion was included by Peppler in 1936 (3) and 1938 (4) and Meldahl in 1941 (5). Although the effect on film thickness was beneficial, the increase was still not enough to accord with observations.

The effects of pressure-viscosity characteristics on rigid cylinder lubrication were examined by Gatcombe (6) in 1945, and Blok (7) in 1950, and Cameron (8) and Blok (9) in 1952 using various pressure viscosity relationships. These all increased the film thickness relative to the Martin conditions but the assumption of rigid materials again led to very thin oil films.

The combined effects of elastic deformation and the pressure dependence of viscosity were studied by Ertel in Russia and the work was published by Grubin and Vinogradova in 1949 (10). In his work he had assumed the shape of the deformed surface of the cylinder to be close to that for dry contact given by Hertz (11). He had used the exponential pressure viscosity relationship to convert it into a straightforward integral equation of a function of the film shape. This enabled him to get a formula for the film thickness at the centre of the contact, which predicts films far thicker than did previous theory and of a magnitude that would enable a fluid film to separate typically rough surfaces. He also gave a qualitative analysis of the difference between his model of film shape and that which would be found in practice. He concluded that there would be a constriction in the film shape prior to the outlet with a pressure spike followed by a sudden drop in pressure immediately before this constriction.

Ertel's qualitative conclusions were confirmed by Petrusevitch (12) in 1951 when he obtained a common solution to the hydrodynamic and elastic equations by a trial and error method. Numerical solutions were also obtained in 1954 by Weber and Saalfeld (13). However, the elastic deformations which they used were small and thus their solutions differed

qualitatively from the solutions obtained by Petrusevitch. They did, however, show the effect of the viscosity variation with pressure.

In 1959, Dowson and Higginson (14) presented a numerical method for the simultaneous solution of the Reynolds equation and elasticity equation to determine the pressure distribution and oil film thickness for a line contact. Fig.1.1a shows the set of results they produced at a constant surface velocity but variable load. There was no evidence of a secondary pressure spike. In 1960 (15) they published a more extensive set of results for conditions of greater severity. The pressure spikes were now clearly visible. The existence of such a pressure peak was also found by Archand, Gair and Hirst (16) at about the same time, although the shape and size of the pressure peak was slightly different as simplifying methods did not cater for the very fine detail. They showed the effect of various parameters on the inlet and exit side of the pressure profiles very systematically for an incompressible lubricant. Higginson and Whitaker (17) extended the method to include compressibility of the lubricant and found that it greatly reduced the peak pressure. Most of the results of Dowson, Higginson and Whitaker were published later in 1966 (18) in the form of a book which also gave details of the numerical method they used. Some of the interesting results are reproduced here for future reference.

Fig.1.1b shows a set of pressure profiles obtained for an incompressible lubricant at a fixed load but variable surface velocity covering four orders of magnitude of speed. The pressure distribution approaches the Hertzian distribution as the speed is reduced. The pressure curve closely follows

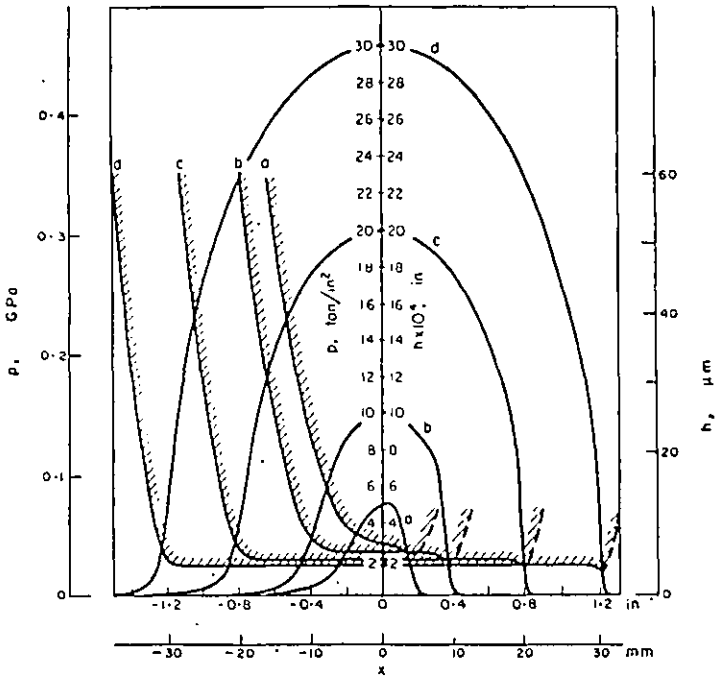

a Pressure distributions and film shapes with pressure-dependent viscosity and elastic cylinders.

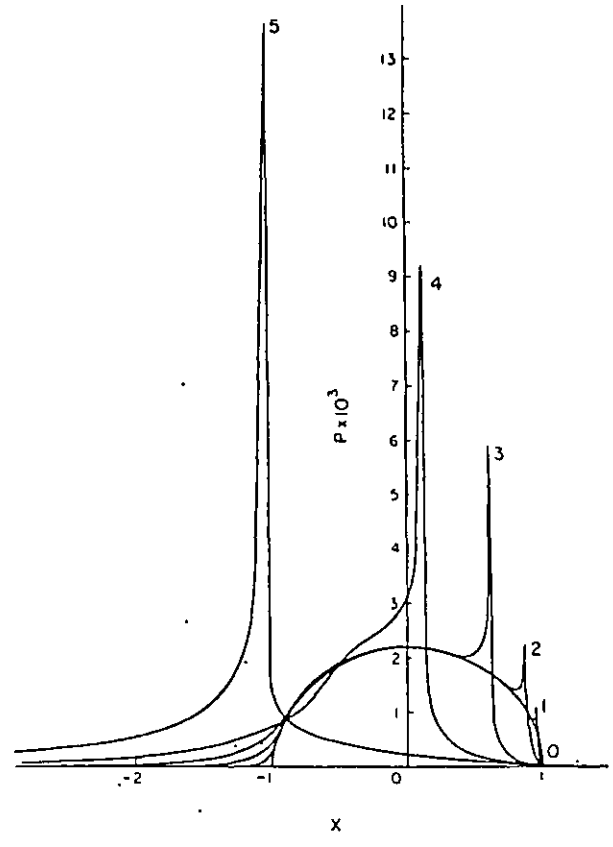

b Pressure distributions for an incompressible lubricant. $W = 3 \times 10^{-5}$, $G = 5000$. $U =$ (0) 0 (dry contact), (1) 10^{-13}, (2) 10^{-12}, (3) 10^{-11}, (4) 10^{-10}, (5) 10^{-9}.

Fig 1.1 Theoretical solutions by Dowson and Higginson (a)early solution (b)refined solution under more severe conditions.

the Hertzian ellipse at the inlet and a pressure peak is retained at the outlet. With increasing surface velocity the pressure profile deviates from the Hertzian distribution and at very high speed hardly any similarity exists between the two. The secondary pressure peak increases with the increase of surface velocity and its position moves towards the inlet of the contact. The height of the secondary pressure peak could reach a value which is far in excess of the Hertzian maximum with an incompressible lubricant. The pressure rise at the inlet starts earlier with the increase of surface velocity.

Figure 1.2a shows a second set of pressure profiles with identical operating conditions as for Figure 1.1b, but with a compressible lubricant. The reduced height of the secondary pressure peak for the compressible lubricant is clear . For a compressible lubricant the position of the secondary pressure peak is slightly closer to the exit. The pressure profile at the highest surface velocity shown in Figure 1.2a is similar to pressure distribution obtained from rigid cylinder theory.

The effect of load on pressure distribution can be assessed by comparing the pressure traces in Figure 1.2 , where the load is ten times that in Figure 1.2a . The effect on the shape (apart from scale) of a tenfold increase in load is much the same as a reduction of two orders of magnitude in speed. The increase of load moves the secondary pressure peak towards the exit and reduces its width. The pressure profile in general follows the Hertzian profile more closely. Solutions for an incompressible lubricant show that the height of the secondary pressure peak does not alter much due

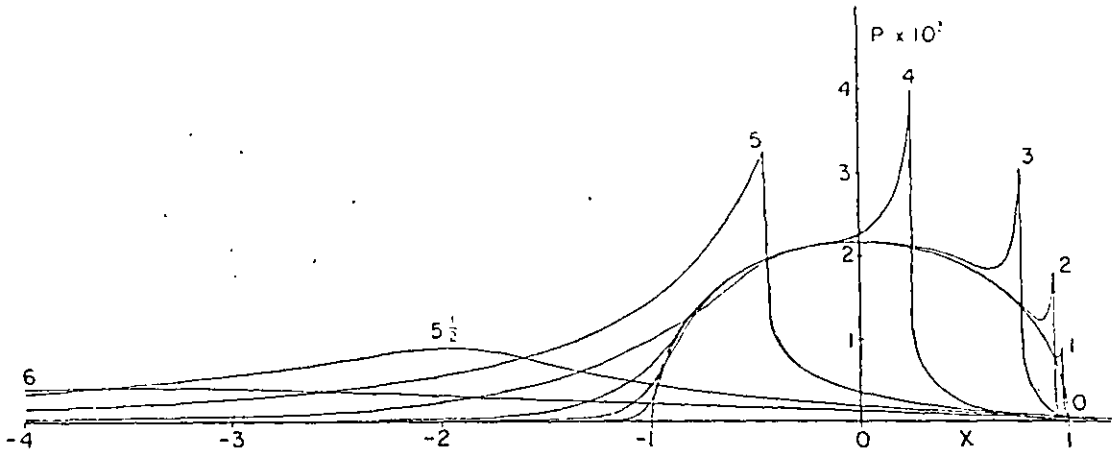

a Pressure distributions for a compressible lubricant. $W = 3 \times 10^{-5}$, $G = 5000$. $U = (0)\ 0$ (dry contact), (1) 10^{-13}, (2) 10^{-12}, (3) 10^{-11}, (4) 10^{-10}, (5) 10^{-9}, ($5\frac{1}{2}$) $10^{-8\frac{1}{2}}$, (6) 10^{-8}. [Reproduced by kind permission from the *Proceedings of the Institution of Mechanical Engineers Symposium on Fatigue in Rolling Contact*, 1963.]

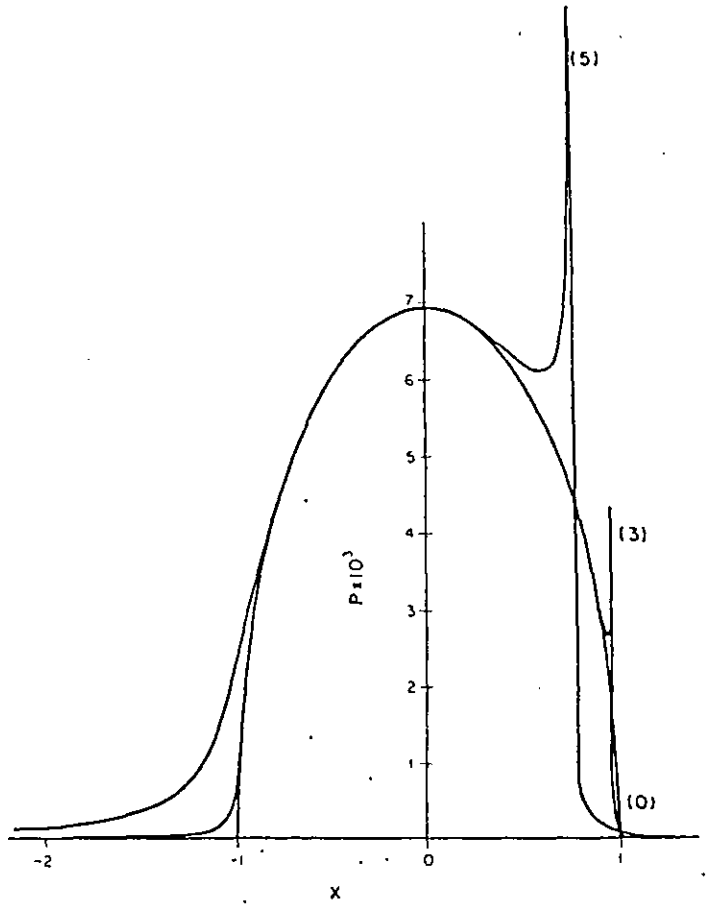

b Pressure distributions for a compressible lubricant. $W = 3 \times 10^{-4}$, $G = 5000$. $U = (0)\ 0$ (dry contact), (3) 10^{-11}, (5) 10^{-9}.

Fig 1.2 Theoretical solutions of Dowson and Higginson (a)fixed load, variable surface velocity;(b)load increased by an order of magnitude.

to the change in load, however, substantial changes in height can be seen with a compressible lubricant.

The effect of the pressure-viscosity co-efficient on the pressure profiles was not discussed independently by Dowson and Higginson (18), but the material parameter G is the product of α and E' (reduced elastic modulus) and so the effect of α would be the same as the effect of the variation of G keeping E' constant. Figure 1.3 shows the effect of G on the pressure profile in an incompressible lubricant, which is mainly to change the height of the secondary pressure peak. At very low values of G the secondary pressure peak disappears. Archard et al. (19) showed that the effect of increasing the α value produces a shift of the secondary pressure peak towards the inlet but the effect on the inlet side of the pressure profile is negligible as shown in Fig.1.4

All the numerical results discussed so far were obtained by solving the hydrodynamic and elastic equations simultaneously. To study the effect of temperature variation within the contact on the secondary pressure peak, Sternlicht, Lewis and Flynn (20) in 1961 included an energy equation in their solution. However, they neglected the conduction of heat from the contact by the bounding solids in the energy equation. This was included by Cheng and Sternlicht (21) and later Cheng (22) refined the analysis to allow the temperature and consequently the viscosity to vary across the film. He produced results for pure rolling and partial sliding conditions.

For moderate to high slip between the rollers, the temperature effects are significant. In general, temperature tends to reduce the severeness of the pressure peak at higher

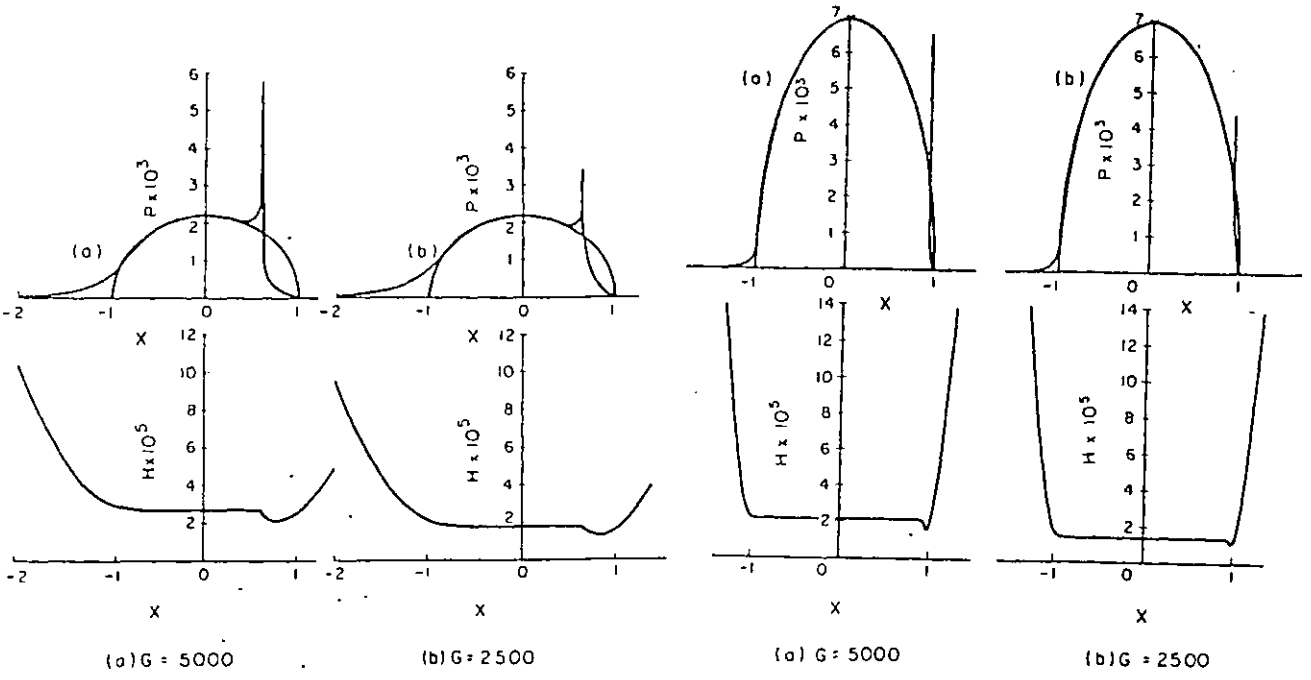

a Pressure distributions and film shapes. $W = 3 \times 10^{-5}$. $U = 10^{-11}$. (a) $G = 5000$. (b) $G = 2500$.

b Pressure distributions and film shapes. $W = 3 \times 10^{-4}$. $U = 10^{-11}$. (a) $G = 5000$. (b) $G = 2500$.

Fig 1.3 Theoretical solution of Dowson and Higginson. Effect of material parameter G, (a) under low load (b) higher load.

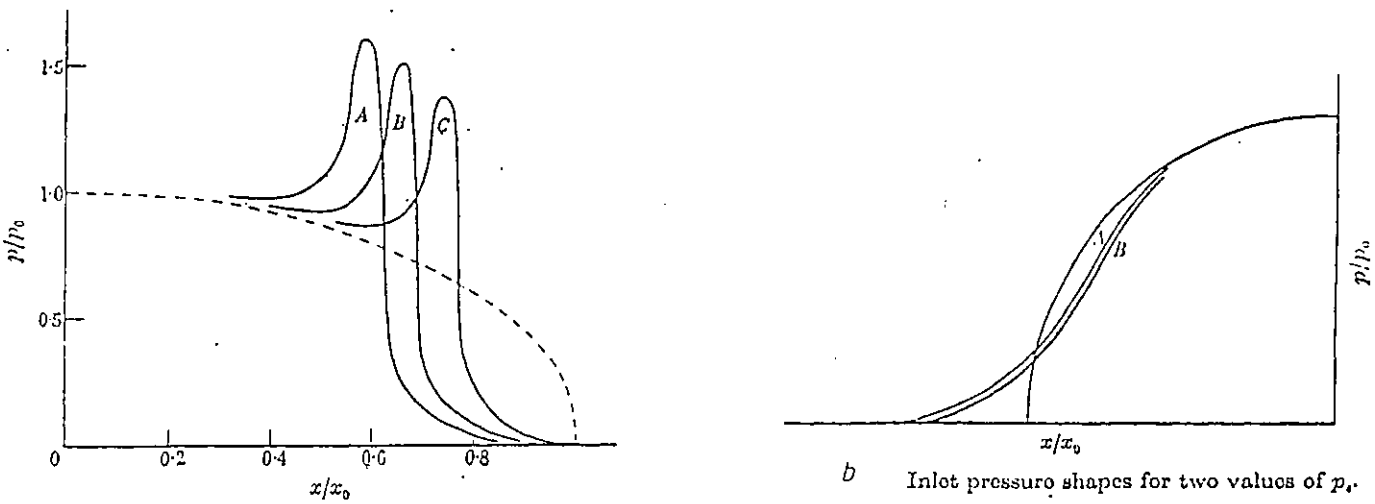

a Outlet pressure shapes for varying pressure coefficient of viscosity p_α.

$U = 130$ cm/s (51 in./s)
$\eta_0 = 0{\cdot}4$ P
$p_0 = 4{\cdot}8 \times 10^9$ dyn/cm² (31 tons/in.²)
$1/\beta = 3{\cdot}5 \times 10^{-2}$ dyn/cm² (22 500 tons/in.²)
$R = 1{\cdot}9$ cm (0·75 in.)
A, $p_\alpha = 2 \times 10^8$ dyn/cm² (1·25 tons/in.²)
B, $p_\alpha = 4 \times 10^8$ dyn/cm² (2·5 tons/in.²)
C, $p_\alpha = 8 \times 10^8$ dyn/cm² (5·0 tons/in.²)

b Inlet pressure shapes for two values of p_α.

$p_0 = 31$ tons/in.² ($4{\cdot}8 \times 10^9$ dyn/cm²)
$\eta_0 = 0{\cdot}4$ P
$U = 130$ cm/s (51 in/s)
$R = 1{\cdot}9$ cm (0·75 in.)
$1/\beta = 3{\cdot}5 \times 10^{12}$ dyn/cm² (22 500 tons/in.²)
A, $p_\alpha = 2{\cdot}5$ tons/in.² (4×10^8 dyn/cm²)
B, $p_\alpha = 1{\cdot}25$ tons/in.² (2×10^8 dyn/cm²)

Fig. 1.4 Theoretical solution of Archard etal (a) effect of pressure viscosity coefficient of oil on the exit side of pressure profile, (b) on the inlet side.

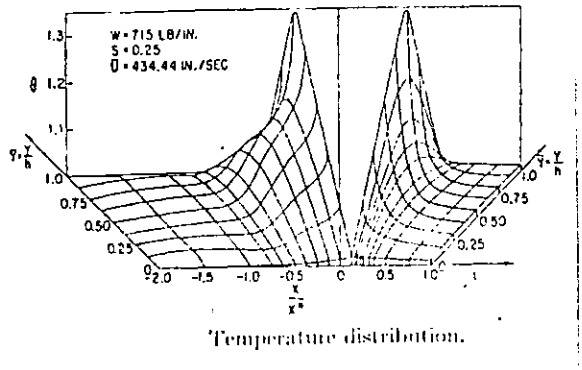

Fig. 1.5 Vriation of the oil film temperature through the EHL contact (after Cheng).

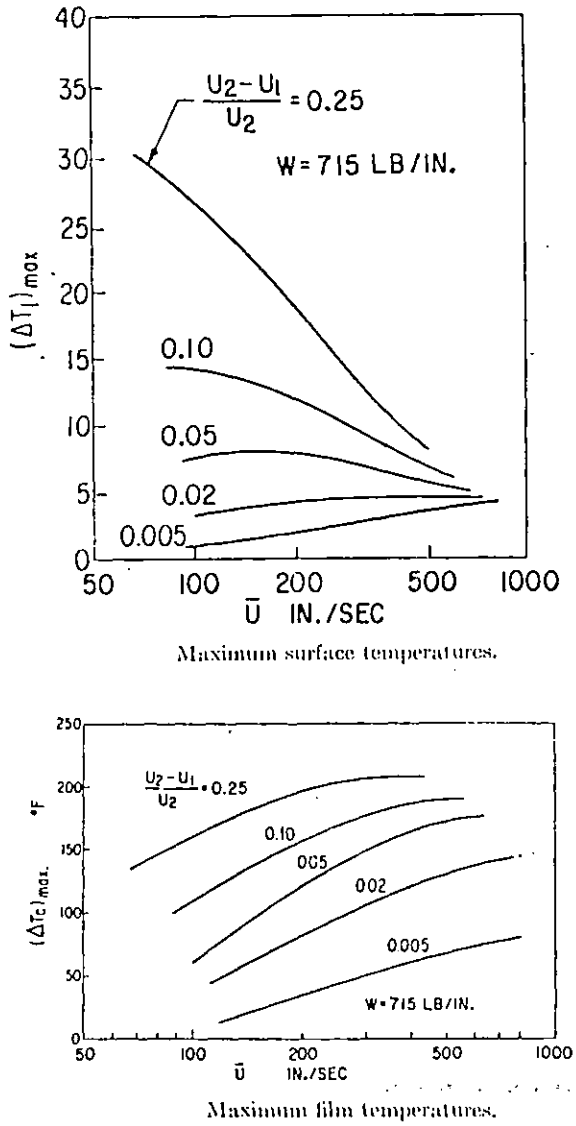

Fig. 1.6 Maximum surface and oil film temperature under different slip-ratios and surface velocities (after Cheng).

speed, but tends to increase the pressure peak at low speed. Dowson and Whitaker (23) in 1968 produced a similar solution including the energy equation and found that the secondary pressure peak heigh reduces with increasing sliding and its position moves towards the centre of the contact.

The last three papers mentioned above also presented temperature profiles within the contact zone under pure rolling and partial sliding conditions. The profiles under sliding conditions show a sharp rise of temperature near the secondary pressure peak zone. Cheng (22) explained it as the heat generated due to sliding at very high viscosity of the oil. Figure 1.5 shows the oil temperature variation through an EHL contact.

Cheng (22) also plotted the maximum temperature rise within the oil film and on the surface of the rollers at various amounts of sliding introduced at various surface velocities. It was found that at low slip ratios the peak surface temperature rises steadily with rolling speed but at high slip ratio the trend was reversed and an increase of rolling speed reduced the surface temperature. These two plots are reproduced in Figure 1.6.

Figure 1.7 shows the film thickness profiles, at a fixed load but different surface velocities, derived by Dowson and Higginson (24) in 1964 for an incompressible lubricant. This set of film thickness profiles was obtained under the identical operating conditions to those of the pressure profiles in Figure 1.1h. The incompressible lubricant produces a distinct constriction zone at the exit, and the beginning of the constriction zone, which is associated with the sharp pressure drop, changes position with the pressure peak. In

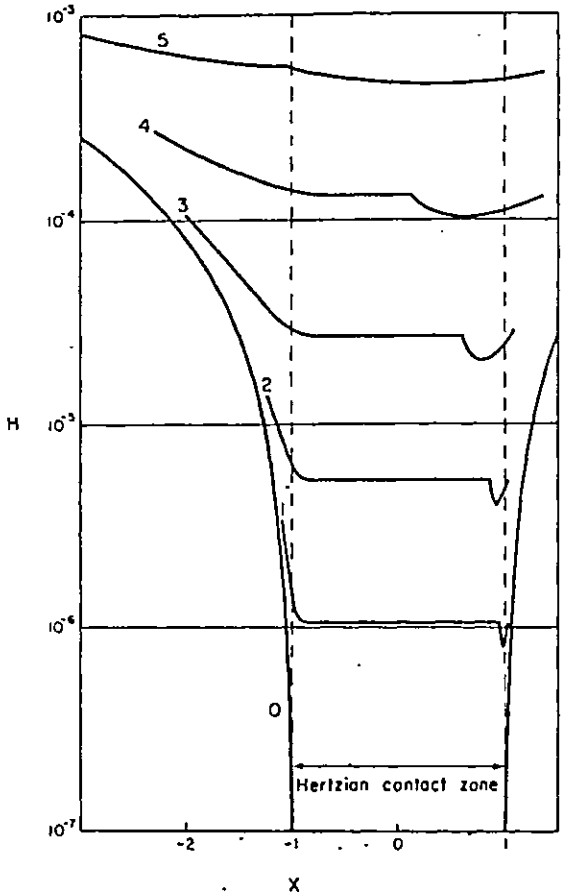

Film shapes for an incompressible lubricant. $W = 3 \times 10^{-5}$, $G = 5000$. $U =$ (0) 0 (dry contact), (1) 10^{-13}, (2) 10^{-12}, (3) 10^{-11}, (4) 10^{-10}, (5) 10^{-9}.

Fig. 1.7 Theoretical solutions of Dowson and Higginson, fixed load but vriable surface velocity.

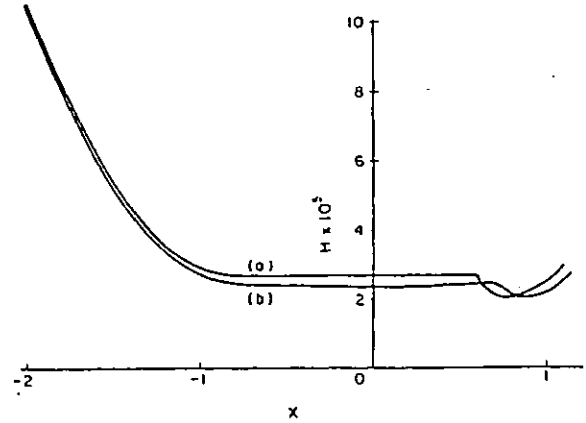

Film shapes. $W = 3 \times 10^{-5}$, $G = 5000$, $U = 10^{-11}$. (a) Incompressible lubricant. (b) Compressible lubricant. [Reproduced from the *Journal of Mechanical Engineering Science*, Vol. 4, No. 2, pp. 121–6 (1962) by kind permission of the Institution of Mechanical Engineers.]

Fig. 1.8 Theoretical solution by Dowson and Higginson, effect of compressibility of the lubricant on oil film profiles.

all cases the minimum film thickness was found to be about three-quarters of the thickness at the point of maximum pressure. The minimum film thickness was found to be much more dependent on surface velocity and material parameters than on the load parameter, as can be seen from their predicted formula for minimum film thickness

$$H^* = \frac{1.6\ G^{0.6}\ U^{0.7}}{W^{0.13}}$$

which when written in dimensional terms, become

$$h = \frac{1.6\ \alpha^{0.6}\ (\eta_o U)^{0.7}\ (E')^{0.03}\ R^{0.43}}{W^{0.13}}$$

where η_o is the inlet viscosity of the lubricant.

The general form of the film shape was not altered by the introduction of the compressibility of the lubricant but there were changes in detail. Fig.1.8 shows comparable shapes for compressible and incompressible lubricants. The minimum film thickness remains the same, but the sharp change of shape at the exit constriction gives way to a smoother change. Also the minimum film thickness is no longer three-quarters of the central film thickness and this ratio now depends on lubricant compressibility and on the magnitude of the pressure.

The isothermal prediction of minimum film thickness was shown, by Dowson and Higginson (24), to remain unaffected when thermal effects were introduced. However, the thermal EHL solution by Cheng (22) showed a slight lowering of the film thickness value and thus a better fit with the experimental results available at that time.

Although the isothermal film thickness formula produced by Dowson and Higginson (24) was widely accepted, several researchers produced experimental results which deviated widely from the theoretical prediction. Data obtained by Crook (25), for example, showed an index value of 0.5 instead of 0.7 in relating the film thickness to $\eta_o U$. At the other extreme Christiansen (26) found a value of 0.83. Sibley and Orcutt (27), in 1961 using an X-ray technique for measuring film thickness showed that their results followed the theoretical prediction reasonably well, although deviating at high surface velocity. A similar effect was found by Dyson, Naylor and Wilson (28) in 1965, using an inter-disc capacitance method. At low surface velocity the film thickness was found to fit the theoretical prediction but at higher velocities the measured thickness was below the prediction. The divergence becomes more marked with sliding as shown in Figure 1.9 . The reason was thought not to be due to non-Newtonian oil behaviour, as both Newtonian and non-Newtonian oils showed the effect to a similar extent. They, for the first time, suggested that inlet shear heating could be the cause of this discrepancy and this effect was expected to increase in importance when sliding was introduced. Crook (25) also noticed a reduction of the film thickness once sliding was introduced. The change, however, was small, only about 10 - 20%.

The inlet shear heating idea was developed in 1972 when Cheng (29), for the first time, tried to implement it into his calculation of film thickness and found that it could substantially reduce the film thickness. However, the properties of the lubricant used were such that the effect was

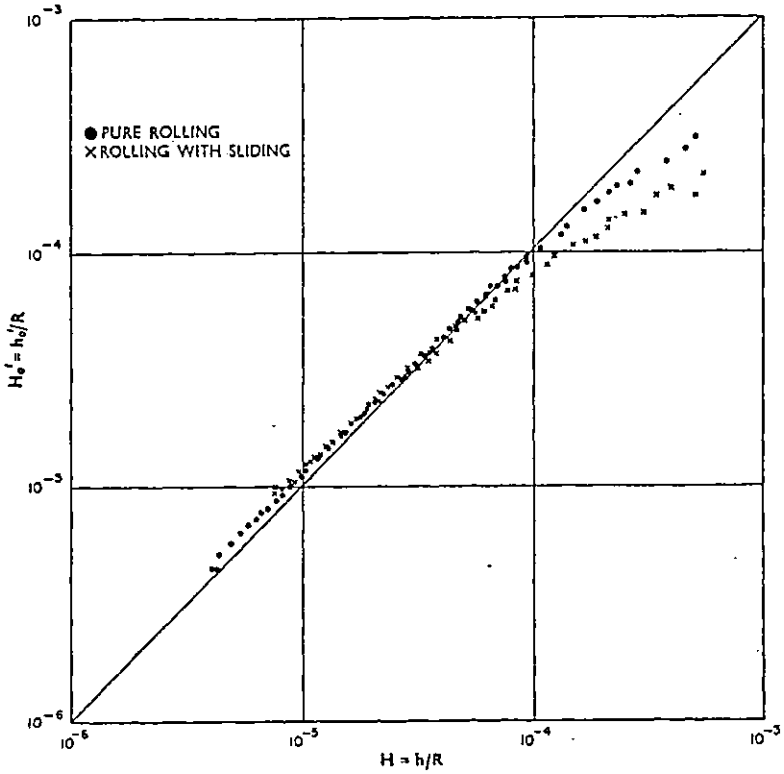

Lubricant D: comparison of measured non-dimensional oil-film thickness $H_0' = h_0'/R$ with predicted values $H = h/R$

Fig. 1.9 Experimental film thickness results of *Dyson* etal under pure rolling and partial sliding conditions.

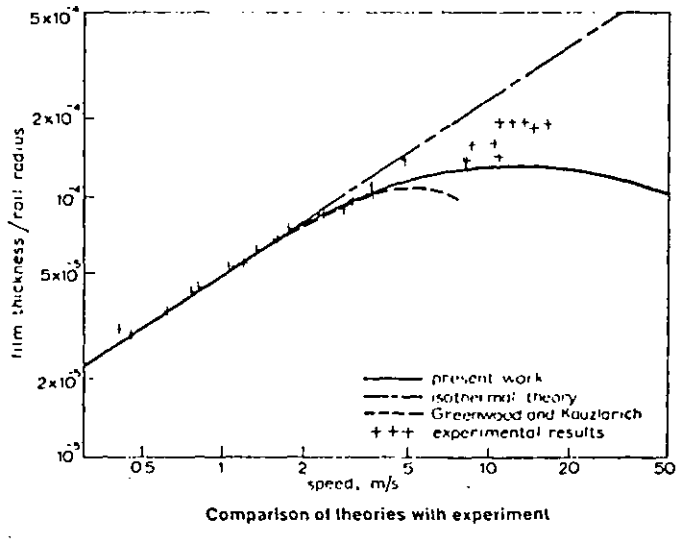

Fig. 1.10 Comparison of theoretical and experimental results compiled by March and Wilson.

only manifest at a very high surface velocity.

Greenwood and Kauzlarich (30) in 1973 presented a general analysis for the inlet sheer heating and its effect on film thickness. They showed that the reduction of film thickness from that of the isothermal prediction occurred at all surface velocities, but the reduction became more pronounced as the velocity increased. In their Grubin type analysis of the contact zone they assumed that the pressure and temperature effects on viscosity were independent. The analytical results in this work were obtained for the properties of Oil A from Dyson et al. (28) and agreed better with the experimental measurements. Dyson, in discussing the Greenwood and Kauzlarich's (30) paper, put forward a second analysis of the inlet zone heating and its effect on film thickness.

Murch and Wilson (31) in 1975 produced an analysis with a more realistic model of viscosity variation with pressure and temperature using Grubin type assumptions. The thermal Reynolds equation they used in the analysis was actually derived by Wilson & Wong (32). All these analyses showed a reduction in the film thickness from that predicted by the isothermal theory and they all showed better correlation with experimental results as shown in Fig 1.10.

The three analyses mentioned above determined a thermal correction factor, Y (a ratio of film thickness considering the inlet shear heating to the isothermal prediction), which was shown to depend roughly on a single parameter termed the thermal loading parameter $X = \frac{\bar{U}^2}{K} \left(\frac{-d\eta_o}{d\theta}\right)$ where $\bar{U}$ is the average surface velocity, K the thermal conductivity of the oil and $\frac{d\eta_o}{d\theta}$ is the rate of change of viscosity with

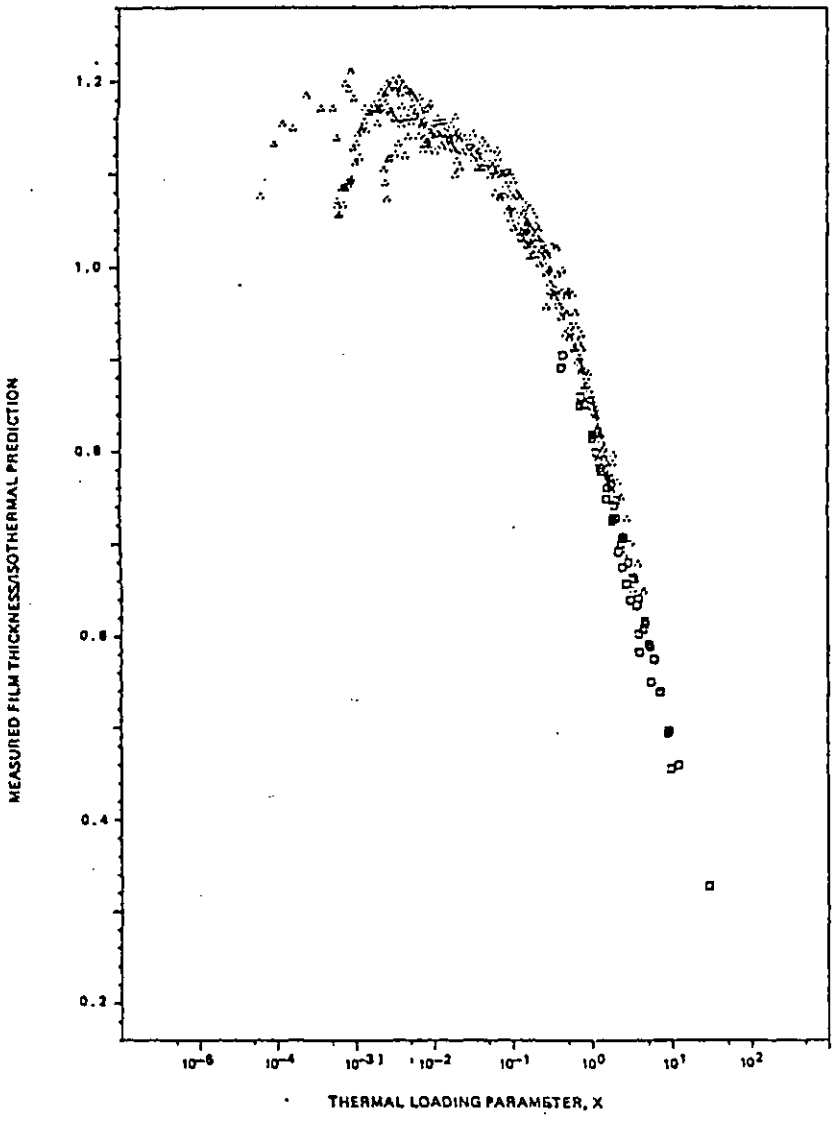

a Variation of measured to predicted film thickness ratio with thermal loading parameter, X (all measurements included)

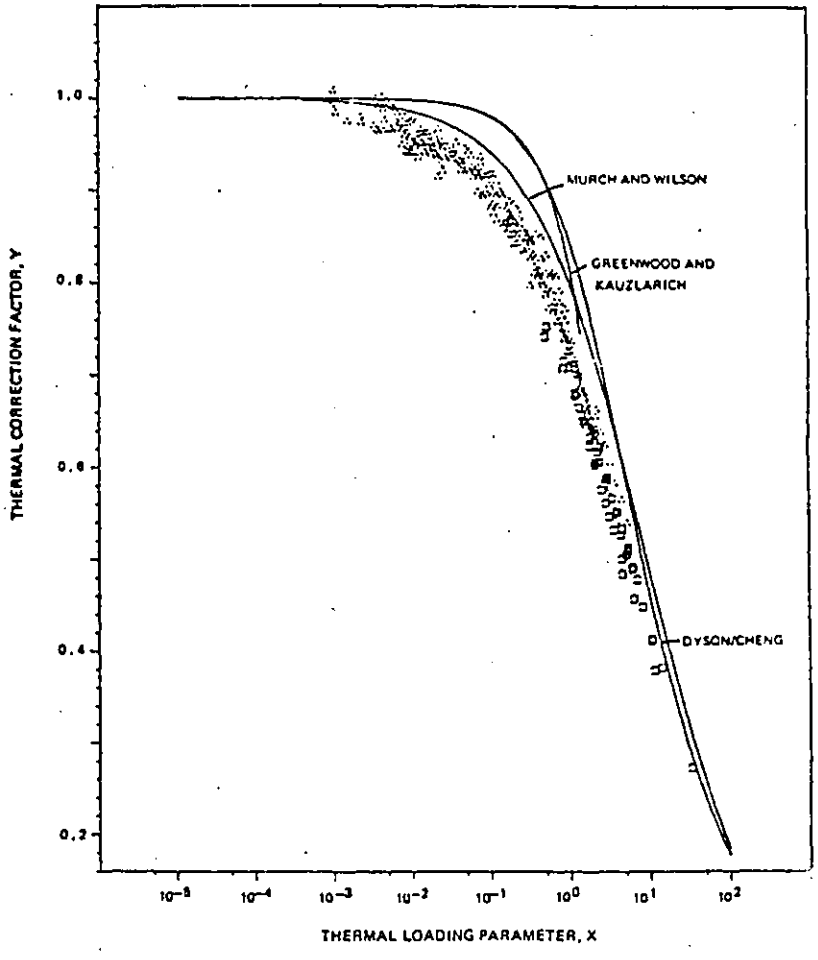

b Comparison between measured and predicted thermal correction factors for film thickness

Fig. 1.11 Comparison of theoretical and experimental film thickness results by Wilson, (a) experimental results; (b) experimental results after processing, and theoretial predictions by various authors.

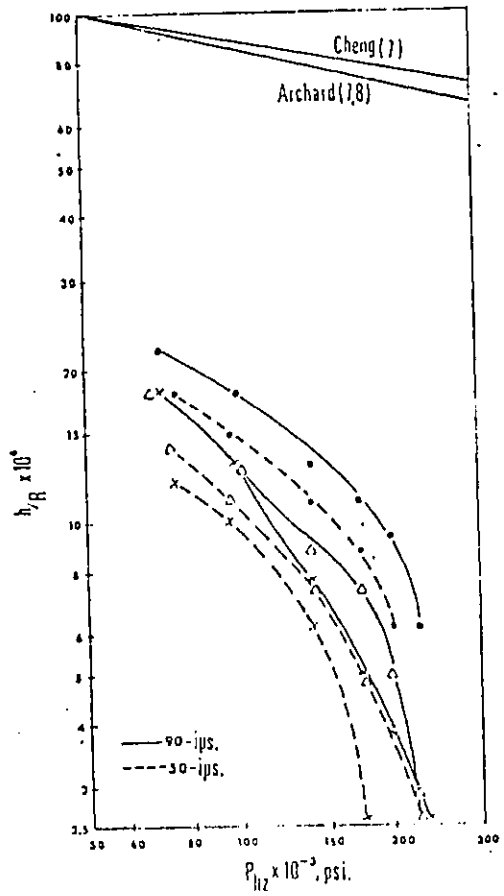

a Center (h_c---), minimum (h –x–), and trailing edge (h_t–Δ–), film thickness versus pressure for a modified polyphenyl ether

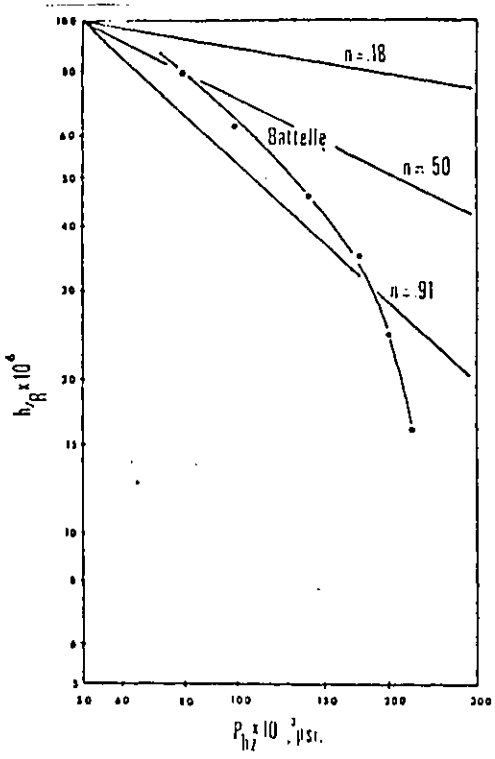

b Battelle data [1] on polyphenyl ether at 178 deg F and 6800 fpm rolling velocity

Fig. 1.12 Effect of load on film thickness, (a) Lee etal's experimental plot and Arcahrd's and Cheng's predictions, (b) Kannel etal's experimental results plotted by Lee etal.

temperature at the temperatures of the disc surfaces. Wilson (33) presented a comparison of capacitive film thickness measurements with some of the predictions. Figure 1.11b shows this comparison. The relations he used were

$Y = (1-0.24x)^{0.75}$ - Greenwood and Vauzlarich (30)

$Y = (1 + 0.458x)^{0.45}$ - Dyson (31)

$Y = 1 + (0.254\, x^{0.62})^{-1}$ - Murch and Wilson (31).

The minimum film thickness formula put forward by Dowson and Higginson indicated a very small dependence of film thickness on load. Early experimental work generally supported this. However, in 1971, Kannel and Bell (34,35), and Parker and Kannel (36,37) found that the dependence of film thickness on load was much larger than the theoretical prediction, particularly when the maximum Hertzian pressure exceeded $0.55\ GN/m^2$ (80,000psi). Kannel and Bell (34) after discussing all the possible sources of error in the X-ray film measurement technique, came to the conclusion that the effect was genuine. In 1973, Lee, Sanborn and Winer (38) found a similar effect in point contact using an optical interferometry method. Lee's (38) film thickness results for point contact along with the theoretical prediction by Cheng (39) and Archard (40) are shown in Figure 1.12a. In Figure 1.12b, Kannel's (39) result (as plotted by Lee et al.) is reproduced where m is the exponent in the equation $h \propto (P_h)^{-m}$. Kannel and Bell (34,35) in 1971 considered the possible reasons for this deviation. They examined three effects (i)generalised pressure variation of viscosity, (ii) a non-Newtonian rheology of Ree-Eyring form and (iii) a time delay of pressure effect on viscosity. They decided that the third effect was the most probable reason for the deviation.

Further works on rheology of lubricating oils have been done by Hirst & Moore (90-95), Winer et al (98-102), Johnson et al (95,103) and other researchers (96,97,104,105)

The theoretical solutions of Dowson and Higginson cover the range most commonly found in practice, namely high elastic modulus materials lubricated under heavy load by a fluid whose pressure viscosity relationship resembles that of a mineral oil. In 1965, Dowson and Witaker (23) presented a survey of isothermal solutions showing how the nature of the lubrication changes from the lightly loaded 'rigid' region covered by Martin's formula, through the moderately loaded region of Weber and Saalfield, to the high load elastic region of Dowson and Higginson. They showed the presence of an intermediate zone in which the surface could be considered as rigid, but the viscosity of the lubricant was enhanced by pressure. This situation does not occur for low modulus materials. The elastic iso-viscous region has received theoretical study by Herrebrugh. Broadly, it is possible to define four regimes of hydrodynamic lubrication: rigid and isoviscous, elastic and isoviscous, rigid and variable viscosity, and elastic with variable viscosity. Johnson (41) in 1970 presented these regimes in the form of a map after considering the theoretical results of a number of workers.

Johnson in the same paper compared the various sets of non-dimensional parameters used for theoretical solutions. He used the non-dimensional parameters introduced by Theyse (42) to plot the map and these parameters are

$$g_1 = \left[\frac{\alpha^2 w^3}{\eta_o U R^2}\right]^{1/2} \qquad g_3 = \left[\frac{w^2}{\eta_o U E' R}\right]^{1/2} \qquad \bar{h} = \left[\frac{h_o w}{\eta_o U R}\right]$$

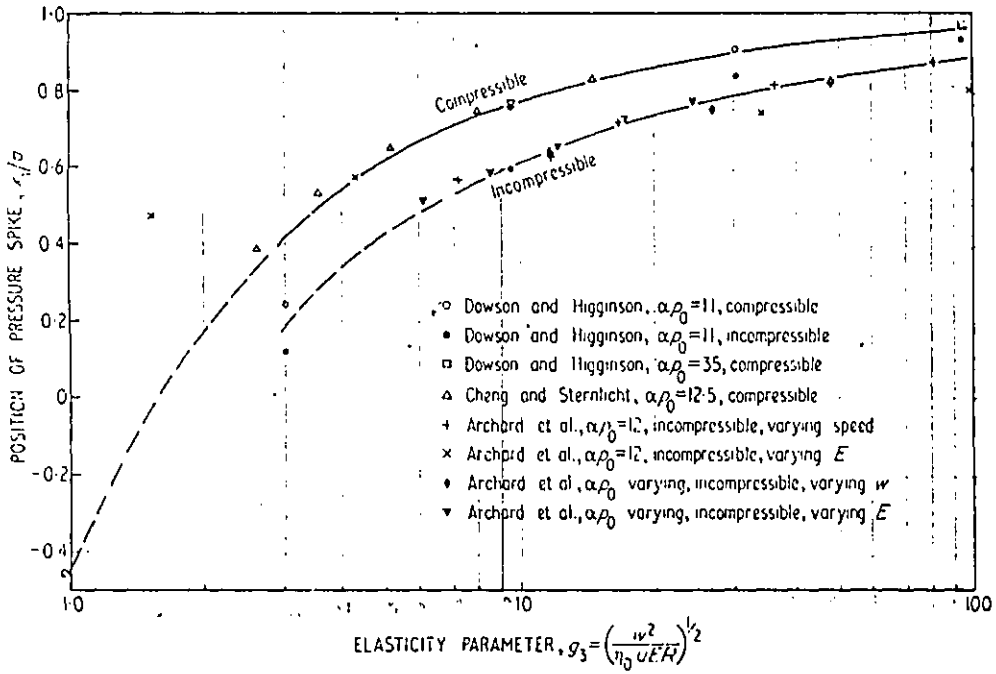

a Position of pressure spike at exit correlated on the basis of the elasticity parameter $g_3 = (w^2/\eta_0 uER)^{1/2}$

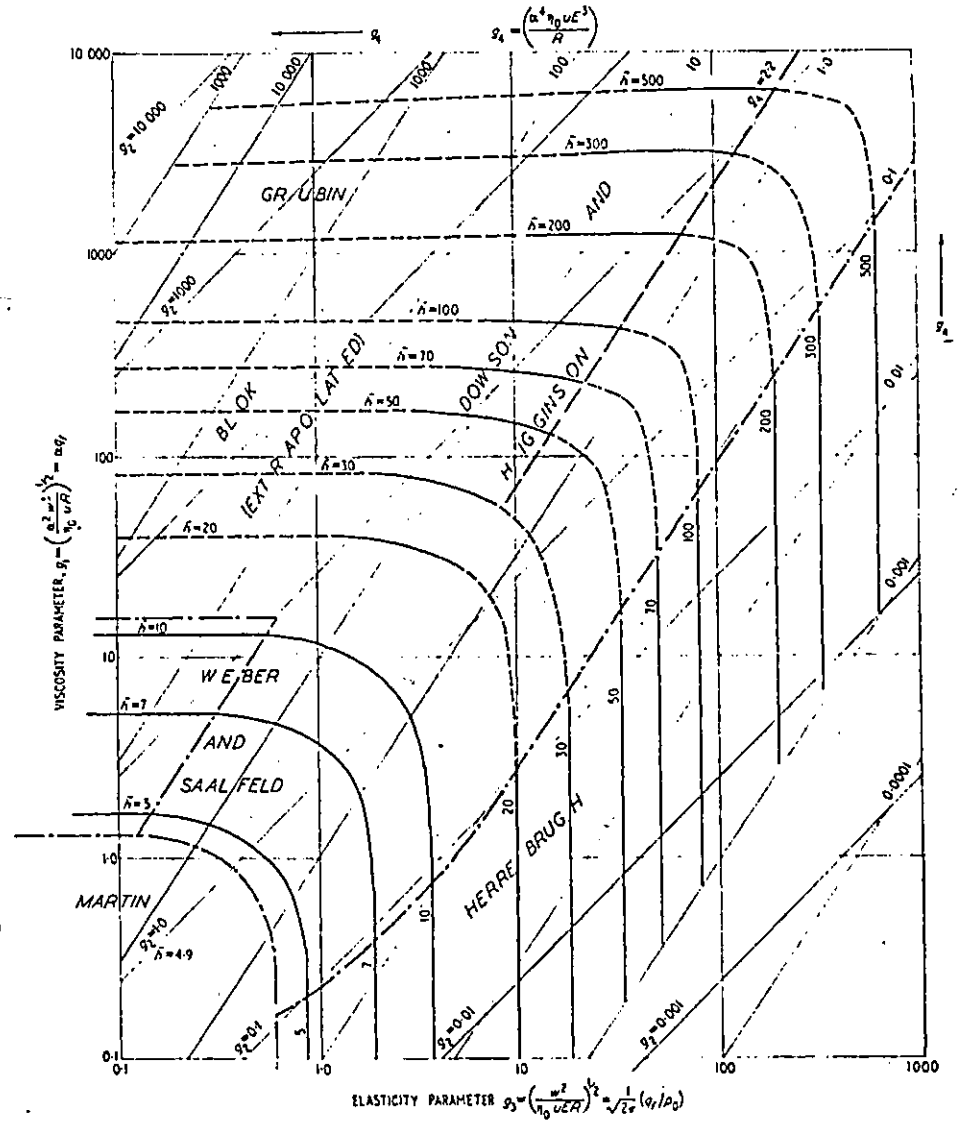

b Contours of film-thickness parameter $h = h_0 w/\eta_0 uR$ *superimposed upon the map of Fig. 1*

Fig. 1.13 (a)Jonsons postualation of the position of secondary pressure peak against g parameter (b) Jonson's map showing the various regimes of lubrication.

The non-dimensional parameters used by Dowson separates the operating variables: speed (u) and load (w) keeping material properties and geometries (α , E and R) constant. Theyse has choosen the independent parameters to separate the physical effects of viscosity increase with pressure (α) and elasticity (E'), and the dependent film thickness parameter which is exclusive of α and E'.

Johnson also discussed the presence or absence of the secondary pressure peak using Archard's (43) argument that the peak should show up when $g_4 > 1.8$ where $g_4 = \left[\frac{\alpha^4 E^3 \eta_o U}{R}\right]^{1/4}$, which is one of Archard's non-dimensional parameters. After considering various theoretical solutions of different authors, Johnson came to the conclusion that the secondary pressure peak should show up when $g_4 > 2.2$.

He has also shown that the pressure distribution within the contact zone can be approximated by $\frac{P\,(x/a)}{P_o} \simeq f(g_3)$. He plotted the position of the pressure spikes (x_1/a) from the published theoretical pressure profiles obtained by different authors. He found that most of the data fall on two distinct curves, one for compressible and the other for incompressible lubricants. The plot is reproduced in Figure 1.13a.

1.2 A SURVEY OF EHL - EXPERIMENTAL WORK

1.2.1 Direct Measurement of Pressure

The direct measurement of the rapidly varying pressure within the small EHL contact zone has proved to be one of the most difficult tasks in studying the characteristics of EHL. To ease the problem, researchers have tried to increase the contact zone by using softer material or by using rolling bodies of large effective diameter. Both these methods have the same drawback, namely that the pressure within the contact that can be achieved is limited, and it is the high pressure within the contact region that gives rise to most of the EHL phenomena.

Higginson (44) in 1962 studied the pressure profile at the contact between a rubber block and a 0.27 m diameter bronze drum with a pressure tapping of 500 μm in diameter. The maximum pressure achieved at the contact was very low at 0.21 MN/m^2 (30 lbs/in^2) and there was no effect of the pressure on viscosity. Even at this low loading the pressure profiles showed a transition from rigid solids to near Hertzian pressure profiles.

More realistic conditions were achieved by Dowson and Longfield (45) in a sliding contact, using a brass shoe and steel disc of effective diameter 1.98 m (78 in) for which the contact width was large enough to provide reasonable resolution with a 200 μm diameter pressure tapping on the fixed shoe as shown in Figure 1.14a. With a hydraulic press as the loading device they were able to generate enough load to produce primary peak pressures of over 0.21 GN/m^2 (30,000 psi) and in some of their profiles they detected the

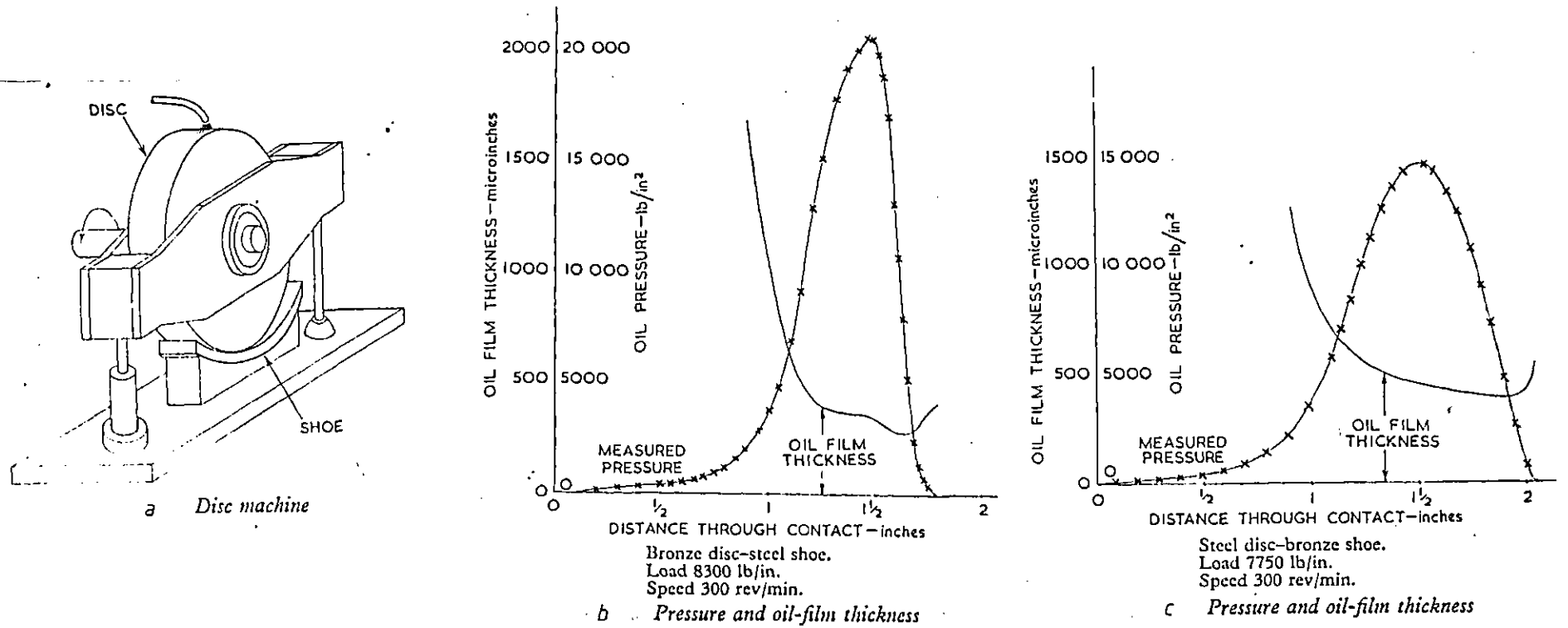

a *Disc machine*

b *Pressure and oil-film thickness*

c *Pressure and oil-film thickness*

Fig. 1.14 Dowson and Longfield's experimental system for measuring pressure in an EHL contact. Measured pressure profiles, bronze disc-steel shoe (b), and steel disc-bronze shoe (c).

formation of a secondary pressure peak zone. In addition to pressure they also monitored the temperature variation within the contact zone using embedded thermocouples. These showed a rise of temperature in the inlet zone, reaching a maximum just before the outlet. As the load was increased so did the maximum temperature. The maximum temperature rise was found to be 36°C with the bronze shoe and steel disc contact; however, the temperature rise increased to 47.5°C with the reversed combination and this was taken to be the reason for the difference in pressure profiles recorded under the two different combinations as shown in Figure 1.14b.

1.2.2 Measurement of Film Thickness

Most of the work in studying the EHL contact zone experimentally has been concentrated on measuring the lubricant film thickness in a contact zone. Several attempts were made to measure the electrical resistance of the oil film between the two electrically isolated discs and to correlate the measured value to the film thickness. This method was used by Lane and Hughes (46) in 1952 to show the existance of an effective lubricating film between gear teeth. They estimated that the resistance of a micron thick film would have a value of around $10^9 \Omega$, consequently resistance of a few ohms must indicate some sort of metallic contact or extremely thin-film. They found that the resistance and thus the film thickness decreases with sliding and load.

The same method was tried in disc machines later by Cameron (47) in 1954, Lewicki (48) in 1955, Crook (49) in 1957 and El-Sisi and Shawki (50) in 1958. However, attempts at measuring the film-thickness by this method were unsuccessful, because of the resistivity of the oil, which is very dependent

on temperature and moisture content. El-Sisi and Shawki (50) stabilised the resistivity to some extent by adding 4% sodium petroleum sulphate but this still did not give dependable results, as the values of the film thickness obtained, even at low loads, were an order higher than the isothermal predictions.

Cameron (47) during his attempt at relating resistance to film-thickness noted that for a current of less than 0.5 A through the oil film, the film behaves like an ohmic resistance, however, above 0.5 A the voltage drop across the film remains constant and this was termed a discharge voltage. This discharge voltage was found to depend on film thickness. This method was applied to gear teeth by McConoche and Cameron (51) in 1960. The method was found to be considerably affected by dirt particles and surface irregularities resulting in considerable scatter of the results. The flow of heavy current (upto 5 A) through the oil was also suspected of causing drastic changes to oil behaviour. Dyson (52) in 1967 examined the technique by making direct comparisons with capacitance measurements. He found that the agreement was not good and in particular he was unable to show the linear relationship between discharge voltage and film-thickness as Cameron et al. had done.

The inter-disc capacitance method consists of measuring the capacitance between two electrically isolated discs separated by an oil film. To convert the capacitance result into film thickness, the shape of the contact zone and the dielectric constant of the test oil under the contact conditions must be known. Lewicki (53) in 1955 tried this method in a disc machine. However, in interpreting the results, he

assumed the contact to be the same shape as a Hertzian contact with a parallel film separating the discs at the contact and the dielectric constant of the oil to be constant. Due to this error of interpretation, it is believed, his results are rather confusing. The film thickness value of around a micron found in his work was later found to be representative of such contacts by Crook.

After this initial work, capacitance measurement of film thickness became very popular. The dielectric constant of the oil plays the vital role in interpreting these results. The theoretical interpretation of the dielectric constant has been discussed by various authors, e.g. Bondi (54). The conclusion drawn from this work is that if the oil does not contain an appreciable polar component, the measured value of relative permitivity, E_r, at room temperature and pressure will not require any major correction when applied to the contact between heavily loaded specimens where high pressure and temperature will occur. Thus for a non-polar oil it can be assumed that the dielectric constant should vary only with changes of density, hence E_r should obey the Clausius-Mosotti relationship.

$$\frac{(E_r - 1)}{(E_r + 2)\rho} = \text{constant, where } \rho \text{ is the density.}$$

Crook (49) in 1958, with his measurement of E_r and ρ at atmosphere pressure and temperature up to 250°C found his test oil to satisfy this equation. However, Galvin, Naylor and Wilson (55) in 1964 measured the dielectric constant of a number of lubricating oils as a function of temperature and pressure. They found that some lubricants show substantial

changes in relative permittivity with applied pressure and temperature.

As Archard (56) in 1965, mentioned in his review paper, given that a non-polar oil is used, the major ambiguity in interpreting the capacitance results concerns the shape of the contact. Crook (49) in his earlier work in 1958 used this method only at very low load and assumed that the specimens were undistorted; with his later work (1963 , (57)) he assumed the contact to be similar to a Hertzian contact with a parallel film separating the elements. He, however, showed that his results from the inter-disc capacitance are consistent with his floating pad capacitance method, described below. Dyson, Naylor and Wilson (28) in 1965 published a large amount of film thickness results using this method with the same assumptions as Crook.

Because of the possible ambiguities associated with the shape of the surfaces, Crook devised the floating pad method which was independent of the deformed shape of the discs at the contact and measured the volume rate of flow through the conjunction of the discs. This volume rate of flow, which was measured on the exit side of the contact, was obtained by recording the capacitance between a very lightly loaded pad and the disc. The pad floated on the thin layer of oil adhering to the disc surface and since the lubricant was only subjected to low pressures the relationship between the capacitance and film thickness could be established more accurately.

Sibley, Bell, Orcutt and Allen (58) in 1960 developed a new method for measuring film thickness where they transmitted a collimated beam of X-rays through the contact zone, along

the direction of rotation of crowned discs, in their precision disc machines. The intensity of the transmitted beam measured on the opposite side of the disc was proportional to the film thickness. The beam width used was 0.75 mm and the minimum film thickness was measured. Later, Kannel, Bell and Allen (59) in 1965 changed the position of the X-ray beam from the direction of rolling to perpendicular to the direction of rolling. As a result, instead of only getting the minimum film thickness, as in the earlier method, the new arrangement could be used to monitor the whole contact along the direction of rolling. The size of the slit was also reduced to 0.75 μm to improve resolution. The advantage of the method was that it was fairly direct and was independent of the physical properties of the disc and the lubricant. However, the main drawback of the method seems to be the high degree of alignment necessary to pass the beam through the contact region. Using this technique they have measured film thickness for a wide range of running conditions.

Optical interferometry is another very useful method of monitoring the contact condition which involves the use of at least one transparent specimen loaded against another transparent or opaque specimen. The interference pattern formed at the contact due to the change in oil film thickness, and thus the gap in the contact, can be calibrated accurately to provide a reasonably accurate overall film thickness profile within the contact. This method was used by Gohar and Cameron (60) in 1963 to study the point contact formed between a steel ball of 2.54 cm diameter against a rotating circular glass plate. The method was further improved by Foord et al. (61) in 1967 when he replaced the high refractive index glass plate

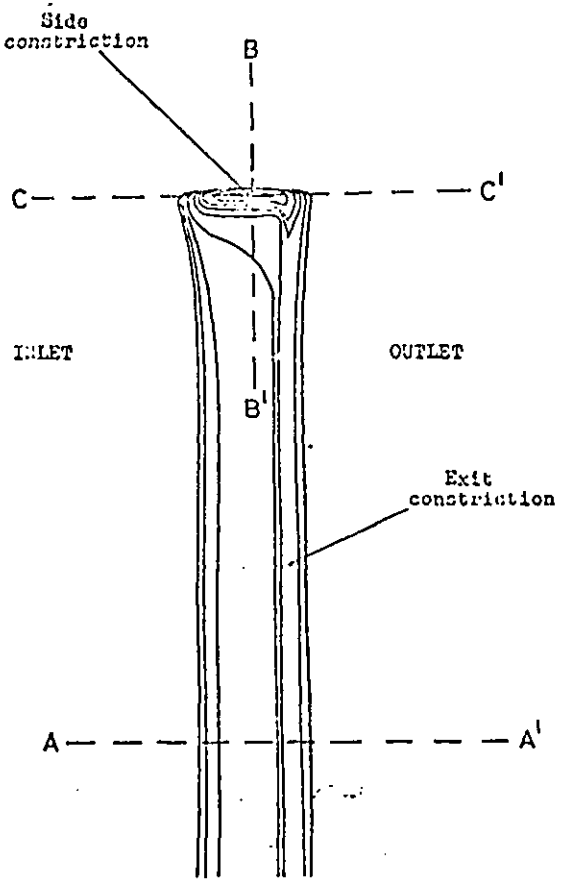

AA': Section through central region in direction of rolling
BB': Section through side constriction in axial direction
CC': Section through side constriction in direction of rolling

Sections through contact for film profile measurements

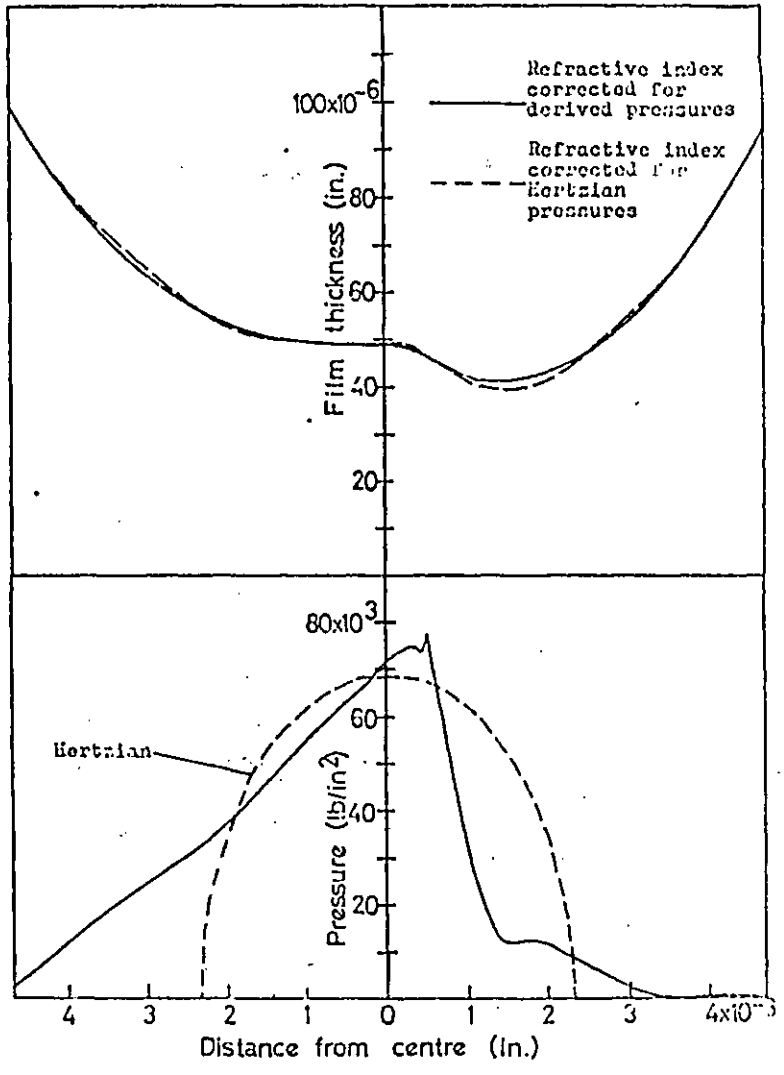

Computed pressure distribution and modified film profile

Load 138.5 lbs. $U^* = 66 \times 10^{-11}$

Fig. 1.13 Optical interferometric pattern of a line contact rcorded by Wymer; film thickness profile determined by the interferometric method is converted to pressure profile by inverse hydrodynamic equation.

with a plate of crown glass with a thin layer of chromium on the side in contact with the ball. Several other researchers from Cameron's laboratories used this technique to study point contact conditions. Wymer (62) in 1972 used the same method to study line contact in a specially prepared thrust bearing rig, where a window of sapphire on the race was made, through which light was shone on the contact formed between the sapphire window and the steel roller. By taking photographs of the contact, the whole area of the contact was analysed. In Fig.1.15a, a fringe pattern is reproduced from this work, the film thickness at the side constriction can be seen to be much lower than at the exit constriction.

Very careful measurement of the optical fringe changes in the contact is essential. In Fig.1.15b, a conversion of a film thickness profile into the corresponding pressure profile using the inverse hydrodynamic equation is shown. The main drawback of this system is that it requires one element of the contact to be transparent, thus the study of steel to steel contact is not possible and the set-up requires extensive calibration for proper interpretation of the interference fringes.

1.2.3 Thin-Film Transducers

Crook (63) in 1961 published a short article in "Nature" describing a novel method for measuring the film thickness in an EHL contact using a strip of evaporated chromium on a glass disc, the configuration of which is shown in Figure 1.16a. As the leading edge of the strip enters the contact zone the capacitance builds up between the strip and the opposing metal disc and this rate of capacitance increase is monitored by measuring the current into the capacitor. Using this method

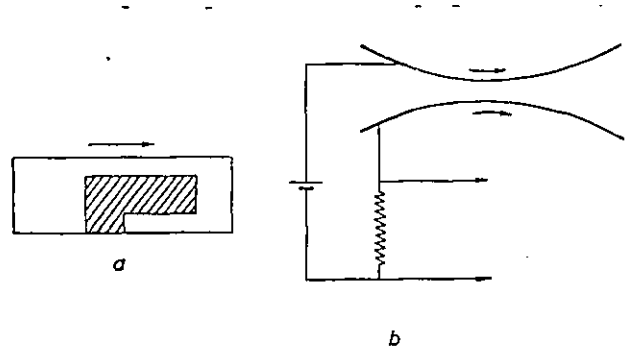

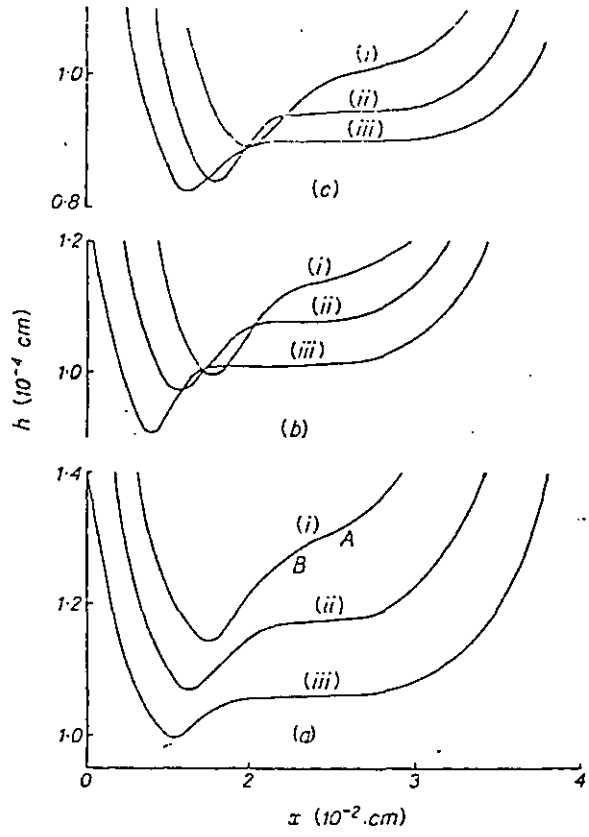

(c) FILM SHAPES
Rolling speeds: (a) 25; (b) 9·2; (c) 3·3 ft s^{-1}.
Loads: (i) 230; (ii) 360; (iii) 500 lb in^{-1}.

Fig. 1.16 Rate of change of capacitance method to measure film thickness, (a) device configuration, (b) electrical circuit, (c) film thickness profiles obtained using glass disc. (after Crook)

the deformation profile of the whole contact zone is obtained. Crook (64) in 1963 presented more detailed film profile results obtained with such a device also using a glass disc; the set of results published in this paper is reproduced in Figure 1.16c. The fairly parallel film formation with a dip at the exit zone can be clearly seen in these pictures at low surface velocity. At high surface velocity the parallel zone shows greater inclination, although even at the highest surface velocity the angle of inclination was only 0.03 degrees. Another interesting theoretical prediction, that the film thickness increases noticeably from the centre to the constriction, was also confirmed in this work.

Kannel, Bell and Allen (65) in 1965 and later Kannel (66) introduced the thin-film manganin strip as a pressure measuring device in an EHL contact. The change in resistance of a manganin strip about 50 μm wide and 0.1 μm thick deposited by vacuum evaporation, was monitored as it passed through the contact zone.. This variation of resistance is proportional to the pressure applied on to the film. In his early work presented in 1965, Kannel (65), fabricated the devices on a glass disc and the loading condition was limited. However, later in the same year Kannel (66) presented another paper where he had applied the technique to a metal disc using an evaporated film of SiO_2 to electrically isolate the transducer from the metal disc. However, the SiO_2 film was found to be piezo-electric in nature and, as a result, the signal from the transducer was obscured by the piezo-electric voltage developed by the SiO_2 film. To overcome this problem he tried to average out the voltage generated by the SiO_2 film

but this procedure was thought to have eliminated the secondary pressure peak. Later, differentiating circuitry was used to avoid the piezo-electric voltage during monitoring In Figs.1.17a,b, two sets of pressure profiles are reproduced from reference (66) where set (a) was obtained by the averaging method and set (b) by the differential amplifier method. It is interesting to note the position of the secondary pressure peak. Although the pressure profiles followed the Hertzic profile closely, it was felt that the position of the secondary pressure peak was very close to the preimary peak pressure for the loading and surface velocity conditions used for the traces. As a result it is doubtful whether the total effect of piezo-electric voltage had been eliminated.

Kannel (68) in 1974 presented some new pressure readings obtained with a thin-film device of the same width but with the length reduced to 150 μm and a layer of alumina was used to replace the SiO_2 film. He used the devices in a sophisticated disc machine where the relative position of the discs could be changed accurately thus making it possible to study the pressure variation across the whole contact length. Fig.1.17c shows a pressure profile presented in this work. Substantial changes in the profiles in Fig.1.17b and Fig.1.17c are noticeable particularly in the position of the secondary pressure peak zone, even though the operating conditions are not too dissimilar. The later profile fits the various theoretical predictions better. None of the pressure profiles show the secondary paresure peaks clearly, which is not surprising considering the width of the device.

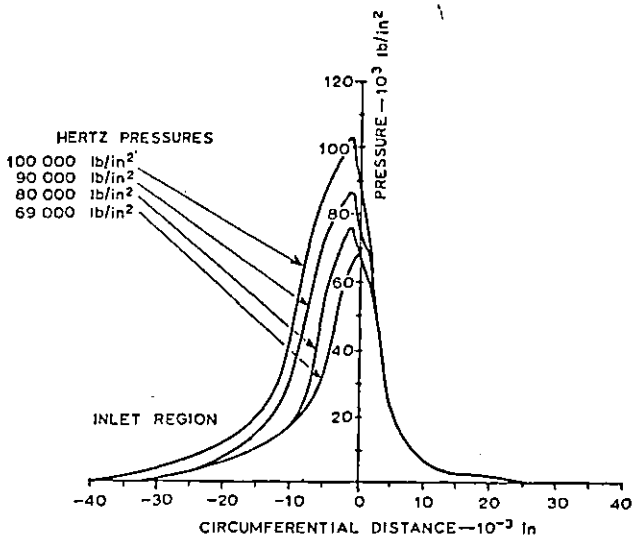

Temperature: $T = 110°F$.
Rolling speed: RS = 1400 ft/min.
Lubricant: polyphenyl-ether.

(a) *Preliminary film-pressure profiles obtained using averaging process for four loading conditions*

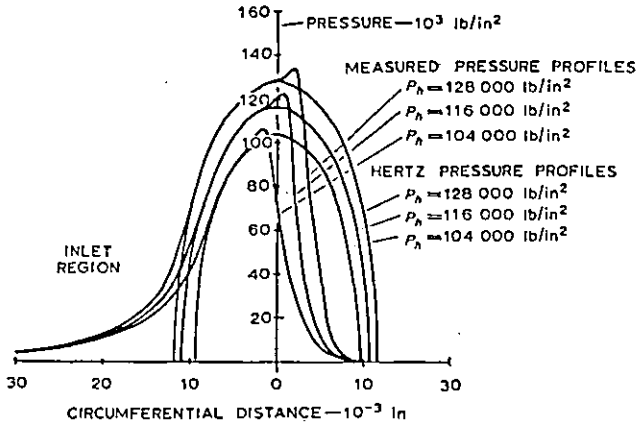

$T = 115°F$.
RS = 1400 ft/min.
Lubricant: polyphenyl-ether.

(b) *Measured variation in pressure profile with disc loading*

(c)

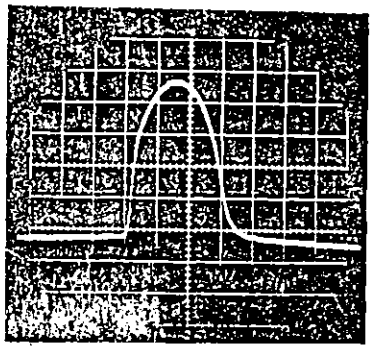

(d)

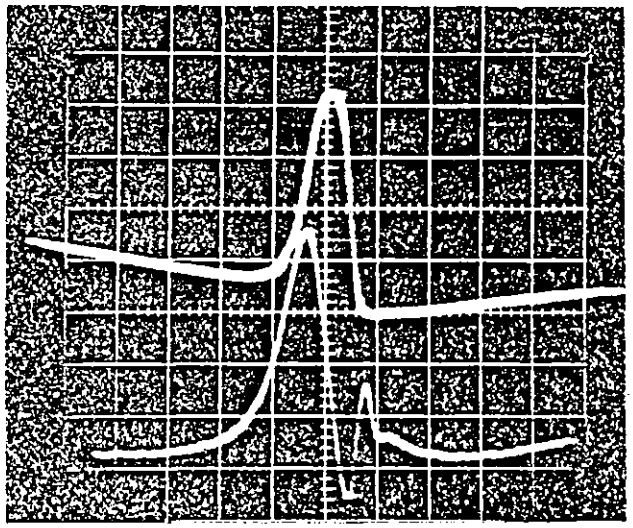

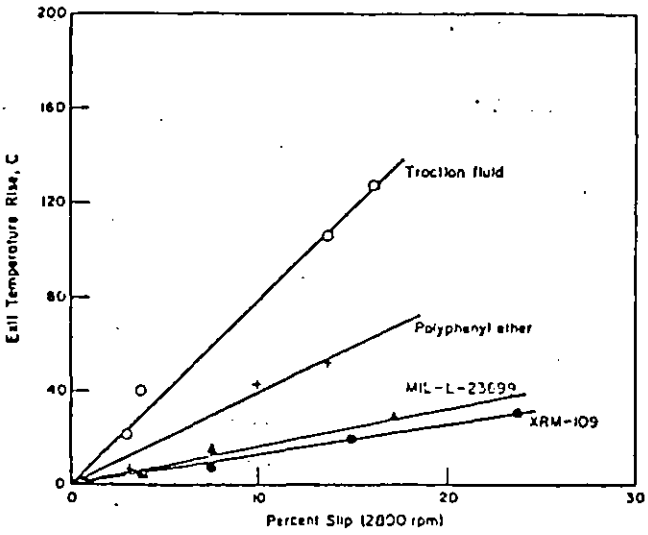

Effect of slip on exit temperature rise for selected lubricants

(e)

Fig. 1.17 Pressure and temperature profiles obtained with thin film devices, (a) & (b) early work using silica as insulator, (c) recent work using alumina as insulator, (d) synchronised temperature and pressure profiles and (e) temperature rises under various amounts of sliding with different oils. (after Kannel et al.)

Kannel and Dow (69) in 1974 presented a paper where they used thin-film titanium as a temperature transducer, having similar dimension to the pressure transducers fabricated earlier. Later in a report Kannel and Zugaro (70) in 1976 presented more details of the temperature profile recorded with these devices. At this stage they had produced superimposed temperature and pressure transducers with a layer of alumina between them. In Fig.1.17d the synchronised temperature and pressure profiles generated by such a combination of transducers are reproduced. The effect of pressure on the temperature profile was substantial. This was later corrected electrically by using the signal from the pressure transducer and the pressure co-efficient of the temperature transducer, which was determined by running the temperature transducer under dry contact conditions. This method of correction is suspect as a slight misalignment between the temperature and pressure transducer can substantially distort the temperature profile.

Kannel and Dow (71) in 1979 presented some more temperature results under pure rolling and partial sliding conditions and the effect of speed, and load and sliding on the temperature profiles were discussed briefly. Fig.1.17e reproduced from this work shows the effect of percentage of slip on temperature rise within the contact. The effect of load on temperature distribution was shown to be substantial, a change of 50% of load from 0.7 GPa to 1.1 GPa produced a temperature change from 30^{o}C to 50^{o}C. Similarly a temperature rise from 27^{o}C to 37^{o}C occurred with the doubling of the surface velocity from 1400 rpm to 2800 rpm in pure rolling.

Orcutt (72) and Cheng and Orcutt (73) in 1965 presented

papers with results obtained from thin-film transducers fabricated on glass disc to measure pressure, temperature and oil film profile in a glass-steel contact. For pressure measurements they used an evaporated manganin strip, 25 to 50 μm in width, running across the whole width of the disc. Temperature transducers were fabricated with the same dimensions as the pressure transducer using platinum paint, which was put on to the disc using a fine wire covered with platinum paint and later converted to bright platinum by heating it in air. The measured relative temperature co-efficient of such a device was quoted as $2.55 \times 10^{-3}/^{o}C$. The film thickness profile was determined using a strip of metal film of the same dimensions as the temperature transducer, where the capacitance between the strip and the mating steel disc was monitored as the strip passed through the contact zone.

Unlike Kannel, Orcutt calibrated his pressure transducers beforehand by slowly rolling the manganin strip through the contact zone in an attempt to avoid the hydrodynamic effect and supposing the contact as equivalent to a dry elastic contact, he equated the maximum height of the calibration pressure trace to the peak Hertzian pressure. However, examination of his calibration profiles reveals that the pressure drop at the exit is much sharper than the pressure development at the inlet. Thus it is rather doubtful whether the hydrodynamic effect was completely removed. The pressure transducers also suffered from high relative temperature co-efficients, which were quoted at $2 \times 10^{-4}/^{o}C$. The pressure profiles used for analysis in the paper were recalibrated to remove the temperature effect by using the temperature co-efficient in conjunction with the temperature

(a)

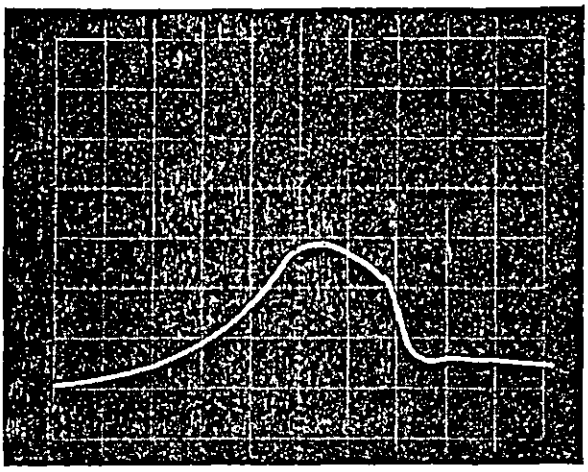

Pressure distribution: 135 in/s, S = 0, 1000 lb/in, Oil H

(b)

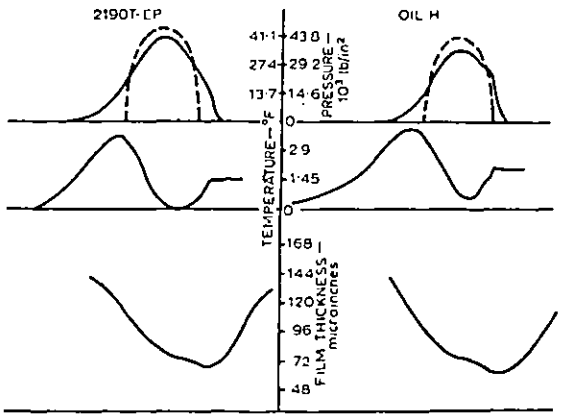

430/430 rev/min, 1000 lb/in.

Broken lines are Hertzian contact pressure distributions according to calibration. The pressure and deformation profiles are corrected for temperature and non-linear effects, respectively.

Effect of lubricant on pressure, temperature, and deformation

(c)

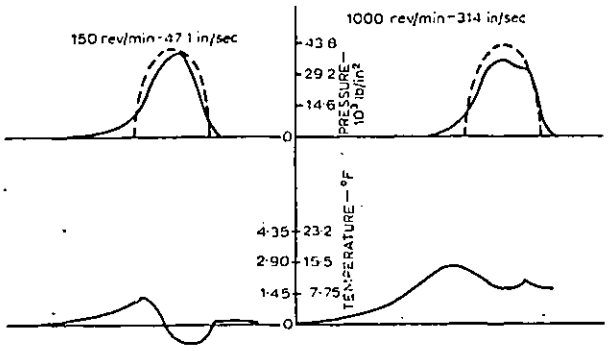

Load 1000 lb/in, Acme H oil.

Broken lines are Hertzian contact pressure distributions according to calibration. The pressure profiles are corrected for temperature effects.

Effect of rolling speed on pressure and temperature—50 and 1000 rev/min

Fig. 1.18 Pressure, temperature and film thickness profiles obtained by Orcutt et al.

profile recorded by the platinum temperature transducers. Some of the results obtained in this work are reproduced in Fig.1.18 . Fig.1.18a shows the zero level shift between the inlet and exit which was thought to be due to the temperature effect and was removed once the above calibration was done.

Fig. 1.18b shows the temperature profiles recorded from the platinum transducer. In explaining the negative excursion of the temperature profile Orcutt suggested a genuine cooling effect within the contact as he could find no pressure effect on the temperature transducer when it was rolled slowly through the loaded contact. This is rather surprising as bulk platinum has a pressure co-efficient similar in magnitude to bulk manganin. This would produce for a pressure of 150 MN/m^2 a change in resistance of about the same order as a few degrees rise in temperature. This is in most cases the kind of temperature rise that he measured at the inlet.

Orcutt found the characteristic change in slope in the pressure profile at the position of the secondary pressure peak and this point was found to move toward the exit with the increase of load; however, with the increase of surface velocity, this point of slope change was also found to move towards the exit substantially, as shown in Fig.1.18c. This is in contrast to the theoretical findings. The effect of sliding on the pressure profile was tried but no result was presented as the effect of temperature on such a profile was found to be large.

Some very interesting observations were made in this work: the pressure drop at the exit showed a steeper change with the increase of load and the secondary pressure peak zone

becomes more prominent for the oil with higher pressure viscosity co-efficient, which agrees well with the theoretical prediction.

An increase in temperature at the inlet was detected in this work with the increase of load. The temperature rise at the inlet was also found to vary with the variation of the surface velocity. A change in surface velocity from 135 in/sec to 314 in/sec produced a change of inlet temperature from 4 ^{o}F to 15^{o}F. The temperature rise within the contact was also found to increase substantially once partial sliding was introduced. The maximum temperature rise recorded at 40% sliding was 25^{o}F whereas under pure rolling it was about 4.5^{o}F at the inlet.

The film thickness measurements in this work have suffered from the fringing effect of the surrounding metal, particularly at the inlet and the exit zone. However, the minimum film thickness value was thought to be correct, as the fringing effect within the contact should ne negligible. The minimum film thickness value measured was 60 to 70% of the theoretical prediction. Dependence of film thickness on load was found to be small. An increased deformation of the surface was detected with increased load, however under none of the operating conditions was a substantially flat region detected. The effect of surface velocity on film thickness profile was omitted in this work due to the difficulty of obtaining readings at low surface velocity, where oil film breakdown occurred.

Further developments of the thin-film transducers were made by Hamilton and Moore (24, 75) who presented two papers in 1967 and 1971 on their work with these devices. Glass to steel contacts were studied using a napthenic mineral oil with a pressure viscosity co-efficient of 2.92×10^{-8} m^2/N.

Pressure and temperature were measured with devices of around 40 μm wide by 0,5 mm long using manganin and nickel respectively as the sensing materials. A single pressure transducer, however, was made with an active element of width 7.6 μm and was operated successfully. Film thickness was monitored using the above mentioned devices, applying the Crook's(63,64) rate of change of capacitance method . Although the same devices were used for measuring pressure and film thickness or temperature and film thickness, they were able to get a high degree of alignment between corresponding profiles.

Although the maximum Hertzian pressure in this work was limited to about 0.3 GN/m^2 , the pressure profiles recorded were found to be consistent with theoretical predictions, particularly regarding the movement of the position of the secondary pressure peak with operating conditions. In analysing the results, the authors computed the theoretical pressure and film thickness profiles for the exact operating conditions for some of their measured profiles. In Fig. 1.19, the set of such comparison profiles and the corresponding original traces are reproduced from this paper.

In positioning the measured profiles relative to the theoretical one, they matched the inlet region of the pressure curves in the two profiles, as this region is, in all cases, well defined. One rather interesting phenomenon was noticed in these comparative theoretical profiles against measured pressure profiles, which is that the secondary pressure peak position shows greater movement with surface velocity at a fixed load in the theoretical profiles than in the measured profiles. Under a fixed surface velocity, the movement of the secondary pressure peak with load is similar in both

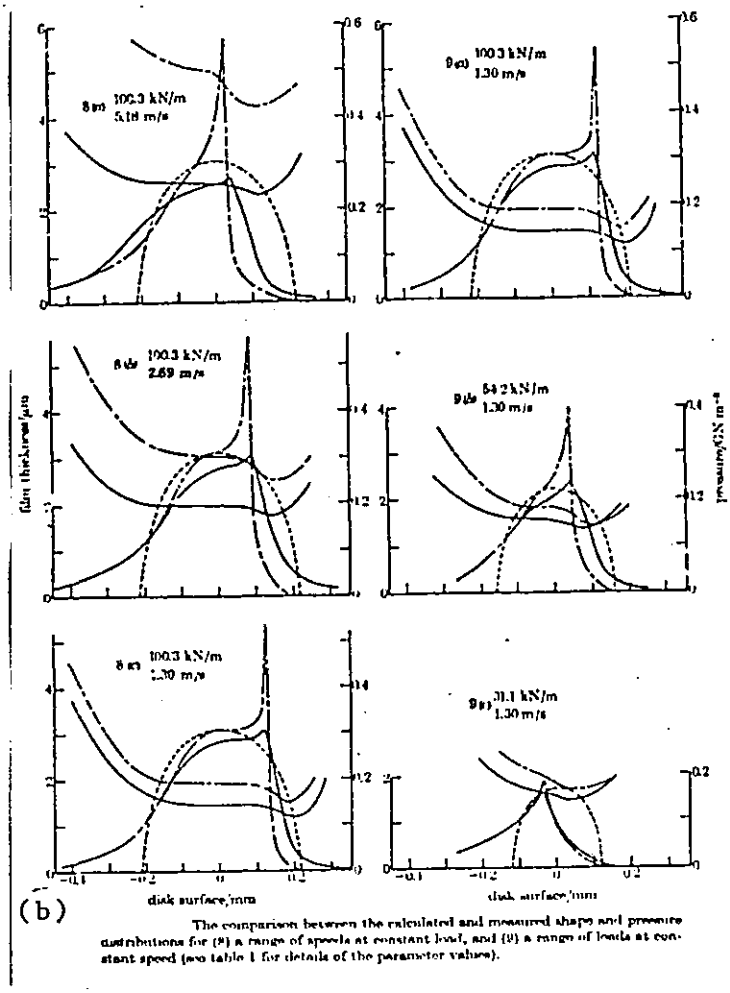

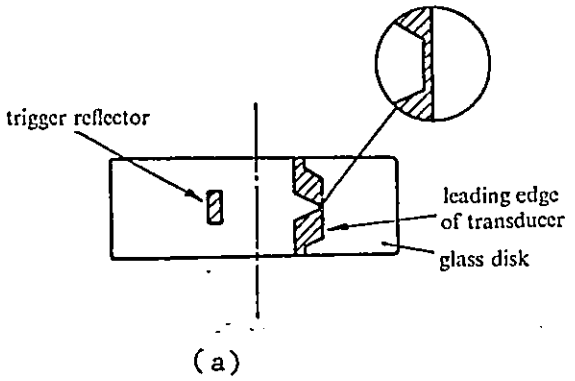

(a)

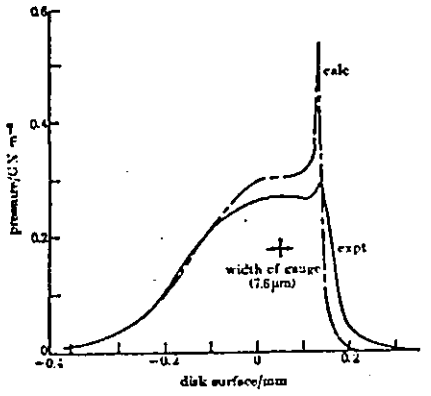

(c)

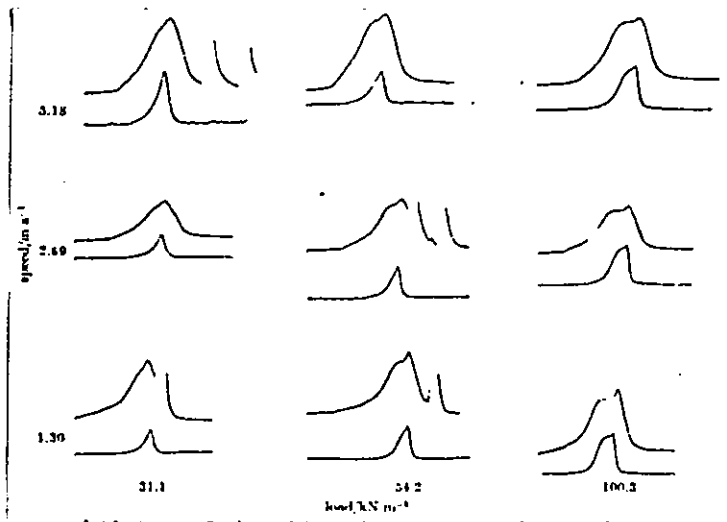

(d)

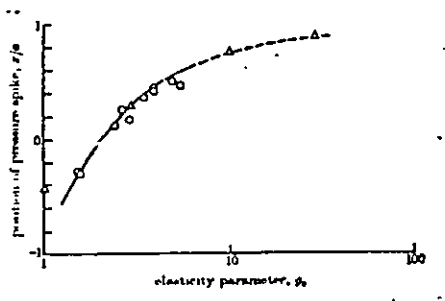

(e)

Fig. 1.19 Thinfilm pressure transducer (a), pressure and film thickness profiles (b), pressure profile obtained with 7.6um device and corresponding calculated profile (c), original recordings (c) and position of pressure peak, x/a against g . (after Hamilton and Moore)

theoretical and measured profiles. However, the relative position of the secondary pressure peaks plotted against the g_3 parameter, were close to Johnson's (76) postulation as shown in Fig. 1.19e.

The presence of the secondary pressure peak is shown clearly for the first time in this work; however, reducing the size of the device from 40 μm to 7.6 μm of width did not produce a large change of spike height, although the point at which it breaks away from the rest of the curve is sharper, as can be seen in Fig. 1.19c.

The film thickness profiles recorded by the rate of change of capacitance method are interesting since instead of a well defined leading edge followed by a constant width electrode along the direction of rolling as shown by Crook (63, 64), the configuration of the pressure and temperature transducers shown in Fig. 1.19a is used. However, a closer examination of this complicated configuration reveals that the effective width of the electrode immediately after the leading edge remains almost the same for some distance. As a result the configuration should produce reasonably accurate film profiles, though some fringing effect may have occurred from the electrode. However, the film thickness values obtained were found to be consistent. At low surface velocity the measured film thickness was close to the theoretical prediction whereas at high surface velocity the deviation is substantial. Unlike Orcutt's (72) result where he failed to find any parallel zone in the film thickness profiles, most of the profiles in this work show a fairly parallel film with the constriction at the exit. However, the authors of this work discussed in detail the discrepancy they noticed between the theoretical

profiles and the measured profiles, regarding the change in size of the constriction with surface velocity. At high surface velocity theory predicts an increase in the constriction while measured profiles showed little change. This was thought to be consistent with the unchanging height of the secondary pressure peak with surface velocity.

The nickel temperature transducers used in this work were applied for a preliminary study to ensure that large temperature rises did not occur within the contact zone. The limited use was mainly because of the high pressure effect on temperature profiles.

Further study of the EHL line contact using thin-film devices was carried out by Schouton (83). In fabricating his devices on metal discs, he used similar shaped devices to those used by Hamilton and Moore (75). Electrical insultation between the devices and the metal discs was accomplished by means of an evaporated layer of SiO_2. The resistive pressure and temperature transducers were made from evaporated manganin and titanium respectively.

In Fig.1.20 some of his recorded traces are reproduced. Traces 'a' and 'b' were recorded with relatively large devices and without any electronic aid to remove zero level shift. These traces do not show any secondary pressure peak. In trace 'c', the width of the device was reduced considerably to 10 μm and the secondary pressure peak shows up clearly. Very little analysis of these traces is given. Traces 'd' and 'e' are temperature traces recorded under pure rolling and partial sliding between the discs. No comments could be found of possible pressure effects on the temperature transducer, nor was any mention made of the possible piezoelectric effect on SiO_2.

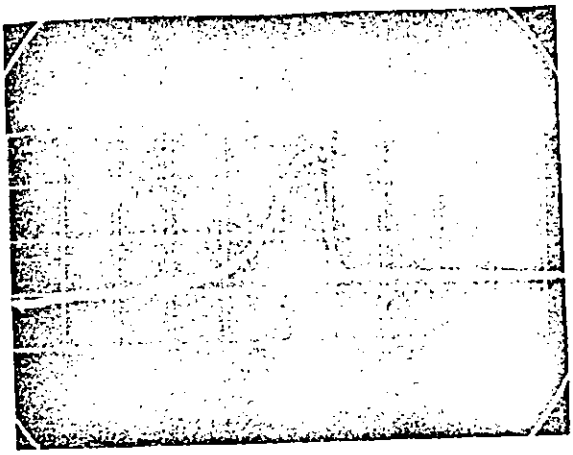

F_o = 2090 N; σ_{Hz} ≈ 6160 bar (a)

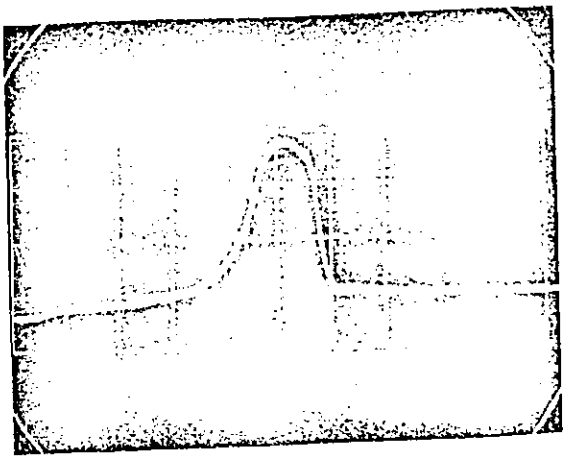

F_o = 4100 N; σ_{Hz} ≈ 8700 bar (b)

n = 30 U/s

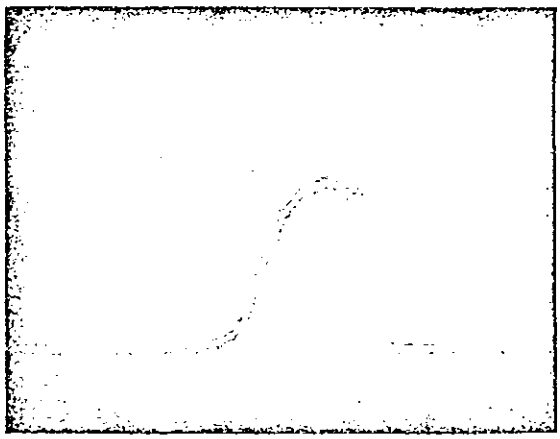

(c)

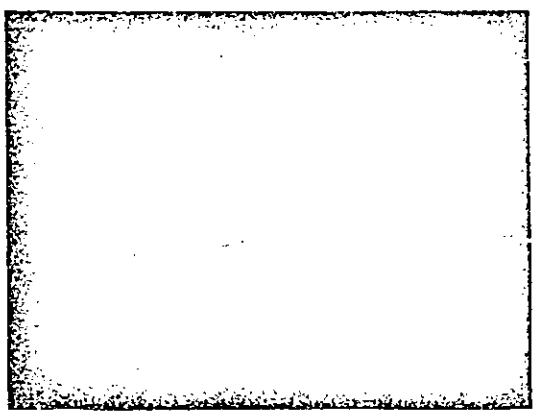

n_2 = 20 U/s (d)

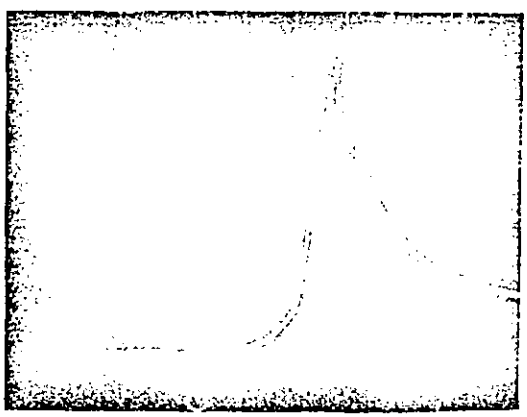

n_2 = 15,0 U/s (e)

Fig. 1.20 Pressure traces recorded with wide device (a) & (b), with 10um device (c) & temperature traces recorded under rolling and sliding conditions (d) & (e). (after Schouton)

Thin-film devices have also been used by Bartz and Ehlert (84) to study the effect of the pressure viscosity co-efficient of lubricating oil on pressure, temperature and oil film thickness in a disc machine. They used the same techniques for fabricating the pressure and temperature transducers (10 μm x 1000 μm) as Schouton (83). For film-thickness measurements, the capacitance between a conducting line (of 100 μm width) deposited on a disc and the opposing disc was measured as the line passed through the contact. In fabricating the film thickness electrode they changed from an evaporated SiO_2 layer, used with their pressure and temperature transducers, to evaporated Al_2O_3. No explanation was given for this change.

The bulk of this work was carried out with a mineral oil with high viscosity (0.85 Pa-sec) and a high pressure viscosity co-efficieint (4×10^{-8} Pa^{-1}). However, they also used other oils with varying α and η values. Figure 1.21a shows a set of pressure profiles reproduced from this work. Traces 4, 5 and 6 were obtained with an oil viscosity of 0.165 Pa-sec and α values of 1.89, 1.68 and 2.37×10^{-8} Pa-sec respectively. Traces 1, 2 and 3 refer to ~~an~~ oils viscosity of 0.85 Pa-sec and α values of 1.26, 2.06 and 4.03×10^{-8} Pa^{-1}. It is interesting to note the change in secondary pressure peak height in traces 1, 2 and 3 with a relatively large change in α values. They found that the pressure distribution resembled more closely the Hertzian pressure distribution with reducing α , and increasing load as shown in Fig.1.21*a,b* In this publication, however, no original recording of any profiles are given.

Four redrawn temperature profiles under pure rolling conditions shows an increase in the maximum temperature rise within the contact of 12°C to 15°C with a change in load from 2.6×10^5 N/m to 4.6×10^5 N/m with Oil 3. A similar change in temperature was found with their Oil 1, where the surface velocity was increased from 5.65 to 7.55 m/sec. In Fig.1.21, two of the temperature profiles are reproduced and they look remarkably similar to pressure profiles under the same operating conditions. This was explained as being due to the fact that, for pure rolling, only compression of the oil can effect any temperature rise within the contact. It is interesting to note a rapid decay of temperature towards the reference level at the exit in these traces whereas the work of Kannel (70) and Schouton (83) suggests a much more gradual decay. No static loading tests on these devices were performed.

Film thickness profiles due to change in load is reproduced here along with dependence of minimum film thickness on load plotted in Figure 1.21. Within the load range from 2.1×10^5 to 5.07×10^5 N/m, they concluded that their results agreed with the isothermal prediction. However, a closer examination suggests a value of m, in the relation $h_{min} \propto (w)^{-m}$, of 0.12 for the lowest loads which increases to 0.24 for the highest loads. Using two data points at 5.03 m/sec and 7.55 m/sec, they showed that the dependence of film thickness on α and η_o value was close to the isothermal prediction.

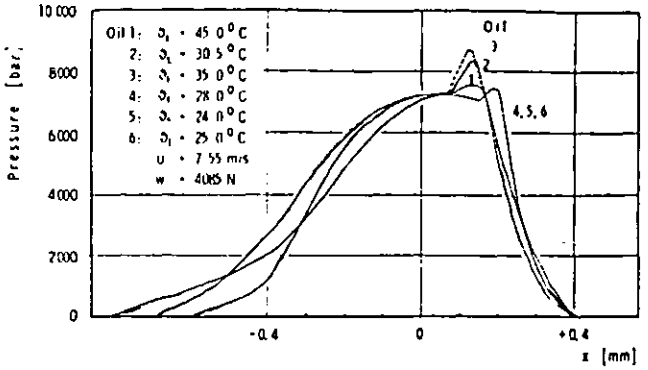

Fig. 10 Pressure distribution for several test oils

(a)

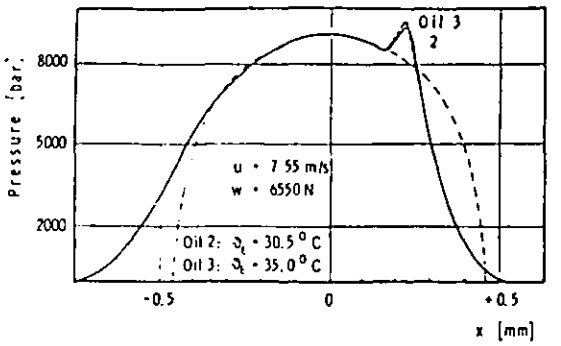

Fig. 11 Pressure distribution for several test oils

(b)

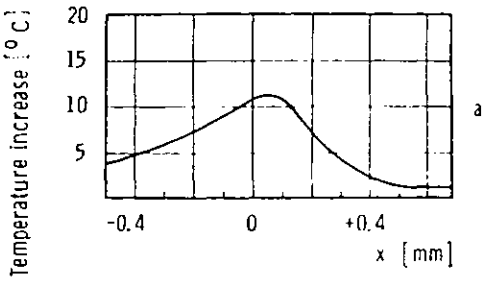

Test oil 3

u = 7.55 m/s

ϑ_E = 35 °C

a: w = 2600 N

b: w = 4578 N

(c)

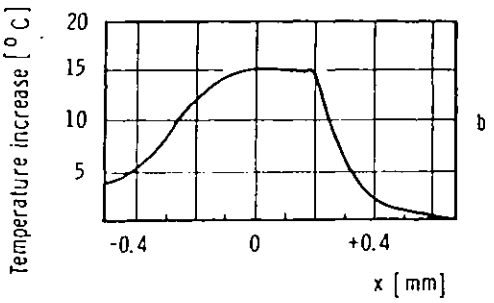

Fig. 14 Influence of load on temperature distribution

(d)

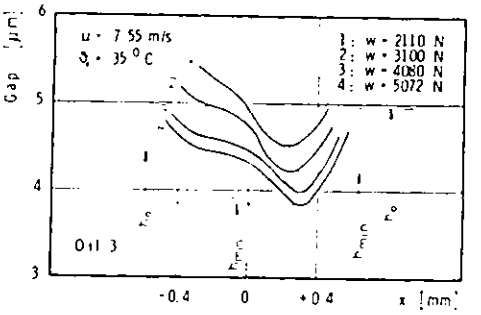

Fig. 16 Influence of load on the shape of gap

(e)

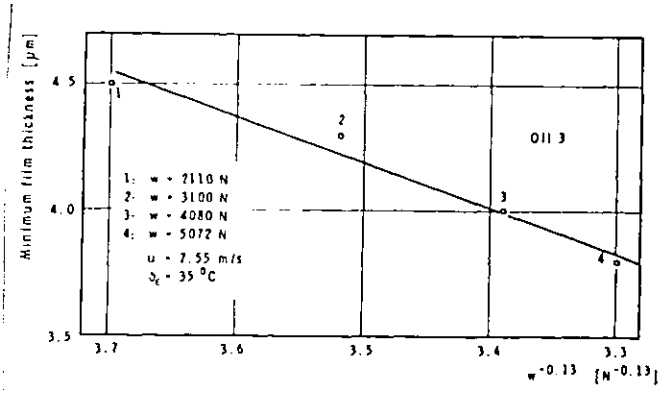

Fig. 17 Measured minimum film thickness depending on the expression $1/w^{0.13}$

(f)

Fig. 1.21 Pressure profile recorded with 10um device using various oils (a)&(b), temperature profiles (c)&(d), film thickness profiles (e) and effect of load on minimum film thickness (f). (after Bertz and Ehlert)

1.3 A Survey of Materials and Devices Related to Thin-Film Transducers

Bridgeman (77) found an almost linear relationship between the resistance of manganin and the pressure applied on it up to 3 GN/m^2 (30 Kbar) in his pioneering work with high pressure. Following the discovery, manganin wire has been used extensively as a pressure sensor in hydrostatic pressure vessels. Bridgeman found it necessary to season the device formed by winding the wire round a sleeve, by annealing it at 140°C up to about 24 hours and then cooling it with liquid nitrogen, followed by a pressurisation cycle to 30 Kbar. This was intended to stabilise the pressure co-efficient and the resistance. The necessity for seasoning was also discussed in detail by Adam et al. (78) in 1937. They found that the resistance of manganin wire changes considerably during physical operations, such as winding the wire in the form of a coil. They detected a change of up to 2.7% in resistance; while annealing at 140°C a change of up to 2% was detected and during pressure seasoning at 8 Kbar a change of up to 0.03% was found to occur. Once the whole seasoning process was over the gauge was found to be stable to within 0.1% and reproducible, provided the operating temperature was not allowed to go beyond a certain value. A sudden change of temperature from 25°C to 65°C and back to 25°C was found to reduce the pressure coefficient value by about 0.4%. In the seasoning process used by Adam et al., they found it unnecessary to use the cooling cycle and later researchers found that the pressure seasoning was also of no great consequence.

Pressure co-efficients of manganin wires were found to vary between 2.1 to 2.4 x 10^{-6}/bar, as noted by Bridgeman, and the variation occurs between supplies from different manufactuerers and between batches. The pressure coefficient was normally determined with a hydrostatic pressure vessel where very little shear stress exists. Some researchers, e.g. Lees (80) and Adam et al. (78), noticed the sensitivity of the pressure co-efficient of manganin to shear stress. Samara and Giardini (79) developed a gauge using a manganin coil wrapped round a AgCl sleeve packed with Ta, Ba and Bi calibrants which change phases at known pressures. They tried this gauge in a piston cylinder and multi-anvil apparatus using a solid pressure transmitting medium; shear stress to some degree is expected in the solid pressure transmitting medium. The linearity of the manganin gauge was found to be good in between the transition stages as shown in Fig.1.22a but at the transition points they detected a rapid change of resistance which was found to be proportional to the volume change of the sleeve.

Lees (81) in 1970 published a research note where he has shown some drastic changes of the pressure co-efficient of a manganin coil wound on different types of sleeves with a solid pressure transmitting medium as shown in Fig.1.22b However, recently Fujioka, Mishima and Kawai (82), using a precision multi-anvil apparatus found that manganin exhibited a highly reproducible and linear pressure co-efficient up to about 180 Kbar and although the pressure transmitting medium was a magnesia cell, the pressure co-efficient remained within (2.322 $\pm$ 0.008) x 10^{-3} $Kbar^{-1}$.

The variation of resistivity of manganin with temperature is well known to be extremely small which makes it very suitable

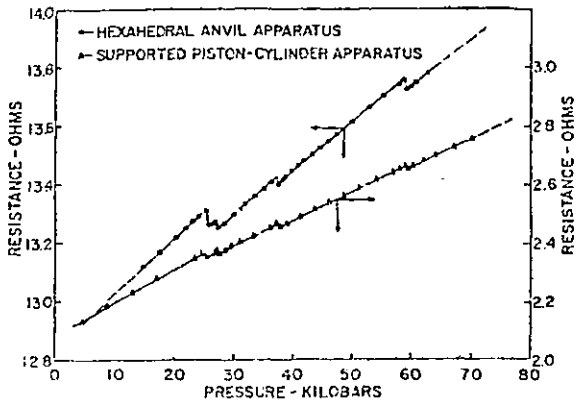

Typical gauge responses in the hexahedral anvil and piston-cylinder apparatuses.

(a)

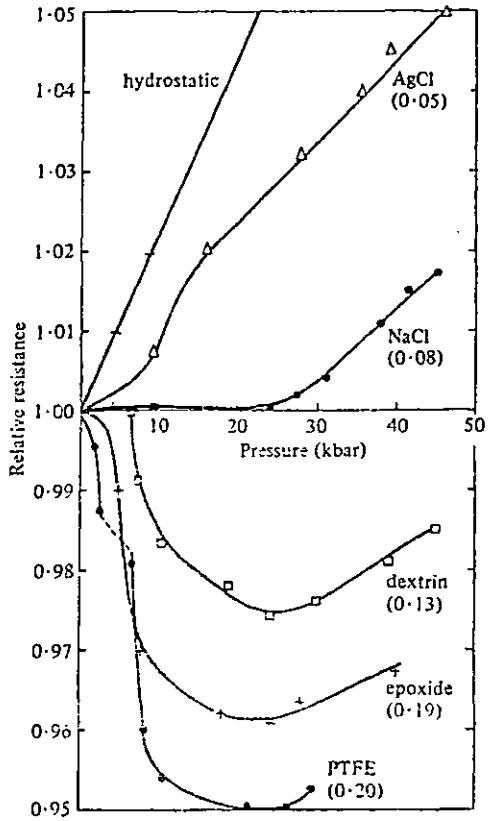

(b)

Dependence of resistance on pressure for Manganin wire in various sleeves (figures by the curves indicate compression at 25 kbar).

Fig. 1.22 (a) Effect of volume change of multi-calibrant sleeve on pressure coefficient of resistivity of manganin (after Samara and Giardini), (b) change in pressure coefficient of resistivity with the change of sleeve material (after Lees).

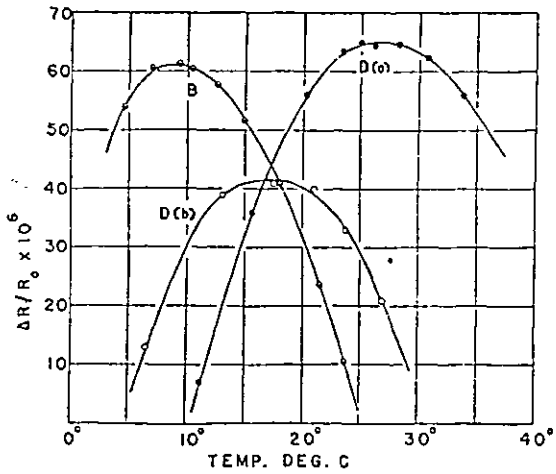

Relative resistance change, $\Delta R/R_0$, *vs.* temperature of two samples of manganin wire. "*B*" refers to the wire supplied by Baker & Co. and "*D*" to that supplied by the Driver-Harris Co., of which (a) and (b) signify after and before "heat treatment" respectively. The scale for $\Delta R/R_0$ is reckoned from an arbitrary "zero."

Fig. 1.23 Temperature coefficient of resistivity of manganin. (after Adams et al.)

for application as a pressure sensor. However, the resistance vs. temperature profile of manganin shows a pronounced maximum at around room temperature as is shown in Fig.1.23 due to Adam et al. (78). The temperature co-efficient at around the maximum is very small and it remains small at around $5 \times 10^{-6}/^{o}C$ even at temperatures well away from the maximum.

No references in the literature to thin-film manganin being used as a pressure sensor in high pressure work have been found, except for the applications in EHL mentioned previously.

Many thin-film temperature transducers have been reported in the literature mainly for the purpose of measuring substrate temperature during thin-film deposition. As a result no mention of any pressure effect could be found in these papers. However, both resistance thermometers and thermocouple type devices have been used in such work and either one is generally suitable for application in the present work.

CHAPTER 2

2.1 DEFINITION OF THE PROBLEM

The process of elastohydrodynamic lubrication depends on several interdependent phenomena that occur within a narrow zone of contact between two machine elements. In instrumenting such a machine element, in order to study the various properties of the EHL contact, one must be careful not to disturb any of the factors which eventually give rise to the EHL contact condition. The severity of the problem can be better understood if physical dimensions are considered for a typical EHL contact as shown by Dowson (85).

The width of the contact zone generally lies between one quarter of a millimeter to a millimeter and the pressure within that zone changes from atmospheric to a value which could be of the order of a few GN/m^2. The oil film that separates the machine elements within this zone could be as little as a fraction of a micrometer thick, while the surface speed of these machine elements could be as high as 20 to 30 m/sec. The transit time for the lubricant passing through such a contact can thus be as small as 10^{-4} or 10^{-5} sec. In other words the lubricant enters a typical contact close to atmospheric pressure, is subjected to a maximum pressure in the range of GN/m^2 as it traverses a passage one thousand times longer than its height and is ejected into atmosphere in a total time of 10^{-4} or 10^{-5} sec. While passing through the contact the viscosity of the oil is increased dramatically by the high pressure. This, coupled with the temperature variation and the elastic deformation gives rise to

complicated pressure and deformation profiles. The temperature variation within the contact zone is also complicated by effects such as inlet shear heating, shear heating within the contact, compressional heating and conduction and convection of heat.

A set of ground rules has been put forward by Kannel and Dow (69) regarding the instrumentation of such a machine element to achieve successful monitoring of the EHL contact conditions.

(i) The transducer should in no way perturb the hydrodynamic action of the fluid in the contact zone between the rolling elements. Practically, however, it should be sufficient to specify that the transducer does not disturb the hydrodynamics any more than would a normal irregularity of the surfaces of the rolling elements.

(ii) The transducer must not perturb the stress patterns on the surface of the rolling elements since the perturbation would, in turn, affect the hydrodynamic pressure.

(iii) The transducer must be capable of detecting transient pressures of extremely large magnitude.

(iv) The transducer must be capable of detecting pressures over increments of area which are small in comparison with the area of the contact region.

These four criteria can be met by thin-film transducers fabricated directly on to the machine elements. Satisfying the first two criteria depends on the overall structure of the transducer, while the choice of transducer material and the technique of its deposition is reflected in the last two criteria.

2.2 Simulation of the EHL Contact

In this project the EHL contact condition has been simulated in a disc machine where two cylindrical discs of 8.3 cm in diameter were loaded one against the other to give rise to a nominal line

contact. The width of the disc surfaces were 2.54 cm but one of the discs were chamfered on two sides to produce a track of either 6 mm or 8 mm wide at the centre. The transducers were fabricated on the disc without the chamfering.

2.3 Structure of Thin-film Transducers

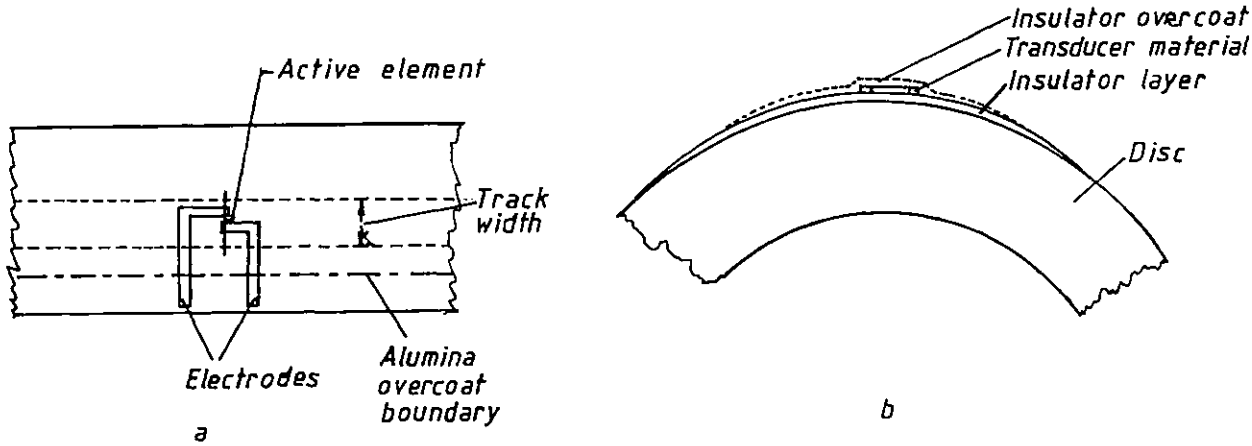

Figure 2.1 - Structure of Thin-film Pressure Transducer: (a) Top View, (b) Side View.

The structure of the thin-film transducers comprises a layer of insulator material, deposited by a vacuum deposition technique, on to the surface of the disc to isolate the transducer electrically from the conducting metal of the disc, as shown in Fig. 2.1b. The transducer material is then deposited through the appropriate mask on to the insulator film. A second layer of insulating material may be deposited on top of the transducer pattern to prevent the transducer from touching the mating disc when operating with thin oil films.

The pattern of the transducer itself is shown in Fig. 2.1a . The fine line at the centre is the active element of the device, which is connected to the external circuitry through the two broader electrode patterns. This pattern was used for the pressure and resistive temperature transducers; the patterns for

other types of devices vary considerably and are described later.

In the overall structure of the transducer shown in Fig. 2.1 , the maximum thickness of the deposited films occurs in the transducer region and the thickness generally varies from 1 to 1.5 μm. Of this thickness the major part comes from the first layer of insulator, which is about 1 μm in thickness, the transducer pattern contributes about 0.1 μm or less and the final insulator overcoating is generally 0.5 μm thick. To prevent this 1.6 μm structure from disrupting the formation of the oil film in the contact, the two insulating layers are deposited over a third of the circumfrence of the disc having maximum deposition at the crown of the disc, where the sensors are positioned and then gradually falling off to zero thickness at the two sides. This leaves a hump of about 0.1 μm or less height at the transducer pattern, which is almost equal to the roughness of the surface and hence it is supposed that it would not disturb the formation of the oil film.

The effect of the extra layers of material on the deformation profile and hence the stress pattern is rather difficult to predict. However, as the thickness of the overall structure is only 1.6 μm compared to the typical Hertzian contact width of around 500 μm over which the deformation takes place, it was assumed that this very thin extra layer does not change the steel to steel contact properties outstandingly.

Similarly, this extra layer of alumina on the steel would also affect the temperature distribution as the conduction of heat from the contact region would be different

from the steel to steel contact. Thus the temperature sensor fabricated on the alumina would encounter a higher temperature. However, alumina has one of the highest thermal conductivity coefficients amongst the ceramic materials with a value about half that of steel (K. Thermal conductivity, steel, 65 ; alumina, 30 watts/meter. Kelvin). Thus, considering the very thin layer of alumina used one would expect it to have a negligible effect on temperature distribution.

2.4 Operating Principles of the Transducers

In this project three types of thin-film transducers were used; (a) resistive type pressure and temperature transducers, (b) thermoelelectric emf type temperature transducers and (c) capacitive type film thickness monitor.

2.4.1 Resistive Type Pressure Transducer

The active element of the pressure transducer may be any suitable piezo-electric or piezo-resistive material. However, it is also desired that the material be insensitive to surface stress, temperature and, as far as possible, dimensional changes. These stringent demands have led to the use of one alloy, manganin, to the exclusion of any other material, in tribological applications.

Manganin is an alloy of copper (84%), manganese (12%) and nickel (4%). It has an extremely low temperature co-efficient of resistance and a linear pressure co-efficient over a wide range of pressure. Bulk manganin is widely used as sensing material in pressure vessels, following the pioneering work of Bridgeman (77). The piezo-resistive property of manganin is used in the thin-film pressure transducer. The change of resistance of the active element made

of manganin in Fig. 2.2a is monitored while it passes through the high pressure contact zone. The change of resistance is proportional to the change of pressure applied on the active element. To determine the calibration factor the area under the pressure profile generated by the device in passing through the contact is equated to the known load applied on the disc. Thus separate calibration is not required. Hamilton and Moore (75) showed, by dropping small steel balls on the thin-film and monitoring its response, that the transient response of the thin-film manganin to pressure is excellent.

2.4.2 Resistive Type Temperature Transducer

In the lubricated contact pressures are high and temperature rises are relatively small. This necessitates the use of material with a very low pressure co-efficient of resistance and a high temperature coefficient of resistance. Titanium has the lowest pressure coefficient of resistivity amongst the metals which have a reasonable temperature coefficient of resistance, which makes it most suitable for resistive temperature transducers.

Unlike the pressure transducer, however, the resistive temperature transducer has to be separately calibrated beforehand. Otherwise the operating method for both these devices is the same.

2.4.3 Thermoelectric EMF Method of Measuring Temperature

Bridgeman (77) with his hydrostatic high pressure work has shown that the effect of pressure on the thermoelectric voltage generated, when the junction of two dissimilar materials is heated, is extremely low. This, coupled with the fact that a very good linear relation exists between the

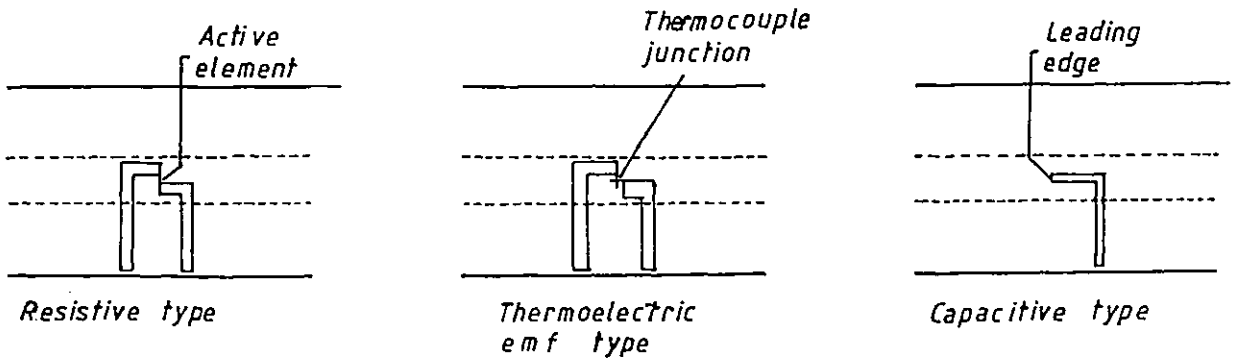

Fig. 2.2 Configurations of various transducers.

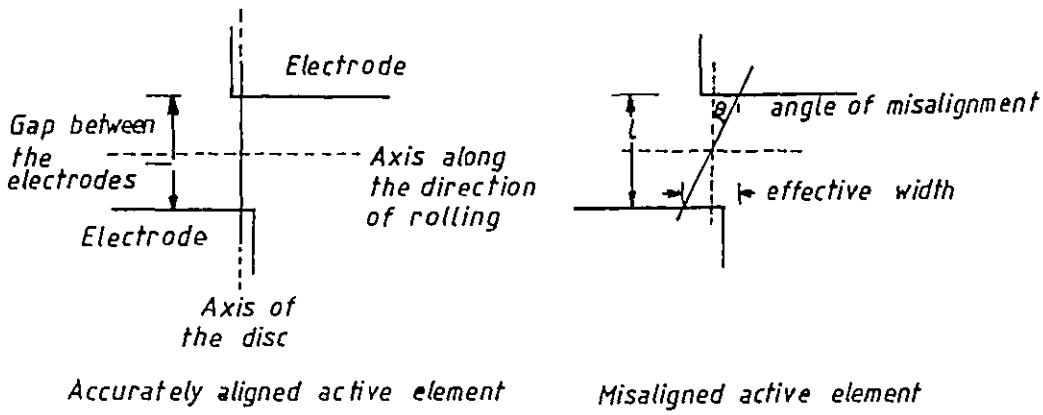

Fig. 2.3 Effect of alignment of the active element on the effective width of the transducer.

thermocouple voltage and temperature, makes the thin-film thermocouple a good alternative for the resistive temperature transducers.

Any of the well-known combinations of materials can be used for fabricating the thin-film thermocouples. In this project chromel (alloy of chromium and nickel) and alumel (alloy of aluminium and nickel) was chosen mainly because of their very good adhesion in thin-film form. The potential difference that develops across the minute junction formed by the overlap of the two materials, as shown in Fig.2.2b , is monitored when the junction enters into the EHD contact zone.

2.4.4 Capacitive Type Film Thickness Monitor

There are two capacitive methods of monitoring the oil film thickness and both of which were developed by Crook (64,49). The most widely used method, as discussed in the literature survey section, could only predict the central film thickness, with the assumptions that the shape of the contact zone is Hertzian and all the capacitance measured between the discs originates from the contact zone.

The second method measures the rate of change of capacitance between the leading edge of an electrode, shown in Fig. 2.2c , and the opposite disc, as the leading edge of the electrode enters into the contact zone. This method of film thickness monitoring provides not only the minimum and central film thickness but also the whole deformation profile within the contact. Crook (64) as well as Hamilton and Moore (75) used this technique with the glass-disc under limited loading conditions. In this project the method has been applied to steel discs under much higher loads.

Any high conductivity material is good enough to form the thin-film electrode pattern required for this method. A simple charging circuit is necessary to charge up the capacitor formed by the electrode and the opposing disc and the charging current is monitored.

The transient response of this device depends on the external circuitry and can be made to be very fast.

2.5 Resolving Power of the Thin-Film Transducers

The necessity for very fine devices to study the minute EHL contact zone becomes apparent when the secondary pressure peak in the theoretical pressure profile (such as in Fig. 1.2b) of the contact zone is considered. The secondary pressure peak zone under most operating conditions occupies a very small part of the contact zone. Resolution of the peak to any significant extent requires devices which are smaller in width than the peak itself. A wider device would simply average out the peak.

In the case of pressure and temperature transducers the resolving power depends on the effective width of the active element. The effective width in turn depends on two factors: (a) the width of the element in the direction of rolling and (b) the accuracy of alignment of the active element with the axis of the disc. Fig. 2.3a shows a device with a properly aligned active element in which case the effective width of the device is equal to the width of the active element itself. Fig. 2.3b shows the active element misaligned by an angle of θ degrees, which produces an effective width, w_f, given by $w_g = w_f + l \tan \theta$, where w is the actual width of the device and l is the gap between the two electrodes.

Thus an active element of 0.5 mm long and 10 μm wide would have an effective width of 19 μm for 1^{o} of misalignment. Hence to improve the resolving power one must align the active element very carefully and keep the length of the element as short as possible.

The nature of the distortions produced by the electrode in the capacitive method of monitoring the film thickness profile is much more complicated. However, to avoid such distortions one must make the leading edge of the electrode a straight line and as nearly aligned to the axis of the disc as possible and the width of the electrode should be kept equal throughout the leading side of the electrode.

In Appendix I, a more detailed analysis of the interpretation of the profiles obtained by this method is given, which shows that even with the slightly simplified interpretation method the minimum film thickness obtained at $\frac{dV}{dt} = 0$, where V is the voltage across monitoring resistor, is accurate.

2.6 Disadvantages of the Thin-Film Transducers

The major disadvantage in using these devices is their limited life under severe operating conditions, such as heavy sliding, etc. The improvement of adhesion between the various layers of thin film in fabricating a device was one of the major problems in this project. The change in the value of the pressure and temperature coefficients for the resistive pressure and temperature transducers from device to device was another difficulty and, because of it, each device had to be calibrated before use.

2.7 Factors Affecting Film Adhesion

The adhesion of the deposited thin-film was a major concern in fabricating a device, hence it is of importance to

know the factors affecting the property. Studying the growth of thin-films in the transmission electron microscope, it was found that the initial growth of a thin-film generally occurs from individual nucleation sites, forming islands which gradually increase in size with further deposition to form a continuous film. This type of growth requires that the incident atoms which are absorbed on the surface are able to move freely on the surface to join existing nuclei. As a result the adhesion of the film depsoited depends mainly on the adhesion at the initial nucleation sites and on the number of the nucleation sites. Generally materials with very high melting points tend to form a larger number of nucleation sites on a given substrate and, as a result, show better adhesion than the materials with lower melting point. It is concluded that the higher melting point material has a higher binding force to the substrate, decreasing the surface mobility of the evaporated atoms and increasing the number of initial nuclei, with a resultant improvement in film adhesion.

Adhesion is closely related to the cleanliness of the substrate upon which the evaporated film is deposited. If the film is grown on the contaminated top layer of the substrate, the adhesion of the contaminated layer, which is generally poor, would basically decide the adhesion of the film. Inspite of rigorous cleaning, the substrate still brings some form of a surface layer of contaminants into the vacuum system, since the cleaning procedures performed outside the vacuum system are unable to eliminate the last monomolecular layer of adsorbed gases. Heating the substrate to a temperature of around 400^{o}C under vacuum is one of the effective ways of removing the last layer of adsorbed gases, but this

method cannot remove the hydrocarbon contamination completely. Plasma etching the top layers of the substrate produces much better results. Contamination of the deposited film can also occur due to residual gases or vapour in the vacuum system, gas released from the evaporant and the heater material itself. This can be reduced by degassing the chamber and the materials inside by baking them at a higher temperature and by depositing materials at a higher rate. Higher rates of deposition are particularly suitable for active materials, since they act as getters during deposition,

Thin-films deposited by any method show some internal stress which can be cpmpressive or tensile in nature and if the stress is too high it can force the film off the substrate. These intrinsic stresses are often a function of filn thickness and sometimes of deposition rate. Internal stress can also arise when the thermal expansion co-efficient of the substrate is different from the film and deposition is done at a temperature different from ambient.

2.8 Methods of Thin-film Deposition

There are various methods of depositing thin-films of different materials, of which two methods under high vacuum are widely used. They are vacuum evaporation and sputtering. Evaporated films result from heating a material in a vacuum enclosure to such a temperature that large numbers of atoms or molecules leave the surface of the material and deposit on to the substrate. Because of the low background pressure few of the evaporated molecules suffer collisions with the residual gas molecules and the majority travel in straight lines to the substrate. Hence it is a line of sight process. Sputtering entails the bombardment of a target with energetic

particles, usually positive gas ions, which cause some surface atoms to be ejected from the target. These ejected atoms deposit onto any surface which may be close to the target. The sputtering process relies on momentum transfer and takes place under higher pressures than evaporation. As a result ejected target materials can go through a number of collisions and approach the substrate from a wide range of angles. Thin-films of most of the materials could be deposited either by evaporation or by sputtering but the physical properties of the films deposited by the two methods differ. A short discussion of the two methods follows.

2.8.1 Evaporation

A very simple evaporation system is shown in Fig.2.4 This is adequate for slow evaporation of most of the elements but if alloys are evaporated in this set-up, fractionation may occur due to the differing vapour pressures of the constituent elements. For example, consider the case of manganin, which is an alloy of copper, nickel and manganese and the most important material for pressure transducers. With the help of the vapour pressure vs. temperature curves it is possible to determine the evaporation rate of individual components of an alloy using the following equation

$$G_A = 0.058 p_A' \sqrt{\frac{M_A}{T}} \text{ grams/cm}^2 \text{ sec.}$$

where p_A' is that part of the vapour pressure of the alloy which is contributed by component A, and M_A is the molecular weight of A. Again $p_A' = X_A p_A$ where X_A is the mole fraction of A and p_A is the vapour pressure of pure substance A. Hence $G_A = 0.058\ X_A p_A \sqrt{\frac{M_A}{T}}$. With 12% manganese,

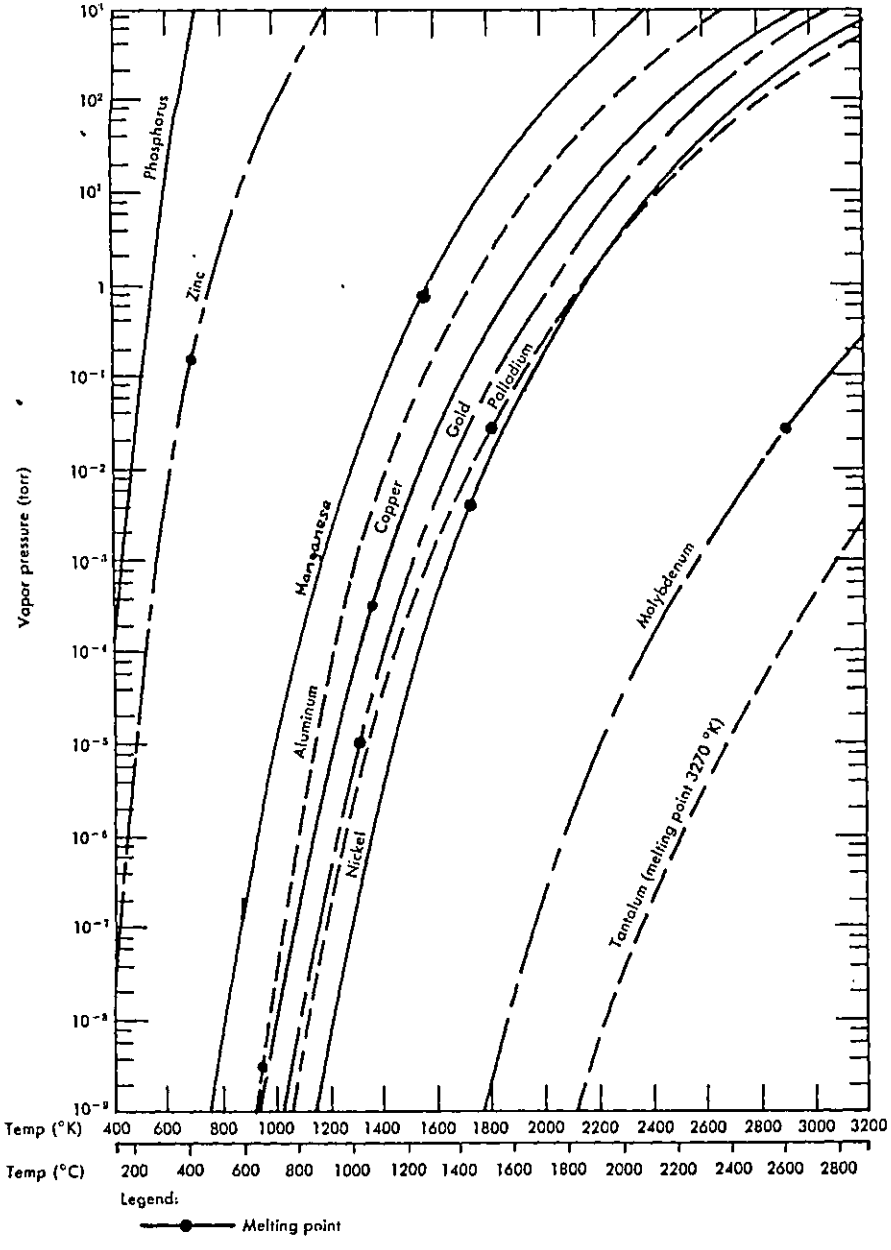

Fig. 2.5 Vapour pressure against temperature plots for various elements.

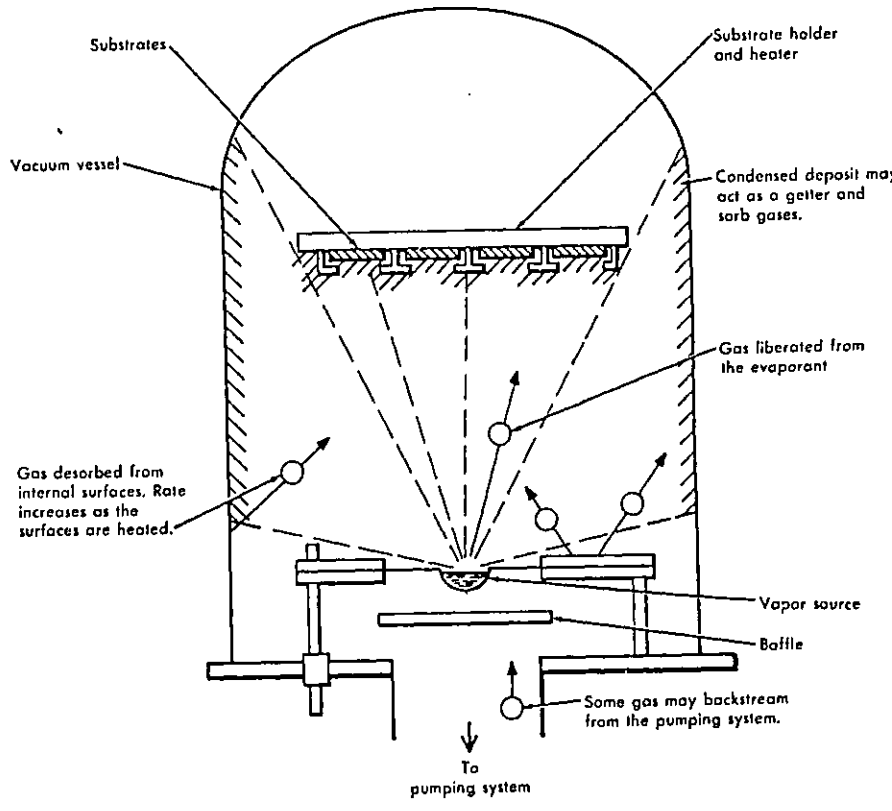

Fig. 2.4 A simple evaporation apparatus.

4% nickel and the rest copper, the mole fraction of manganese is given by

$$X_{Mn} = \frac{W_{Mn}/M_{Mn}}{(W_{Mn}/M_{mn}) + (W_{Ni}/M_{Ni}) + (W_{Cr}/M_{Cr})} = 0.1358$$

from Figure 2.5 the vapour pressures of pure manganese, copper and nickel are 20, 0.4 and 0.015 torr respectively at 1500°C. Hence $\frac{G_{Mn}}{G_{Cr}} = 7.68$. Similarly $G_{Cr}/G_{Ni} = 538.29$. This means manganese would evaporate initially 7,68 times faster than copper and copper would evaporate 538.29 times faster than nickel from the alloy, with slow evaporation at 1500°C. Instead of a thin film of manganin with proper composition, one might observe three distinct layers of manganese, copper and nickel.

The composition of evaporated alloy films may be controlled by several techniques, of which the most widely used method is flash evaporation, in which finely divided particles of the alloy are dropped onto a surface so hot that the particles evaporate almost instantaneously.

The alloy films in this project were all prepared by flash evaporation. The alloys were available in the form of fine wires which were cut into small pieces, thus avoiding problems of spitting. Spitting is a major problem with flash evaporation, and is caused by the large gas content of very finely divided particles. The rapid release of this gas produces a high background pressure which then forces solid or molten particles to leave the source and strike the substrate. Although fractionation does occur during the evaporation of

each piece of wire, a slow but steady feeding of wire pieces to the hot boat leaves different pieces at different stages of evaporation at any time and the total evaporation of all the pieces results in a homogenious deposit.

2.8.2 Sputtering

This method of thin-film deposition relies on the bombardment of a 'target' of the material to be deposited by high energy ion or *nutral* gas molecules derived from a plasma of ionized, inert gas in the vacuum chamber.

The energies of the molecules ejected from the target are generally much higher than those of evaporated molecules and, as a result, the thin-films deposited by sputtering show much better adhesion than the evaporated films. Another advantage of sputtering is its capability of depositing any material, including the refractory metals and their compounds, at a reasonable rate. Control of the deposition parameters is somewhat more tenuous than in the case of evaporation, due to higher complexity of conditions in sputtering, but once the system is calibrated it is relatively easy to obtain reproducible films by this method. The process of sputtering generally requires a vacuum of 10^{-3} torr but to obtain a film of good purity it is necessary to evacuate the chamber to a much lower pressure and then backfill the chamber with the pure gas with which the sputtering is carried out.

Fig. 2.6 shows a simple sputtering apparatus where the target (cathode) is surrounded by a cathode shield. The electrical power is connected to the target and produces a voltage between it and an earthed counter electrode (the substrate assembly). This voltage causes ionization of the low pressure argon in the chamber and sets up the required plasma.

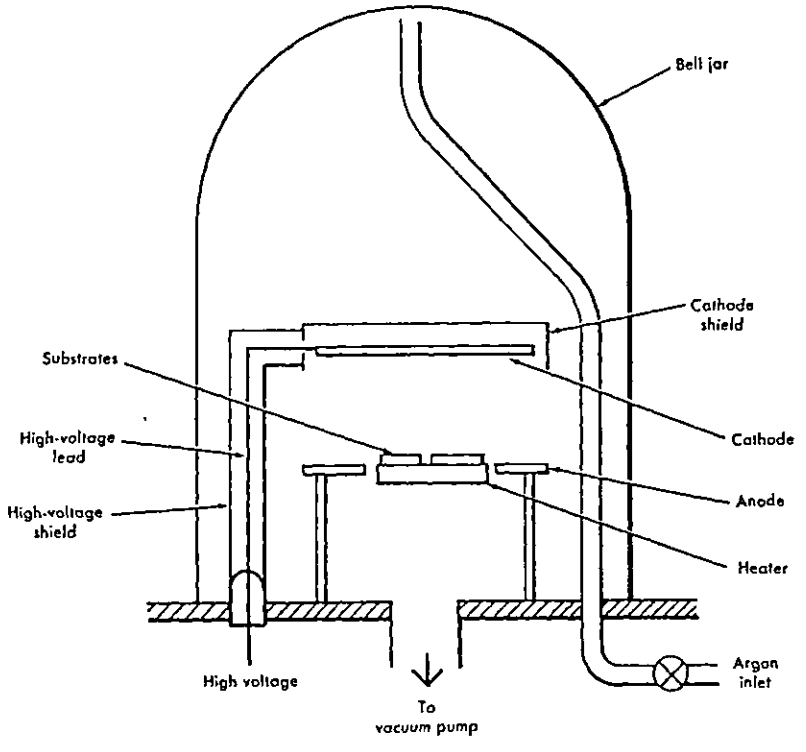

Fig. 2.6 A simple sputtering apparatus.

The shield around the target is within the Crooke's dark space of the plasma and is, therefore, not subjected to ion bombardment. It therefore serves to protect the target assembly from being sputtered leaving only the target as a source of sputtered atoms. This simple system is good enough for d.c. sputtering with a conducting metal target.

2.8.3 R.F. Sputtering

Insulators as well as metals may be sputtered but a simple substitution of an insulator for the metal target in a conventional d.c. sputtering system does not work because a layer of surface charge of positive ions build up on the surface of the insulator, which then prevents any further ion bombardment.

Radio-frequency sputtering overcomes this problem of charge build-up with the insulating material. This process relies on the fact that the mobility of the electrons is much higher than that of ions. An a.c. potential applied to an electrode in the plasma draws much larger electron than ion current and acts, therefore, like a rectifier. If one arranges a large capacitor in series with a metal electrode in the plasma and applies an a.c. voltage of high frequency, the capacitor will charge negatively, due to the excess of electron current, and will produce a negative bias on the electrode. This reduces the electron current until it equals the ion current and a steady bias results on the electrode.

To enhance the r.f. discharge, it is useful to have a magnetic field parallel to the electric field in the case of the r.f. sputtering.

Efficient plasma generation by this process requires

frequencies above 10 MHz and usually r.f. systems operate at the industrial frequency of 13.56 MHz.

In this project the ceramic insulating materials as well as some metals and alloys were deposited using this technique.

CHAPTER 3

FABRICATION OF THIN-FILM TRANSDUCERS

3.1 INTRODUCTION

Although the main objective of this project was to fabricate thin-film devices on steel discs, a major part of the development work was carried on glass slides and metal foils. Their flat smooth surface and their small size make them convenient to handle in high vacuum systems. They also permit simple methods for studying various properties of the thin-films deposited. Thus most of the work done in choosing materials and techniques of deposition for the different layers of a device was carried out on glass slides and metal foils before they were transferred to the steel disc. Equipment had therefor to be built which could handle all three types of substrate.

In this chapter the general procedure followed for the fabrication of a thin-film transducer in the vacuum system is discussed along with the description of the system itself. The important aspects of the fabrication techniques are then discussed in greater detail.

3.2 Vacuum Equipment

Two vacuum systems were used at the various stages in the development of the thin-film transducers. One of

them can be called a "general purpose system" while the other one was purpose built. From the outset the special purpose vacuum system had been developed to handle only the metal discs and to fabricate transducers with as few vacuum breaks as possible. It was found inconvenient to use this arrangement for the general purpose of depositing thin-films of different materials by evaporation on glass slides and metal foils to study their properties. The R.F. sputtering facility, however, was only available in the special purpose system, hence all depositions of ceramic materials by sputtering had to be carried out in this system. In the case of metal foils this was done by wrapping the foil around a disc so that the combination could be sputter coated. The metal foil was then separated and cut into small pieces to be used as specimens.

3.3 General Purpose System

Both the vacuum systems had similar vacuum generating equipment, the chamber to be evacuated being placed on a bottom plate mounted on an oil diffusion pump which was backed by a rotary pump. This general purpose system had a glass bell jar 30 cm in diameter as the chamber and the bottom plate was available for the various mechanical and electrical feed throughs. Among the permanent facilities available in this system was a high current, controllable supply for the evaporation boat the temperature of which was determined by the current supplied. The boat was

clamped between two extended stainless steel bars, rigidly bolted to the high current feed-throughs. A stand was used as the substrate holder which could hold the mask and the substrate directly above the boat, at a distance of about 10 cm from the boat.

For flash evaporation in this system, a simple hopper was made by bending a piece of molybdenum sheet, 8cm long and 1cm wide, through its longer axis by 90^{o}. One end of the hopper was bolted to the top end of a stainless steel studding, rigidly mounted on the base plate. The hopper was slightly bent in such a way that the floating end of it remained about 1cm above the centre of the boat. Because of the inclination, granules placed on the hopper would move towards the boat when vibrated by a striker. A rotary feed through, at a distance of 5cm from the hopper mount, was used as the striker by fixing a stainless steel rod at a right angle to the feed through.

In addition to the high current feed throughs, the system had a low current and a four contact signal carrying feed throughs. The low current feed through was used for the substrate heating element while the signal feed throughs were generally used for thermocouple connections.

This system could achieve a vacuum of better than 10^{-5} torr in the chamber. Its major disadvantage was the absence of a liquid nitrogen cold trap, but it was nevertheless, adequate for the initial work.

3.4 Special Purpose System

The necessity for this system was realized early in the development work, when it was found that for best adhesion between the different thin-film layers, they must be deposited with the least number of vacuum breaks. This meant that the substrate had to be moved from station to station with high precision, so that it could be coated with different materials through appropriate masks and still register properly to form a useful transducer. The final configuration was reached through several changes and modifications. With the final arrangement it was possible to sputter etch the substrate, sputter deposit the first insulator layer, flash or slow evaporate three times in succession through three different masks with acceptable registation between them and finally overcoat the whole structure with another layer of ceramic material, without allowing air into the system.

The system consisted of an Edward 4" diffusion pump stack, backed by a 11 m^3/hr rotary pump, with a cold trap mounted directly on top of the diffusion pump and a baffle valve. The 45cm Diameter bottom and top plates were made of duralumin. The chamber used was a 30cm diameter glass cylinder 45cm in length. The top plate supported the 12.5cm target assembly, which was specially designed for the 8.3cm dia. disc specimen. The top plate also supported the shutter assembly as well as the

(c)

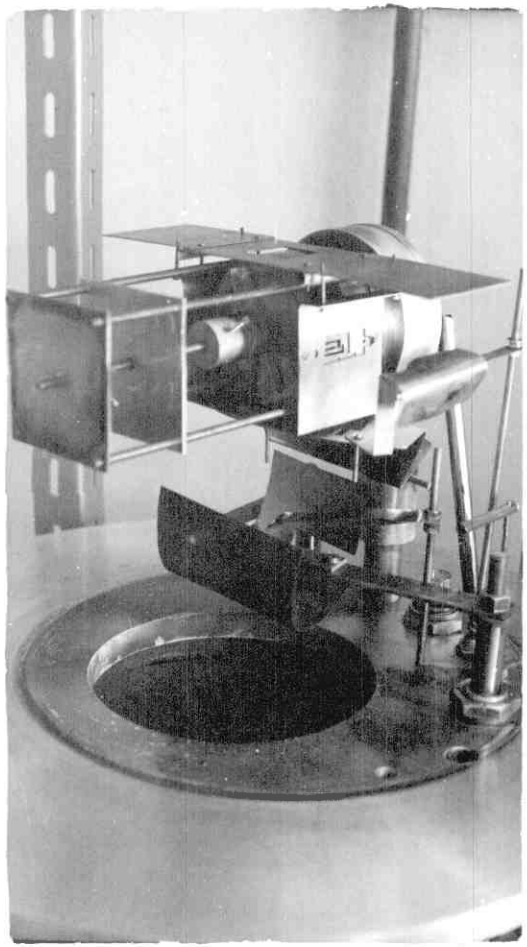

(b)

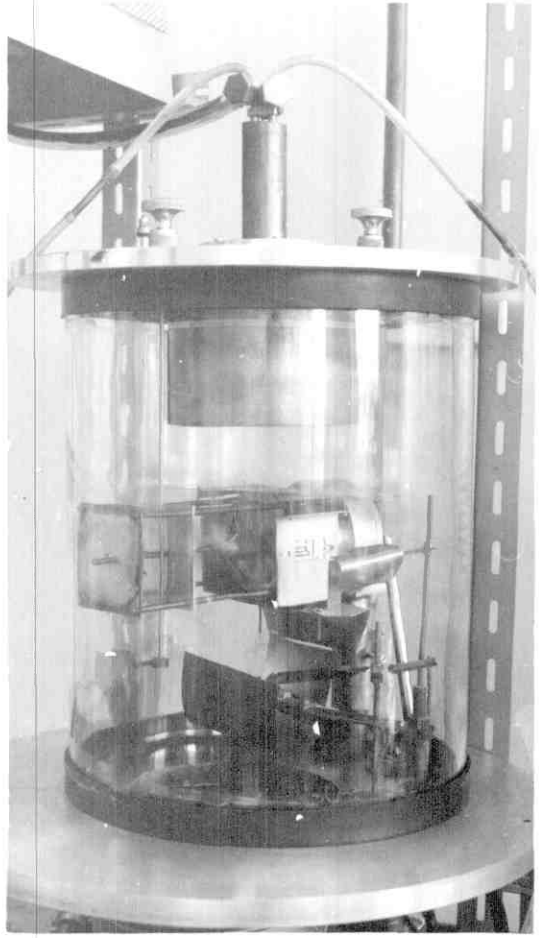

(a)

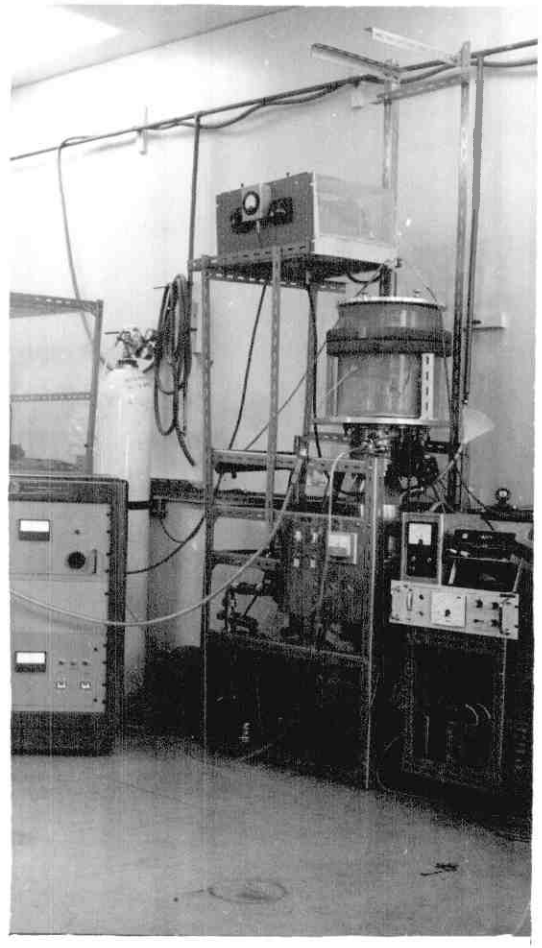

Fig. 3.1 Overall view of vacuum system used for fabrication of thin film devices (a); vacuum chamber (b); evaporation apparatus in vacuum chamber (c).

mechanical arm which was used for rotating the disc under vacuum from the outside.

The biased platform, designed to hold the disc rigidly in its place and sputter clean it, was mounted through the bottom platform along with the mask holders, the high current feed throughs required for the three boats, and the vertical posts to hold the hoppers and the strikers. An iorization gauge and an argon gas leak valve were also mounted on the bottom plate.

3.5 Substrate Assembly

Figure 3.1c shows the arrangement of the boats and the mask assembly surrounding the biased platform. The biased platform basically consisted of a cylindrical water chamber which was electrically isolated from its back-plate and the mounting with a circular PTFE disc which was water and vacuum sealed with 'O' rings as shown in Fig.3.2. To prevent sputtering from the exposed parts of the water chamber, a cylindrical earth shield was attached to the back-plate by four stainless steel studs. These four studs also provided support for the disc rotating mechanism. A gap of 2mm was maintained between the water chamber and the earth shield throughout, which was much less than the dark space length at the sputtering pressure of 5×10^{-3} torr generally used. The outside diameter of the water chamber was made about 25μm

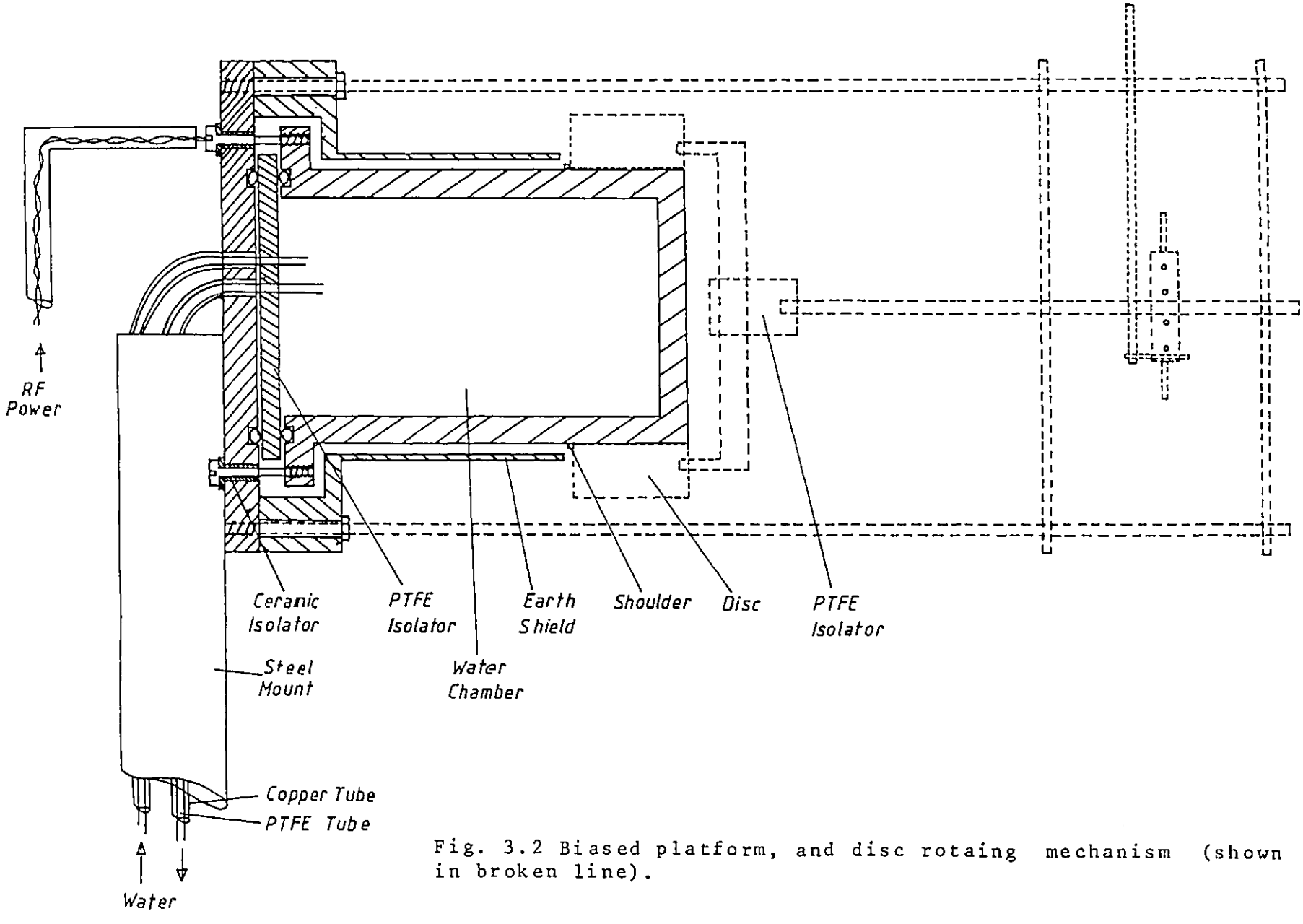

Fig. 3.2 Biased platform, and disc rotaing mechanism (shown in broken line).

smaller than the inside diameter of the disc for easy movement. The disc was mounted on the exposed end of the water chamber and a 1mm thick shoulder built on the water chamber kept the disc firmly aligned to the water chamber at all times. Six screws rigidly held the water chamber to the back-plate and all of them were electrically insulated from the back-plate by ceramic insulators. PTFE tubes were used to feed the cooling water to the chamber. These tubes passed through two vacuum sealed copper tubes which were in turn placed inside a 2.54cm outside dia. mounting tube. PTFE tubes were necessary to isolate the cooling water from the supply for some distance as electrical conduction can occur at the high voltage used in R.F. sputtering.

A simple mechanism was devised to rotate the disc in contact with the water chamber as shown by the broken lines in Fig.3.2. The rotating wheel with the centre shaft was supported between two parallel plates which were in turn mounted on the four extended studdings. The disc was connected to the centre shaft of the rotating wheel through a 1mm thick stainless steel plate, which had two extended fingers pressed inside two slots in the disc, and a cylindrical block of PTFE, which joined the plate to the shaft as well as providing electrical insulation between disc and the rotating mechanism. The mechanism was rotated by a linear motion feed-through which was anchored to the wheel via a connecting rod.

3.6 Mask Holder Assembly

The fabrication of transducers of small width and accurate registration and alignment with the electrode pattern requires a sturdy mask holder assembly. There should be no detectable vibration in this assembly either from the rotary pump or from the hopper. The complete assembly was supported by two steel studs solidly mounted on the bottom plate. A 17cm by 15cm stainless steel plate was used as the platform, bolted to the studding and sitting just below the substrate assembly. This platform carried the vertical evaporation mask at the centre while the other two mask holders were mounted on this platform on two sides of the substrate assembly. The position of these mask holders on the platform could be adjusted for proper alignment of the masks with respect to the disc. The complete mask holder assembly could be moved up or down by changing the position of the platform on the two studdings. The masks themselves could be clamped in various positions to the mask holders. Once the masks were positioned properly and clamped the whole structure was sufficiently immune to vibration. To facilitate the alignment of the masks with respect to the disc, both the mask and the mask holder had precise lines passing through the centre of them, which could be aligned with a line on the front edge of the disc.

3.7 The Evaporation Boat Assembly

The three evaporation boats used in the system were all inter-connected and powered from two high current feed throughs, the third being connected to electrical earth. Two stepdown power transformers were used, one of them through a switch to supply power to either of the two horizontal evaporation boats. Two variacs of 7A and 10A ratings were used to control the current flow through the boats.

For flash evaporation, initially, molybdenum were tried as boat material but they were found to form an alloy with nickel, present in manganin, giving rise to a porous material. Tungsten foil was found to be satisfactory. To avoid shadowing effects in horizontal evaporation, the height of the boats was kept exactly at the same height as the finest part of the mask.

For evaporation of single elements like copper, titanium and chromium,multi-stranded tungsten spirals were used as filament heaters.

3.8 Sputtering Facility

Figure 3.3 shows a cross-sectional view of the 12.5cm diameter target assembly used in this system. It consisted of a disc shaped water chamber, having two stainless steel water tubes welded to one face and a tapped hole at the centre of the opposite face for mounting

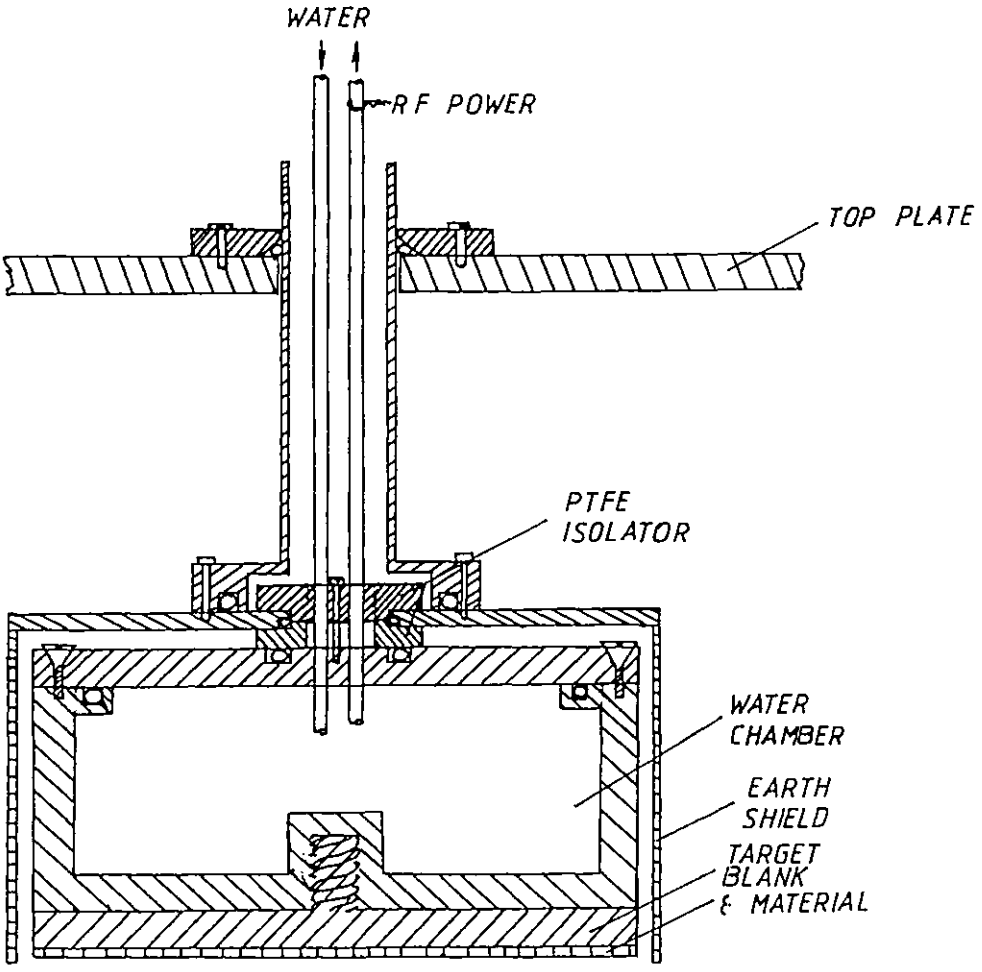

Fig. 3.3 R.F. sputtering target assembly.

the target. The water chamber was electrically isolated from the rest of the assembly by two glass spacers and power was supplied to the water chamber and the target through the water tubes. All the exposed parts of this chamber, except the target face, were enclosed within an earth shield. A copper tube was mounted on the earth shield, surrounding the water tubes, and acted as the support for the complete assembly. The height of the target assembly could be adjusted by a clamp which held the copper tube and the rest of the assembly.

The 13.65 MH_z R.F. power was generated by a commercial unit which could provide upto 1.25 kW.

3.9 General Procedure Followed For Vacuum Deposition Of A Device

Great care was necessary in preparing this special purpose system for deposition. A polished and properly cleaned disc was mounted on the biased platform with a thin layer of sllicon grease to aid the conduction of heat. With the plane side of the disc pressed against the shoulder ring,the disc rotating mechanism was mounted on the substrate holder assemply. The whole mechanism was checked for easy rotation of the disc.

Because of the electrical contact arrangement in the disc machine, only one quarter of the disc on either side of the two slots were available for the fabrication of a device. A length of about 2cm within these two available zones was chosen after a close check for any blemish or scratches which might give rise to a defective device. The chosen area was made to face upwards for sputter deposition. At this point an alignment mark was put on the disc using a small T-square. It consisted of two short, fine lines on the two edges of the disc surface and a broader mark on the front face of the disc using a permanent ink felt pen. The active element of the device was to be deposited along this alignment mark.

Before the masks could be mounted on the mask holders, it was necessary to decide which material would be evaporated from the various boats. Magnetic materials like iron or alumel could only be deposited from the

central evaporating boat, because of the surrounding electromagnet which attracts the loose magnetic material to the centre of the chamber. Furthermore the central boat which evaporates vertically upward was found to give the best pattern definition, hence it was most suitable for the deposition of the active element. For a resistive type pressure and temperature transducer, where the electrodes and the active elements were deposited separately, the active element was deposited from the central boat while one of the horizontal evaporation boats was used for the electrode deposition. In the case of the thin-film thermocouples, alumel was flash evaporated from the central boat and chromel from one of the horizontal boats.

During the deposition of titanium for the resistive temperature transducer it was noticed that, even at low (5×10^{-6} torr) chamber pressure, the deposited film showed very high resistivity compared to its bulk value, which suggested that part of the titanium was being oxidised. To overcome this problem, one additional tungsten filament, with titanium wrapped around it, was used as a getter. The titanium from the additional filament was evaporated, in a remote part of the chamber, immediately before the titanium on the main filament was heated for evaporation. This additional evaporation brought the pressure down to 7×10^{-7} torr, and the deposited film of titanium showed much lower resistivity.

All the masks, except the one for the active element, were mounted slightly away from the disc, to prevent the masks from damaging the previously deposited film layers, during the rotation of the disc. The mask for the actual transducer, however, was mounted generally with a slight pressure between the disc and the mask, to avoid undercutting and loss of definition. The distance between the central boat and the mask was maintained at 10cm while the two side boats were placed at a distance of about 7cm. each from their respective masks.

The amount of material needed to deposit a certain thickness of a particular film, either by slow or flash evaporation, were determined in advance, in calibration runs. Those predetermined amounts of material were then placed in the hoppers or wrapped round the tungsten filament boats. Immediately before the glass jar was positioned on the bottom plate, the disc was blown gently with compressed air to remove any dust particles that might have settled during the setting-up operations. Once the glass jar had been positioned properly, the top plate was mounted on it immediatedly and its position was adjusted, so that the disc rotating mechanism was in proper alignment with the linear motion feed through. A distance of about 10cm was maintained between the target and the substrate. The system was then ready for evacuation.

It took about an hour for the pressure inside the chamber to drop down to below 10^{-5} torr provided there was

no appreciable leakage in the system. This initial vacuum was adequate for sputter etching the substrate and for the first deposition of the ceramic material. Before the sputter etching process was started, the cold trap was filled with liquid nitrogen, which reduced the pressure to below 5×10^{-5} torr. For sputter etching as well as sputtering, the pressure inside the chamber was raised to 5×10^{-3} torr, using 99% pure argon gas, whose flow in the chamber was controlled by the leak valve and the baffle valve. The cooling water was then circulated through the system. The R.F. power was, at first, connected to the biased platform while the rest of the system was earthed. The two halves of the shutter were positioned at a distance of 8cm from the substrate, in the space between the substrate and the target, to prevent sputtered material from the substrate being deposited on the target. A period of 5 minutes was required to heat up the filament in the R.F. power supply unit before the plate voltage could be turned on to provide the R.F. power. A bluish-violet argon plasma formed between the target and the substrate assembly which become intense with the electromagnet switched on and proper tuning of the matching network. The disc was sputter etched for 10 minutes at 200 watts and this produced a shiny surface on the disc. Then the R.F. power was switched from the substrate to the target assembly, the position of the shutter was lowered by 5 or 6cm. and the matching network was adjusted for maximum

power transfer to the target, while the substrate assembly was grounded. At a power of 400 watts, it took about an hour and a half to deposit the first layer of alumina of 5000Å thickness at the crown of the disc. The deposition rate was measured in calibration runs, whenever there was any major alteration to the system. Thickness of the insulating layer could also be estimated by counting the number of Newton's fringes which were formed by the gradual reduction of the film thickness to zero at the sides of the disc.

It was virtually impossible to deposit a perfectly insulating layer without pin holes in one deposition as the system was not located in a clean environment. To achieve proper insulation, the system was let up to air pressure at this stage and the surface of the freshly deposited alumina was blown with compressed air, with the belief that any dust would not settle in a previously contaminated spot. The chamber was again evacuated in order to deposit the second layer of alumina. Sputter etching was found not to have any effect on the adhesion of the second layer of alumina.

Once the full thickness of 1μm of alumina was deposited, sputtering was stopped and the shutter was replaced between the substrate and the target assembly to prevent any evaporated material from contaminating the target. The leak valve was closed and the baffle valve was fully opened to bring the pressure down to its lowest level.

Once the pressure was below 10^{-5} torr, the disc was rotated through 90^{o} to bring the alumina layer under the 1st horizontal evaporation mask, where the line on the front face of the disc was matched with the central line on the mask.

Generally the electrode pattern or one leg of the thin-film thermocouple was deposited at this horizontal evaporation station. For flash evaporation of manganin or chromel, the tungsten foil boat was preheated one minute at a temperature of 1500^{o}c to remove the absorbed gases. During this process the pressure inside the chamber generally increased to 5×10^{-5} torr, but once the pre-heating was completed the pressure gradually dropped back to around 5×10^{-6} torr. The temperature of the boat was then raised a second time to 1500^{o}c and was carefully monitored by an optical pyrometer. Once the complete boat had stabilised at this temperature, the granules were dropped slowly but steadily on the boat from the hopper by light taps on the hopper column by the striker. Granules generally evaporate immediately after landing on the boat but the wire pieces take about a second to melt and then evaporate. The evaporant was not allowed to gather on the boat, or it stopped the process of flash evaporation and damaged the boat. Severe spitting occurred if the temperature of the boat was allowed to rise much higher than 1500^{o}c. A period of 30 minutes was allowed for the freshly deposited material to cool down naturally as the

water cooling to the substrate assembly was turned off during the evaporation process. After this period the disc was rotated again for the second evaporation from the vertical evaporation boat. The process was continued until the device was ready, for the final over-coating of alumina.

This final over-coating of alumina was found to be a rather delicate process. The shutter used for masking part of the electrodes to keep them exposed for the electrical connection, had to be placed a fraction of a millimeter above the disc surface. Too large a gap led to undercutting of the shutter, making electrical connection impossible. If the shutter was placed on top of the fabricated device in partial contact with the electrode then oxidation occurred, particularly if the electrode material was manganin film. The shutter temperature could rise up to 300^{o}c during sputter deposition. Similar problems occurred with manganin films, when an attempt was made to deposit an overcoat of alumina by sputtering at 400 watts. This problem was overcome by depositing about 1000Å of alumina at a low sputtering rate at 200 watts power and the raising the power gradually to 400 watts. The overcoating thickness used, varied between 0.3 to 0.5μm. During the disc machine tests, however, it was found that within the operating range of the disc machine and with the two heigher viscosity oils used, no sporadic breakdown of the oil film occurred which can short out the transducer.

Because of this, the overcoating was used only under special circumstances.

The process of fabrication of the devices became relatively simpler, once the composite masks, made by a laser milling method, were introduced. The necessity for seperate active element and electrode deposition was removed and this made the two delicate horizontal evaporation facilities redundent. These two mask holders were then replaced by two heating element assemblies which could heat up the substrate quite uniformly. These two heaters were used to study the effect of various substrate temperatures on the adhesion of the evaporated films. Temperature was monitored by a thermocouple pressed against the disc and it was never allowed to rise above $150^{o}c$ during the actual fabrication of a device even though it was found, particularly in the case of thin film manganin, to show better adhesion at heigher substrate temperatures.

Once the fabrication of a device was complete, it was left under vacuum up to a period of about 3 hours before it was brought out for inspection. The device was then given a thorough check for different faults e.g.

i) continuity, to determine whether the active element had been deposited properly,

ii) electrical insulation from the substrate,

iii) adhesion, by scratch testing a small portion of the exposed electrode, and

iv) the alignment of the active element.

At the end of these tests, the properly deposited device was ready for annealing.

3.10 Annealing Set-Up for the Thin-Film

In fabricating a thin-film transducer of the resistive pressure or temperature type or thermocouple type, we have relied on the bulk properties of the materials used. During the process of deposition, however, a number of properties can change e.g. the composition of the alloy, oxidation, and several types od structural defects, which can alter the behaviour of the thin-film. The first two problems and their solutions have been discussed elsewhere. The third problem could be overcome to a large extent by mild heat treatment of the deposited films. In most cases the resistivity of the film decreases with heat treatment but in some cases it can increase because of oxidation and/ or agglomeration. To avoid oxidation, the process of annealing was carried out in an inert atmosphere.

A standard annealing set-up, using a tube furnace of 7cm diameter, with a 'Eurothem' controller was used for annealing films deposited on glass slides and metal foils. Before switching on the furnace, the pyrex tube, containing the specimens, and all the other connections were flushed with nitrogen to remove oxygen in the system. Annealing thin films of most of the materials was found satisfactory with this arrangement, except for the manganin films, which were found to oxidise very readily. Changing from nitrogen to normal grade

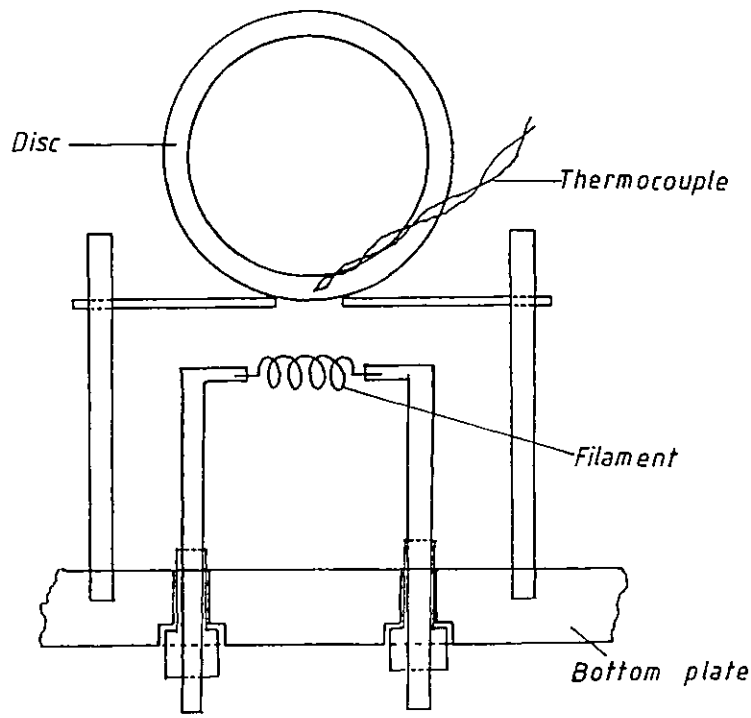

Fig. 3.4 Annealing apparatus in vacuum.

argon did not help. A second problem was faced with the steel discs, which were too large to fit inside any available tube furnaces. This made it necessary to build a second annealing system.

The second furnace was built inside the general prupose vacuum system, where a simple platform, with a 2.54cm square hole at the centre, could hold a glass slide or a disc rigidly using a simple clamping mechanism. The film on the glass slide or the fabricated device on the disc was positioned on the hole, facing downward. A heater assembly, made of tantalum wire, was mounted rigidly about 2cm below the platform, directly beneath the hole as shown in Fig.3.4 A chromel-alumel thermocouple was mounted either on the disc or the glass slide with a spot of silver paint, as near to the hole as possible, for monitoring the temperature at the film. In this set-up the process of annealing was carried out at a pressure below 10^{-5} torr. The problem of oxidation of the manganin film never occured.

Temperatures of around 250^{o}c over a period of 2 to 3 hours are generally required to anneal a metal film, but because of the problem of detempering of the steel disc, the annealing of the fabricated devices were carried out at a temperature of 150^{o}c for a period of up to 6 hours. It was found that even this extended period was not enough to produce the full annealing at the lower temperature. Comparisons were made by annealing films on glass slides at 250^{o}c and at 150^{o}c and then by determining their respective changes in resistivity from the pre-annealed state. A difference of up to 20% was noticed.

3.11 ELECTRICAL CONTACTS TO THE DEVICE

1.5cm long 50μm thick copper wires with a coating of burnished insulator were used for the immediate contact with the thin film electrodes. Initially a spot of silver loaded paint was used as a conducting glue to stick one end of the bared wire to the electrode. Although the adhesion of the dried paint was found to be quite good, a layer of epoxy resin was used to cover up the junction to prevent the lubricating oil from seeping in under the painted contact, as well as to provide heigher strength to the contact. Care was taken that the overall thickness of these contacts were smaller than the gap between two discs mounted in the disc machine. This was necessary to prevent any pressure build-up on these contacts when they passed through the contact zone during a test.

The flimsiness of the wire used for the initial contact necessitated the use of some form of anchoring of these wires, to prevent them from being torn away while mounting the disc in the disc machine or during high speed rotation through the test oil. The anchoring was provided by glueing 1m.m. thick plastic coated copper wires, on to the front face of the disc just below the devices. The ends of the fine wires coming from the electrodes were soldered to the thicker fixed wires. All the outside connection to the devices were made through these thick wires.

Although the silver painted contacts were found to be reasonably tough it was thought that slight zero level shifts noted in the pressure traces were caused by these contacts. Static pressure tests on these contacts were tried to assess whether any change was produced in resistance in the overall device or any voltage generated across it, but before any steady change could be detected the contact fractured either partially or totally from the electrode, giving rise to large erratic variations of resistance. This form of contact was then replaced by soldering the fine copper wire on to the electrode. It was found possible to solder the copper wire using a commercial solder for stainless steel. Great care was necessary in depositing a small amount of solder over the junction, as a long contact between the hot iron and the electrode generally produced oxidation or peeling off of the electrode. The strength of these soldered contacts was found to be remarkable. Soldering was found possible with manganin, chromel and alumel films but not with titanium. This problem was overcome by depositing manganin on part of the titanium electrode and forming the contact with the manganin film. The problem of zero level shift, however, remained even with the soldered contacts.

3.12 PREPARATION OF THE SUBSTRATE

3.12.1 Polishing the Disc

The discs which were used for this project were made of EN29 steel and were ~~surface~~ hardened. The surfaces

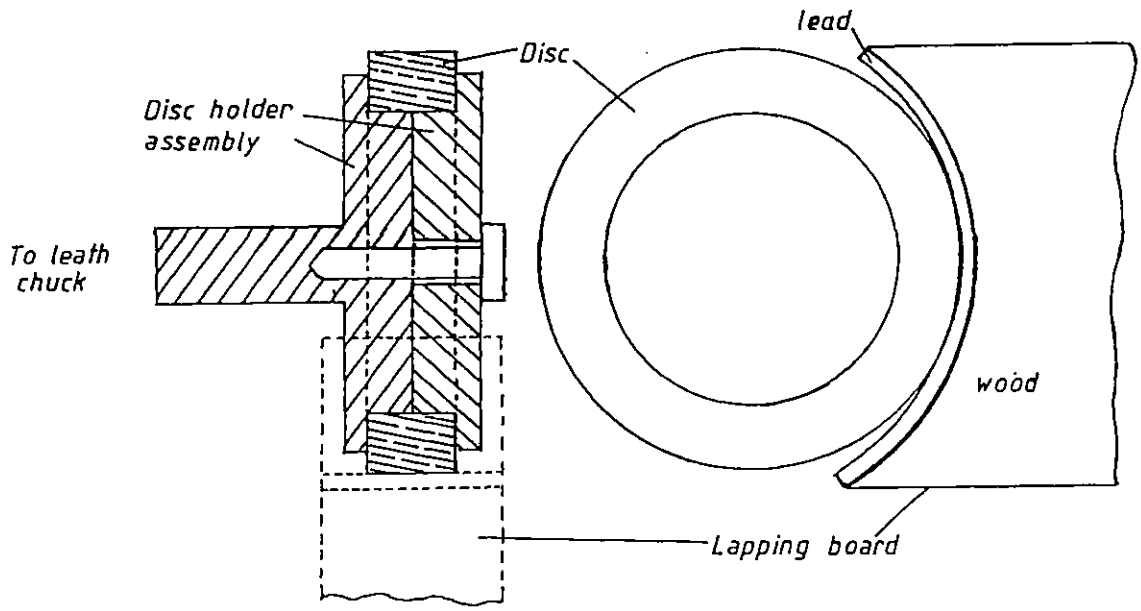

3.5 Lapping apparatus for polishing the disc.

of these discs were finished by grinding and had a surface roughness of 1 to 1.5μm peak to valley. It was found virtually impossible to deposit a properly insulating thin layer either of alumina or chromic oxide, even when the insulating film thickness was 1.5μm. Polished stainless-steel with a surface roughness of less than 100Å could be well insulated with a layer of 0.1μm thick alumina. Thus polishing the discs was found to be of major importance.

To achieve the high finish required of the disc surface, diamond polishing pastes of various sizes were used in conjunction with a specially built polishing rig. The rig was built on a lathe which could hold the disc at a distance of about 8cm from the chuck and rotate it at different speeds without any appreciable excentricity or vibration. The lapping board was made from a block of hard wood of 3cm thick, a 9cm diameter hole was bored at the centre of the block of wood and the inside wall of this hole was lined with 2mm thick lead sheet. The block was cut into three pieces through the centre of the hole to form three lapping boards and each of them was used with a particular grade of diamond paste.

Generally the lapping was started with 16μm oil based diamond paste, thinly spread on the lead, which was then lightly pressed against the surface of the disc, rotating at a speed of 100rpm as shown in Fig.3.5. This combination of coarse polish and low speed was used to remove upto a micron of material and helped to remove the deep scratches. At the end of this first step a uniform surface roughness of about 1500Å was obtained. In

the second stage of polishing the grade of diamond paste was reduced to 6μm and the rotational speed of the disc was raised to 500rpm which reduced the surface roughness to about half of its previous value. Finally the speed of disc was raised to 1000rpm and the grade of the diamond paste was lowered to 1μm size. At this stage hardly any material was removed but the amount of high frequency roughness was lowered drastically which gave the surface a mirror finish. During the lapping process one must be careful to maintain a sufficient amount of lapping fluid at the contact, and a constant and steady movement between the disc and the lapping board is essential.

The surface roughness of the discs were measured by a 'Talysurf' profilometer at the end of each stage to determine whether the average required roughness had been reached and whether there was any deep scratch on the surface. Even a single scrat ch on the surface could short the electrode to the metal substrate below, rendering the whole device useless.

3.12.2 Substrate Cleaning

The adhesion of the thin-film of a particular material on a particular substrate could vary over a wide range depending on several factors such as the cleanliness of the substrate, the vacuum pressure of the chamber, temperature of the substrate, purity of the evaporated material etc. Most of the above factors could be controlled,

and set at near optimum values, except the substrate cleaning. This factor plays a vital role in the adhesion of the fabricated device.

The same cleaning procedures and apparatus were used for glass slides and for metal foils, but for the metal disc these were changed to some extent because of its size and surface roughness. Both glass slides and metal foils had surface roughness less then 100Å peak to peak and both of them were available in pre-cleaned form. Liquid detergent diluted with water was used as the first step of cleaning. Gloved hands were used for rubbing these substrates vigorously with the diluted detergents and then they were thoroughly washed with hot water before they were given a critical check for any grease mark. In the absence of any such marks, the substrates were rubbed and rinised in distilled water and dried off with paper. The substrates were then put into a vacuum degreaser, in which they were washed twice with hot distilled iso-propyl alcohol. The degreaser had to be turned off in such a way that the thimble containing the substrates was left empty of solvent, hence the substrates could dry within the enclosed thimble chamber. If IPA droplets sticking on the substrate were dried outside, a residue was generally left behind which eventually gave rise to poor film adhesion. The substrates were then quickly transfered into the vacuum chamber where all the arrangements for vacuum deposition had been prepared. Covered glass dishes were used for transportation of substrates between every operation.

Because of the greater roughness of the metal discs, they were put through an extra step of cleaning, where the discs, already cleaned with the liquid detergent, were immersed in distilled water in an ultrosonic cleaner. This step was thought necessary in the event of particles from the polishing stage remaining embedded in fine groves on the disc surface. At the end of this stage the disc was returned to the usual cleaning procedure by placing it in a large vapour degreaser.

3.13 CHOICE OF MATERIAL AND TECHNIQUE OF DEPOSITION OF THE INSULATOR LAYER

Two major points considered, in choosing the material and technique of deposition of the insulator layer, were the piezo-electric voltage that can develop across the film under pressure and the adhesion of the film on to metal disc. Three commonly used ceramic materials which show good adhesion in thin film technology are SiO_2, Al_2O_3 and Cr_2O_3. All three materials had high melting points which ruled out the straightforward evaporation of these materials in their oxide form. However, SiO_2 can be deposited by a reactive evaporation method, where SiO is evaporated in an oxygen *rich* atmosphere and reacts in its gaseous phase to deposit SiO_2. At an early stage of the project, this method was tried by evaporating SiO from a tungsten foil boat with different partial pressures of oxygen. The adhesion of the films deposited were never found to be satisfactory. Later, following Kannel's finding

that the SiO_2 film shows piezo-electric effects, this material was abandoned. The electron beam evaporation method was tried with Cr_2O_3. The adhesion of a thin-film of Cr_2O_3 on a glass slide was found to be good. As this facility could not be incorporated in the special purpose vacuum system, the R.F. sputtering method was evaluated. It was found difficult to deposit a good film of Cr_2O_3 on to a metal substrate using R.F. sputtering, particularly when the temperature of the substrate was kept at a value of around $50^{\circ}C$ by water cooling. Upto a thickness of about 1000Å the film adhered very well but as the thickness increased the film would start to peel off and by the time the thickness had reached about half a micron, almost all the film from the centre of the substrate would come off in powder form leaving thinner layers of Cr_2O_3 films at the two edges of the deposition area. Better results were obtained when the substrate was allowed to heat up to a temperature of around $150^{\circ}C$ or more. But as detempering of the steel disc starts to take place at this temperature, it was decided that Cr_2O_3 was not the best material for the insulator layer.

R.F. sputtered Al_2O_3 showed a far better adhesion when deposited on the metal disc at a temperature of around $50^{\circ}C$. However, if the temperature of the disc was allowed to rise above $100^{\circ}C$, the alumina would start to peel off once the thickness had reached 3 to 4 x 10^3 Å. This peeling-off did not occur while the sputtering was going on, but the process would start once the sputtering had stopped and the substrate was allowed to cool down. The probable reason

for this was the higher co-efficient of thermal expansion of the steel compared to the thin film alumina. The stress that was generated within the alumina film, when the steel substrate contracted more than the film, forced the film to peel off the substrate.

A 1 micron thick alumina film deposited by R.F. sputtering on a metal disc, usually showed total transparency except for interference fringes caused by a reduction in thickness at the two sides of the disc. Occasionally, however, the alumina film was found to deposit with a deeper blackish colour, though retaining transparency. It was thought to be caused by some impurity, most probably duralamin, sputtered from the side of the target assembly. No change in resistivity could be determined between the two types of film even though the adhesion of the totally transparent film was found to be better.

The adhesion of the alumina film deposited, after sputter etching the substrate, was found to be extremely good. Generally it was found impossible to scratch the film off the substrate. During the polishing of a disc for re-use once a fabricated device had failed, it was found that part of the alumina film withstood the initial 16 μm lapping stage for 5 minutes whereas other deposited film layers disappeared within seconds.

Thin-film alumina was checked for any piezo-electric effect by two types of loading. A thin-film of alumina deposited on a stainless steel sheet was load statically and by load impulses. A piece of highly polished stainless-steel sheet was coated with a layer of alumina. An electrode

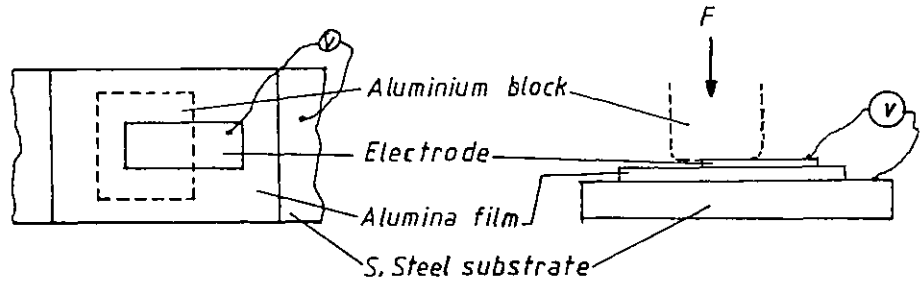

Fig.3.6 - Test Arrangement for Piezo-Electric Effect in Alumina

of manganin, was deposited on top of the alumina layer. Electrical connections from one end of the electrode and from the stainless-steel substrate were formed by soldering on copper wires. The composite structure was then placed between the two jaws of a hydraulic press for static loading. The pressure was transmitted to the structure through a block of aluminium, positioned on the electrode and covering part of it. The edges of the block were rounded off to prevent any sudden change of pressure which might crack the alumina layer during loading. A piece of paper was used as electrical insulation between the aluminium block and the electrode. To match the high impedance of the set-up, a digital voltmeter with very high input impedance was used for monitoring the voltage. But the voltmeter showed readings similar to the floating electrodes condition throughout the whole pressurisation and depressuriation process. No firm conclusion could be taken from this test. For the impulse loading test, the digital voltmeter was replaced

by an oscilloscope and the loading was provided by sudden hammering on the aluminium block. No signal could be detected over the slight noise level and it was concluded that the film does not produce any appreciable piezo-electric voltage.

3.14 CHOICE OF MATERIAL AND TECHNIQUE OF DEPOSITION OF THE ELECTRODES

During the disc machine test of the devices it was found that the weakest link in the whole device was the electrodes. Usually the electrodes determined the useful life of a transducer under test. It has already been shown in the literature survey, using Wymer's (62) work, that the most severe pressure condition arises at the two side constrictions in a line contact. In practice it was found that the electrodes fail precisely in that zone. Hence the adhesion of the electrodes had to be as good or better than the active elements themselves. From the electrical point of view, the resistance of the electrodes should be negligible compared to the active element resistance, so that the electrical phenomena that occur at the active element can be monitored accurately. To achieve this, in the case of the pressure and resistive temperature transducers, the width of the electrodes was made 20 to 100 times larger than the active element width and the material used had a resistivity equal to or smaller than the active element itself.

In the early stages of the project, the special purpose system had only one evaporation facility and it was

used for the deposition of the active element immediately after the deposition of the insulator layer without the vacuum break. Hence materials were tried as electrodes which would have the necessary adhesion to the alumina layer even after the vacuum break. Aluminium was the first choice as it was found to show very good adhesion to an alumina layer. Generally the aluminium film deposited on alumina would withstand the scratch test. But the combination was found to be rather brittle and it came off in small patches in disc machine tests particularly in the side construction zone. Copper and manganin were also tried as the electrode. Although manganin showed much better adhesion than copper, the life of the manganin electrodes deposited after a vacuum break, was found to be short, lasting up to 3 minutes.

It is widely known that the adhesion of both chromium and titanium films is very good to almost any substrate. These two materials, however, are not suitable for use as electrodes on their own, as their resistivity in the thin-film form is very high, but they can be used as an intermediate adhesive layer between two films with poor adhesion. Electrodes were fabricated using this technique, a layer of about 100Å of chromium was evaporated from a tungsten rod coated with electrolytically deposited chromium, on to the alumina layer through the electrode mask and then through the same mask was deposited a layer of manganin of 1000Å thickness to complete the electrode. Similar electrodes were also fabricated with titanium underlayers. Widely varying results were obtained. Some fabricated electrodes survived in the disc machine for 10 min. before the manganin

layer was damaged but in some cases the adhesion was so poor it could not survive the adhesive tape test.

To further improve the life of a device, sputter deposition of the electrodes was tried. It has been mentioned that sputtered films generally show much better adhesion than evaporated films. Initially copper electrodes of 1000Å thickness were fabricated by sputtering from a 12.5cm target at 150 watts for 10 minutes after pre-sputtering the target for 10 minutes to clean the top surface of the target. Copper electrodes deposited by this method could withstand the adhesive tape test but failed in the disc machine. A 12.5cm diameter manganin target was made using a manganin foil. The sputtering rate of manganin was found to be almost equal to that of copper. The adhesion of the sputter deposited manganin film on freshly deposited alumina was very good. Transducers fabricated with sputtered manganin electrodes could survive more than one run in the disc machine, each run lasting well over 30 minutes. To achieve this adhesion it was found necessary to have a good initial vacuum of around 10^{-6} torr and required the use of liquid nitrogen in the cold trap to remove the moisture. It was also necessary to sputter etch the substrate and target at around 150 to 200 watts for 10 to 15 minutes.

Although the adhesion of the electrodes deposited by sputtering was found to be much better than any of the evaporated ones, their use was limited to a few larger devices as it was found virtually impossible to generate a very fine gap between the electrodes due to the undercutting that takes place during sputter deposition. Several methods

were tried to produce a fine gap by preventing the depositing particles from penetrating beneath the mask. These met with little success, either producing poor adhesion of electrodes near the active element area or damaging the deposited active element.

The necessity for finer devices led to the return to evaporated electrodes. For the disc machine test of pressure tranducers it was noticed that usually the active elements, which had been deposited without a vacuum break, remained undamaged while the evaporated electrodes deposited after a vacuum break, had failed. Usually manganin films deposited without a vacuum break could withstand the scratch test successfully. It was also noticed that the films show much better adhesion when the thickness of the film is low, the adhesion gradually deteriorating as the thickness is increased beyond 1000Å and generally the film starts to peel off once a thickness of around half a micron is reached. Two types of manganin had been tried, one with 2% Ni and 12% Mn which was produced commercially, and the other with 4% Ni and 12% Mn which was made by the author. No appreciable difference in adhesion was noticed. Neither was there any difference of adhesion when the charge of manganin for flash evaporation was in the form of 12.5 um wire in 1 mm long pieces or very fine granules produced by filing a 1 mm diameter wire.

Further improvement in the adhesion of the evaporated manganin films was detected with the use of laser milled composite masks. This was thought to be due to fewer steps being required in fabricating a device, which in tunr reduced the number of feedthrough manipulations required.

As the system occasionally leaked a small amount of air into the chamber when the feedthroughs were manipulated, less handling of feedthroughs meant less chance of contamination and hence better adhesion. The life of these devices fabricated through the composite masks were found to be almost as good as the devices with sputter deposited electrodes.

3.15 FABRICATION OF MASKS

Masks played a vitally important role in fabricating the thin-film devices. The active elements as well as the electrodes were deposited either by evaporation or by sputtering materials through the masks. The dimensions of the mask pattern determined the dimensions of the devices deposited through them. Masks required for the wider patterns, like the electrodes of the resistive tranducers and the capacitive film thickness monitor, were relatively easy to make. On the other hand masks of minute dimensions required for the deposition of the active elements for the resistive devices were quite difficult to achieve. In this project several techniques for fabricating the masks were tried, broadly they can be divided into two groups: (i) conventional methods, mainly using photolithographic technique and (ii) the laser milling method.

3.15.1 Conventional Methods

In the early stage of development all the wider masks were fabricated using the conventional photolithographic technique on molybdenum foil. The thin-foil masks

produced this way required a background support which was provided by spot welding the foil mask onto a m.m. thick stainless-steel of about 2.54cm by 4cm in size with a similar but much wider pattern milled into it.

This method had been tried to make a composite mask containing both electrodes and the active element. Due mainly to large undercutting during the etching process, the finest slot achieved for the active element was about 150 um wide and about 0.75mm long. This large width was not acceptable for resistive type transducers. This forced us to use one mask for electrodes fabricated by photolithographic technique and a second mask for active element.

The mask for the active element was made by spot welding two pieces of razor blade with their cutting edges facing each other onto a m.m. thick stainless-steel with a cm long slot at the centre as shown in Fig.3.7 . To achieve a fine and uniform gap, it was found essential to examine the cutting edges of the blade under a microscope and choose two pieces of about 1.5cm long area from a blade where it showed the least unevenness at the edge. The two lengths were then cut off from the blade carefully with a shearing machine, making sure that the ends of the pieces do not bend. One piece of the blade was then spot welded on to the stainless-steel in such a way that its cutting edge covered exactly half of the slot along its length. A spot of araldite was used to hold the second piece of razor blade on to the stainless-steel with its cutting edge covering the remaining half of the slot. The whole assembly was then placed on a light box, which in turn was placed

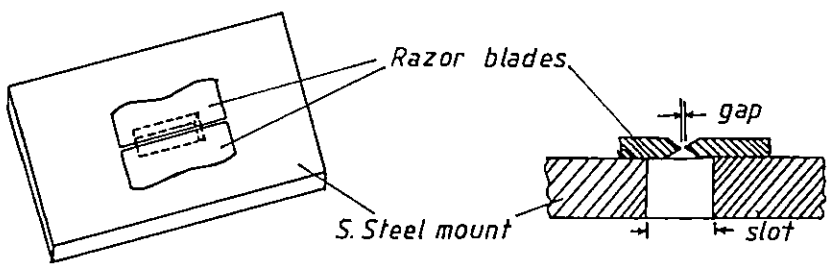

Fig. 3.7 Mask fabricated with razor blades.

under a travelling microscope. The second razor blade was then carefully manipulated under the microscope to generate a uniform but very fine gap between the edges. The araldite was then allowed to harden and the second piece of blade was also spot welded in its position. Using this technique a gap of down to 20 microns could be made.

3.15.2 The Laser Milling Method

In this method of fabricating the masks a laser milling set-up was used which was developed for fabricating model rough surfaces by De-Silva (86). The system consisted of a pulsed ruby laser in which the power and frequency of pulsing could be varied. The horizontal beam coming out of the laser was reflected through 90^{o} by a mirror, and was then focussed onto the cutting platform by a microscope objective. The diameter of the focussed beam could be controlled by controlling the aperture of an iris placed in the unfocussed beam path, or by changing the objective lens on the microscope. The position of the beam and its size on the milling platform could be monitored through the microscope. The milling platform was mounted on an X-Y platform, the movement of which was controlled by two stepper motors which were in turn driven by a mini-computer. The minicomputer also controlled a Q-switch which was positioned on the unfocussed beam path and could turn the beam on or off from the microscope attachment.

A single step in the stepper motor produced a linear movement of 1.25 μm in the X-Y platform. By providing

the computer with the number of steps it has to rotate one or both the motors in positive or negative directions along with the status of the Q-switch, it was possible to make the X-Y platform traverse, relative to the fixed laser beam, the outline of complicated mask pattern.

By using a X20 objective in the microscope and setting the iris to 1/10th of its maximum aperture, a minimum beam diameter of about 4 μm could be obtained with the fundamental mode of operation of the laser. However, as the iris is closed down the power of the beam drops drastically. At 4 μm beam diameter it was found just possible to cut slits in molybdenum foil of 20 micron thickness at 1000 pulses per second and at a platform traverse rate of 60 μm/sec. The foil mask with 4 μm slit was used to replace the razor blade mask but it was found that if these thin-foil masks were mounted on a stainless-steel plate and used for deposition in the usual way, no evaporant passed through the slit. The reason was thought to be the slight bending of the foil when the disc was pressed against it, which moved the slit out of alignment. Then if the 4 μm slit was not in perfect alignment with the boat and the disc, the 20 μm thick slit wall forms a large shadow thus preventing any material from passing through it.

This problem was overcome by wrapping the foil on the disc with the slit properly positioned on the previously deposited electrodes and aligning the slit very carefully over the boat. This way active elements of upto 6 um width were achieved. But as the vacuum had to be broken to place the mask, the adhesion of these active elements were found to be poor.

The masks fabricated for the electrodes using photolighographic technique needed a minimum gap of about 0.5 mm between the electrodes which made 0.5 mm the minimum length obtainable for the active element. As we have seen earlier, a slight misalignment of the active element over this length would increase the effective width of the active element dramatically. Because of this, a programme was developed to mill a composite mask using the laser milling equipment. Initially the length of the active element was chosen to be 300 μm long and to get a positive cut throughout the whole outline of the mask, the beam power was raised by opening up the aperture to 1/5th of its maximum value, increasing the beam diameter to 10 μm. Later with a second programme the shape of the electrode at the active element zone was changed to reduce the length of the active element to 30 um while the width was kept at 10 μm as shown in Fig. 3.8.

Mounting these thin-foil masks with relatively large pattern on them was found to be rather delicate. If the pattern had been removed from the foil leaving large holes on it, before it was mounted, the slighest stress generated during the spot welding of the foil distorted the slit for the active element. This problem was overcome by stepping up the linear motion of the X-Y platform from 60 μm to 100 μm/sec. At this speed it was found that the laser could not produce a positive cut, instead it occasionally left uncut lengths of a few micron at a time. As a result of this circumscribed areas did not detach from the foil once the whole pattern was traversed by the laser beam. Once the foil was properly mounted on the metal plate a slight pressure on the pattern zone was enough to remove it from

the foil. In this method, however, to achieve a positive cut at the active element zone, the laser beam was made to traverse the line twice. This process does not increase the width of the slit, as the backlash of the X-Y platform was negligible but actually improves the uniformity of the slit by removing the ragged edges of the slit produced by a single cut due to the stepping motion of the platform and the roundness of the beam.

Two alignment slits were milled in the mask 20 mm apart and each 3 mm long on the same line as the active element as shown in Fig.3.8c. These two slits produce two fine lines at the two edges of the disc when the transducer material was evaporated through the mask, thus helping to determine the precise alignment of the minute active element.

No problem was encountered in evaporating material through these composite masks.

The results obtained with these laser cut composite masks encouraged the development of multiple device masks with a high degree of alignment between the active elements of the devices. Fig.3.8 shows the patterns used for the resistive pressure and temperature transducer mask. The two active element slits and the two alignment slits were cut in one operation so that one axis of the X-Y platform remained locked. This precaution was taken to make sure that these four slits were made in the best straight line for accurate alignment. The active elements were made 300 μm long and 10 μm wide.

In using these multiple device masks, one needs a shadowing device which can keep one pattern under its shadow

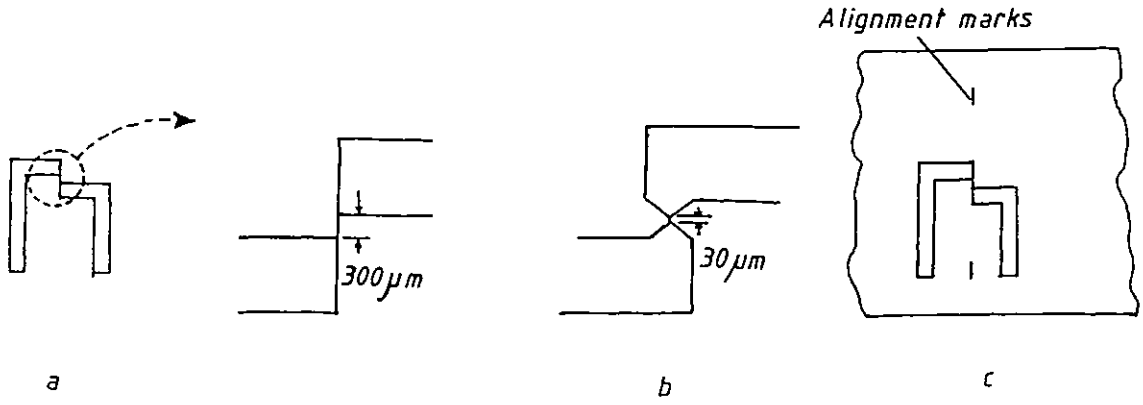

Fig. 3.8 Mask pattern for resistive transducer, (a) 300um long active element, (b) 30um long active element, (c) alignment cuts relative to active element.

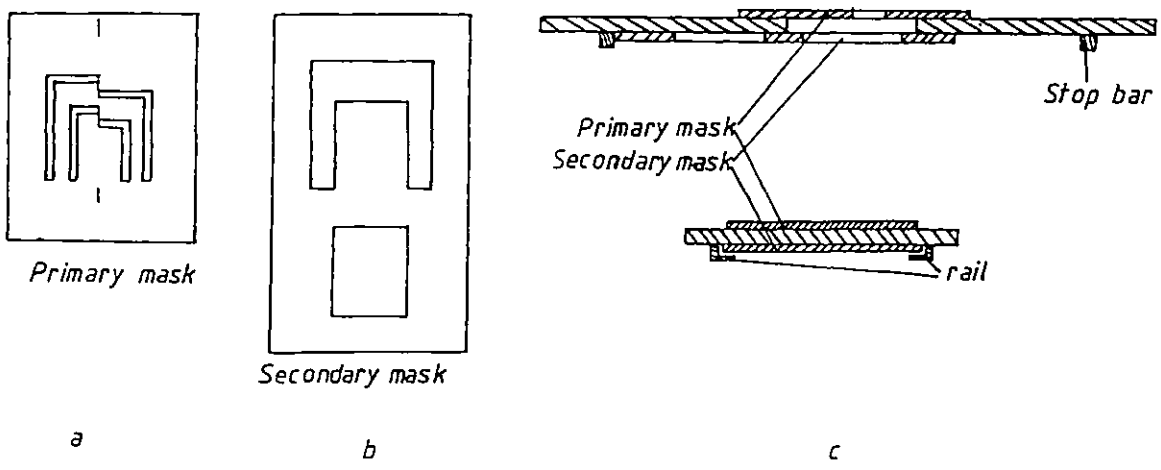

Fig. 3.9 Multiple transducer mask(a);secondary mask(b); relative mounting of two masks in the special mount(c).

while material is deposited through the other pattern and vice versa. To achieve this a secondary mask was fabricated as shown in Fig.3.9b, using a 100 μm thick molybdenum sheet. The secondary mask was also mounted on a stainless steel plate in the same way as the main mask. The secondary mask mount was then placed between two guide rails devised on the back of the main mask mount. Two stop bars were also spot welded on the back of the main mask mount at the two extreme traverses of the secondary mask mount as shown in Fig. 3.9c. As a result when the secondary mask was at one extreme traverse it exposed one pattern and shut off the second one completely. Exactly the opposite happens when the secondary mask was pushed to the other extreme position. A 10 cm long by 1 mm diameter stainless steel rod was welded at one end of the secondary mask frame and by coupling this rod with an external feedthrough, it was possible to change the position of the secondary mask relative to the main mask from outside the chamber.

No such elaborate 'masking a mask' procedure was needed for using the multiple pattern mask made for pressure and capacitive film thickness transducers, as the same material was used for fabricating both the devices.

CHAPTER 4

EXPERIMENTAL STUDY OF THE PROPERTIES OF MATERIALS USED IN FABRICATING THIN-FILM TRNSDUCERS

4.1 Study of the Properties of Manganin

The composition of manganin is not very well defined, some authors like Adams et al. (78) have used manganin of composition 84% Cu , 12% Mn and 4% Ni, while Hamilton and Moore (75), in fabricating their thin-film pressure transducers, used manganin with 3% Ni, 85% Cu and 12% Mn. Most of the authors while discussing their pressure sensors have mentioned that the composition of manganin is very important in relation to their pressure coefficient and linearity. However, although work has been carried out by various authors to determine the pressure coefficient and reproducibility and linearity of pressure coefficient of bulk manganin using hydrostatic pressure equipment, no such work has been reported regarding the thin-film manganin or bulk manganin with different compositions.

4.1.1 Sources of Manganin

In this project most of the thin-film pressure transducers were fabricated using manganin with 85% Cu, 12% Mn and 3% Ni supplied by Goodfellow Metal Co. However to study the properties of manganin with different compositions, some manganin wires were obtained from Driver-Harris Co. and, in addition to these two sources, the author had made a wide variety of manganin with different compositions.

An M.R.C. arc furnace was used for alloying manganin with different percentages of manganese in it. High purity copper and nickel foils and electrolytically deposited manganese

were used as the basic materials. In alloying the materials in the furnace, the accurately weighed materials were placed in the water cooled thimbles formed in the copper base plate of the furnace and in a second thimble an ingot of titanium was kept. The furnace was evacuated to a vacuum of about 0.1 torr and backfilled with pure argon gas. The arc was then struck and transferred to the titanium ingot which was melted and kept in that state for a few minutes. As the titanium acts as a good getter, it removes the residual oxygen from the chamber. The arc was then transferred to the alloying mixture which was totally melted and a thorough mix was produced, in about 1 minute, by the swirling action generated by the off-centre arc. The alloy was kept in inert atmosphere for about an hour to cool down. These alloys were later checked for their composition using the microprobe analysis. In all cases there was a slight loss of manganese, which was not surprising as manganese has very high vapour pressure at the temperature at which the alloying was done.

The 3 cm. diameter slightly oval shaped ingots were then pressed in a large tensile testing press to a load of $\sim$ 360,000 Kg to flatten them so that they could be used as 5 cm. diameter sputtering targets after slight machining.

For flash evaporation part of an ingot was filed off to produce very fine granules which were then placed under a powerful magnet to remove any steel particles arising from the file itself.

4.1.2 Hydrostatic Pressure Test Equipment

To study the pressure co-efficient of manganin, initially a simple hydrostatic pressure apparatus was devised, in the absence of a proper hydrostatic pressure vessel. As shown

in Fig. 4.1, two circular discs of PTFE of 0.5 cm thickness and 7 cm in diameter were used to form a sandwich with the test wire laid in between. The combination was then mounted inside a short heavy steel cylinder with a 7 cm diameter steel rod being used as plunger. The pressure on the apparatus was generated by a hydraulic press with 30,000 Kg capacity. The ends of the test wires were brought out through two holes in the cylinder and a Wheatstone bridge with a DVM was used to monitor the resistance change. However, with this system pressure on the wire could be raised only upto $\sim$ ~~165~~ 75 MN/m^2 (~~24~~,000 psi), so that, with the low resistance of the wire, very little change in resistance would occur and detection of it was found to be difficult. This apparatus, however, proved to be totally inadequate when it was tried to determine the pressure co-efficient of thin-film manganin deposited on a glass slide. None of the glass slides withstood more than $\sim$14 to 20 MN/m^2 (2 to 3 x 10^3 psi), before they cracked due, presumably, to the pressure generated within the cell not being totally hydrostatic in nature. As a result it was found necessary to design and build a hydrostatic pressure vessel with a liquid pressure transmitting medium.

4.1.3 Construction of Hydrostatic Pressure Vessel

The monoblock cylinderical hydrostatic pressure vessel with a two times safety factor (maximum operating pressure 480 MN/m^2) was designed following the design procedure given in the text book by Alexander and Lengyel (87). The material used for the pressure vessel was a 15 cm diameter block of EN29 steel which had been ultrasonically checked to ensure the absence of any flaws inside the block. The 2.54 cm

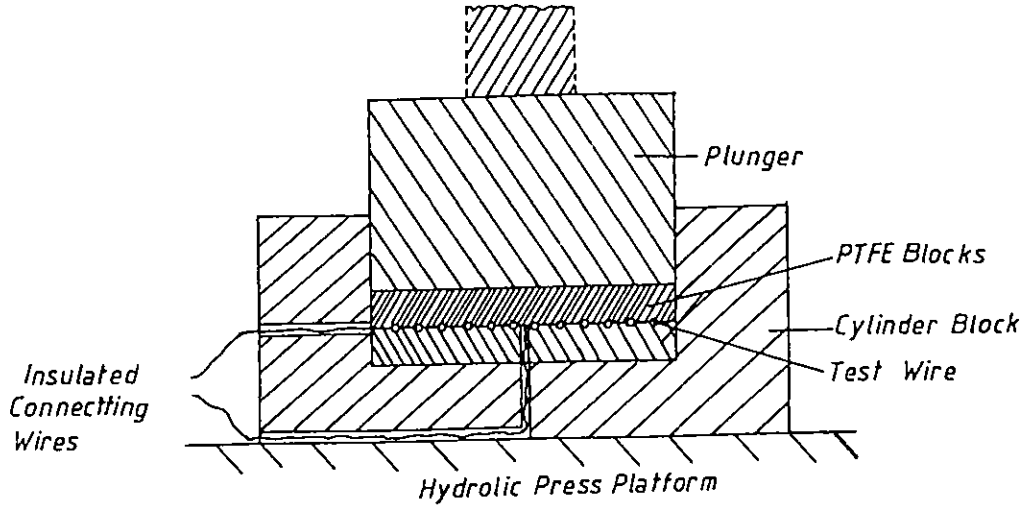

Fig. 4.1 Hydrostatic pressure test appparatus with solid pressure transmitting media.

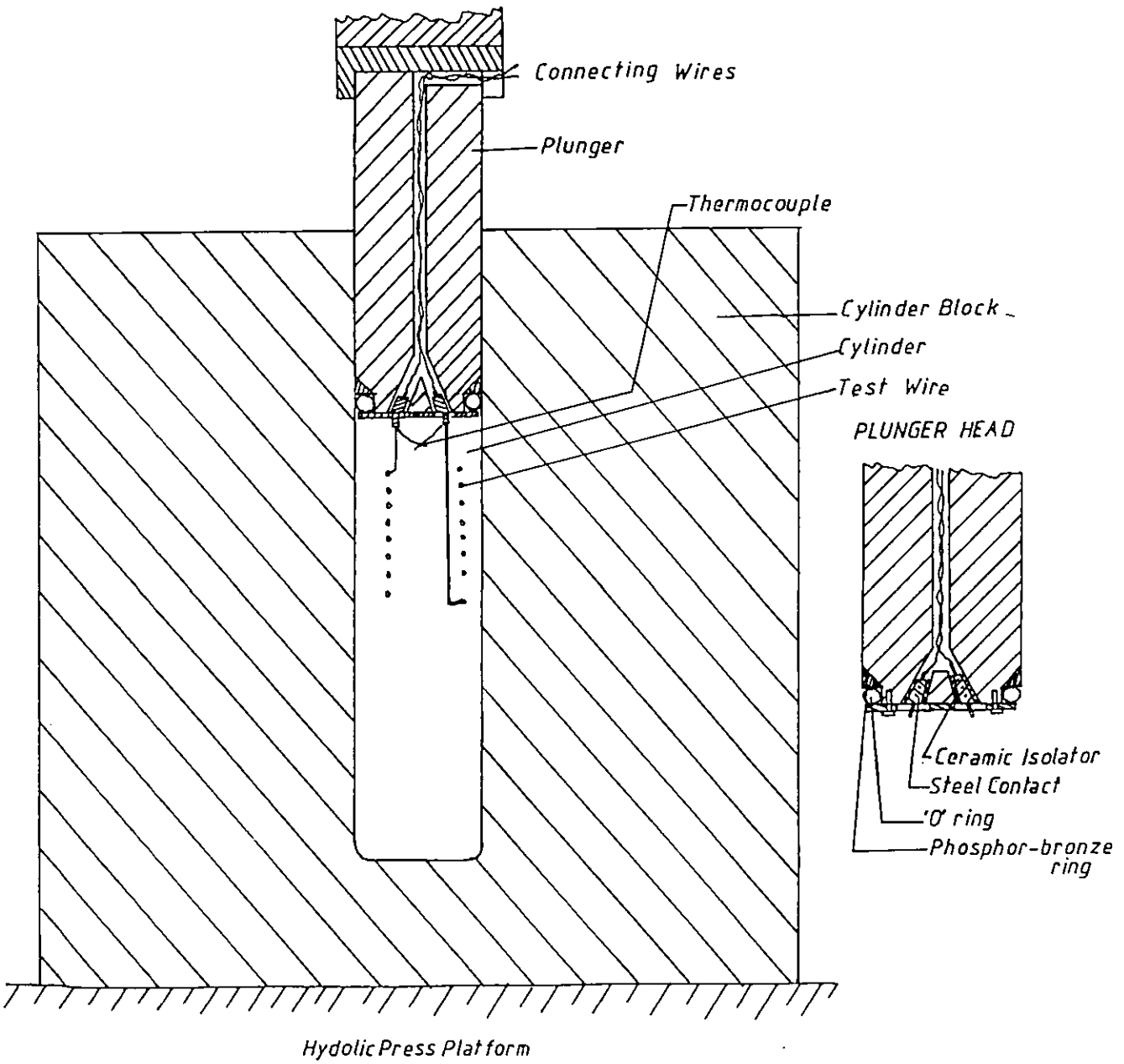

Fig. 4.2 Hydrostatic pressure test apparatus with liquid pressure trasmitting media.

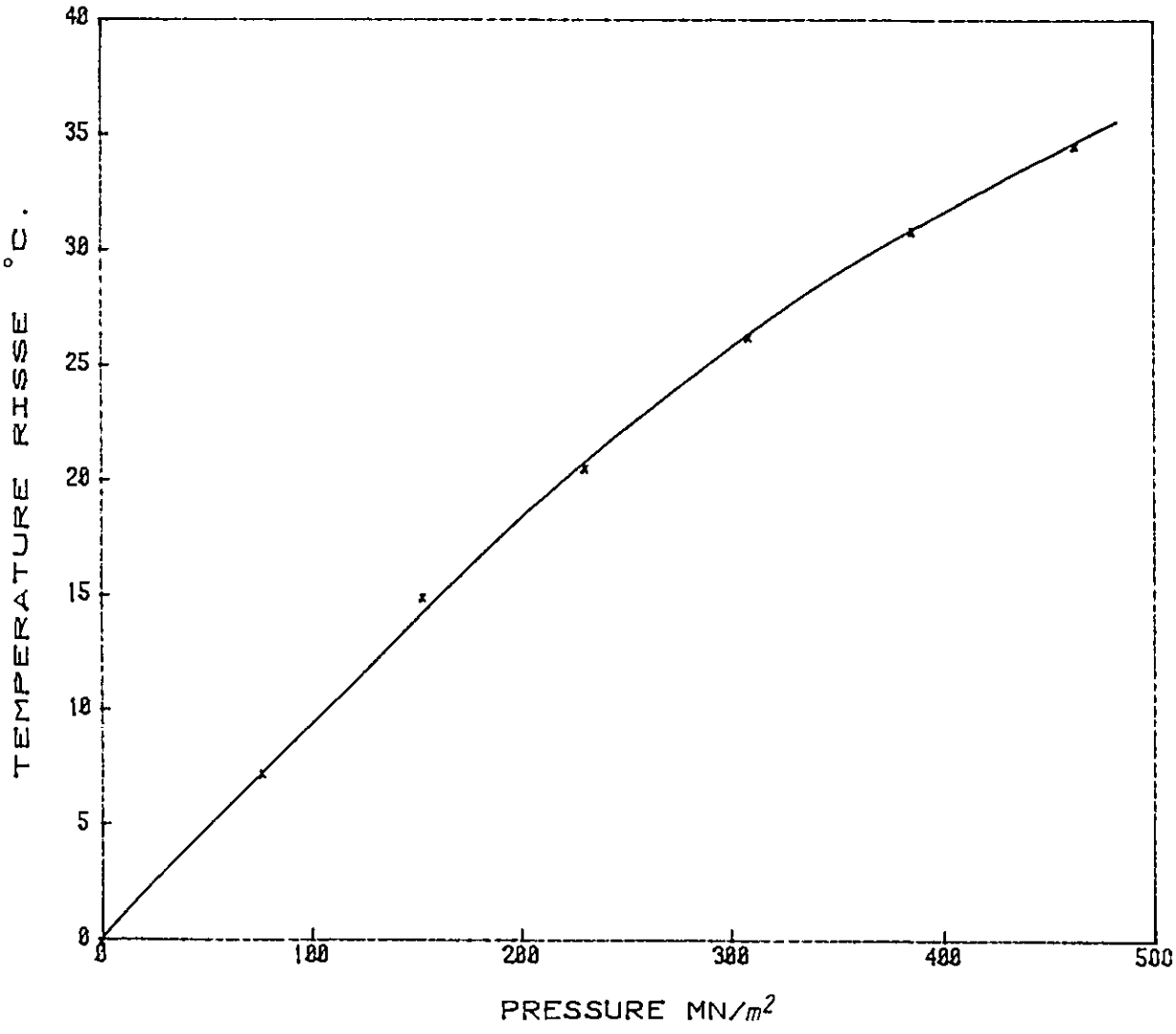

Fig. 4.3 Temperature rise in the pressure transmitting oil (SAE 90) due to increase in pressure.

diameter cylinder made at the centre of the block was 12.5 cm long. The plunger was also made of the same material; the cross-sectional diagram of the equipment is shown in Fig.4,2 . Four electrically isolated lead throughs were fitted through the specially designed ceramic insulators at the cylinder end of the plunger, two of which were later modified to carry the chromel and alumel thermocouple wires without leakage.

To prevent leakage between the plunger and cylinder interface an 'O' ring and a phosphore bronze ring were fitted, the 'O' ring provided the sealing effect at low load and the phosphore bronze at high load. Although this combination worked well when new, the phosphore bronze ring was found to get scratched during operations. As a result after a few initial cycles a slight leakage of the liquid would occur above 275 MN/m^2 (40,000 psi). A slow pumping of the press was found suitable to maintain the pressure at a particular value. However, the phosphore bronze ring was generally replaced after 5 or 6 complete tests.

The working volume available in the cylinder depended upon the compressibility of the pressure transmitting medium and on the applied load, however, for a maximum pressure of 480 MN/m^2 (70,000 psi) with glycerin, a working volume upto 7.5 cm long was available.

The heat generated due to the compression of the pressurising fluid was found to be substantial. Using the built-in thermocouple the temperature rise in the pressure transmitting fluid (in this case SAE90 oil) was measured and is shown in Fig. 4.3. In studying the effect of pressure on thin-film devices in the pressure vessel, the effect of temperature had to be removed, thus before taking any readings

at a particular pressure, the heat generated within the vessel was allowed to dissipate, this being monitored by the thermocouple.

4.1.4 Preparation of Specimens for Hydrostatic Pressure Vessel Test

The pressure coefficient of resistivity of most of the metals and alloys are extremely small, hence even with the comparatively large pressure attainable with the hydrostatic pressure vessel, the actual change in resistance is very small. In preparing a thin-film specimen for pressure testing in the hydrostatic pressure vessel, one must make sure that the change of resistance of all other parts, such as the electrical contact with the thin-film, is negligible compared to the change in resistance of the sensor.

For the test of bulk manganin, the manganin wire was formed into a coil of about 1.5 cm diameter with enough spacing between two turns to avoid short circuits. The top end of the coil was soldered straight onto the binding post while a stiff copper wire, soldered to the second feedthrough, was passed through the centre of the coil and soldered to the other end of the coil, thus acting as a rigid post to keep the coil from vibrating. This procedure worked well with the bulk manganin.

A great deal more difficulty was encountered in connecting the thin-films deposited on glass slides. Initially copper wires were connected to the thin-film using silver loaded paint which was covered up with araldite for better strength. This method of connection worked well at pressures about 69 MN/m^2 (10,000 psi), however, below this pressure the change of resistance with pressure was found to be erratic and

instead of increasing, the resistance of the manganin film (which has positive pressure coefficient) would show a slight decrease due to the contact resistance being reduced by virtue of the firmer mechanical contact.

The above method of connecting the wire to the thin-film was discarded in favour of soldering the wires to the film. However, evaporated manganin film deposited on a glass-slide without prior sputter etching of the slide generally produced poor adhesion and soldering on to these films was found virtually impossible.

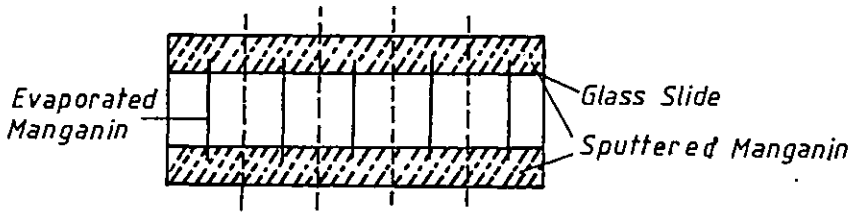

Fig.4.4 - Glass Slides with Sputtered Manganin Contact

This problem was overcome by preparing special slides with sputtered manganin contacts as shown in Fig. 4.4 . The transducer was then formed by evaporation of manganin through thin slits to bridge the gap between these contacts. Soldering of copper wires to the sputtered manganin contacts were found to be reasonably simple.

4.1.5 Tests in Hydrostatic Pressure Vessel

At first glycerine was used as the pressure transmitting fluid in the pressure vessel. After mercury, glycerine has the lowest compressibility amongst the readily available liquids, thus providing the maximum working volume available.

However, glycerine was later replaced with the SAE 90 oil as it was one of the major lubricating oils used in the disc machine tests of the transducers fabricated on discs. A Wheatstone bridge with a DVM as null detector was used to monitor the change in resistance of the test specimens.

4.1.6 Bulk Manganin

Two types of manganin wires: (1) Goodfellow Metal and (2) Driver-Harris, were tested in the hydrostatic pressure vessel to determine the pressure coefficient and linearity of bulk manganin. Authors like Bridgeman (77) and Adams et al. (78) have mentioned the necessity for pressure seasoning of the manganin sensor. To get a clear understanding of the effect of the initial cycles on bulk as well as thin-film manganin, careful readings with some of the samples were taken from the very first pressure cycles. Fig.4.5 shows the effect of the first few pressurisation cycles on Driver-Harris wire. The change in pressure coefficient in the first few cycles for this wire was found to be large. The value, however, was found to stabilise within the first two cycles for pressure over 80 MN/m^2. The pressure coefficient below this pressure was found to change even after 5 to 6 cycles of pressurisation, although the change gradually became very small. Manganin wire produced by Goodfellow Metal, however, showed much less change in pressure coefficient from 1st to 2nd cycle and so on, although the readings below 80 MN/m^2 was found to decrease slightly with the successive pressurisation cycles. The linearity of the pressure coefficient was found to be good for both the wires after the first few pressure cycles as shown in Fig.4.6 . The pressure coefficient of resistivity of the Driver-Harris wire was found to be slightly higher than the Goodfellow Metal wire.

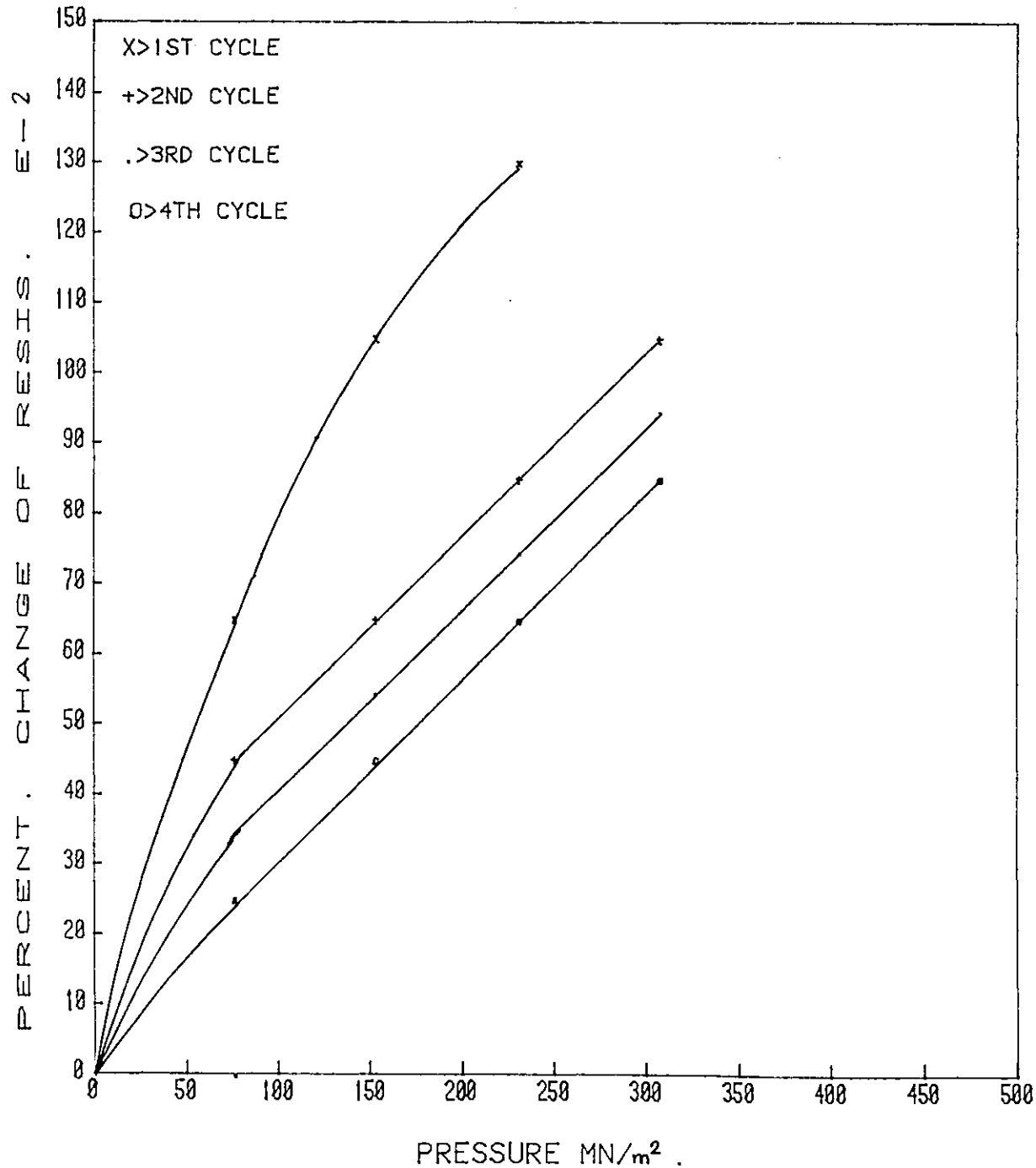

Fig. 4.5 Pressure coefficient of resistivity of manganin wire produced by Driver-Harris Co.

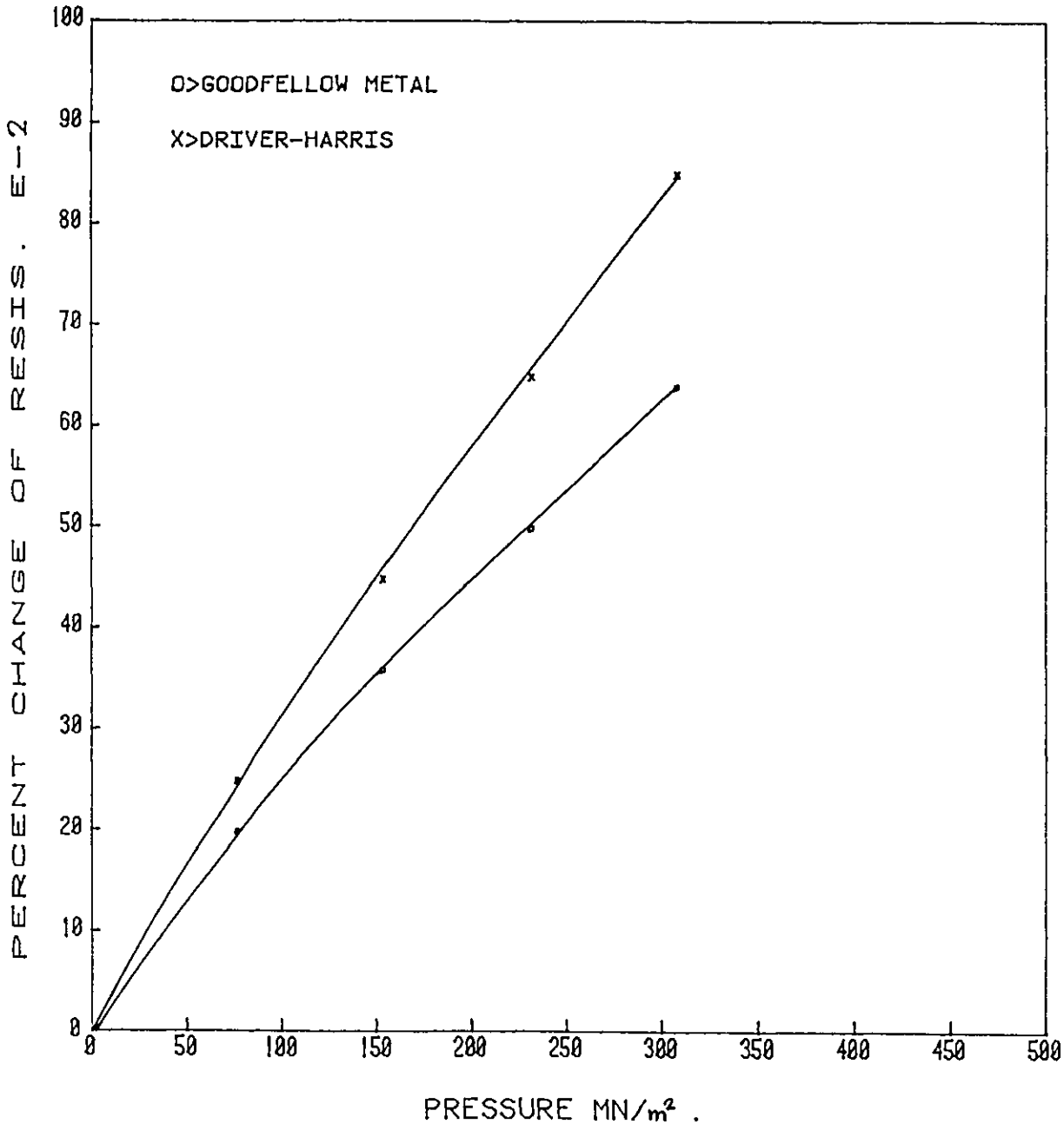

Fig. 4.6 Pressure coefficient of resistivity of manganin wires by Goodfellow Metal and Driver-Harris Co.

4.1.7 Thin-Film Manganin

The effect of pressure seasoning on thin-film manganin was found to be rather small. Hardly any change in pressure coefficient of a particular sample of thin-film of manganin could be detected above 80 MN/m^2 from one cycle to the next. However, below this pressure, most of the samples showed a slight increase in pressure coefficient in the first ~ 5 cycles after which they became quite stable, as shown in Figs.4.7 & 4.8. The linearity of the pressure coefficient of thin-film manganin above 80 MN/m^2 was found to be good from the very first cycle and it generally extends to atmospheric pressure after the first few pressurisation cycles.

The effect of annealing on the pressure coefficient of manganin film was found to be negligible. A 6 hour annealing at 150°C in vacuum was carried out on one segment of a glass slide while a second segment was left unannealed. Fig.4.9 shows the pressure coefficient plots for these two specimens. The annealed sample shows slightly better linearity at the low pressure region, while the non-annealed sample shows slightly higher value of pressure coefficient.

Manganin evaporated fromthe same bulk source at different times, keeping all the deposition parameters as constant as possible, show different pressure coefficients as can be seen from Figs.4.7 and 4.8. However, during the course of the pressure vessel work with thin-film manganin, it emerged that the pressure coefficients of the thin-films of manganin deposited at the same time remains within 10% of each other.

Manganin alloys made in this project with varying percentages of manganese were also tested in the thin-film form. Fig. 4.10 shows the plot for three such different compositions

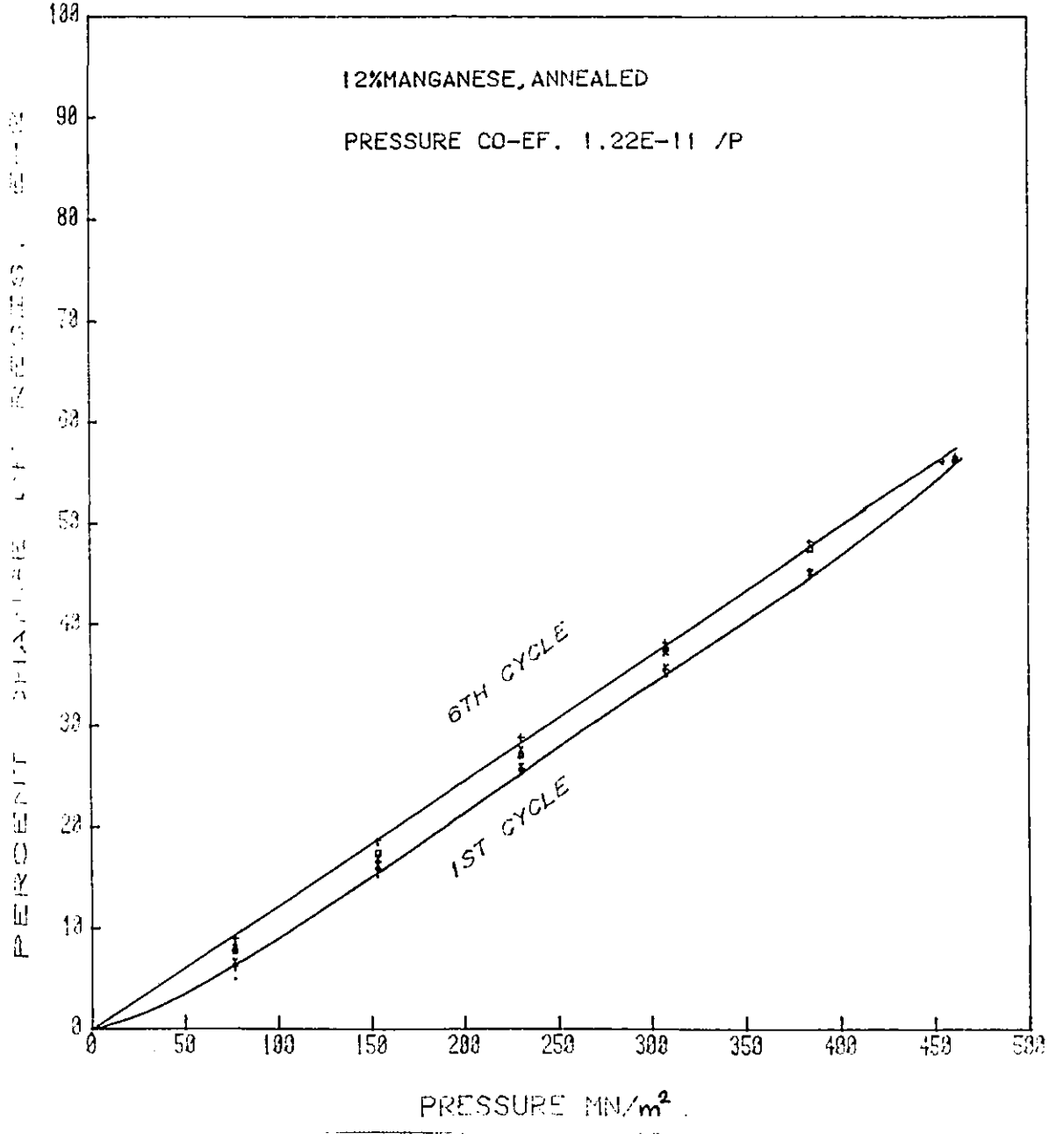

Fig. 4.7 Pressure coefficient of resistivity of thin film of manganin; first few pressurisation cycles.

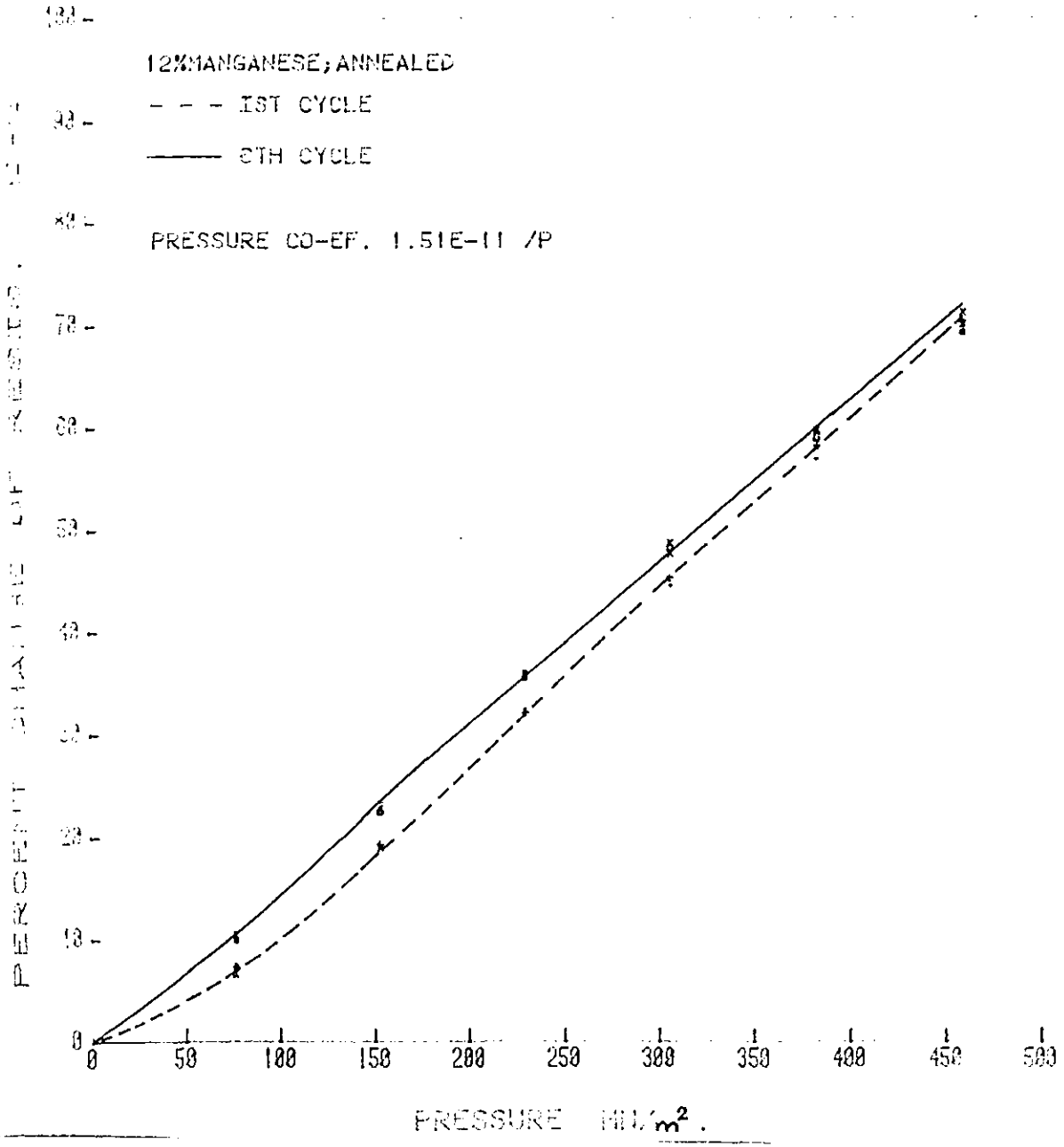

Fig. 4.8 Pressure coefficient of resistivity of thin film of manganin; first few pressurisation cycles.

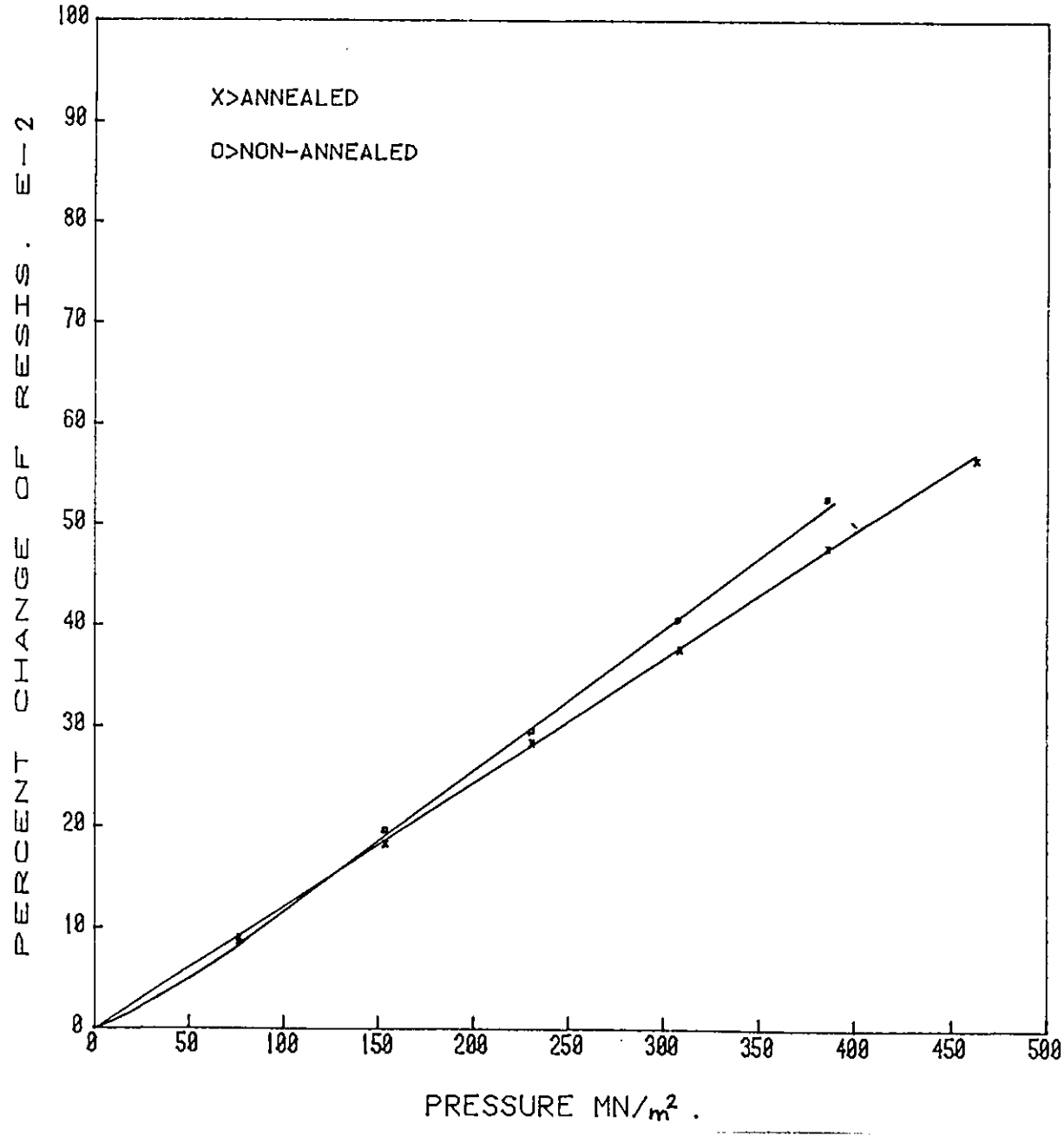

Fig. 4.9 Pressure coefficient of resistivity of unannealed and annealed thin film of manganin.

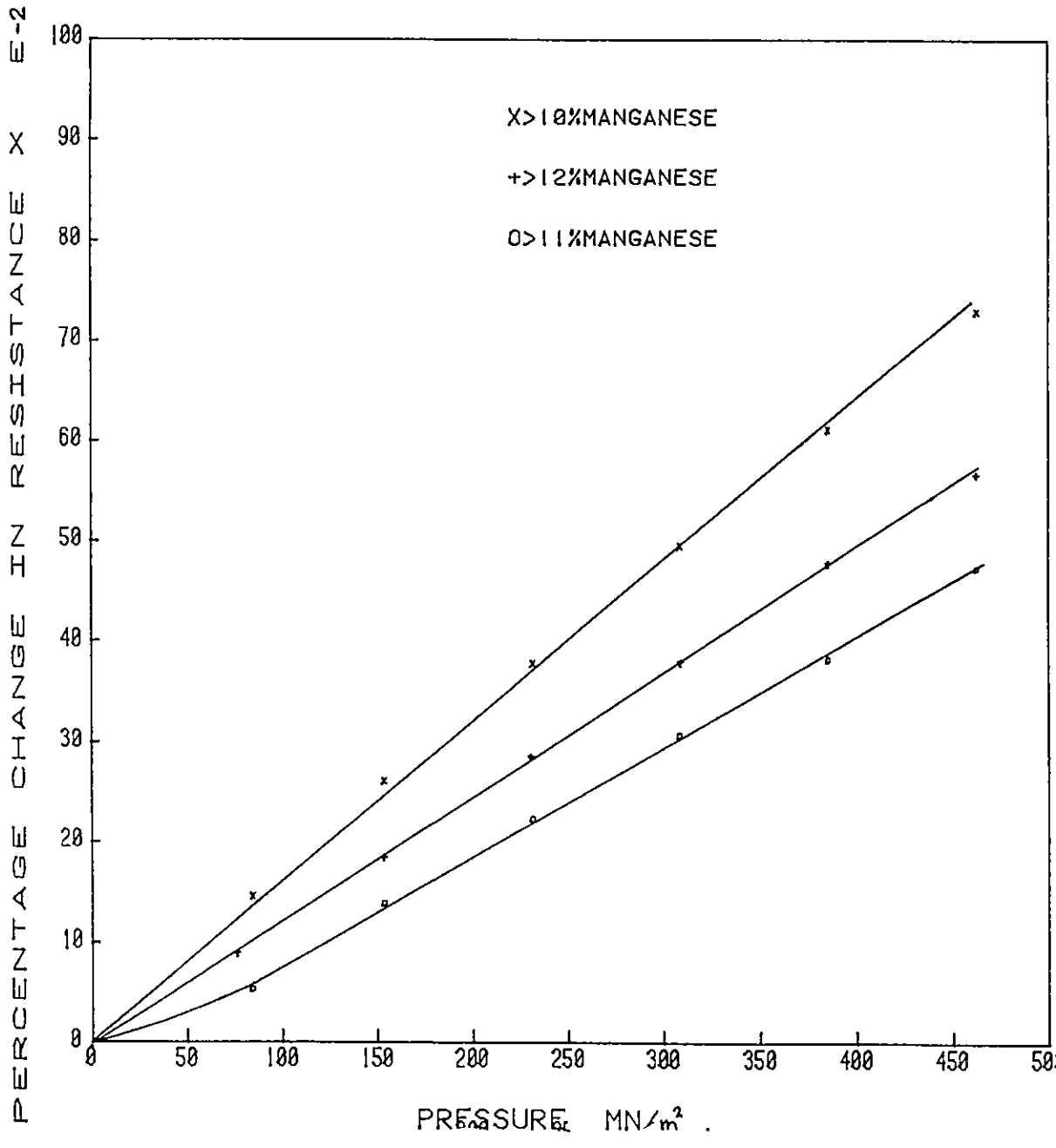

Fig. 4.10 Pressure coefficient of resistivity of thin film of manganin having various composition.

with 10%, 11% and 12% manganese. The degree of linearity of the pressure co-efficient of the three films was found to be similar, but no consistent relation could be found between the pressure co-efficient and percentage of manganese present in the source alloy. This is not surprising, however, as the manganin films deposited from the same source at different times show different pressure co-efficients and although the source alloys had 10, 11 and 12% manganese, the compositions of the evaporated films were unknown. However, two manganin films deposited by evaporation were analysed using a Microprobe machine and both the films showed compositions almost the same as the source material.

Shear stress was supposed to cause drastic ahanges in the pressure co-efficient of bulk manganin, as we have seen in the literature survey section from Lee's (81) work. No suitable experiment could be devised to generate enough shear stress on thin-film. In Lee's work the drastic changes occurred when the sleeves, on which the wires were wound, were changed using different materials. Thus it was thought interesting to examine the pressure co-efficient of thin-film manganin deposited on substrates with different bulk modulus of elasticity, so that under hydrostatic pressure they would compress by different amounts. Pressure co-efficients have already been presented using glass slides (bulk elastic modulus of glass ~ 36 GN/m^2). Two pieces of stainless steel and tungsten (bulk modulus of steel 180 GN/m^2, of tungsten 313 GN/m^2), both of exactly the same dimensions and 250 μm thickness, were simultaneously sputter deposited with 1000 Å thick alumina on to which a manganin film was flash evaporated under the same vacuum and both the films

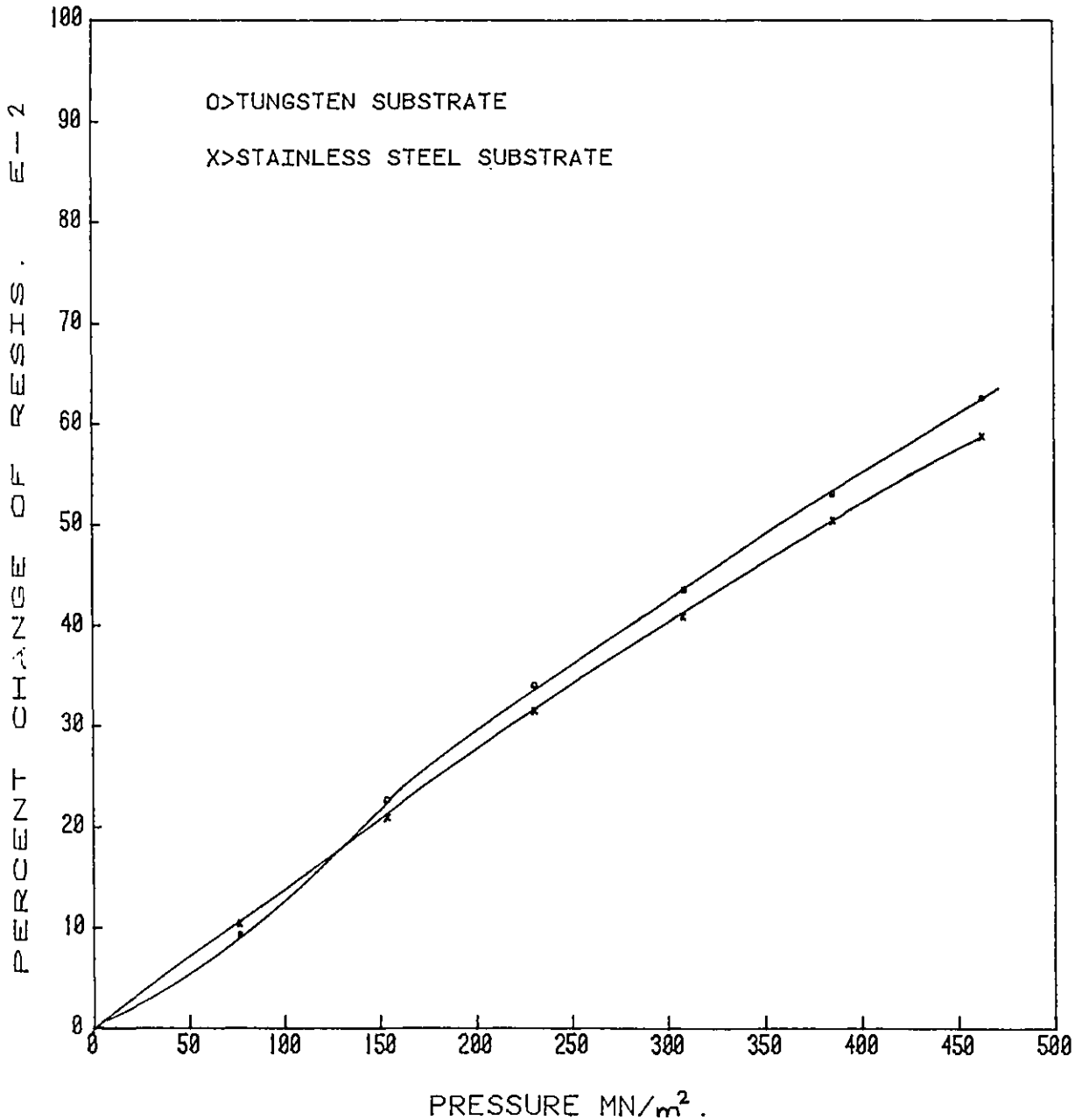

Fig. 4.11 Pressure coefficient of resistivity of thin film of manganin deposited on various substrates.

were subsequently annealed in vacuum simultaneously. In the hydrostatic pressure vessel test both the films behaved in exactly the same way as the films deposited on glass slide. Fig.4.11 shows the plots obtained in these experiments. The two films also show the type of slight pressure coefficient variation that were found to exist in films deposited at the same time. The film deposited on stainless steel showed a slightly better linearity than the film deposited on tungsten.

4.1.8 Sputtered Manganin

As we have mentioned earlier, manganin films deposited by sputtering show far better adhesion than the evaporated films and as the life of a device depends on the adhesion of the film, much effort was made in this project to deposit the manganin films by sputtering. Initially a 12.5 cm diameter target was made from a manganin sheet obtained from Goodfellow Metal Co. Sputtering was done under varying pressures of argon (between 1 to 10 micron) and varying powers (from 50 Watts to 200 Watts), but with all these depositions, the deposited films showed a change in colour compared with evaporated films, which show precisely the same colour as the bulk manganin. The sputtered manganin always showed a very deep almost blackish copper colour. Under Microprobe analysis all the deposited films showed a loss of manganese; generally the percentage of manganese varied between 8 and 10% and in the hydrostatic pressure vessel tests, the change in resistance of the film was found to be very non-linear and occasionally totally erratic. Fig.4.12 shows two such plots, obtained from two different samples, where some

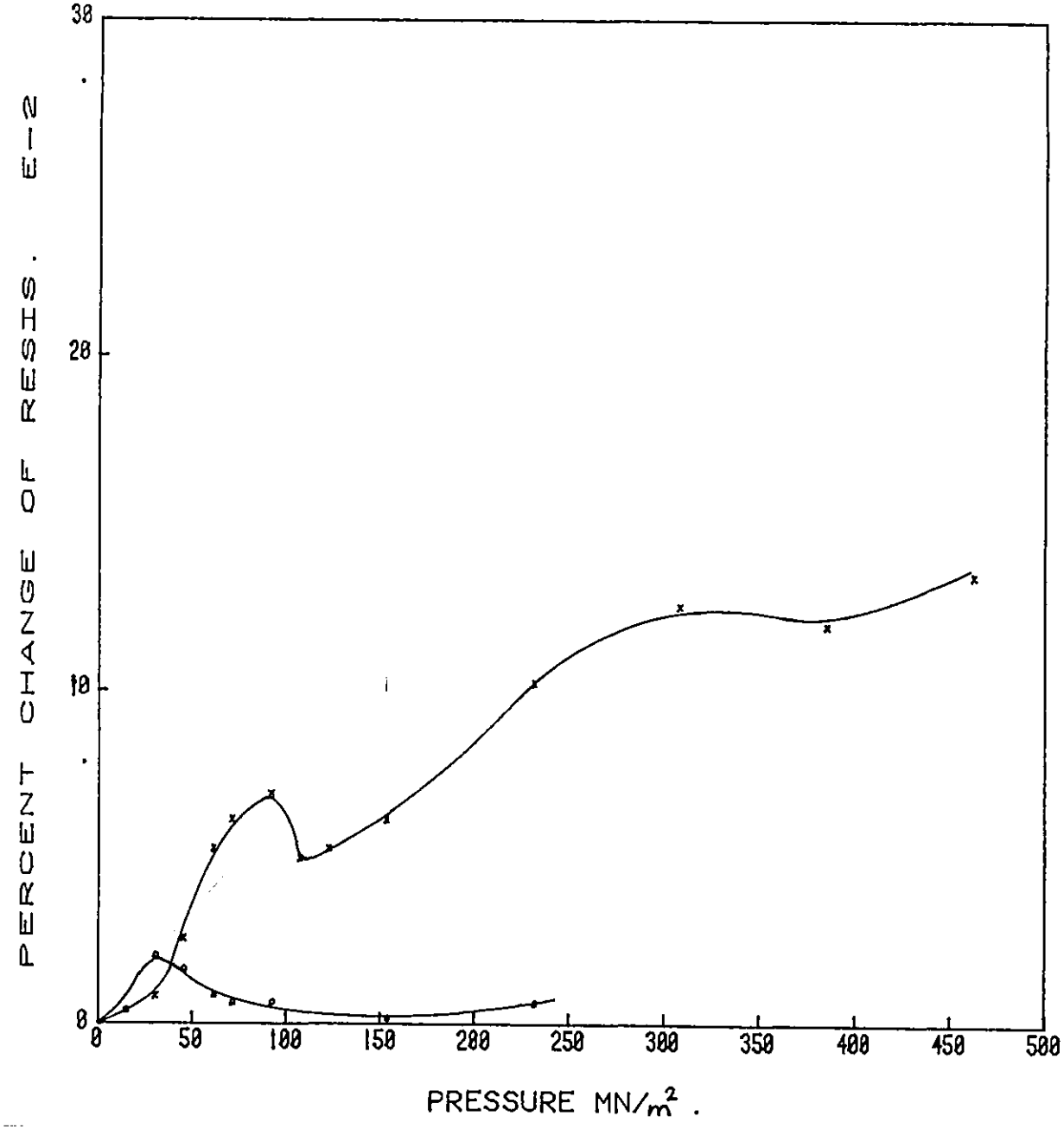

Fig. 4.12 Presssure coefficient of resistivity of thin films of manganin; deposited by r.f. sputtering.

reproducibility was obtained.

After the microprobe analysis, some alloys were made with higher percentage of manganese (upto 18% in 1% steps), which were formed into 5 cm diameter targets as mentioned earlier. Thin films deposited from these targets retained the dark colour and although microprobe analysis showed films with similar composition as bulk manganin, the same erratic change in resistivity under pressure remained in hydrostatic pressure tests. The most probable reason was thought to be due to the formation of manganese oxide during sputtering as manganese gets oxidised very easily and in microprobe analysis oxides cannot be detected.

4.1.9 Temperature Coefficient of Resistivity of Thin-Film Manganin

The temperature coefficient of the thin-film of manganin deposited by flash evaporation on glass slides as well as on discs were measured by dipping the films in an oil bath, which was gradually heated. To monitor the temperature of the substrate and thus the thin film, bulk thermocouples were mounted as close to the thin-film as possible by using silver loaded paint with an araldite overcoating for the glass-slide specimens and by soldering in the case of steel discs. The change in resistance was monitored using the Wheatstone bridge and D.V.M. combination. Electrical connection to the thin-films were made by soldering as mentioned earlier.

The temperature coefficient of an unannealed manganin film was found to be $\sim 2 \times 10^{-4}/^{\circ}C$ and remains reasonably linear up to a temperature of $\sim 60^{\circ}C$. Above that temperature it was found that the resistance of the non-annealed films

increases relatively fast and the change becomes mostly irreversible. A permanent change of upto 0.5% of resistance value was detected when the specimens were heated to 100°C and brought back to room temperature. This effect of permanent change of resistance was found to reduce substantially with the annealing of the films at 150°C over a period of upto 6 hours. Annealing was found to reduce the temperature coefficient of thin-film manganin substantially to a value between 0.8 ~ 1.5 x 10^{-4}/°C. Fig.4.13 shows a plot of the temperature coefficient of such an annealed sample of manganin film (12% manganese). An interesting phenomenon could also be seen in the plot, at temperatures around 75°C where the temperature coefficient shows a slight reduction in value. However, above a temperature of around 110°C it was found some permanent change in resistance starts to take place even with these annealed films. To study the possible effect on resistance of annealed manganin film passing through a high temperature contact zone at high speed in a disc machine, some films were rapidly dipped and removed from an oil bath at a temperature of around 120°C. There was no detectable permanent change in resistance value once the substrate was brought back to room temperature.

A further reduction of the temperature coefficient of manganin was obtained by heating the substrate to 150°C while the deposition of the manganin film was carried out and then annealing the film at 150°C for upto 6 hours. Fig.4.14 shows a plot of resistance change due to temperature for a film prepared by this method. The temperature coefficient of such a film was found to vary between 0.5 to 1 x 10^{-4}/°C at ~ 50°C. The change in temperature coefficient of the

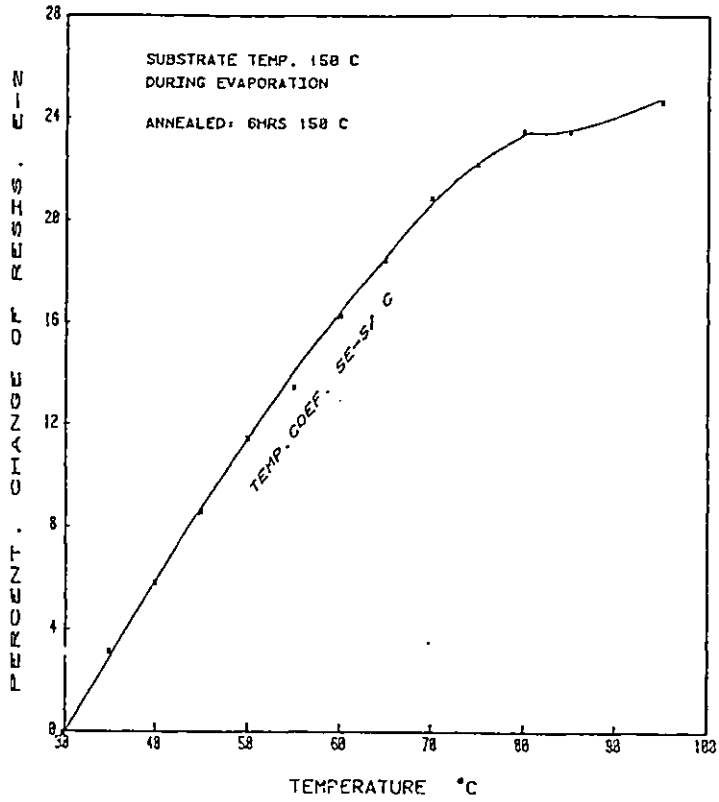

Fig. 4.14 Temperature coefficient of thin film of manganin deposited on heated substrate and subsequently annealed.

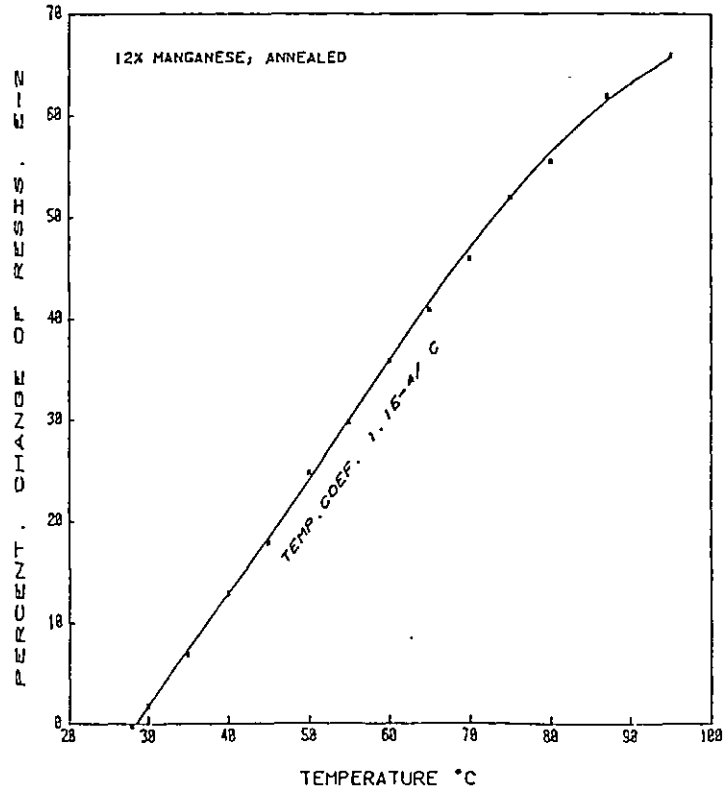

Fig. 4.13 Temperature coefficient of resistivity of thin film of manganin; annealed.

film at $\sim 80^{\circ}C$, as mentioned above, becomes more noticeable with these films, however, the problem of slight permanent change of resistance at ~ 100 to $110^{\circ}C$ was found to remain in these films as well.

The temperature coefficient of the evaporated manganin with 10% manganese in it was also determined and is reproduced in Fig.4.15 These films were annealed but the substrate was not heated during deposition. The change in resistivity of these films with temperature was found to be remarkably similar to the 12% manganese film deposited in the same way.

4.2 Temperature Coefficient of Thin-film Titanium

Thin-film titanium was used as the resistive temperature transducer. The temperature coefficient of titanium in bulk form is about $3.8 \times 10^{-3}/^{\circ}C$. However, in the thin-film form it was found to show a value between 0.5 and $1.25 \times 10^{-3}/^{\circ}C$. The lower values of around $0.5 \times 10^{-3}/^{\circ}C$ were found with the thin-film deposited by electron beam evaporation. The system in which electron beam evaporation was done had a poor ultimate vacuum of 10^{-5} torr, which might have produced slight oxidation of the film and this is thought to be the reason for the lower coefficient of the films deposited by this method. Films deposited by evaporation from a tungsten spiral immediately after a dummy evaporation of titanium to remove the residual oxygen at 5×10^{-7} torr showed the higher temperature coefficient of $\sim 10^{-3}/^{\circ}C$. The linearity of the temperature coefficient of resistivity was found to be much better when deposited by this latter method. Fig4.16 shows the plot of its temperature dependence of resistivity .

An attempt to measure the pressure coefficient of resistivity of thin-film titanium in the hydrostatic pressure

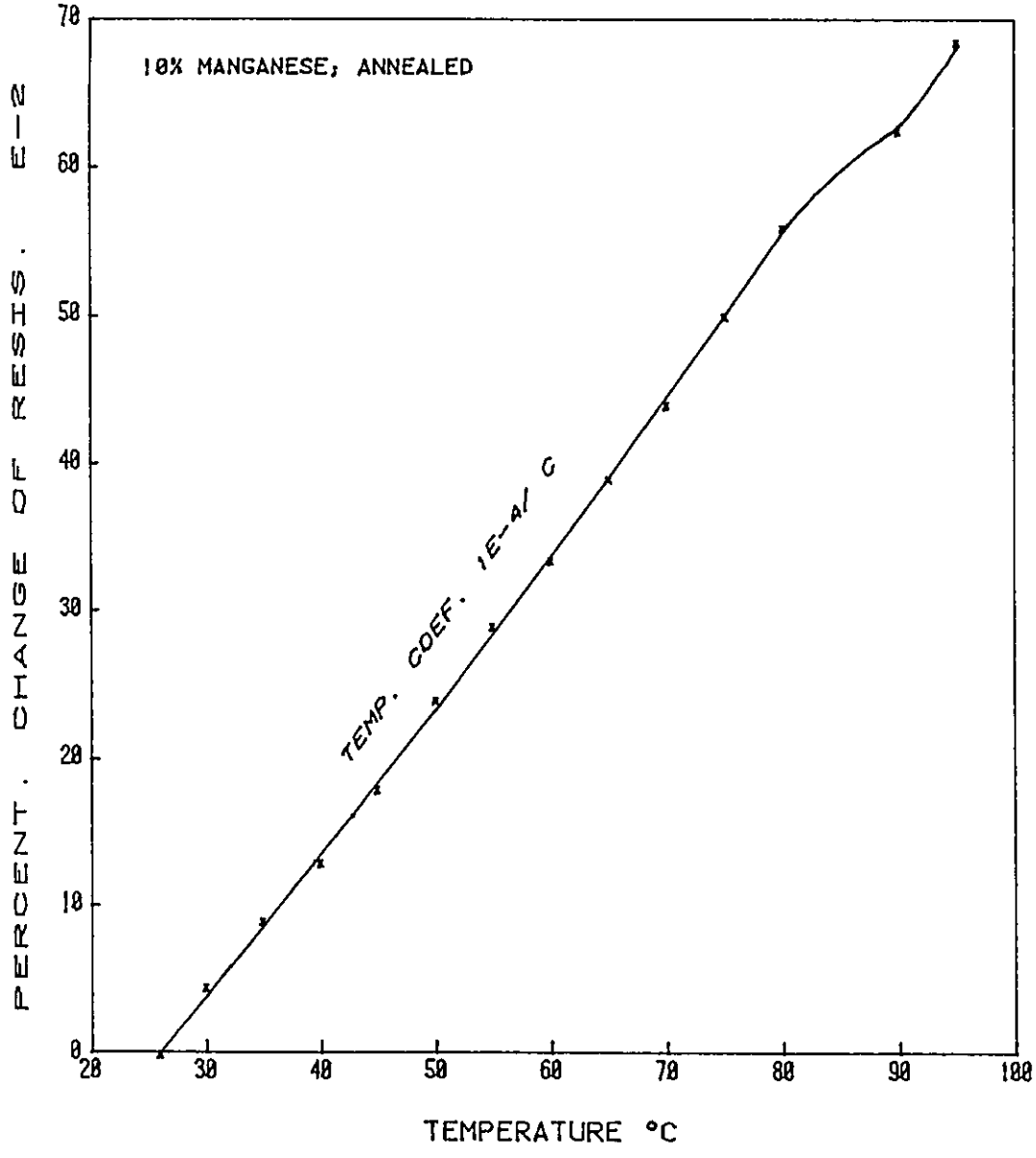

Fig. 4.15 Temperature coefficient of resistivity of thin film of manganin (with 10% manganese); annealed.

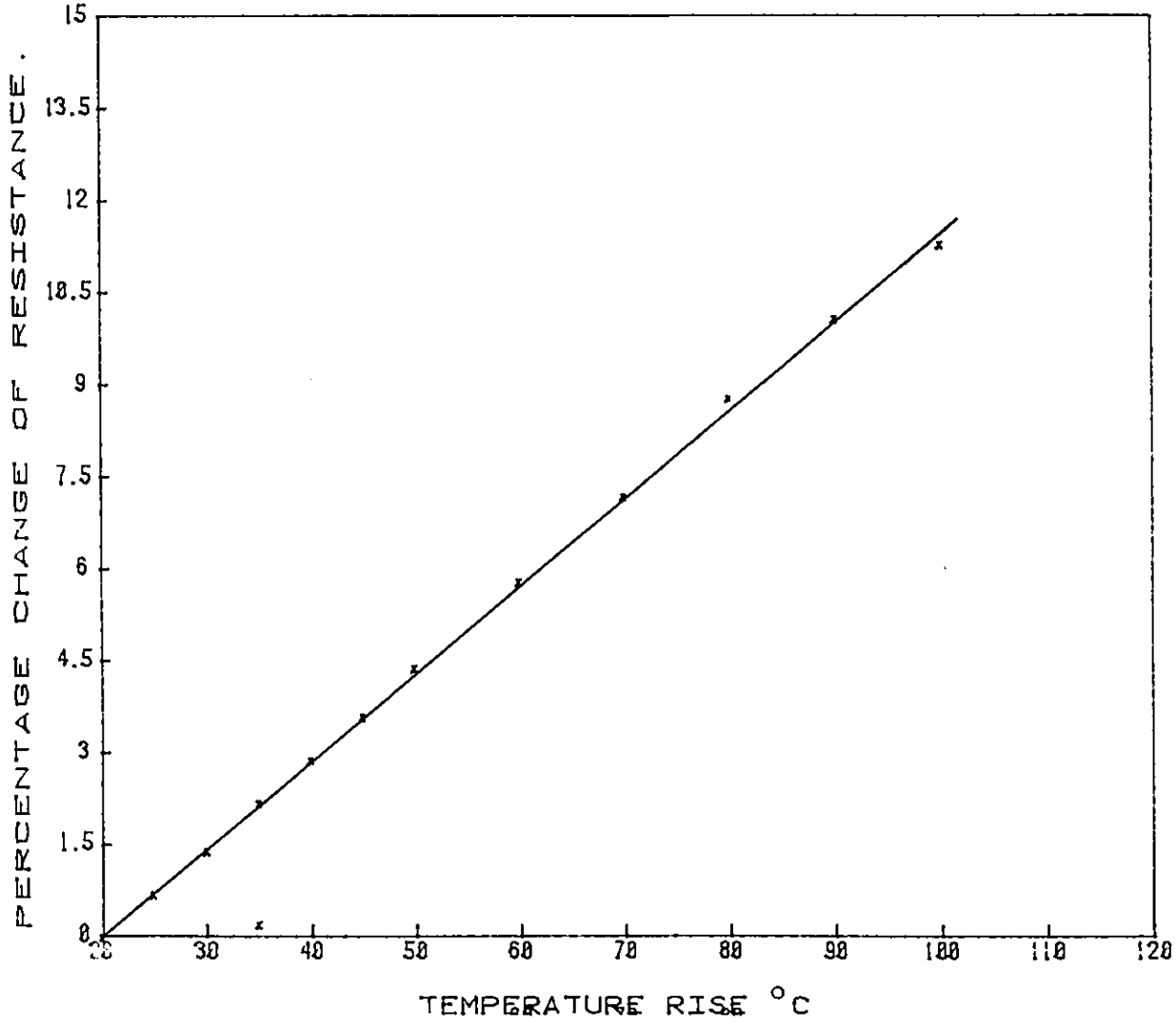

Fig. 4.16 Temperature coefficient of thin film of titanium.

vessel was not successful. This is because of the absence of any facility within the pressure vessel for rapid removal of the heat generated in the pressurising fluid. Thus, every time the fluid is pressurised or depressurised, a long time has to be spent to bring the temperature back to its original level very accurately, as the relatively high temperature coefficient of titanium can mask the effect of a substantial change in pressure even for a one degree variation in temperature. Although it is possible to bring the temperature back to original level, the slight drift present in titanium films makes it impossible to obtain reproducible results.

4.3 Thin-film Thermocouple

4.3.1 Calibration

Chromel (Chromium and Nickel) and Alumel (Aluminium and Nickel) were flash evaporated for the fabrication of the thin-film thermocouples. The film thickness of both chromel and alumel was $\sim$ 1000 Å and the junction area was 25 x 125 μm with the 25 μm in the direction of rolling of the disc. Devices were also fabricated on glass slides and stainless steel sheets. A layer 1000 Å thick alumina was used to isolate the device from the metallic substrate.

Chromel and alumel wires were used to form the electrical connections using silver loaded paint covered by araldite. Bulk thermocouples were either glued or soldered next to the thin-film thermocouples for the purpose of calibration. An oil bath was used to heat up the device and a D.V.M. was used to monitor the thermal e.m.f. generated by the thin-film device while an electronic thermometer was used with the bulk thermocouples.

The thermocouples were calibrated over the range of 30°C to 105°C. The linearity of the e.m.f. generated by the thermocouple output was found to be good, but the e.m.f's generated were found to vary from device to device over a range of about 30 μV to 42 μV/°C. Fig.4.17 shows such a calibration plot for a device deposited on a glass slide. The reproducibility of the signal generated by these devices was found to be remarkably good.

4.3.2 Strain Effect on Thin-film Thermocouples

Bridgeman (77) in studying the behaviour of the bulk thermocouples under hydrostatic pressure showed that the thermal e.m.f. generated by the thermocouples has an extremely low pressure sensitivity but the effect of strain is not very clear from this work. To determine the effect of strain on the thin-film thermocouples, a broad junctioned thermocouple was fabricated, using the usual technique, on a piece of 0.5 mm thick stainless steel sheet which was wrapped round a disc during fabrication. Thus the steel sheet with the fabricated thermocouple on it had a smooth curvature of 8.3 cm in diameter. The device was calibrated with this curvature. Later the steel sheet was carefully flattened out to generate stress in the thin-film and a second set of calibration readings was taken. Both the sets are reproduced in Fig.4.18. Hardly any difference between these two sets of readings could be detected.

4.4 Measurement of the Dielectric Constant of the Lubricating Oils

In measuring the oil film thickness by any of the capacitive methods, the dielectric constant of the oil under various pressure has to be known. As alredy seen from

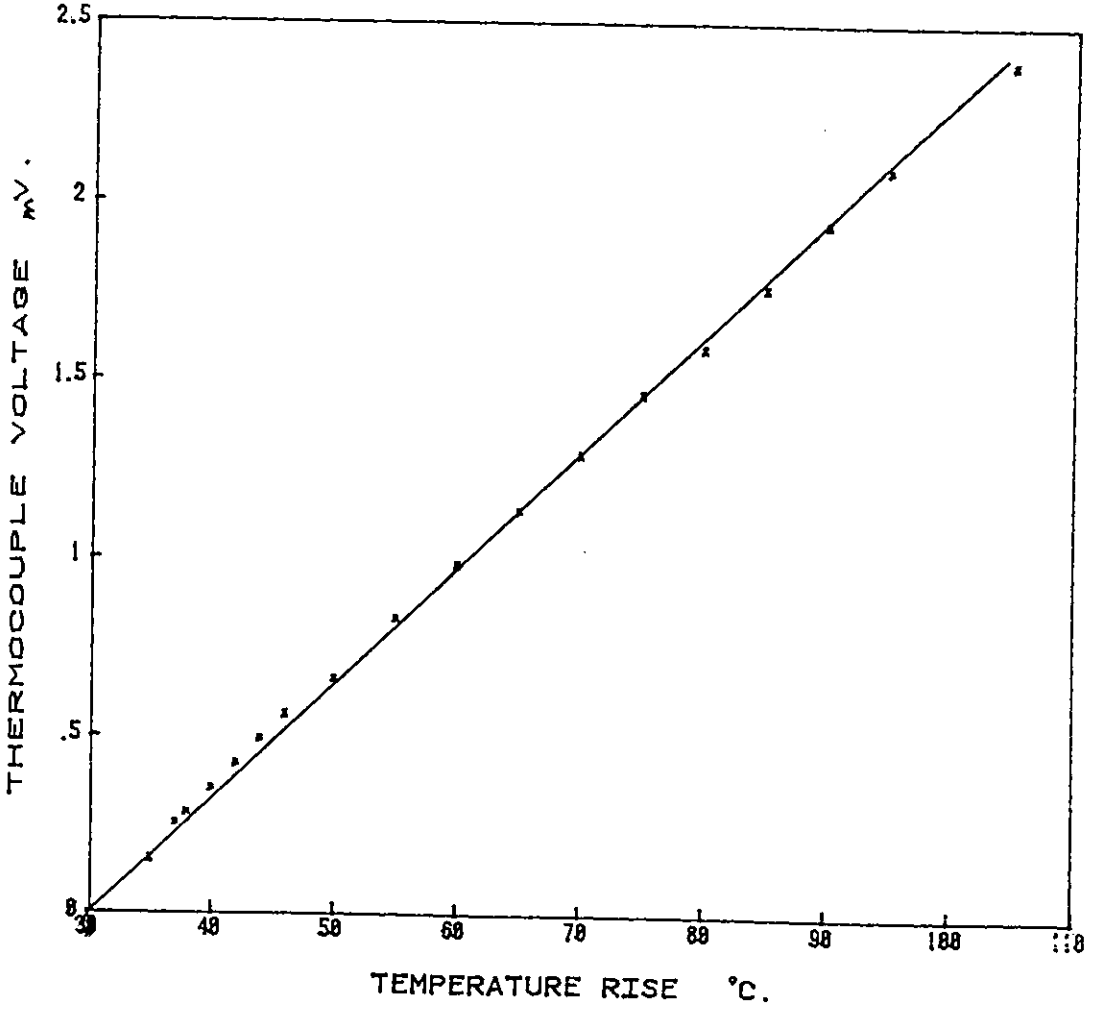

Fig. 4.17 Calibration plot of thin film thermocouple deposited on metal disc; thermocouple voltage against temperature rise.

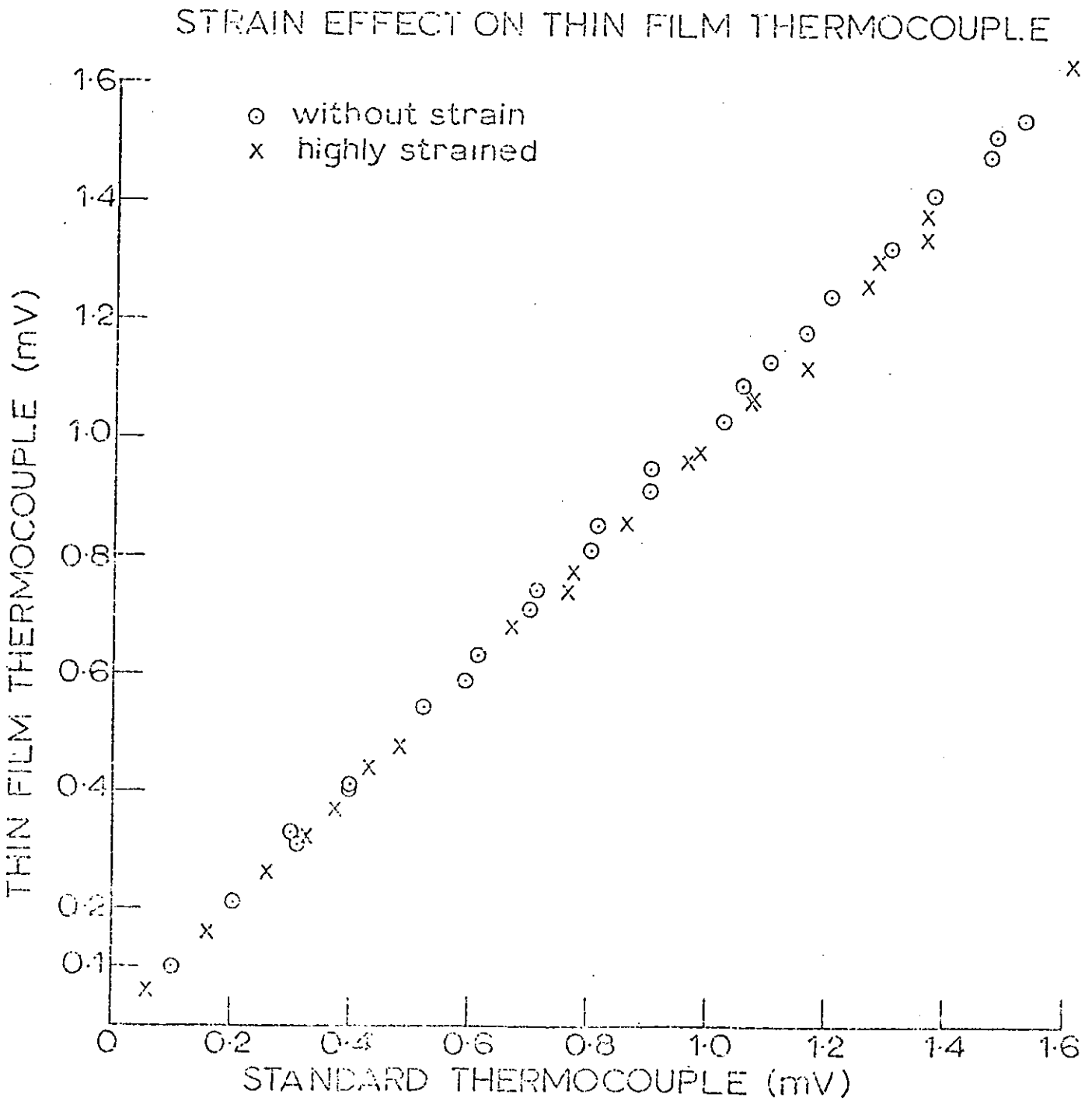

Fig. 4.18 Calibration plot of thin film thermocouple; with and without strain on the thermocouple.

Galvin et al's (55) work, the dielectric constant of the oils varies with pressure and with some oil the variation is substantial. In this project an experimental apparatus was made, using the hydrostatic pressure vessel, to measure the dielectric constants of the three oils used in the disc machine tests, under pressure.

Fig.4.19 shows the cross-sectional view of the hydrostatic pressure vessel with the positioning of a concentric parallel plate capacitor within it. The capacitor is formed by the two concentrically mounted copper tubes of 1.8 cm (o.d) and 2 cm (i.d.) in diameter with 1 mm wall thickness, rigidly mounted in two concentric slots machined on a piece of circular PTFE disc. With the tubes positioned in the slots, the gap between the two tubes was checked carefully for uniformity. Electrical connections were made on the inside wall of the inner tube and outside wall of the outer tube by soldering on copper wires. The whole structure was pushed inside the pressure vessel to sit rigidly on the lower platform of the cylinder of the pressure vessel.

A Wayne-Kerr bridge with 17 KHz signal source was used to measure the capacitance. Prior to taking any reading, the heat generated due to the compression of the lubricant was allowed to dissipate, as monitored by the thermocouple.

The capacitance formed by the parts of the two tubes exposed to the oil is the capacitance that should be used to determine the dielectric constant of the oil. However, the capacitance measured also included the parts exposed to the PTFE and the fringing capacitance due to cylinder wall, etc. To determine the capacitance contribution from the PTFE, the capacitance between the tubes was measured outside the pressure

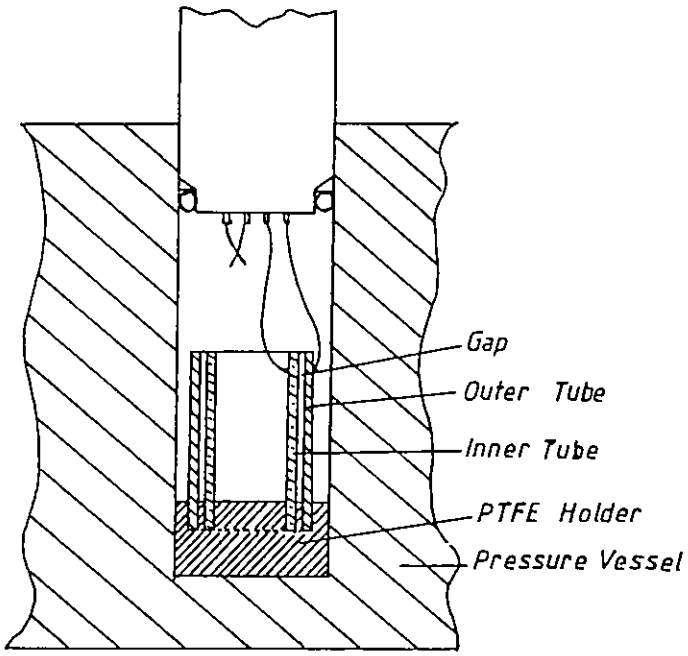

Fig. 4.19 Experimental apparatus for measuring relative permittivity of oils.

vessel. The possible capacitance due to the part exposed to air is calculated theoretically and subtracted from the above measured capacitance to give the capacitance value due to PTFE. The dielectric constant of PTFE was determined from this value and was found to agree with the published dielectric constant value of PTFE. The fringing capacitance value was determined by comparing the measured capacitance of the concentric tubes outside the pressure vessel with the gap between the tubes filled with the oil under test and the capacitance measured while the structure was inside the pressure vessel filled up with oil. Thus in later calculation for the dielectric value of the oils, these two excess capacitance values were deducted. However, this still leaves some uncertainties in the above calculation, as the change in pressure might change the values of these corrections, but as the added value of the above effect is only 10% in the case of the mineral oils and 6% in the case of diester oil, it can be safely assumed that the measured dielectric constant of the oils are reasonably accurate.

Figs.4.20 & 21 show the plot of the dielectric constant values of the oils measured under various pressures. It is interesting to note that the two mineral oils distinctly show a maximum and minimum followed by a gradual increase. This is consistent with the theory of the polar components of the oil. The diester oil did not show any such maximum or minimum over the pressure range covered in these experiments, and the dependence of the dielectric constant value on pressure is larger than the other two mineral oils.

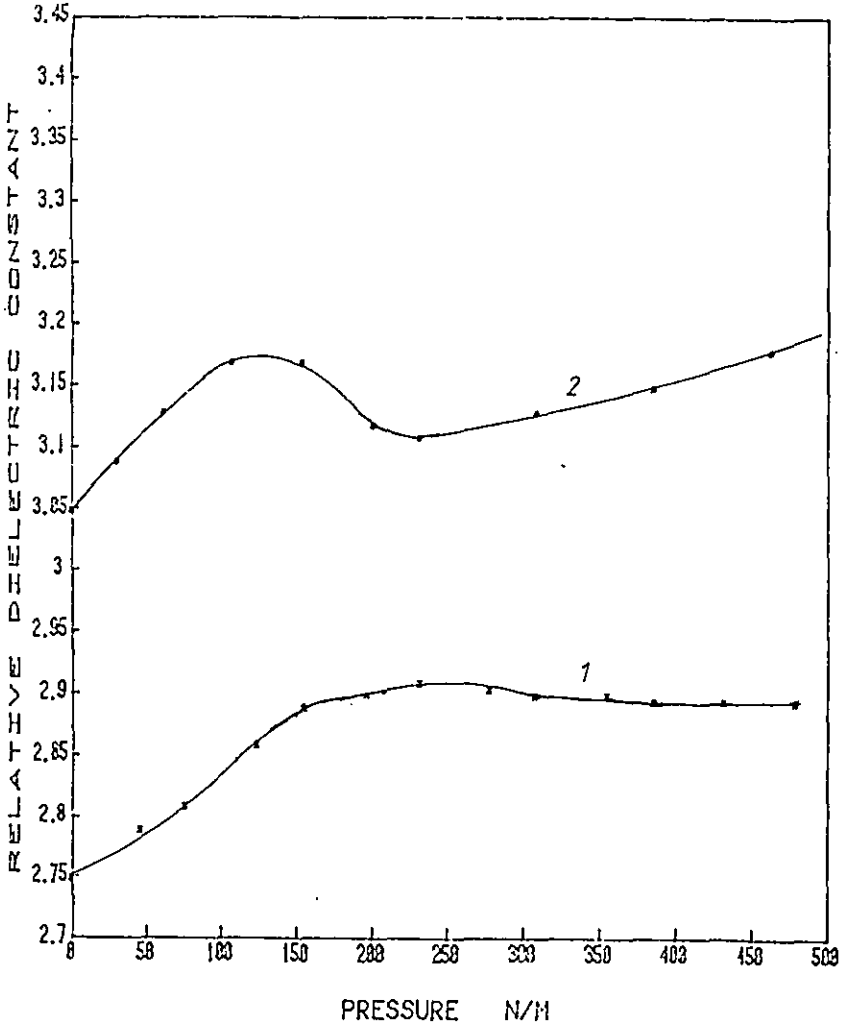

Fig. 4.20 Relative permittivities of oils 1 and 2 under various pressure.

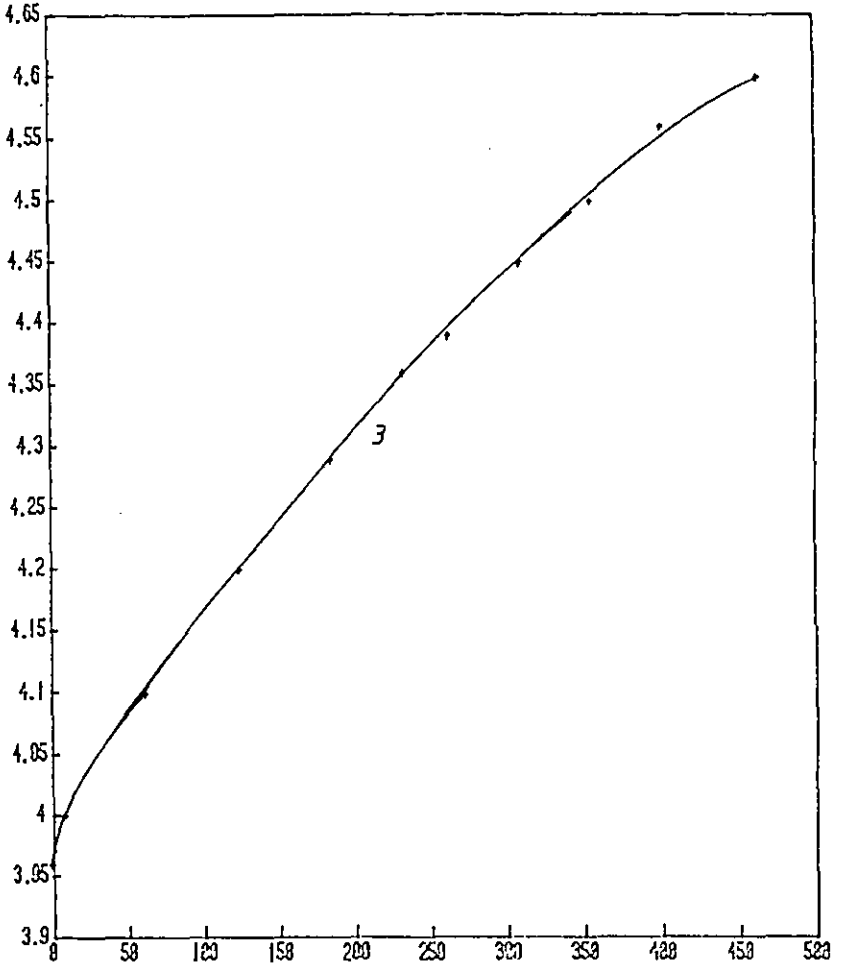

Fig. 4.21 Relative permittivities of oil3 under various pressure.

CHAPTER 5

EXPERIMENTAL APPARATUS AND GENERAL PERFORMANCE OF TRANSDUCERS

5.1 Description of the Disc Machine

A full description of the disc machine can be found in reference 88. A brief description is given below.

A general view of the machine is shown in figure 5.1a. Figure 5.2a shows a photograph of the two discs. These are 83 mm (3.26in dia) of outside diameter, 25.4 mm of axial width and have a wall thickness of 9.5mm. As can be seen one disc is chamfered at 8° to provide a 8mm (or 6mm) wide track.

The discs are arranged as shown in figure 5.2c each forming the outer rotating member of a hydrostatic bearing. Theyare loaded against each other by the three high pressure oil pockets, which form a stable self aligning arrangement, thus ensuring even loading across the track. The discs are driven through the shear pins from drive rings, which are in turn rotated by driving blades centrally clamped through onto the input shafts. An exploded view of the hydrostatic bearing and disc driving arrangement is shown in figure 5.2b.

The discs are driven and braked by a pair of "Dynadrive" units,which control the electromagnetic coupling and eddy current brake built inside the two squirrel cage motor housing. The dynadrive units to enable constant speeds to be maintained, independent of torque, was achieved by electronic feedback circuits. Timing belts were used to drive the shafts for the discs.

The same supply of lubricating oil, through a high pressure gear pump and a filter, is used to pressurise the hydrostatic bearing and to lubricate the discs.

(a)

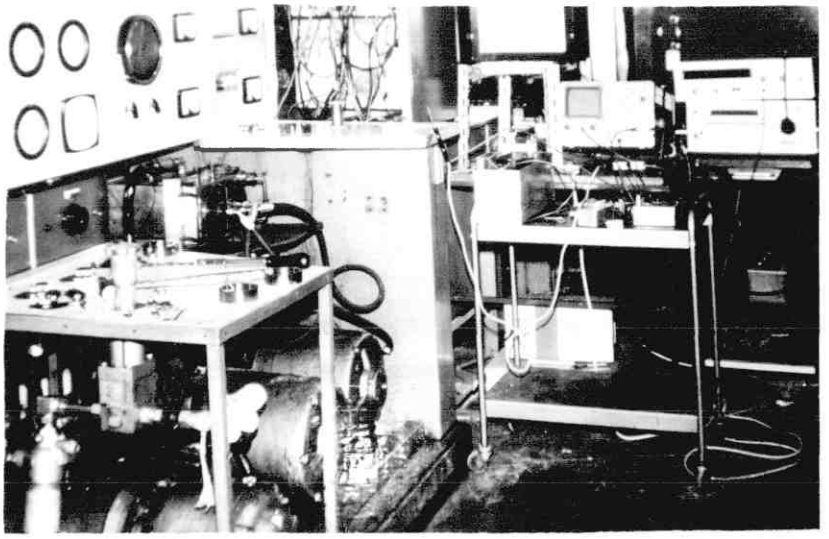

(b)

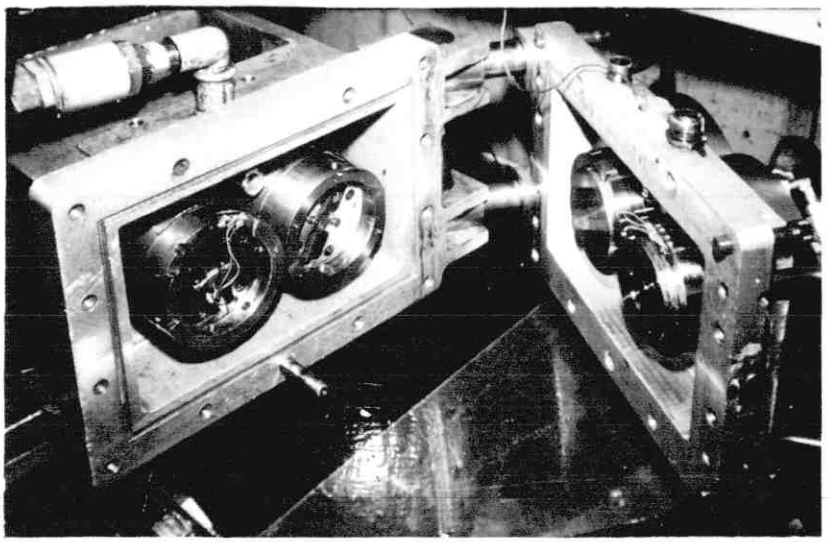

(c)

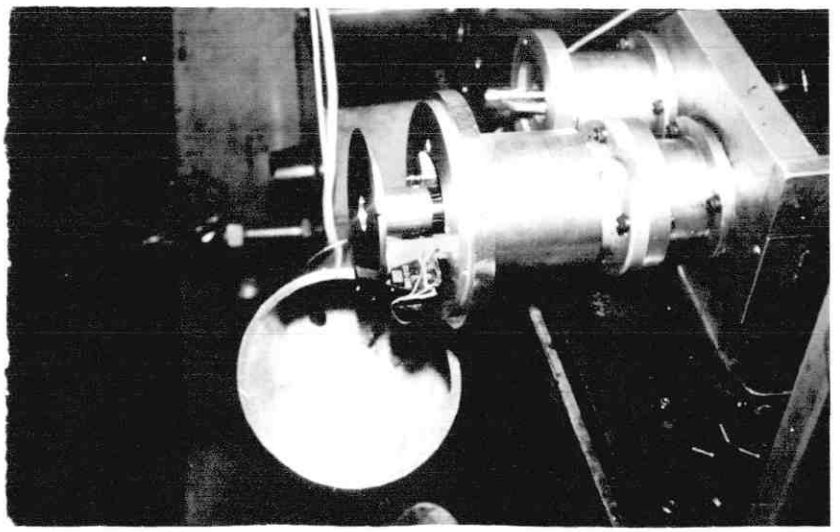

Fig. 5.1 General view of the disc machine(a); disc chamber(b); slipring assembly, triggering disc and the housing(c).

(a)

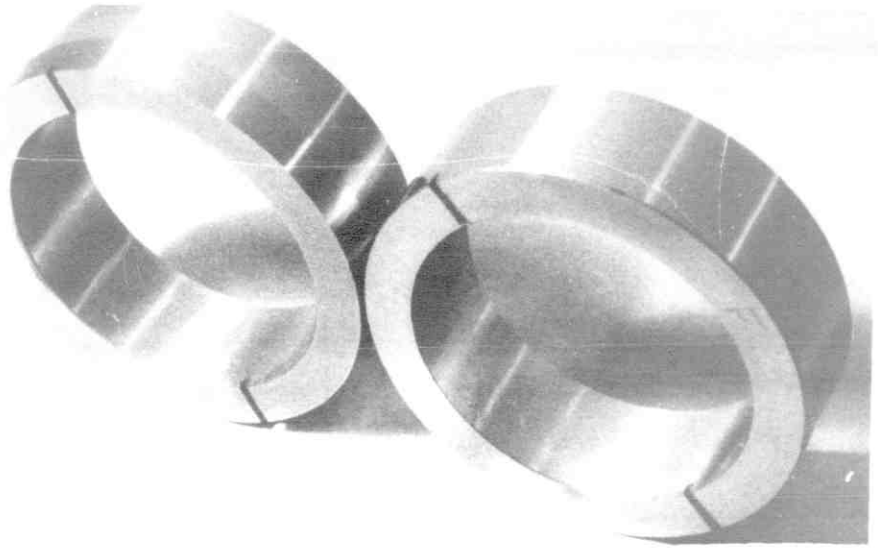

(b)

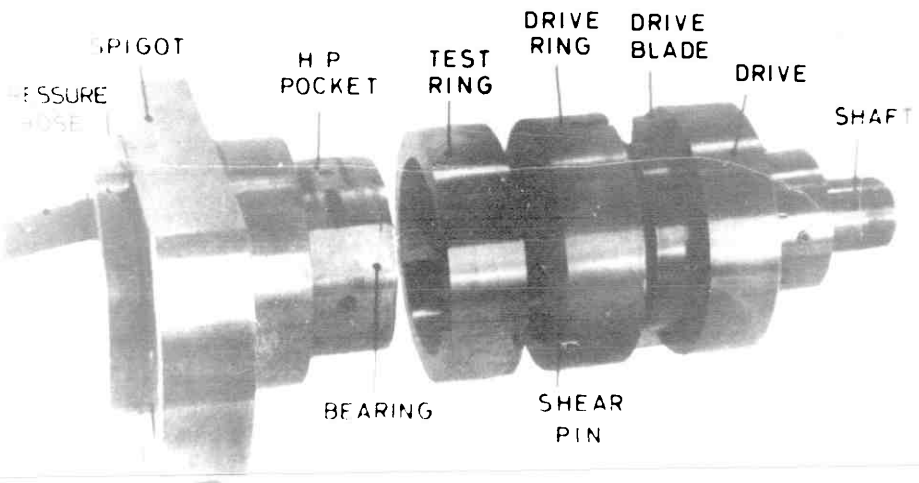

(c)

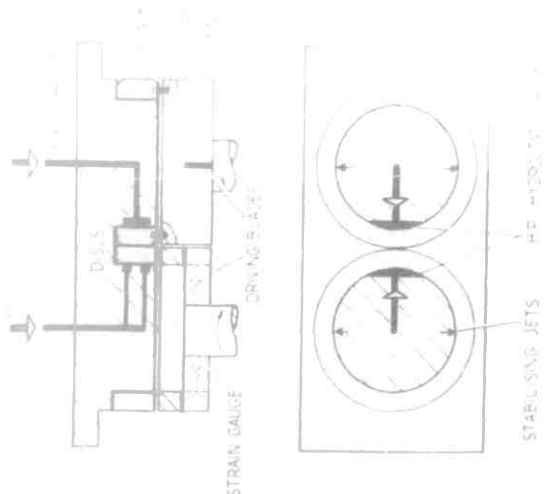

Fig. 5.2 Discs(a); exploded view of a hydrostatic bearing(b); cross-sectional view of hydrostatic bearing(c).

A water cooled oil cooler in the oil circuit provided the necessary temperature control of the oil.

A thermocouple mounted close to the contact point between the discs, in the disc housing, provided the oil temperature; while a pressure gauge mounted on the oil lines to the hydrostatic bearings provided the loading on the discs.

One of the drive rings, shown in figure 5.2b, was modified slightly to carry a set of electrical binding posts without shorting to the disc, as shown in figure 5.1b. A set of 3 wires and a pair of thermocouple wires were passed through this drive shaft to connect the binding posts on one end of the shaft to the slip rings on the other end. A metallic housing was made to cover the sliprings and the triggering device, and this was mounted on the slipring shaft, to avoid any electrical noise pick-up.

The hydrostatic bearing system in the disc machine was capable of providing a load of 1MN/m and a maximum surface velocity of 12m/sec. To start the discs rolling without appreciable sliding between the discs a load of around 0.23MN/m was necessary. At this load it was possible to run the discs upto a surface velocity of 3m/sec; above which sliding between the discs took place. The range of surface velocity that can be covered without sliding increased with the increase of load. Generally, at a load of around 0.55MN/m, the complete range of surface velocity could be covered. Although a minimum load of .23MN/m was necessary to start the discs rolling, it was found possible to lower the load down to 0.1MN/m over a very narrow surface velocity range once the machine was running.

5.2 Development of the Signal Monitoring Circuits

Four types of transducers were fabricated in this project, piezo-resistive pressure transducers, resistive temperature transducers, thin film thermocouples and capacitive film thickness transducers. The circuitry used for each device is described below.

5.2.1 Pressure Transducer

The piezoresistive pressure transducer fabricated with manganin showed a pressure coefficient of resistivity $(\Delta R/R)x(1/\Delta P)$ of $1.5x10^{-11}$ m^2/N. Hence for a change of about 1GN/min pressure 1.5% change of resistance would be expected. As the change is very small a very sensitive and noise free resistance monitoring circuit is necessary.

A high accuracy Wheatstone bridge was chosen for monitoring the resistance of the sensor. This bridge was calibrated for the measurement of the unknown resistance. Once the bridge was balanced with the unknown resistance in place the dials of the bridge gave the direct measured value of the unknown resistance with an accuracy of 0.1%. An amplfier with a gain of 10 was used in place of the usual galvanometer, as shown in figure 5.3. The output of the amplifier was connected to an oscilloscope. The input impedance of the amplifier was 50KΩ. The bridge was excited by a 3V battery which caused a current of 2mA to flow through a transducer having a resistance of 150Ω. This current was low enough not to cause any unwanted heating effect in the transducer.

The variation of resistance in the transducer showed up as the unbalanced voltage at the output of the bridge and was amplified and finally recorded in the oscilloscope. The

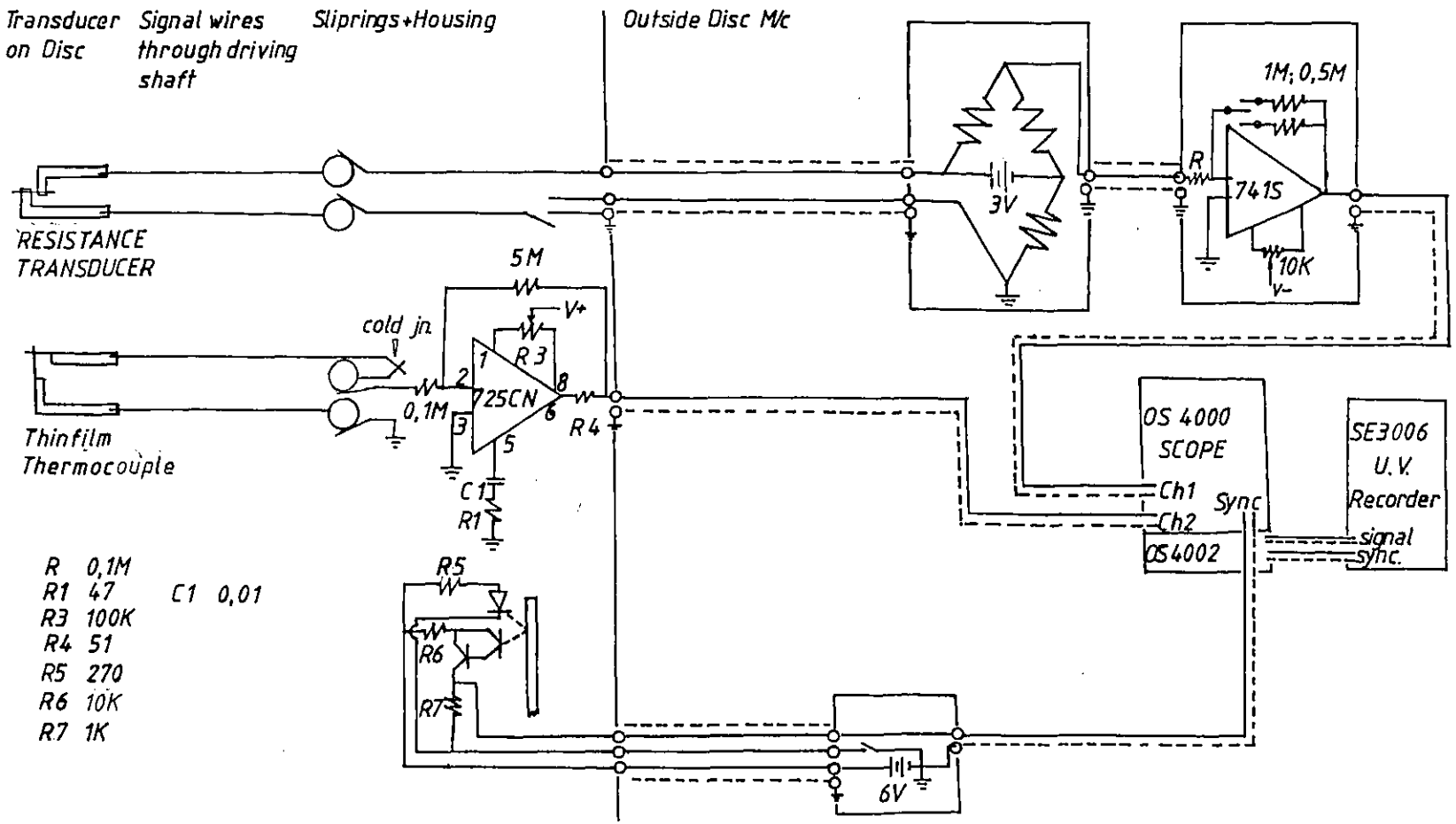

Fig. 5.3 Transducer signal monitoring circuits used with the disc machine.

relation between the change of unknown resistance and the corresponding output voltage change is shown in figure 5.4. A decade box of resistance was used to simulate the transducer and the unbalanced voltage was measured with a digital voltmeter. The bridge was balanced with a 150Ω resistor and higher values in 1Ω steps. The linearity was found to be good.

The frequency response of the complete circuit shown in figure 5.3 was checked with the equipment in position for operation. The bridge was unbalanced slightly with a pressure transducer connected to the bridge through its usual circuitry, the battery was removed and an oscillator was connected across the battery terminals and the unbalanced signal was monitored. Then the oscillator was connected across transducer terminals and again the unbalance signal level was monitored. In both the cases the frequence respose was found to be flat upto 200KHz, falling off rapidly at higher frequencies. The limiting factor was the amplifier.

5.2.2 Temperature Transducer

The circuit used for pressure transducers was also used for resistive temperature transducers.

The materials used for thin-film thermocouples were evaporated chromel and alumel. In the previous chapter it was shown that, even in thin-film form, this combination generates a themoelectric emf of 40μV/°C rise of temperature. Chromel and alumel wires were connected to the appropriate thin-films. These wires, running through the driven disc shaft, were welded together at the slipring end of the shaft to form a cold junction. The signal was taken from a break in the chromel wire, the two ends of which were connected to sliprings.

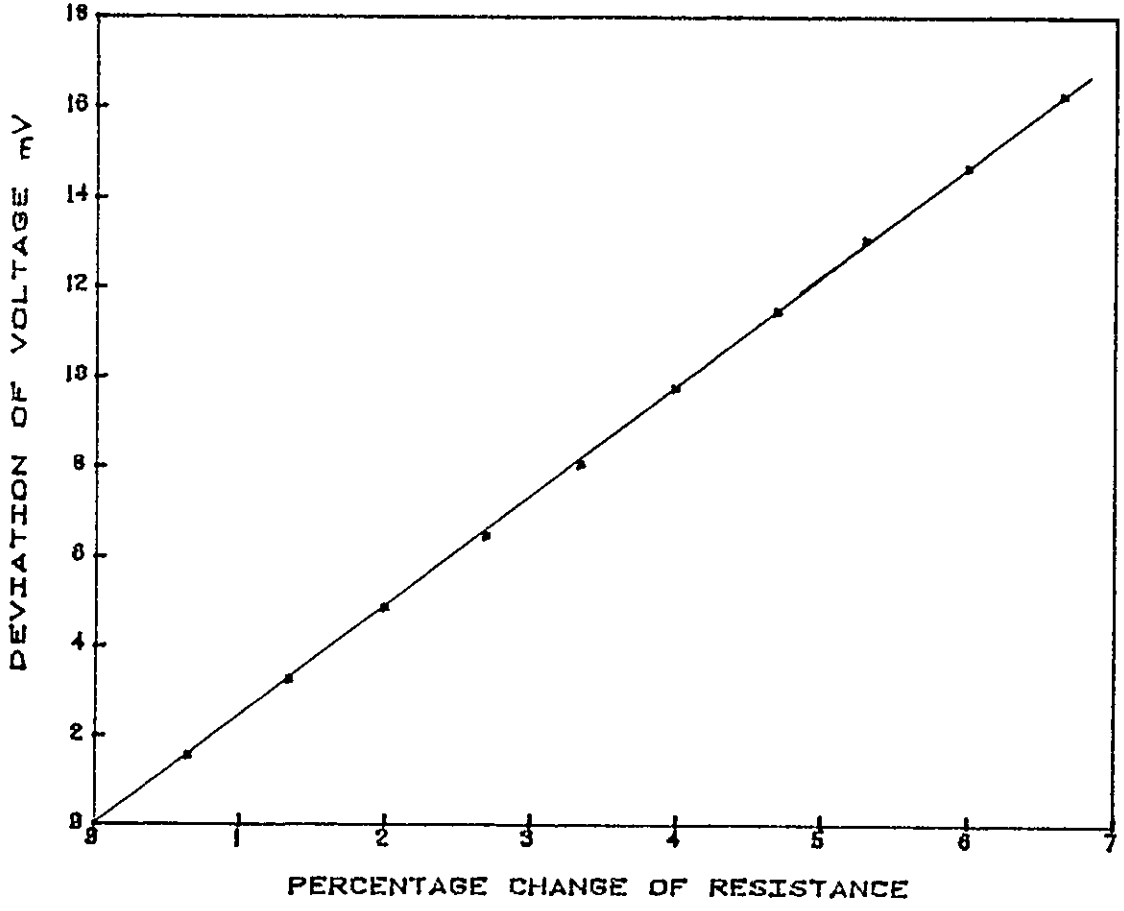

Fig. 5.4 Calibration of the bridge circuit.

An amplifier with a gain of 50 was mounted inside the metal housing of the slipring assembly. The input impedance of the amplifier was made to be 50KΩ. This was a compromise between the high impedance required for the thermocouple and the vulnerability to noise of high impedance cicuit. The amplifier was mounted as close as possible to the discs, a distance of almost 50cm. The signal from the amplifier was transmitted to the oscilloscope by well shielded wires.

5.2.3 Capacitive Film Thickness Monitor

Figure 5.5 shows the simple electrical circuit required for monitoring the oil film thickness with the rate of change of capacitance sensor.

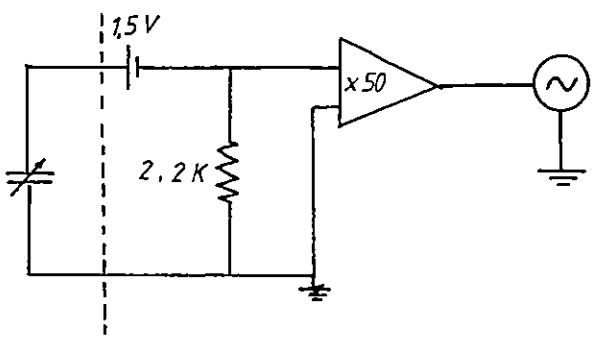

Fig. 5.5 Electrical Circuit Used With Capacitive device

A single 1.5V cell was used to energise the circuit. The voltage that develops across the 2.2KΩ resistor, due to the charging current of the increasing capacitance formed between the device and the mating disc, as the leading edge approaches and passes through the contact, was monitored. The maximum voltage developed across the resistor was generally of the order of a half millivolt. An amplifier with a gain of 50 was found suitable to raise the signal level sufficiently for recording in the oscilloscope.

The possible leakage current in the capacitor formed between the electrode-alumina-metal disc was also checked with the above circuit. The devices used never showed any detectable voltage across the 2.2KΩ resistor when the circuit was energised, thus the leakage current was negligible enough not to cause any error in the signal generated.

5.3 Method Used for Signal Recording

A dual beam analogue oscilloscope was initially used for monitoring and storing the fast transient signal generated by the various transducers. Permanent recording of the stored signal from the analogue oscilloscope was achieved by Polaroid photography. This method of recording was found to have two problems. Firstly, although in its ordinary mode the analogue oscilloscope had a frequency respose of 10MHz, in the storage mode it was unable to produce a permanent recording on the screen of the fast transient part of the pressure profiles, such as the pressure drop in the secondary pressure peak zone. Secondly, the time required to load, unload and develop the polaroid picture limited the number of results that could be obtained from an experiment.

The above method was superceded when a digital storage oscilloscope was acquired. This oscilloscope in the digital mode could sample the analogue signal at a rate of upto 1.2MHz which limits its frequency response to 600KHz. The sampled signals were digitised and stored in a memory which was scanned contineously and displayed on the CRT. This signal which is stored in the memory can be brought out in a form suitable for permanent recording, on a chart recorder. Initially an ordinary chart recorder was used, however, due to the very low frequency response of such a chart recorder, about 5Hz, 3 minutes was required to

record a signal. Later, the chart recorder was replaced by an ultraviolet recorder with two galvanometers with 1KHz frequency response. With this equipment it was possible to transfer a trace in 10 seconds from the oscilloscope to the UV recorder without any loss of information.

5.4 Triggering Device

The circumference of the test disc was 26cm whereas the contact width between the two mating discs under load was less than 1mm. The signals that the transducers generate while passing through this contact is the only interesting part over a whole revolution. Hence to get a resonably large picture of the signal while the transducer is in this zone, the oscilloscope must be triggered just before the transducer enters the contact region.

The discs in the disc machine were enclosed in a metal chamber which was flooded with oil, thus it was not possible to obtain a synchronising signal from the discs. Instead a metal disc, with a fine redial slot, was mounted on the drive shaft at the rear of the slipring assembly. An optical coupling was mounted in such a way as to detect the slot. A more precise and reliable system was developed subsequently using reflected rather than transmitted light. The same disc was used, this time with a thin black line which interupted the light each time it passed infront of the detector.

The output of the optocoupler was a rectangular pulse about 5V in magnitude. To improve the triggering, this pulse was passed through a differentiating cicuit to produce two large, sharp spikes. The oscilloscope was found to trigger well with either of the pulses depending on whether it was set for positive pulse triggering or negative pulse triggering.

For some purposes it was found necessary to study a wider region of the contact, particularly the area where the electrode enters into the contact zone. A variable time delay device was therefore constructed as shown in figure 5.6. It was connected between the optocoupler and the differentiating network, and could delay the triggering pulse by upto 10ms. By placing the black line on the disc well in advance of the leading electrode, the whole area covering the leading electrode transducer and the trailing electrode entering the contact zone could be monitored.

5.5 Measurement of Speed

The disc machine drive units had tachometers fitted, mainly for providing feedback to the speed controllers. The outputs of these two tachometers were connected to two analogue meters showing the rotational speed of the motors. These two analogue meters were found to be inaccurate. Thus to monitor the speed accurately, an electronic speed measurement circuit was devised using the triggering circuitry described above. An electronic counter with accuracy better than 0.1% was used to measure the time lapse between two succesive pulses from the triggering device. As the pulses were taken after the differentiating network, they were clearly defined and the accuracy of speed measurement was found to be very good.

5.6 Procedure Followed for Running an Expriment

5.6.1 Preliminary Test on the Devices

Before a disc with a transducer fabricated on it could be mounted in the disc machine for an experiment, some preliminary checks were carried out on the device itself. For the pressure and temperature transducers, the temperature coefficient was measured by dipping the disc into an oil bath. For a few devices the the

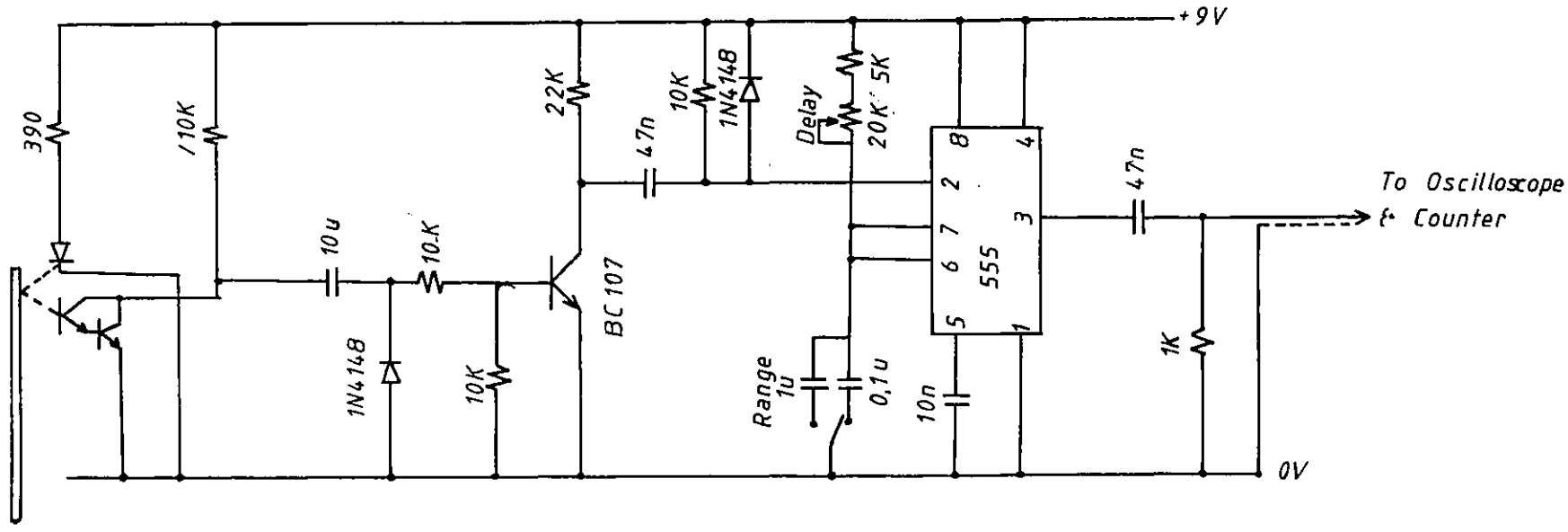

Fig. 5.6 Variable time delay circuit used in conjunction with the triggering device.

temperature coefficient of resistance was found for each 10°C rise of temperature from 20°C to 110°C. For most of the pressrure sensors this was done at 20°C and 60°C only. A calibration curve for a temperature transducer is shown in figure 4.14 in the previous chapter. Within the wider temperature range, temperature transducer showed linear variation of resistance with temperature.

5.6.2 Setting-up of the Disc Machine

The transducers were always fabricated on the plane discs. The mating discs were chamfered on both sides at an angle of about 8° leaving a plane land either 6mm or 8mm wide. The 8° angle allowed enough space at the edge of the discs for joints, soldered to the electrodes, to pass through the contact zone without touching the mating disc or developing excessive pressure.

Once the preliminary tests on the discs were complete, the position of the trigger point was adjusted. Initially, with the fixed trigger, an accurate trigger point was achieved by rotating the two discs on the shafts until the active element was within the contact, and making a mark on the triggering disc in line with the opto-isolator. The discs were then removed and the triggering cicuit was checked for proper functioning by manually rotating the shaft.

Next the discs were properly mounted on their hydrostatic bearings, the chamfered disc was always mounted on the driving side. At this point the position of the thermocouple was adjusted so that the tip lay 10mm away from the contact in the inlet region. The short signal wires from the transducers were soldered to binding posts mounted on the drive ring. The signal monitoring circuits were energised at this stage to check for operation and the circuits were kept energised when the slots on the discs and

the shear pins were matched and the chamber was sealed. The shafts were then rotated manually and the trace on the oscilloscope was monitored. This was necessary to check for possible short circuits from any loose wire touching the disc housing.

5.6.3 Experimental Procedure

The oil pump was allowed to run for about 15 minutes and cooling water was regulated to stabilise the oil temperature in the machine. The hydrostatic bearings were then pressurised (to a load of 0.23MN/m) by opening the loading valve and pressure was monitored on the pressure gauge. The driving motors were then started with the speed controller energised but set at zero position which kept the electromagnetic clutch disengaged. The noise level in the electronic circuitry presented problems initially but was reduced by ensuring that no earth loops occured in the circuit and by running the experiments outside the normal working hours.

Once the initial readings such as the resistance value of the resistive type transducer, the gain of the amplifiers used etc were recorded the oscilloscope and the electronic counters were switched to external triggering. The disc machine was then started by slowly turning the speed controller from the zero position to a speed of about 150 rpm. Extreme caution was necessary to start the machine, as any sudden change of speed always produced severe sliding between the two discs which could destroy a device. In orderto raise the speed further, and develop a reasonable oil film, the load on the discs had to be increased to at least 0.3MN/m. For this reason most of the initial readings in the experiments were taken at this load.

The temperature of the circulating oil was observed to

change once the discs started to rotate. At a speed of 500 rpm a rise of upto 10°C from the initial temperature was noted, equilibrium being attained quite quickly. By regulating the flow of the cooling water the temperature of the oil was set at the operating temperature for the experiment, which was normally 50°C for oil 1, 52°C for oil 2 and 30°C for oil 3. The viscosity for oils 1 and 2 was 0.1 Pa.sec. at the operating temperature of the oils, while for oil 3 it was 0.039 Pa.sec.

When the operating temperature of the oil was stabilised, the signals from the transducers were recorded. To record a signal the trigger set button of the oscilloscope was energised manually so that the oscilloscope would record the signal generated immediately after the next trigger puls. The sweep speed of the oscilloscope was adjusted according to the speed of the discs. The analogue oscilloscope was used upto a sweep speed of 20 μs/div whereas the maximum sweep speed available for the digital storage oscilloscope was 50 μs/div. When the trace was recorded on the oscilloscope, a permanent recording was made by photographing the screen or with the UV recorder for the digital oscilloscope. This operation together with tabulating the relevant data took between 3 to 5 minutes. Thus depending on the life of a device, 10 to 15 traces could be recorded in an experiment. Usually a single recording was made under particular operating conditions. However, to ensure that the trace recorded was reproducible, about ten traces were examined in the oscilloscope before making a permanent recording.

Sliding between the discs was achieved either by applying the eddy current brake on the driven shaft or by raising the speed of the driving shaft beyond the range of pure rolling for a

particular load. The second method was used to avoid the use of the eddy current brake which was found to become unstable, under certain operating conditions.

5.6.4 Disc Surface Temperature Measurement

In conducting the experiments in the hydrostatic disc machine, the temperature of the oil was measured, about 1cm away from the actual contact zone at the trailing end. This was the nearest point to the contact where a thermocouple could be placed safely. However, this temperature was expected to vary from the surface temperature of the disc. As a result an experiment was carried out to determine the difference between the temperature monitored by the trailing end thermocouple and the actual disc surface temperature. To achieve this, a very fine pair of chromel and alumel thermocouple wires were spot welded, 1mm away from the track on the plane disc, to form the hot junction. The thickness of the junction was made to be very thin and it was covered with a thin layer of araldite, so that the temperature measured by the thermocouple was the disc surface temperature and not the oil temperature. The rest of the thermocouple wires were passed through the driving shaft and a cold junction was formed near the slip ring assembly. The chromel wire was broken to form contacts with the sliprings. A DVM was used to monitor the emf generated by the thermocouple. The usual thermocouple near the trailing end was also carefully mounted to monitor the inlet oil temperature.

It was found that a reasonably linear variation of the temperature difference exists (between the disc surface and inlet oil temperature) with the variation of the surface velocity and load. An increase of suface velocity by 1.5m/sec or

load by 0.3MN/m produced an increase of 1°C in the difference between the two themocouple readings over the entire operating range of the disc machine.

This test could only be performed with oil 1 under pure rolling conditions.

5.7 Change of Oil

The disc machine required a charge of 5 litres of oil to operate satisfactorily. In addition to this, a litre of oil was necessary to flush out the system. Major components such as the filter and heat exchanger needed to be dismantled and cleaned in organic solvent. Under the circumstances, all the development work and most of the initial experiments were carried out with one oil, which was Shell Spirax SAE 90, designated oil 1.

The second oil (oil 2) used in this project was a mixture of two different oils, specially prepared to obtain a high pressure-viscosity coefficient.

The third oil (oil3) used in this project was ASTO 555. This was chosen because of its low viscosity and pressure viscosity coefficient. The use of these three oils enabled a wide range of viscosity and pressure viscosity coefficients to be examined. Figure 5.7 shows the viscosity-temperature characterstics of all three oils and table 5.1 shows additional data.

Table 5.1

Oil	Type	Viscosity at Temp.	Pressure Viscosity Coefficient
SAE 90	Mineral	0.0168Pa.sec at 99°C 0.231 Pa.sec at 38°C	2×10^{-8} Pa^{-1}
Special Mixture	Mineral	0.0125Pa.sec at 99°C 0.5 Pa.sec at 30°C	3.05×10^{-8} Pa^{-1}
ASTO555	Diester	0.00125Pasec at 99°C 0.039 Pa.sec at 30°C	0.95×10^{-8} Pa^{-1}

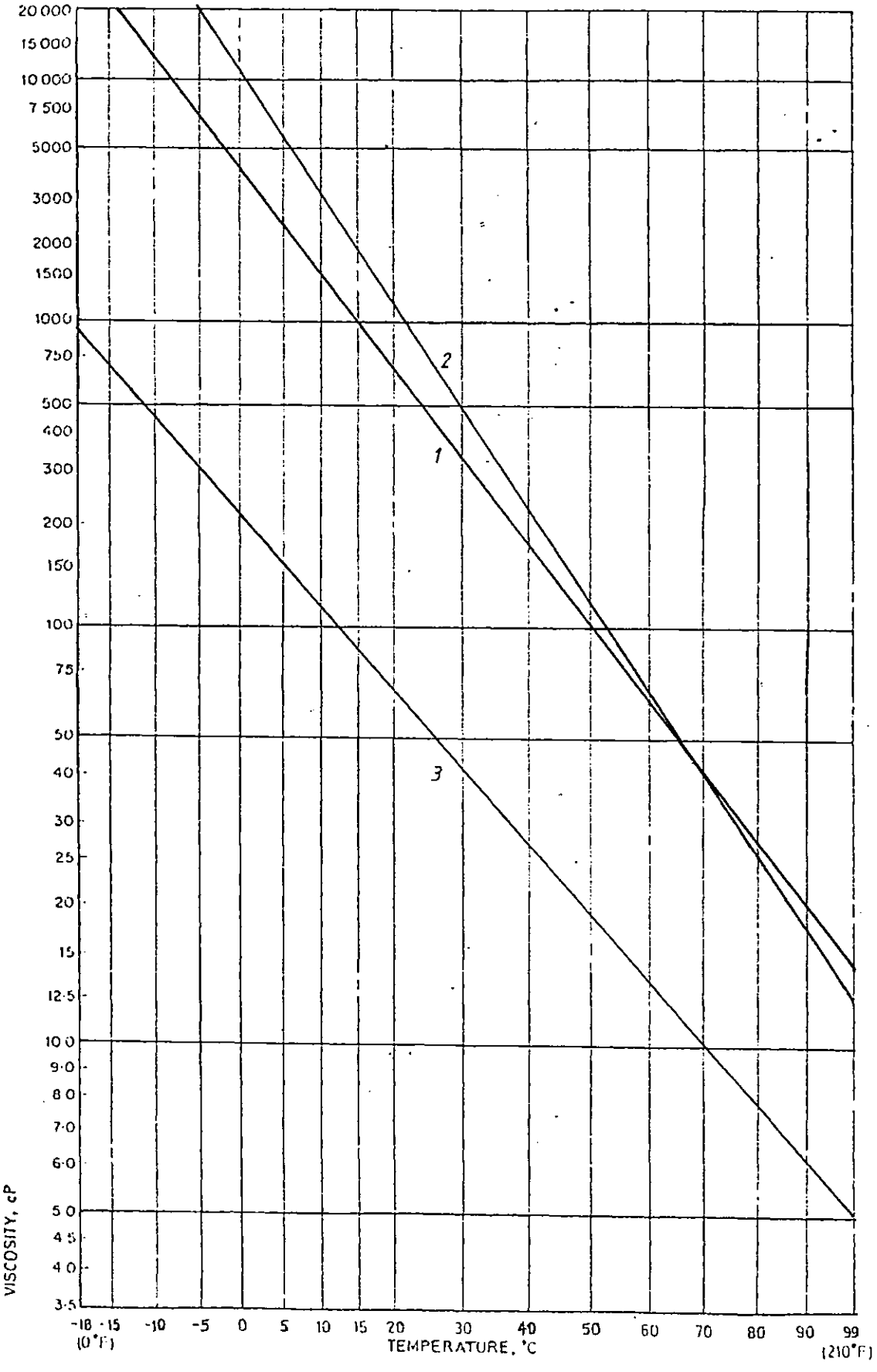

Fig. 5.7 Viscosity-temperature characterstics of the three different oils used in this project.

5.8 Life of Thinfilm Transducers

Two factors primarily determined the life of a thinfilm transducer, the technique used to fabricate the device and the severity of the running conditions of the disc machine. The use of different fabrication techniques to improve adhesion was discussed earlier. The different types of failure that occured in the disc machine are considered now.

Figure 5.8 shows photographs of discs with the earlier type of pressure transducers (two active elements with a common electrode) where the electrode and the active element were deposited seperately. Figure 5.8a shows a device before the disc machine test and figure 5.8b shows a similar device after it had failed in operation. It can be seen that part of one of the trailing electrodes was removed. This type of failure was common in the early stages of development and it was difficult to explain why one of the elctrode should have poorer adhesion than the rest, unless of course that part of the alumina layer was contaminated from the mask holder. However, the majority of the failures occured at the side constriction, as can be seen in the figure 5.8b with the other two electrodes. Wymer's (62) work with the line contacts indicated that the film thickness at the side constriction can be as little as 20% of the film thickness at the exit constriction . Thus the possibility of sporadic penetration of the oil film by surface asperities at the side constriction is higher than any where else within the contact. Hence it is not surprising that the majority of the devices eventually failed in this region. The propagation of this type of failue and its effect on transducer signals are discussed further later. Occasionally even the alumina layer was removed

(a)

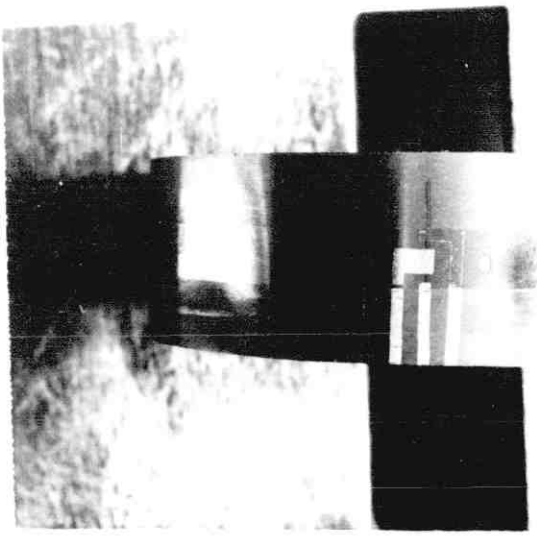

(b)

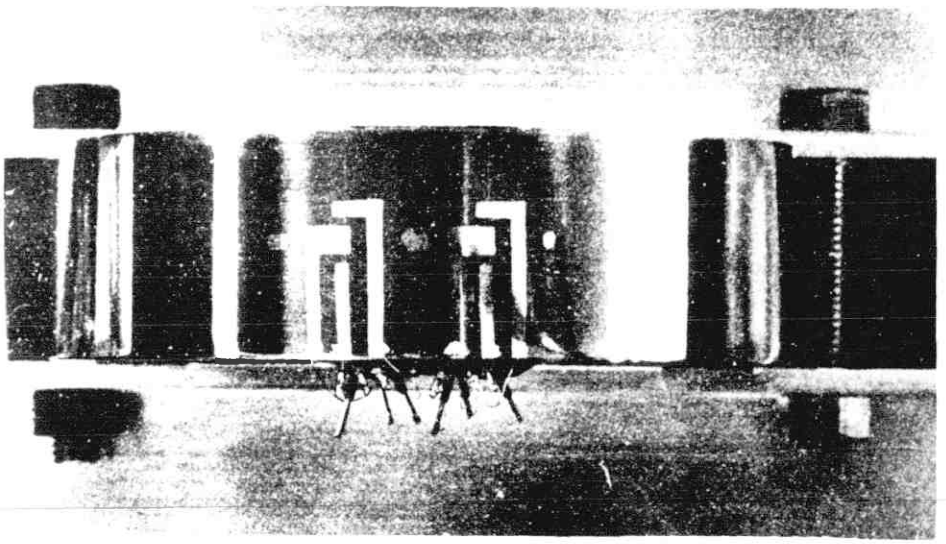

(c)

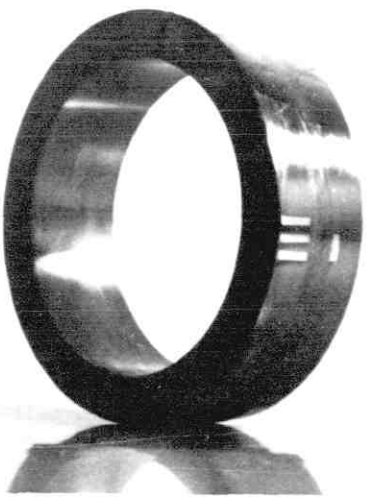

Fig. 5.8 (a) Pressure transducers deposited on metal disc (early work), (b) device failed at the electrode, (c) alumina layer, deposited without sputter etching, was removed at the start of test.

at the sides of the contact. This can be seen in figure 5.9a above the single 10μm x 30μm pressure transducer. However, this type of severe damage was found only under certain operating conditions, when some misalignment occured between the discs. Typically, very high load and high surface velocity produced severe vibration and occassionally broke the shear pins and pulled of the connecting wires. Figure 5.9b shows a pair of aligned pressure and temperature transducers phtographed after an experiment. Partial removal of the elctrode at the side constriction of both the devices is clearly visible. In addition to this, part of the leading electrodes of the pressure transducers was also severely damaged. This photograph also shows a rare type of failure at the manganin overcoated titanium trailing electrode near the soldered contact. Occasionally an otherwise good deposit simply floated off in contact of oil, which happened in this case.

Sliding between the discs produced the largest number of failures. Sliding at the start of an experiment had the most devastating effect on the devices as no oil film formation takes place at this stage. Controlled sliding at reasonably high surface velocity (5m/sec) and moderate loads ($3x10^5$ N/m) was found to be acceptable for a short while with slip ratios of upto 20%, however, as mentioned earlier, the eddy current brake occasionally produced large variations in slip which damaged the devices. Very heavy load at very low or very high surface velocity also damaged the devices. However, with improved deposition technique and careful running at later stages of the project, it was found possible to run even the pressure and film thickness transducers for over an hour and some devices could be

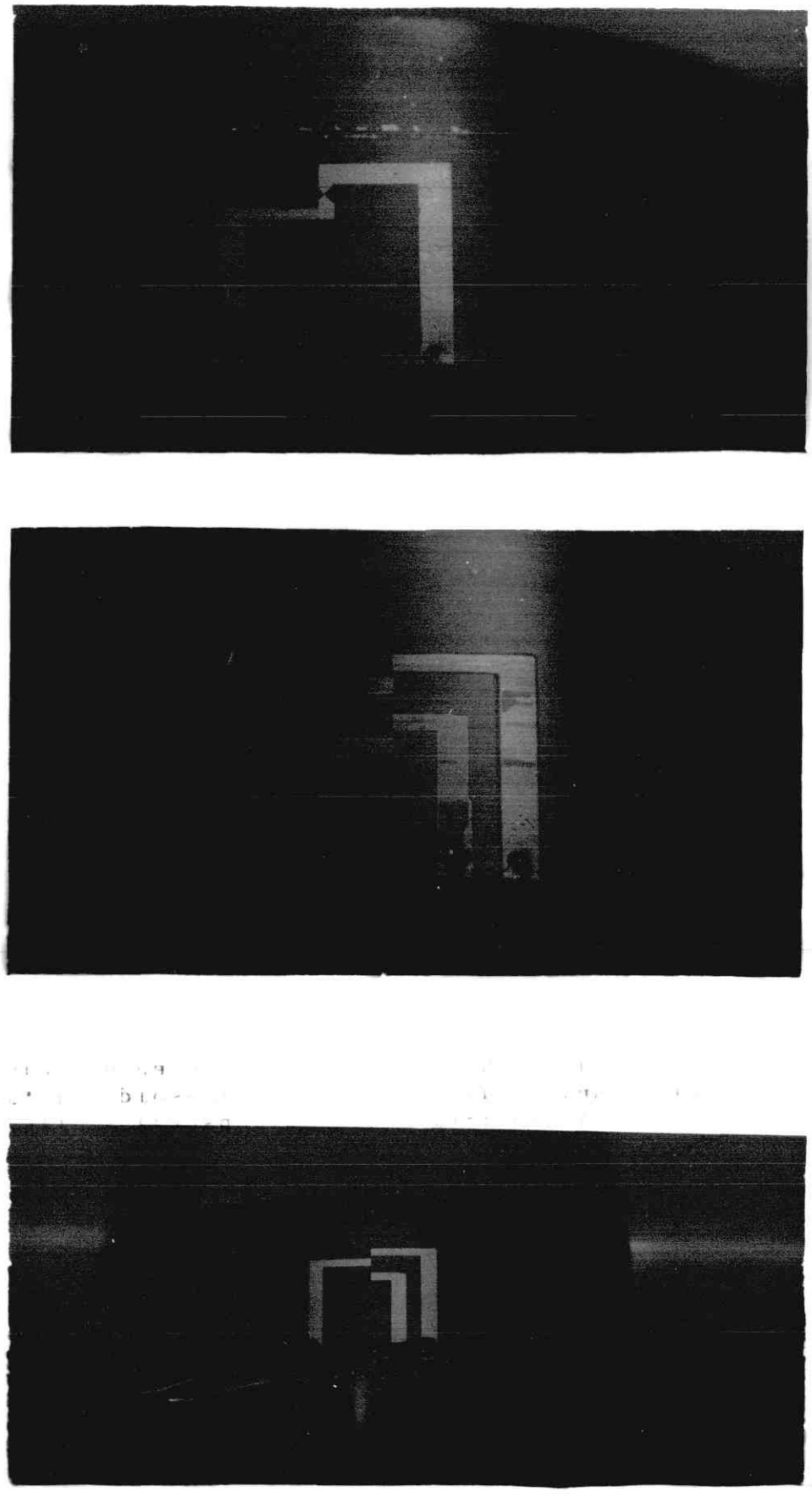

Fig. 5.9 Various transducer configurations (a) pressure transducer, (b) pressure and temperature transducer and (c) pressure and capacitive film thickness transducer.

used for 3 experiments.

5.9 General Performance of Transducers

5.9.1 Pressure Transducer

i) Effects of Transducer Width and Monitoring Circuit

Figure 5.10 shows 5 pressure traces recorded over the course of this project using oil 1. The operating conditions of the disc machine were similar for the four traces b to e, while trace a was at a higher load. The transducer used for traces a and b was 25μm wide, for trace c it was 15 to 18 μm wide, for trace d it was 10 to 12μm wide and for trace e it was 6μm wide. The analogue oscilloscope was used in recording traces a and b while the rest of the traces were recorded using the digital storage oscilloscope. Signal interuption occured in trace a and b in the secondary pressure peak zone. Similar breaks in pressure profiles occured in most of the traces recorded using the analogue oscilloscope, whereas the effect was absent in the storage oscilloscope. The probable reason for this is that, in the storage mode, the analogue oscilloscope has a lower writting speed, making faster changes less visible.

Studying the trace c, which was obtained with a finer device than in trace b, it becomes clear that no secondary pressure peak could exist in trace b. Trace c shows a sharp pressure drop at the exit without any appreciable pressure spike. It was found that devices having an effective width greater than 18μm could not resolve the secondary pressure peak to any extent under the operating conditions of this disc machine and with the oils used in this project. Trace d and e shows the secondary pressure peak clearly.

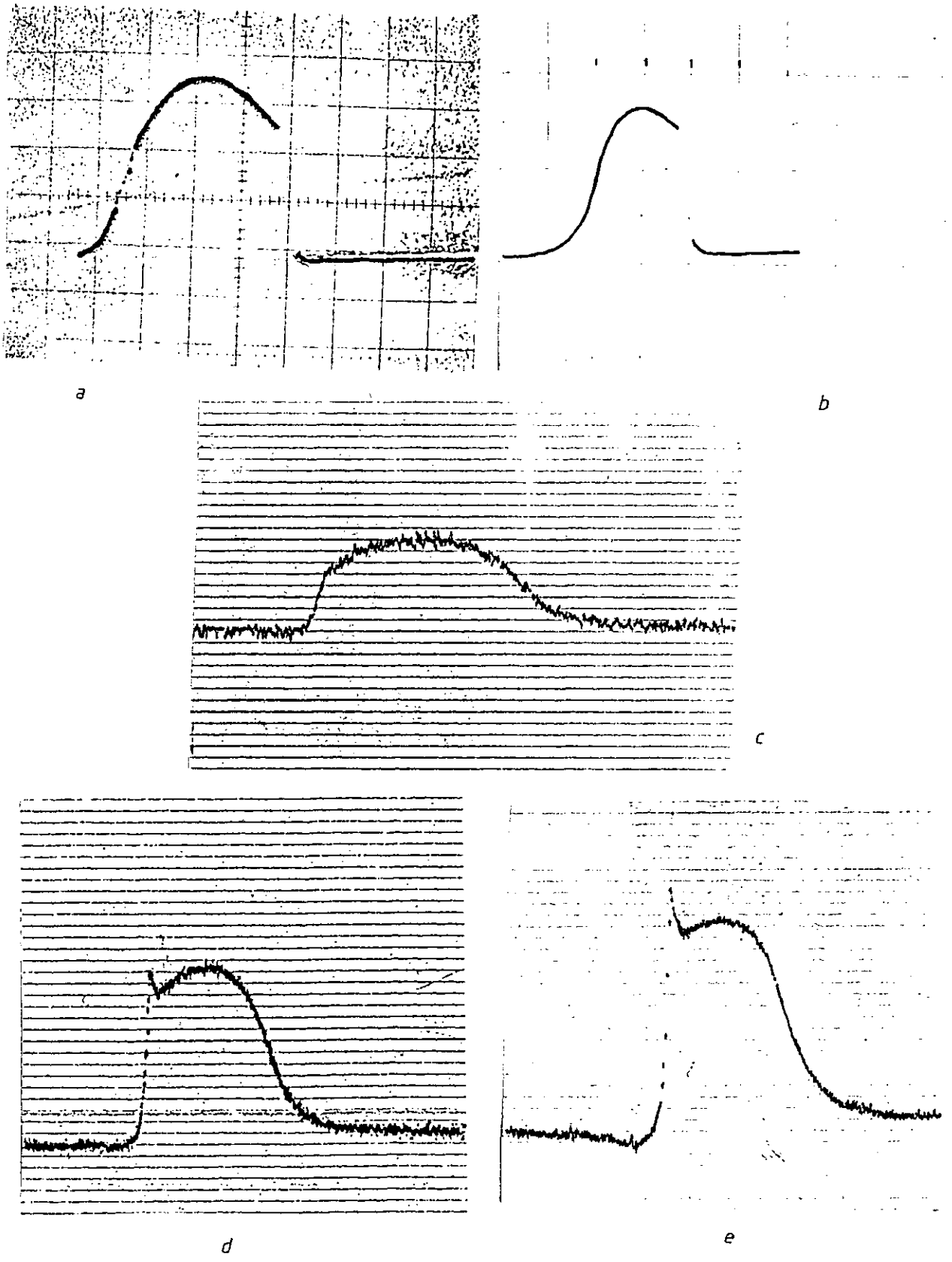

Fig. 5.10 Pressure profiles recorded with transducers of different active element widths, traces b to e were recored under broadly similar operating conditions while trace a was at a higher load. Device width: a and b, 25μm; c, 16 18μm;d, 10 12μm;e, 6μm.

ii) Effect of Electrode Breakdown

In this project most devices failed by electrode damage at the side of the line contact. Failure took the form of a fine line scratched across the electrode in the direction of motion and did not occur in one pass through the contact zone, but started from one end and slowly extended to the other end. When the scratch was long enough, the remaining electrode could behave like a second transducer. Depending on the position of the unbroken part of the electrode relative to the transducer, the pressure trace from the electrode would either superimpose or form a second profile beside the profile generated by the transducer itself. Figure 5.11 shows two such profiles. In trace a the unbroken part of the electrode was on the trailling side of the transducer whereas in trace b, it was on the leading side. In both cases the transducer was in line with the trailing electrode. To prevent the pressure profile generated by the damaged electrode from interfering with that generated by the transducer, the electrode arrangement was redesigned so that the electrodes did not pass through the contact at the same time as the active element.

As the electrode slowly wears off it adds resistance to the transducer. This causes a relative reduction of the output from the transducer which in turn produces pressure profile of reduced height for a given set of operating conditions.

During the experiment the electrode damage could be detected either by the gradual shifting of the signal zero level due to the unbalanced voltage produced at the bridge or by monitoring the electrode as it passes through the contact using the variable triggering facility. Thus in the case of such

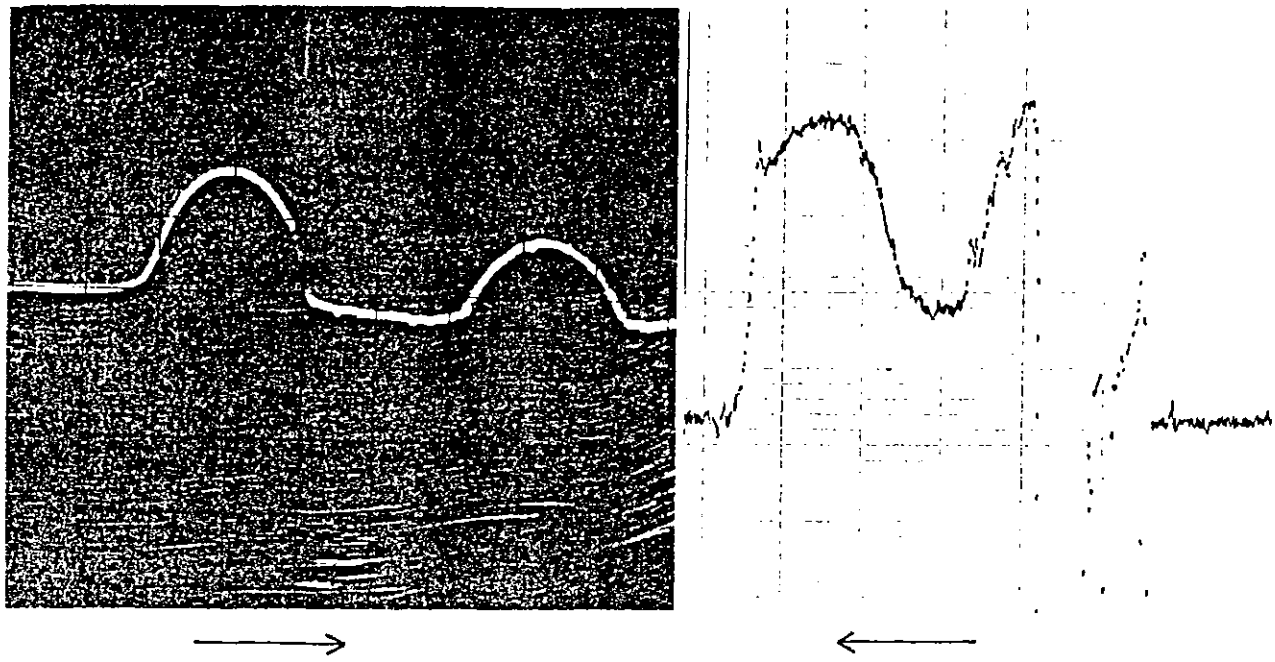

Fig. 5.11 Effect of secondary transducer, formed due to partial electrode breakdown. Secondary transducer on trialing side (a), leading side (b).

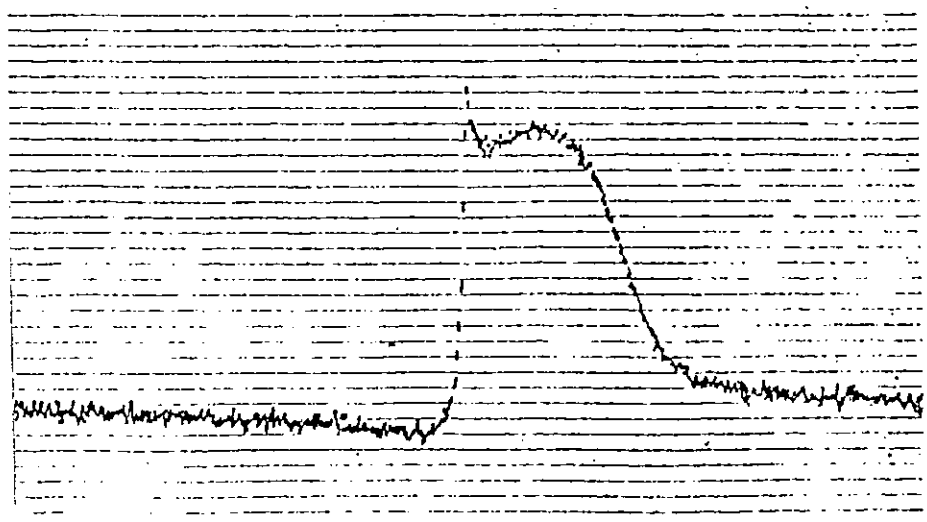

Fig. 5.12 Pressure profile with zero level shift. Proper zero level, at the exit side, is attained within one and a half Hertzian width.

electrode breakdown the bridge had to be re-balanced to bring the trace back to the proper position on the screen.

iii) Zero Level Shift

Figure 5.13 shows a set of four pressure traces recorded in one experiment. Traces a, b and c were at the same load of 2.78x10 N/m and at surface velocity of 3.6, 7.4 and 9.2m/sec whereas trace d was at a high load of $1x10^6$ N/m but at nearly the same surface velocity as in trace b. All four traces show differences between the zero levels at the inlet and at the exit. The extent of zero level shift was found to vary from device to device and also to depend on the running condions. Increasing the surface velocity was found to increase the zero level shift as can be seen in traces a, b and c, but incresing the load reduced the shift as can be seen in traces b and d. With most devices it was found that the zero level at the inlet was correct but on the exit side the signal dropped below the zero level. However, in some devices the zero level at the exit side remained higher than the inlet side. In all cases the signal returned to true zero level over a distance of about one to two contact widths as can be seen in figure 5.12. It was also noticed that the finer devices were generally more prone to this zero level shift than the wider devices.

A single cause could not be found which explained all the above obsevations. The electrode pattern could produce some zero level shift particularly when one electrode become preferentially etched or damaged near to the transducer, as a substantial part of the overall resistance of very small device comes form the electrode (about 30% incase of 30μm x 10μm device). However, that would not produce any dependence of

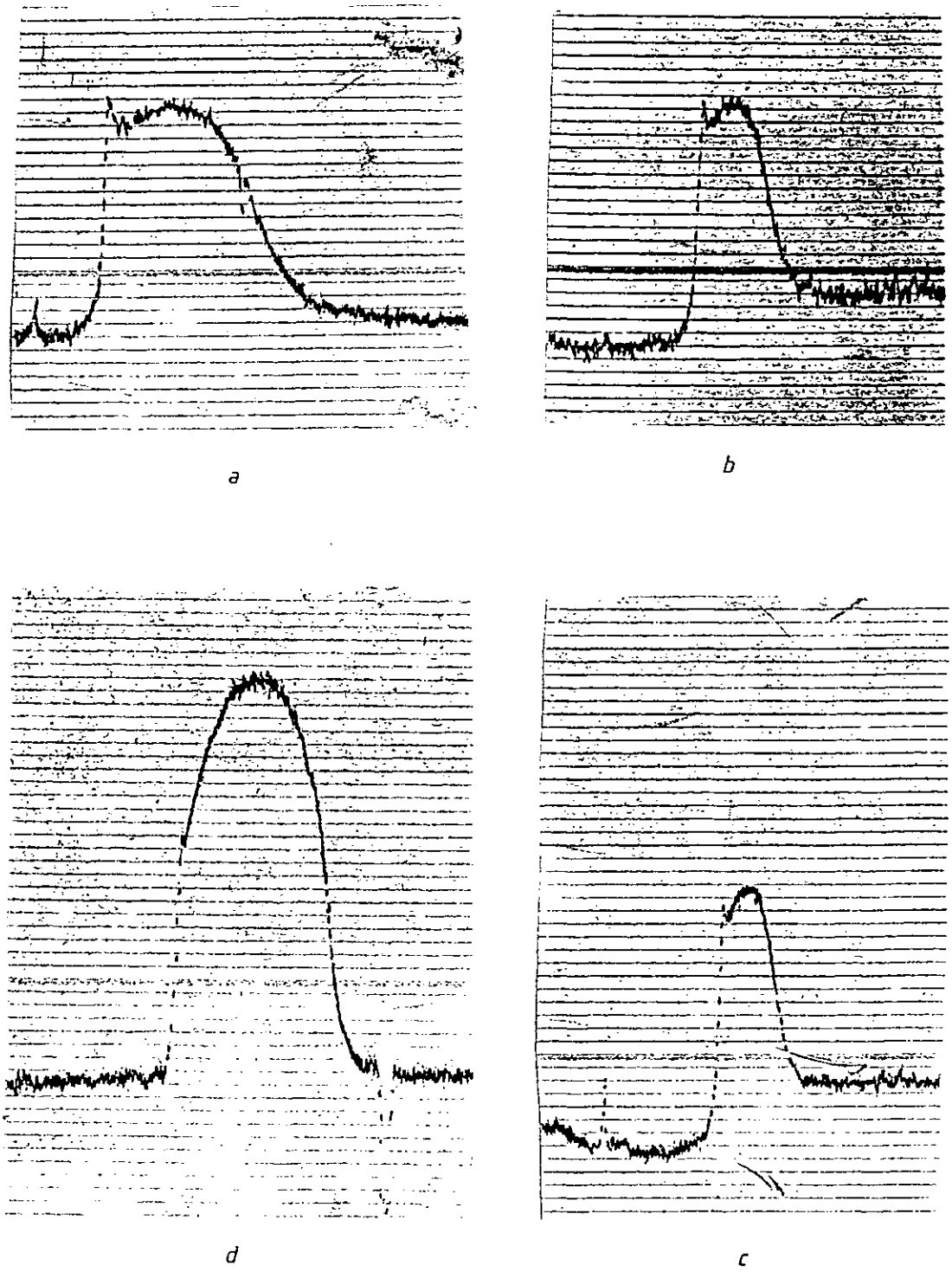

Fig. 5.13 An extreme case of zero level shift. All traces recorded in one experiment. Surface velocity increases the effect, higher load reduces it.

zero level shift on surface velocity.

A second possibility considered was the capacitance formed across the transducer, which could explain the velocity dependence. A simple equivalent circuit of a transducer is shown in figure 5.14

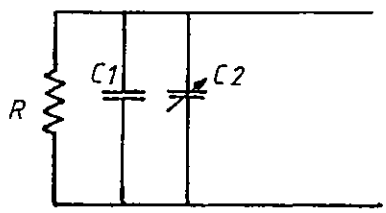

Fig 5.14 Simplified Equivalent Circuit of a Pressure Transducer

where R is the resistance of the active element, C1 is the fixed capacitance that forms between the electrode and the disc on which the device is fabricated andC2 is the variable capacitance that is formed while the transducer gradually enters into the contact zone. The estimated values of C1 and maximum C2 for a 1μm thick film is around 400pf and 30pf respectively. The added value of these capacitances together with a 150Ω resistor produces a very small time constant compared to the large recovery time noticed with the zero level shift. Thus this capacitance alone can not cause the shift.

The third possibility considered was the temperature effect on pressure transducer, however, all prssure transducers were found to show a positive temperature coefficient, hence the zero level on the exit side would have been higher than the zero level at the inlet side as the temperature at the exit remain slightly higher than the temperature at the inlet.

The material property of the thin film manganin was the

prime suspect for this zero level shift. It has been mentioned earlier that to avoid detempering of the metal discs used in this project, the temperature of the disc was never allowed to rise above 150°C. However, it was found that if the transducers were deposited while the disc was heated to 150° C and afterwards annealed in vacuum at 150° C for a period of 5 to 6 hours the zero level shift reduced considerably.

iv) Effect of Temperature on the Pressure Transducer

As we have seen in chapter 4 the temperature coefficient of resistance of manganin varies with the variation of depoasition techniques. The unannealed film shows higher value of temperature coefficient compared to the properly annealed film. During the development of the pressure transducer, some devices were fabricated without annealing. The pressure profiles generated by these devices under pure rolling did not show any apparent change in shape. However, the effect of temperature showed up prominently when sliding was introduced between the discs. Figure 5.15 shows two traces recorded in one experiment where trace a was under pure rolling conditions and trace b was recorded with some sliding. The load for trace a was 0.5MN/m and to introduce sliding, the load for trace b was reduced to 0.22MN/m and the surface velocity was slightly increased. A slip ratio $(U_2-U_1)/U_2$ of 0.2 was obtained. The height of the primary pressure peak of trace b under sliding is about 100% greater than is expected at 0.22MN/m load. Calculations indicate the differences to be caused by the higher temperature in the contact. Non-annealed manganin has a temperature coefficient of 2×10^{-4} /°C and the pressure coefficient of the device was 1.5×10^{-11} /Pa, thus a temperature rise of about 40°C is necessary to

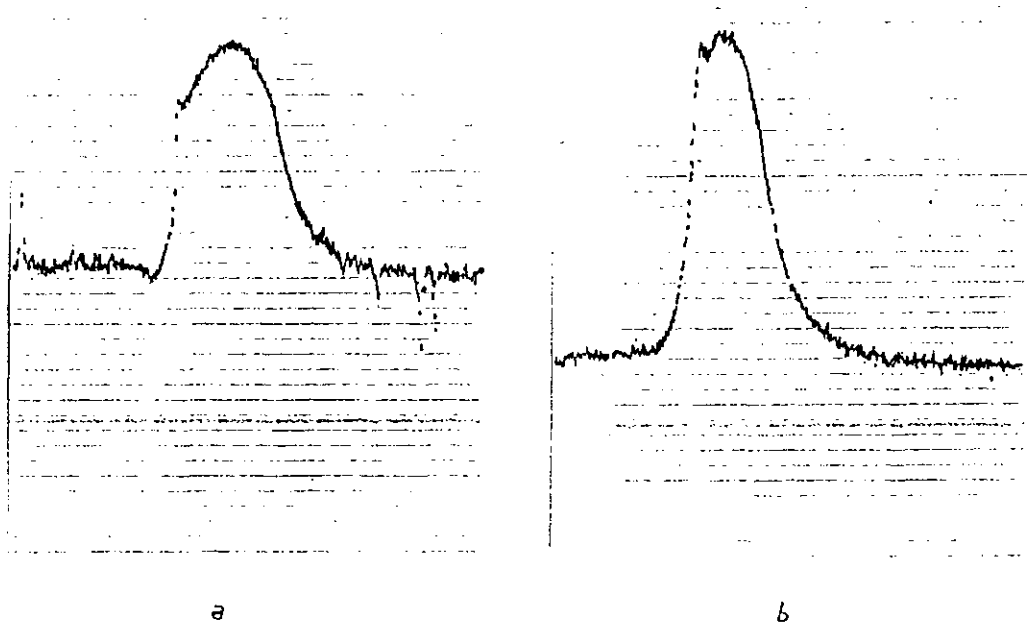

Fig. 5.15 Effect of temperature rise within the contact on unannealed pressure transducer. Trace (a) at higher load and pure rolling condition, (b) low load and sliding condition.

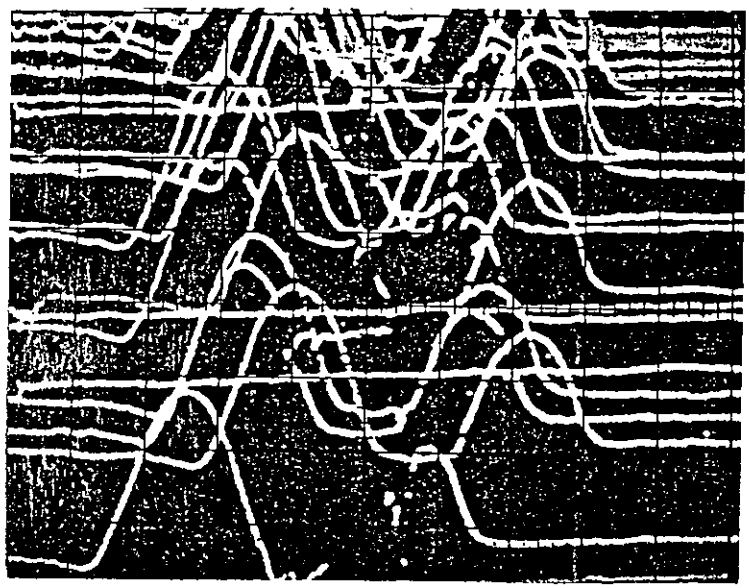

Fig. 5.16 A number of pressure traces recorded to study reproducibility.

produce the observed height of the pressure profile under sliding condition. From work with temperature transducer, a similar temperature rise could be expected under the above sliding conditions.

Once the devices were properly annealed, however, the temperature coefficient was significantly reduced, and the pressure profiles obtained under sliding conditions show little differrence in the primary peak pressure height from profiles recorded under pure rolling conditions.

v) Reproducibility of Pressure Profiles

As described above, before making a permanent recording of a signal generatedby a transducer, several traces were examined in the oscilloscope to check the reproducibility of the signal from rotation to rotation. Without permanent recording, only general features such as the height of the primary and secondary pressure peaks could be checked without wasting transducer life. With the analogue oscilloscope it was possible to record more than one trace on the screen, hence facilitating the above check. Figure 5.16 shows such a recording with several traces under the same running conditions with a few seconds between each of the traces. The levels of the traces were shifted intentionally to obtain a clear picture of each trace. It can be seen that the reproducibility of the pressure signal is good. Unfortunately this type of multitrace recording was not possible with the digital oscilloscope.

vi) Pressure Coefficient of the Pressure Transducer

The pressure coefficient of the pressure transducers was determined in all cases from the first pressure trace recorded by the device. They were found to vary over a range from 0.72 to

2.1×10^{-11}/Pa. with most of the values lying between 0.8 to 1.5 $\times 10^{-11}$/Pa. The pressure profiles recorded by these devices did not show any appreciable difference that could be related to the pressure coefficient.

5.9.2 Resistive Temperature Transducer

Titanium was used for the thin film resistive temperature transducer. In bulk form, titanium shows the lowest pressure coefficient of resistivity among the metals. In thin film form, however, the value of pressure coefficient of resistivity was found to be substantially larger. Figure 5.17 shows two sets of synchronised pressure and temperature profiles generated by aligned pressure and temperature transducers while passing through the EHL contact zone. The temperature traces show the combined effect of positive temperature coefficient and negative pressure coefficient of resistivity of thin film titanium. As the transducer approaches the contact zone, the traces show only the temperature effect as the pressure in that part is negligible. As the device moves into the contact zone the effect of pressure is to reduce the effect of temperature. As the pressure drops sharply at the exit, the effect of temperature again dominates. The position of the secondary pressure peak in the pressure distribution profile correspond to the beginning of the sharp transition, shown as 'a' in figure 5.17, in the recorded temperature profiles. This point of transition is later used for superimposing the temperature profiles.

Figure 5.18 illustrates the much larger relative effect that pressure exerts on the temperature profile under rolling conditions.

To determine the pressure coefficient of the temperature

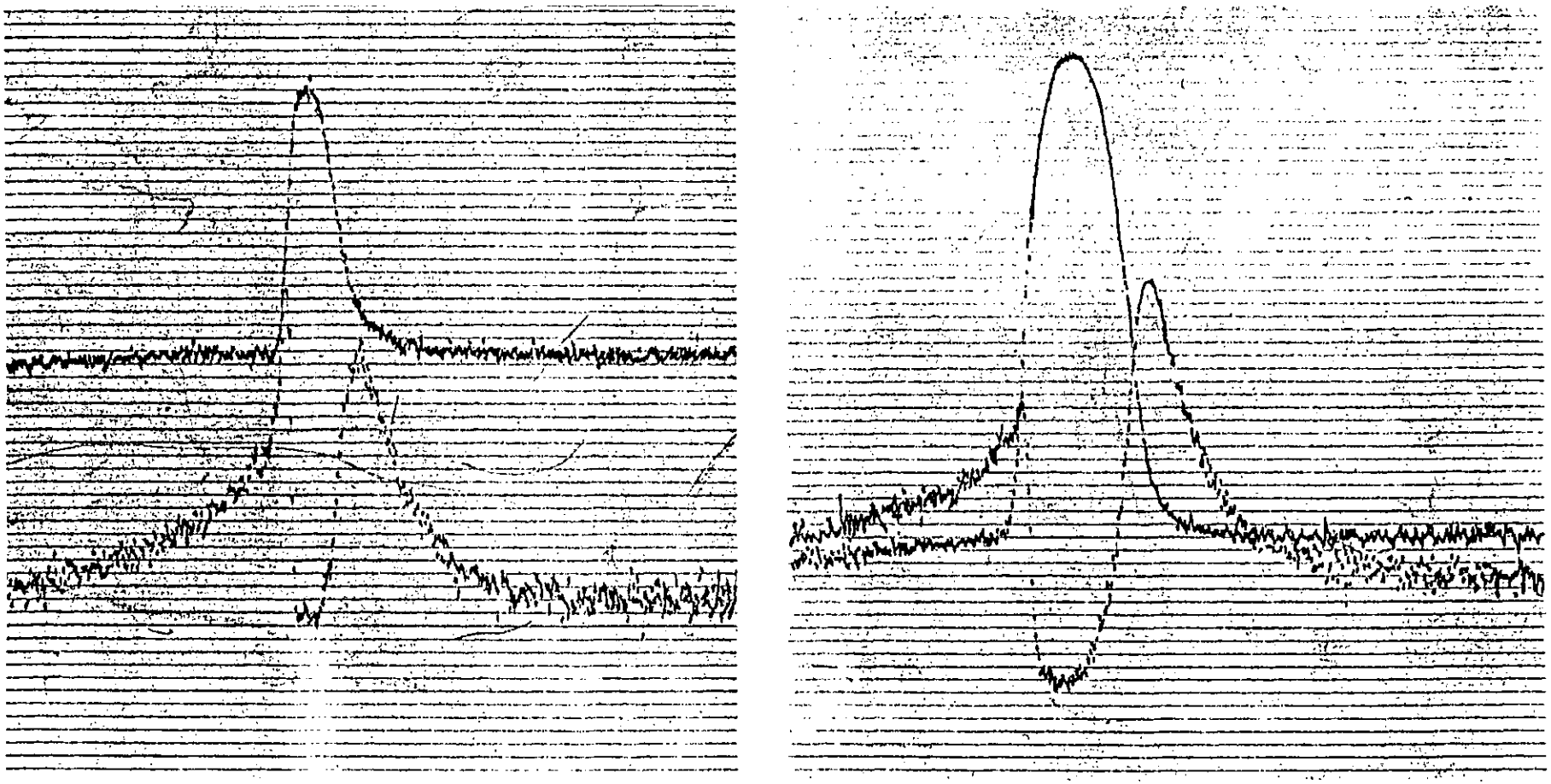

Fig. 5.17 Synchronised pressure and temperature traces generated by aligned pressure and temperature transducers under rolling conditions.

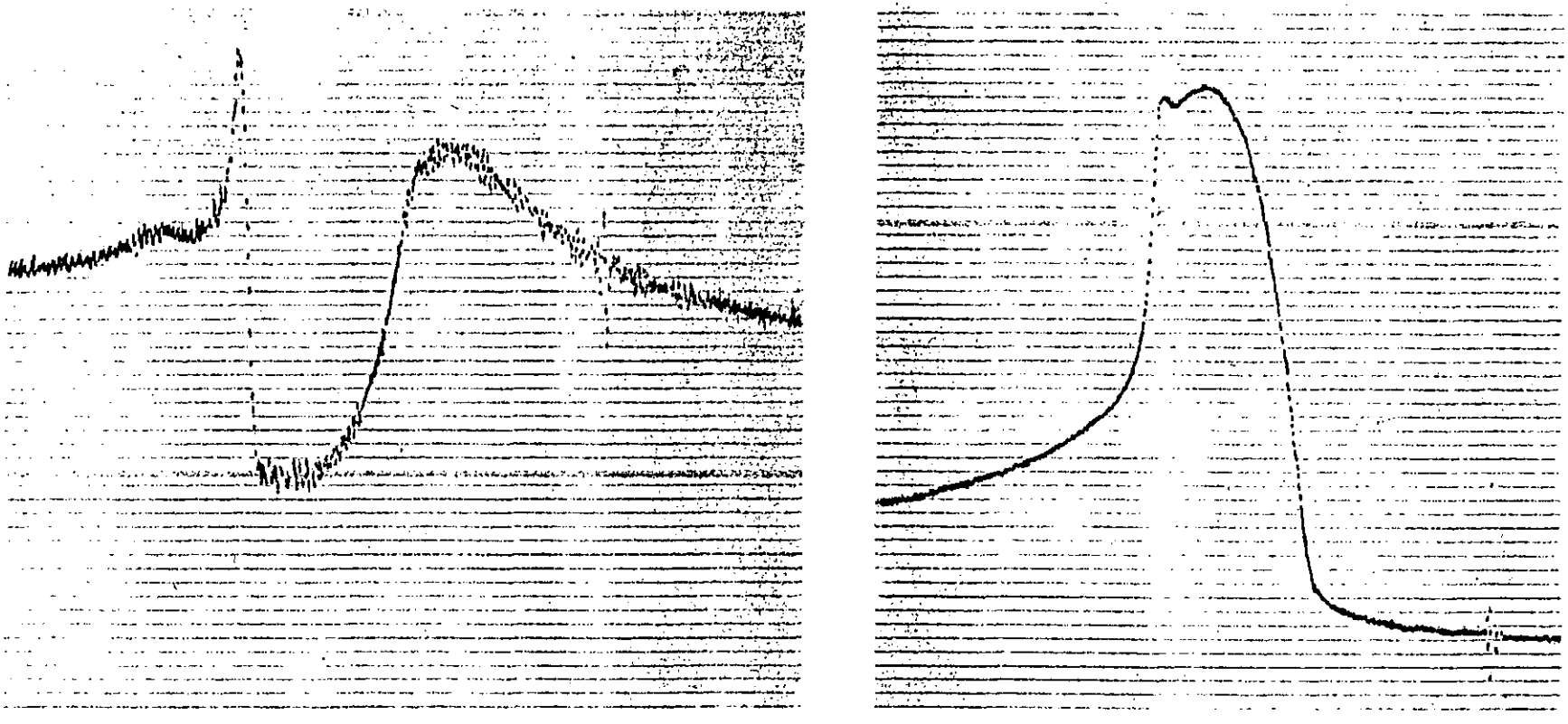

a b

Fig. 5.18 Temperature profiles recorded under (a) rolling, (b) sliding condition.

transducer a rectangular piece of aluminium with a paper covering on one surface was mounted over the temperature transducer. The assembly was then mounted between the jaws of a hydraulic press and slowly loaded upto 890Nf(200lbf) and then unloaded. In the first few cycles the change of resistance of the transducer was found to vary widely with the alignment of the device relative to the bar. But after about 5 cycles the face of the aluminium bar conformed with the disc surface, at which point very little variation of the change of resistance could be noticed with the change of relative position. The pressure coefficient of the temperature transducer determined in this way was 1.5×10^{-11}/Pa. Figure 5.19 shows a synchronised temperature and pressure trace and the temperature trace corrected for pressure effect.

The adhesion of the titanium temperature transducer was much better than that of the manganin transducers and they could be used under more severe conditions. Most of the failure occured due to electrode failure at the side contact. In some cases devices failed by chipping of the alumina layer from the steel disc, complete with the titanium coating.

The formation of a second device by a partially damaged electrode also occured with these devices, but it was found that once damage had started it rapidly progressed and the device failed quickly.

Zero level shift in the traces was difficult to ascertain as the temperature at the exit of the EHL contact is higher than that at the inlet.

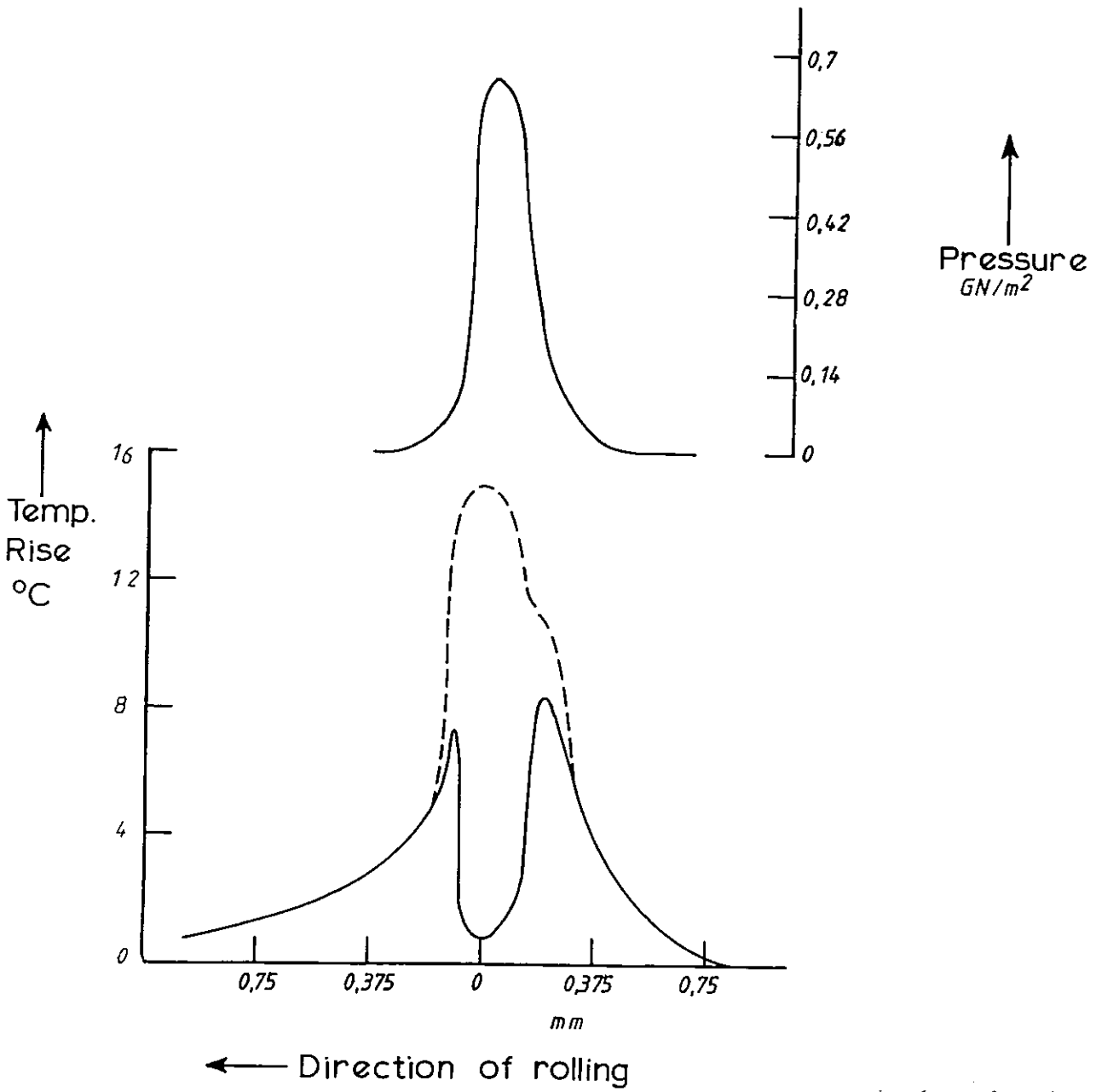

Fig. 5.19 Synchronised pressure and temperature trace, Temperature trace corrected for pressure effect.
Temperature coefficient 0.9×10^{-3}/C
Pressure coefficient 1.5×10^{-11}/Pa.

5.9.3 Thinfilm Thermocouples

The thinfilm thermocouple fabricated on the discs had a rectangular junction 25um long in the direction of rolling and 125μm wide. Each of the chromel and alumel layers was about 1000Å thick. The resistance of these devices was found to be relatively high and varied between 400Ω and 1kΩ from device to device. In the disc machine test none of the devices failed at the start of an experiment and the overall life of devices was found to be better than the pressure transducers. The high device resistance and the high impedance of the monitoring circuit caused the signal from these devices to be noisy.

Figure 5.20 shows three profiles generated by a thinfilm thermocouple under different running conditions. These profiles show a large increase of temperature (well over 30°C) within the contact zone. Once the transducer had passed through the contact zone, the profiles showed a negative excursion suggesting a drop of temperature relative to the ambient value. It can be seen that the temperature rise within the Hertzian zone depended on both load and surface velocity but the negative excursion generally remained close to a value of about 15°C below ambient. All the thinfilm thermocouples fabricated showed positive and negative excursion similar to the figures 5.*20*. Initially it was thought to be due to adiabatic compression and expansion of the oil passing through the contact zone. But the resistive temperature transducer did not show similar negative excursions. In the absence of a good explanation for this negative excursion found with the thinfilm thermocouple, a through examination of the temperarture profiles in the EHL contact zone was not performed with these devices.

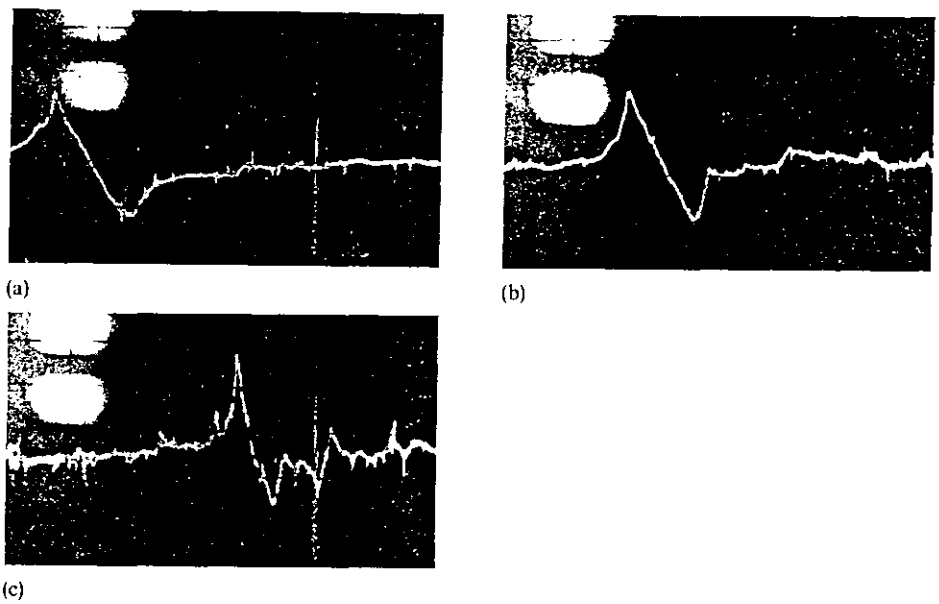

Fig. 5.20 Signal generated by thinfilm thermocouple passing through the contact zone. (a)0.28MN/m, 2.39m/sec; (b)0.33MN/m, 3.09m/sec; (c)0.61MN/m, 5.63m/sec.

5.9.4 Behaviour of the Capacitive Transducer in an EHL Contact.

Figure 5.21 shows a set of synchronised pressure and film thickness profiles generated by aligned transducers. The capacitive nature of the film thickness monitoring device and the differentiating circuit used for monitoring the charging current gave rise to a high level of noise in the film thickness profiles. Assiduous shielding of all the signal wires led to little improvement. Eventually a filter was intoduced between the final amplifier and the oscilloscope. The upper cutoff frequency was set at 40KHz and the lower cutoff frequency was set at 100Hz to remove line frequency noise. Figure 5.22 shows two sets of synchronised pressure and film thickness profiles recorded succesively under the same operating conditions using the filter. As can be seen in trace of figure 5.22a this filter introduced oscillation whenever there was a sharp burst of noise in the signal line. This particular problem became acute at high surface velocities where the noise level was found to be higher and precise determination of the zero level was difficult with these signals. Thus most of the development work and the work with oil 1 and some work with oils 2 and 3 was conducted without the filter. As the high frequency noise level remains more or less constant it was found possible to draw a line through the mean noise and this produced reproducible results.

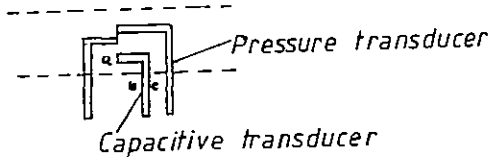

Fig. 5.23 Synchronised Pressure and Film Thickness Transducer

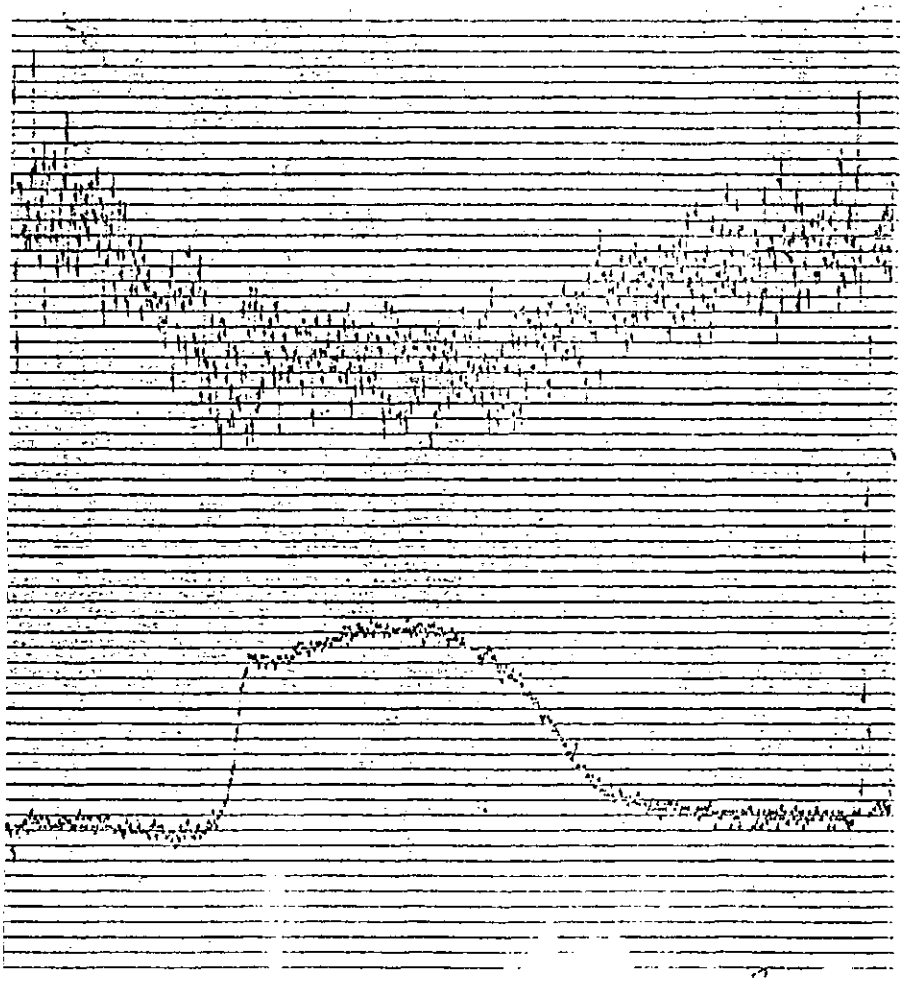

Fig. 5.21 Synchronised pressure and deformation profiles. High noise level in the deformation profile is apparent.

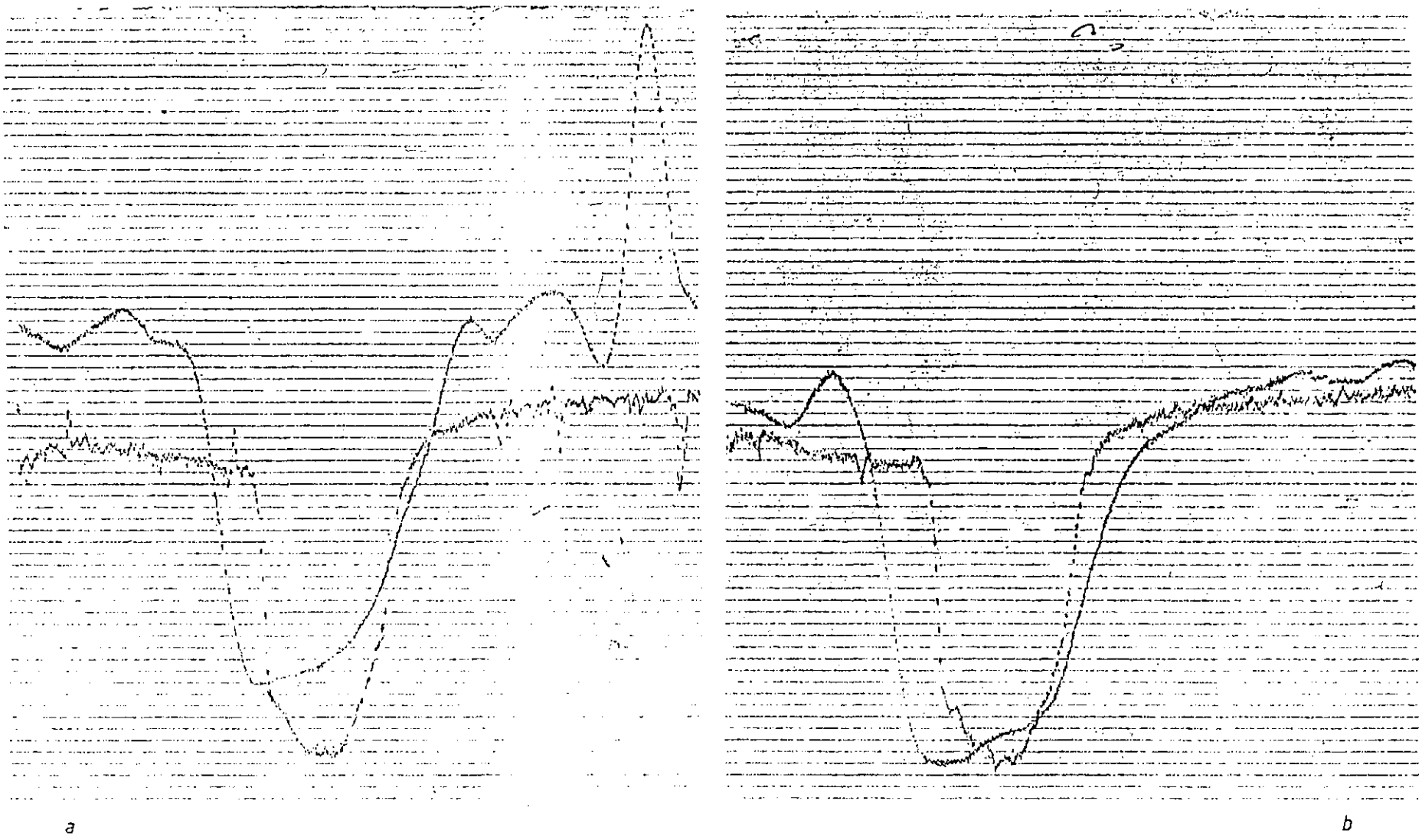

Fig. 5.22 Synchronised pressure and deformation profiles. (a) Effect of of filter on the deformation profile in the presence of transient noise; (b) no noise in the inlet zone, however, noise at primary peak pressure zone distorts the deformation profile in that zone.

The configuration of synchronised pressure and film thickness monitors is shown in figure 5.23. The capacitive device produces three broadly similarly shaped profiles, from edges 1 and 2, in the figure 5.23, entering the contact and edge 3 leaving the contact and producing an inverted signal. For calibration purposes only the leading edge (edge 1) was used.

The trailing electrode of the capacitive device was found to have a second effect on the film thickness profiles monitored. In figure 5.23 the leading edge of the capacitive device was 3mm away from the leading edge of the trailing electrode. With properly deposited devices, the film profile generated by the leading edge of the trailing electrode does not affect the profile generated by the leading edge of the device as shown in figure 5.22b. In figure 5.24a the begining of the second profile may just be distinguished. During the deposition of the device, the leading edge of the electrode sometimes moved slightly due to under cutting or misalignment of the boat and the mask. The effect of this was to prevent the full recovery of the film thickness profile at the exit as in figure 5.24b. However, the shift of the electrode was never found to be enough to cause distortion in the minimum film thickness zone. At a later stage, the configuration of the film thickness monitor and the pressure transducer was changed to that shown in figure 5.25

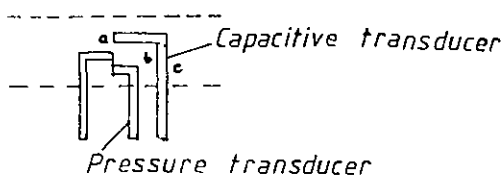

Fig. 5.25 Alternative Pressure And Film Thickness Transducer.

In this configuration the failure rate of the capacitive device during fabrication was higher because the electrode area

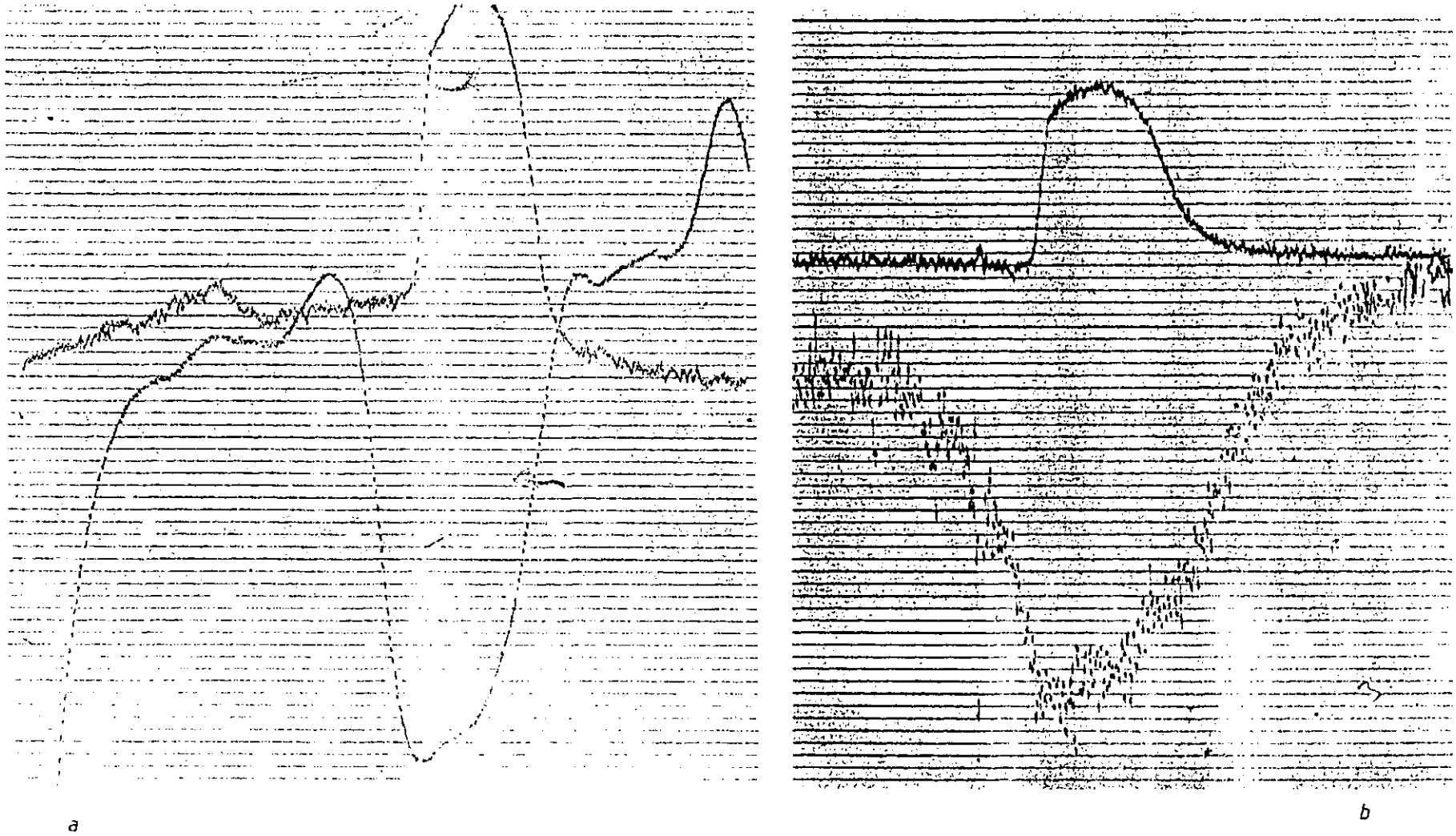

Fig. 5.24 Effect of leading edge of trailing electrode of the capacitive device, (a) part of the deformation profile due to trailing electrode can be seen at the exit side of the main profile; (b) trailing electrode slightly nearer to the leading edge preventing full recovery of the deformation profile at the exit.

was increased, and good electrical insulation was more critical with capacitive devices than with other types of resistive transducer.

The alignment between the leading edge of a capacitive transducer and the active element of the pressure transducer was within one micron at the mask stage, however a gap of about 2.5mm seperates them as can be seen in figure 5.9c. Hence a misalignment of 1° between the disc and the mask would produce an offset of about 44μm between the two devices. However most of the devices fabricated show very good alignment as can be seen in figure 5.26a where the secondary pressure peak in the pressure profile occurs immediately before the exit constriction, as the theory predicts, and this observation holds true for all the traces recorded in this experiment under different operating conditions. Figure 5.26b shows misallignment by about 3°.The pressure transducer was ahead of the capacitive device.

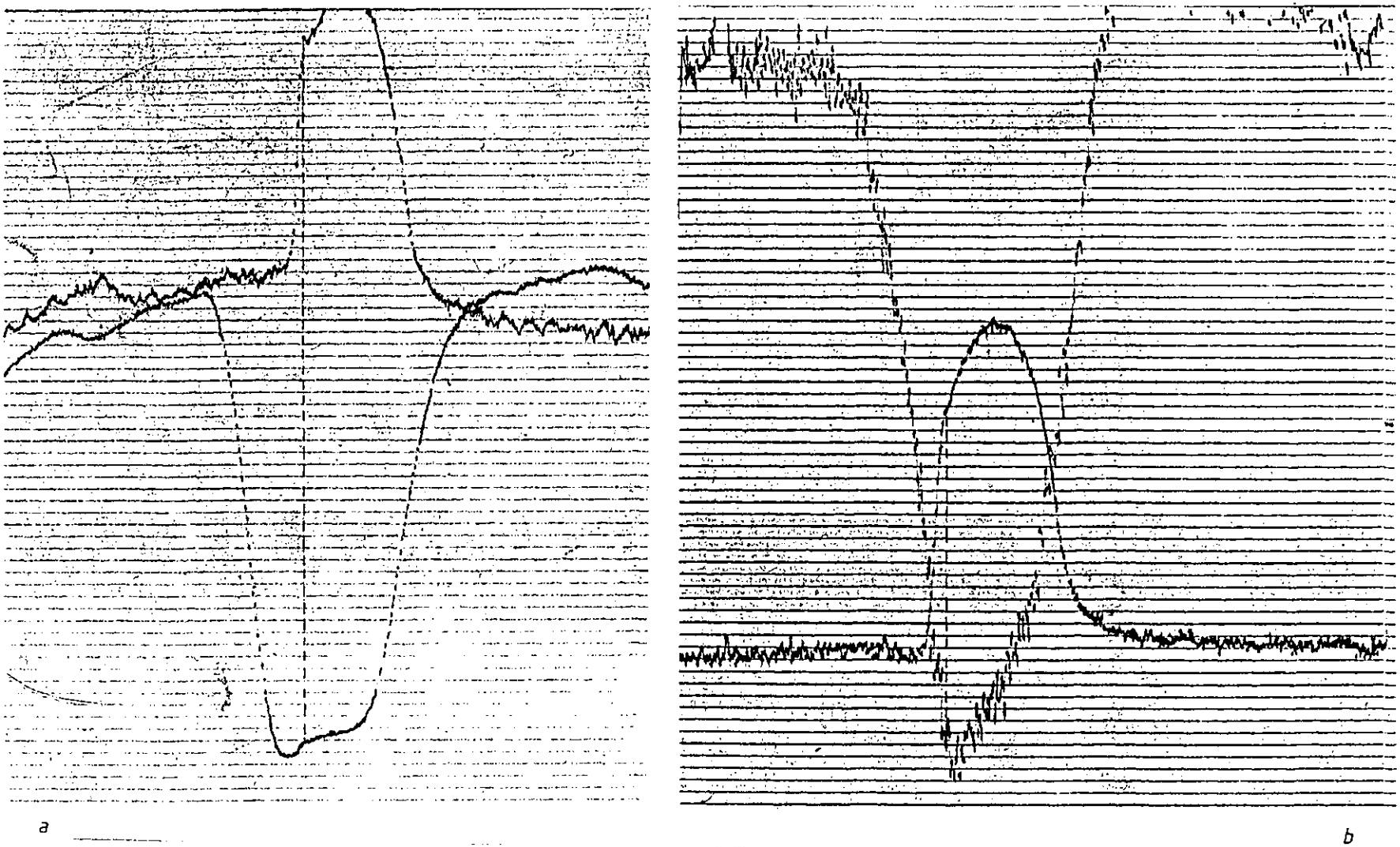

Fig. 5.26 Alignment of pressure and capacitive transducer; (a) properly aligned devices show the secondary pressure peak immediately before exit constriction; (b)pressure transducer slightly in advance of the capacitive device.

CHAPTER 6

ANALYSIS OF TRANSDUCER RESULT

In order to study the effect of the operating variables on signals derived from the transducers it was normally necessary to process the output data to provide a reasonable basis for comparison. The recording oscilloscope had a limited useful range of fixed sweep velocities and the obvious effect of a small increase in the rotational speed of the discs was a reduction in the duration of the transducer signal. The abscissae of recorded signals were therefore converted from units of time to units of distance along the surface of the disc. This was done manually by means of an accurate proportional divider and a multiplication factor determined from the sweep speed of the oscilloscope, the chart speed of the recorder and the surface velocity of the disc upon which the transducer was located. It was also necessary to obtain some reference procedure so that the co-ordinates of comparable recordings could be correctly located. From the theoretical pressure profiles obtained by Dowson and Higginson (18) and reproduced in Fig.1.2 of section 1.1.1, it can be seen that all the pressure profiles with reasonably high loads but low to moderate surface velocities ($W > 3 \times 10^{-5}$ and $U < 10^{-11}$) follow the Hertzian pressure distribution closely in the primary peak pressure zone. The pressure profiles from the thin-film transducers also showed a well defined primary peak pressure zone provided the line load was above about 0.25 MN/m ($W = 6 \times 10^{-5}$). Hence in superimposing the pressure profiles obtained under loads of above 0.25 MN/m, the primary peak pressure was taken

as the reference. However, at loads below 0.25 MN/m, it was found difficult to distinguish the primary pressure peak, from the emerging secondary peak. From study of the theoretical pressure profiles for very high surface velocities ($W = 3\times10^{-5}$, $U > 10^{-10}$) where a similar situation arises, it was decided that the inlet shoulder region was the best place to align the experimental pressure traces at lower loads.

In running an experiment in the disc machine, the load was generally kept constant while the transducer signals were recorded for different surface velocities and then the load was increased and the procedure was repeated. The traces used to study the effect of load at a particular surface velocity were therefore generally recorded at time intervals of upto 15 minutes. Although the wear rate of the devices was low under pure rolling conditions, the accumulated effect over a long run was found to be enough to cause a change in the pressure scale arising from the increased resistance of the electrodes. Hence in superimposing pressure traces, where a change in resistance of the device occurred, the areas under the pressure profiles were measured accurately with a planimeter and equated to the load to determine the individual pressure scales. The recorded signals were then redrawn to the same scale.

Another problem encountered was the determination of the correct zero level for each trace. This was particularly difficult for signals produced from very fine devices where the zero level shift was relatively large. Observation, made during the test, of the signal level produced by the device at a distance of 2 to 5 mm away from the contact, were taken as the true zero level.

6.1.1 Effect of Surface Velocity on Pressure Distribution

Oil 1

Fig. 6.1 shows a set of four pressure profiles, recorded by one of the finest devices fabricated in this project, which had a 6 μm wide active element, covering the velocity range from 2.2 m/sec to 7.44 m/sec at a fixed load of 2.47×10^5 N/m using Oil 1 (SAE 90). Although the oil pressure gauge indicated the same value in all four cases, the superimposed traces suggest a drop of loading in the case of trace 'a'. This type of fluctuation of load was found to occur frequently although the variation remained quite small.

The expectation from theory is that as surface velocity is increased, the width of the secondary peak on a plot of amplitude against rolling distance will be greater. This is borne out by the results shown in Fig.6.1. The peak should move towards the centre of the contact area as speed is increased, if the load remains constant. This is also seen in Fig.6.1, with the exception of trace 'a', at the lowest speed. However the magnitude of the pressure at the centre of the contact indicates that the load was significantly lower in this case. A lowering of the load has the effect of moving the peak towards the centre if surface velocity is constant.

The three profiles 'b', 'c' and 'd' were also found to follow the predicted behaviour of the development of pressure at the inlet of the contact. In the lower surface velocity trace, 'b', the pressure development zone at the inlet shows the least extension beyond the Hertzian zone. Successively larger development zones can be seen to have occurred with the higher surface velocity traces 'c' and 'd' respectively. However,

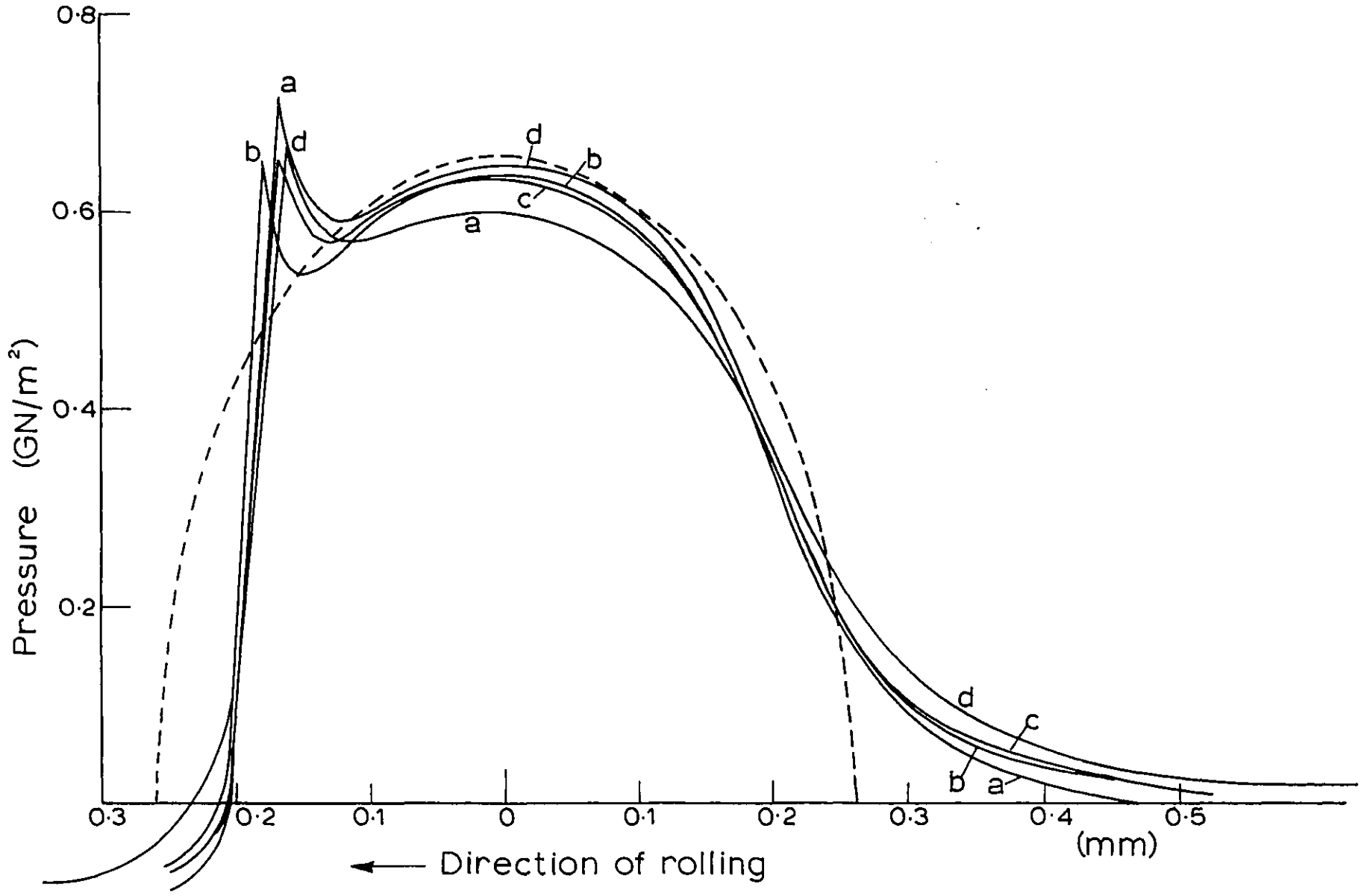

Fig. 6.1 Pessure profiles recorded with 6μm wide activre element, using oil1, at a fixed load of 0.275MN/m and surface velocities of (a)2.2m/sec, (b)3.63 m/sec, (c)5.43m/sec (d)7.44m/sec.

trace 'a' shows an extension which falls between 'b' and 'c', and this is believed to be due to the lower loading in this case.

Oil 2

Two sets of pressure profiles are redrawn in Figs. 6.2 and 6.3 . All the traces were recorded using the same device having an active element 10 μm wide and 30 μm long. In Fig. 6.2 the load was 2.75×10^5 N/m and the surface velocity was varied between 1.54 m/sec and 7.4 m/sec, hence the running conditions for these results were similar to those of Fig. 6.1 . In Fig. 6.3 the load was 8.34×10^4 N/m, and the set covers a surface velocity range from 0.75 to 3.6 m/sec. This set represents the lowest loading condition employed in this project.

As in Fig. 6.1, the slight variation of load between the traces can also be seen in Fig. 6.2. The largest secondary pressure peak occurred in this set was at 3.4 m/sec whereas in Fig. 6.1 using Oil 1, it occurred at 2.2 m/sec. Similarly to Fig. 6.1, the amplitude of the secondary pressure peaks in Fig. 6.2 also reduce to some extent at higher surface velocities. However, the most striking feature of this set of profiles in Fig. 6.2 is the absence or the small size of a secondary pressure peak in the lowest surface velocity trace 'a' in Fig. 6.2. The region where the pressure peak is expected from theory is well defined in the trace and the absence of a distinct peak cannot be explained either by the width of the device, which is much smaller than the secondary peak region, or by the frequency response of the circuitry at the low surface velocity. Similar disappearance of the secondary peak at low surface velocity can also be seen in Fig. 6.3. In Fig. 6.4 two original pressure traces are reproduced, one is the trace 'a' of Fig. 6.2, and the

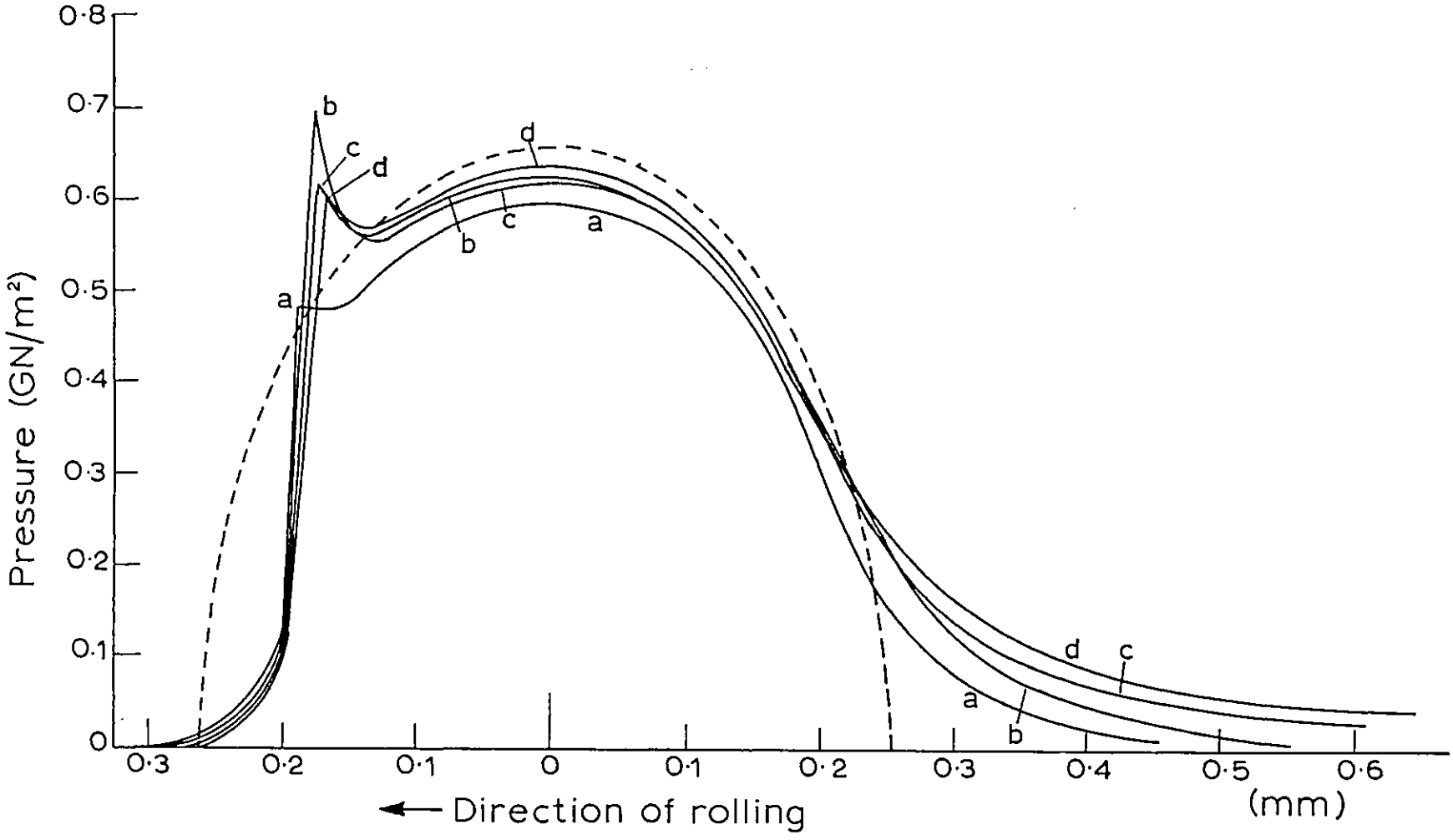

Fig. 6.2 Pressure profiles recorded with 10μm device, using oil2, at a fixed load of 0.275MN/m and surface velocities of (a)1.54, (b)3.4, (c)5.4 & (d)7.4m/sec.

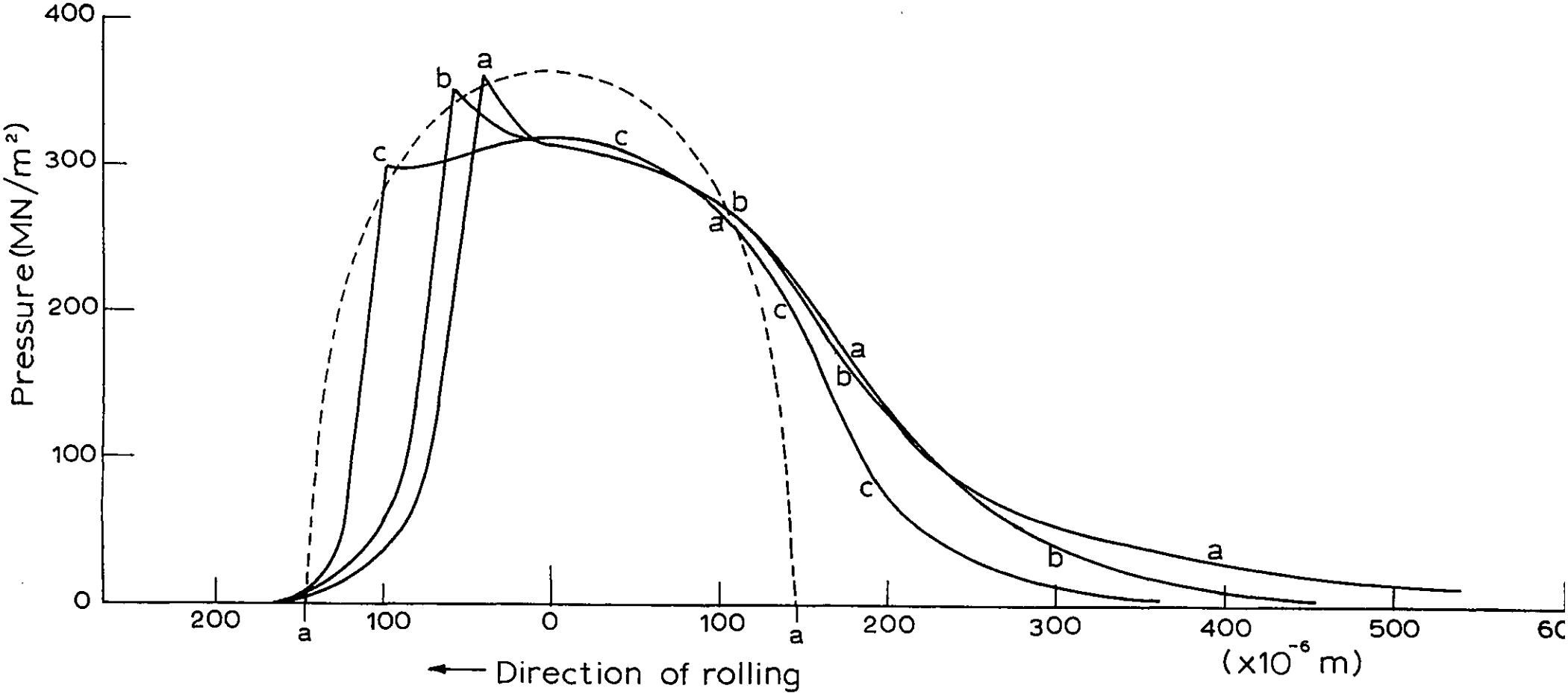

Fig. 6.3 Pressure profiles recorded with 10μm device, using oil2, at a fixed load of 0.0834MN/m and surface velocities of (a)0.75, (b)1.73 & (c)3.6m/sec.

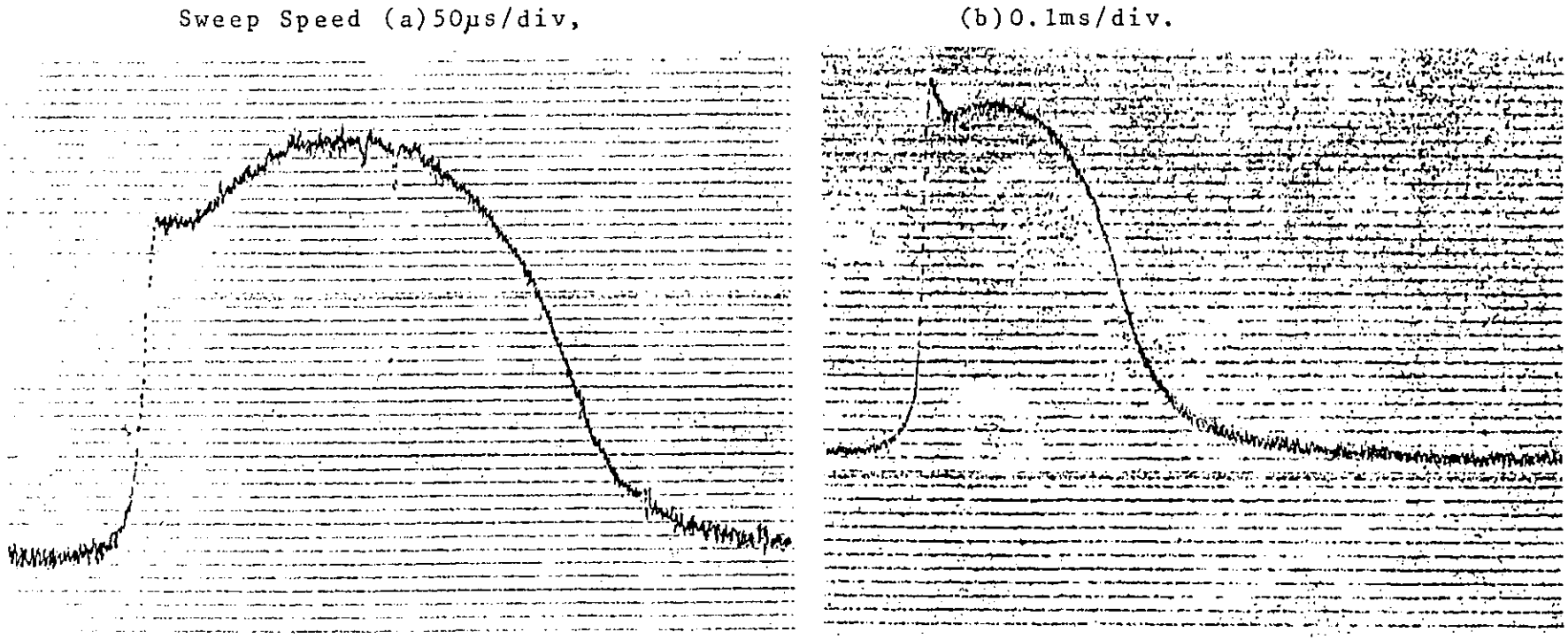

Fig. 6.4 Original recordings of the pressure profiles, both at surface velocity of 1.65m/sec but at loads of (a)0.275 & (b)0.22MN/m.

other is a trace recorded by a different device of similar dimensions and at the same surface velocity but at 20% lower load. It can be seen that the secondary pressure peak reappears at the slightly lower load. Unfortunately, the second device failed immediately after recording this trace due to a sudden heavy sliding between the discs.

The two sets of traces in Figs. 6.2 and 6.3 show the development of pressure in the inlet region quite well. At low surface velocities the pressure development zone at the inlet is quite short but with the increase of the surface velocity this zone extends further beyond the Hertzian zone.

The movement of the secondary pressure peak in Fig.6.2 is not well defined but the profiles at lower load in Fig.6.3 show the shift very clearly. This is expected if we consider the movement of the outlet pressure peak with the $g_3 \left(= \frac{W^2}{\eta_0 u E' R}\right)^{1/2}$ value as predicted by Johnson (41) and demonstrated by Hamilton and Moore (75). The range of values of g_3 for the lower load pressure traces in Fig. 6.3 is such that they fall on the steeper slope region of the plot, as shown in the insert in Fig. 6.3, which suggest larger movement of the secondary peak whereas higher values of g_3 for traces in Fig. 6.2 locates them on the low slope region of the Johnson's plot and the movement of the secondary spike should be negligible.

Oil 3

A set of pressure traces is reproduced in Fig.6.5 using Oil 3 at a load of 3.9×10^5 N/m. This load is higher than in Figs.6.1 and 6.2 to eliminate high sliding with this low viscosity oil. The surface velocity range covered is between 3.47 m/sec to 8.3 m/sec, being limited at the lower end by partial electrical

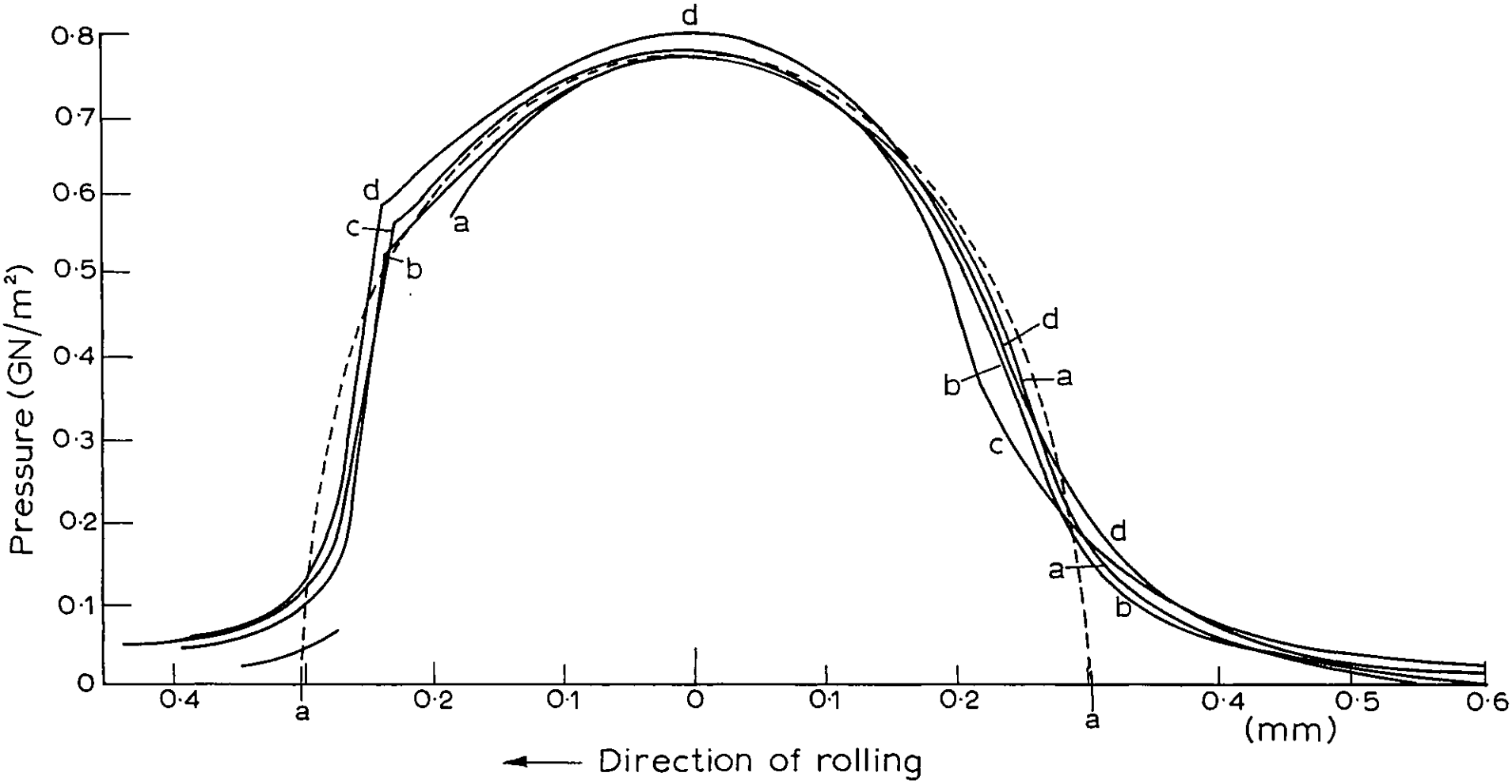

Fig. 6.5 Pressure profiles recorded with 10 um device, using oil3, at a fixed load of 0.39MN/m and surface velocities of (a)3.47, (b)5.2, (c)6.8 & (d)8.3m/sec.

contact through the very thin oil film. Trace 'a' shows the effect of such a short circuit where the part of the profile corresponding to the minimum film thickness disappeared. The probable reason for such breakdown has been discussed in Chapter 5.

The transducers used for recording the traces shown in Figs.6.2, 6.3 and 6.5 had the same width (10 μm). None of the traces recorded using Oil 3 showed any clear secondary pressure peak. This is to be expected however, as the low pressure-viscosity co-efficient of Oil 3 compared to Oils 1 and 2 produces a lower value of the non-dimensional quantity G. (G values for Oil 1: 3.9×10^3; Oil 2: 5.85×10^3 and Oil 3: 1.85×10^3). This low value gives rise to a shorter and narrower secondary pressure peak which even these fine devices cannot resolve.

The traces shown in Fig.6.5 are broadly similar. This was found for all other oils at higher loads.

6.1.2 Effect of Pressure-Viscosity Coefficient on Pressure Profile

In Fig.6.6 three pressure traces are reproduced which were recorded with devices 10 μm in width, but using the three different oils. The 2.78×10^5 N/m load was the same in all three cases and the surface velocities were close to 3.8 m/sec. The main difference between these traces is the height of the secondary pressure peak. The trace for Oil 2, which has the largest value (3.05×10^{-8} m^2 N^{-1}), shows the largest secondary pressure peak. Trace 'a' for Oil 1 (α value of 2×10^{-8} m^2 N^{-1}) shows the second highest pressure peak while Oil 3 ($\alpha = 0.95 \times 10^{-8}$ m^2 N^{-1}) does not show a secondary pressure peak. This strong dependence of the height of the pressure spike on the

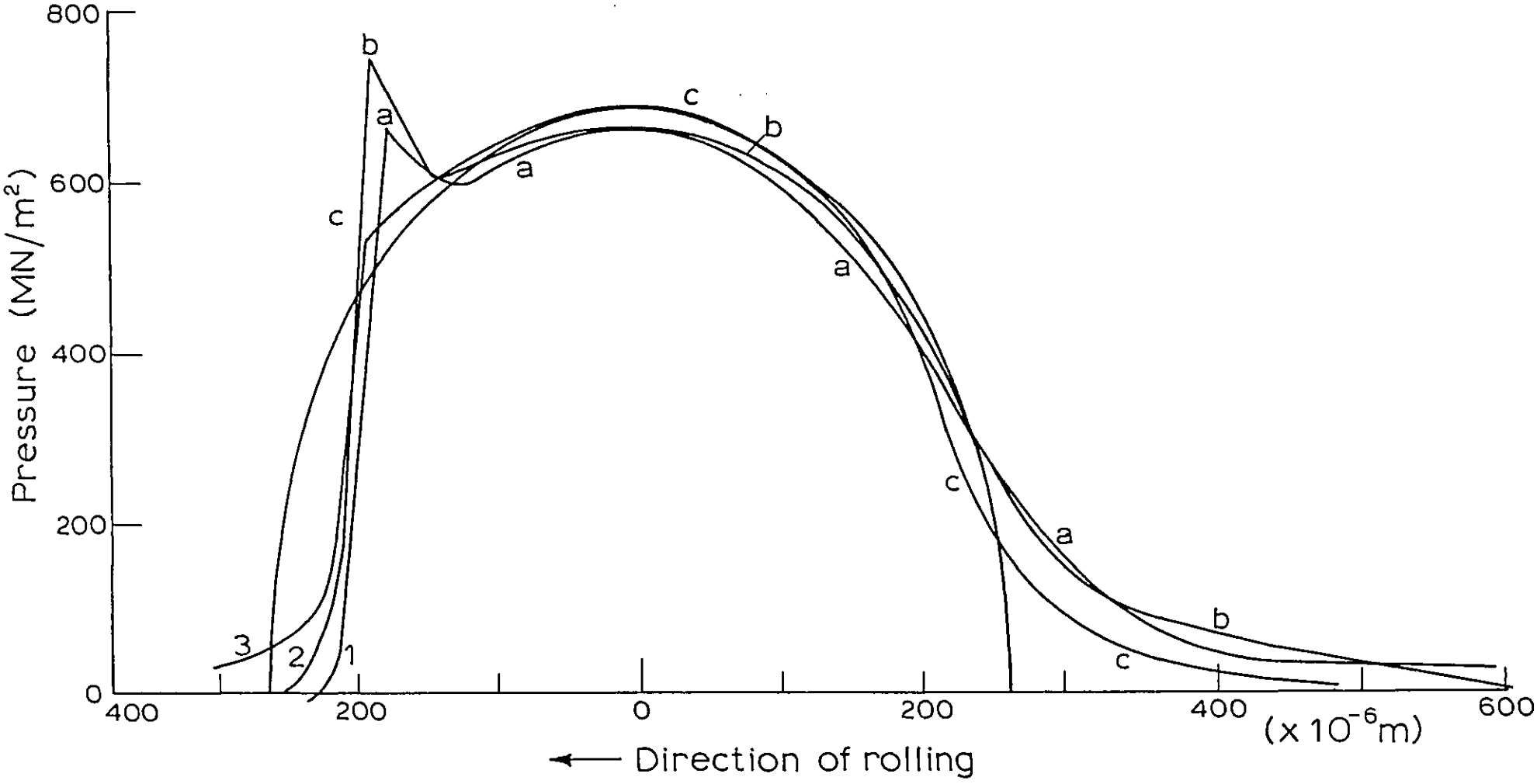

Fig. 6.6 Pressure profiles recorded with 10μm device at a load of 0.278MN/m and surface velocity of 3.8m/sec using (a)oil1, (b)oil2, (c)oil3.

pressure-viscosity co-efficient of the oil was not always observed. At other surface velocities above 3.8 m/sec the height of the secondary pressure peaks produced by Oils 1 and 2 were similar. The effect of α upon the secondary pressure peak zone shows up more clearly at higher loads. With Oil 1, even the finest transducer could not resolve the secondary pressure peak much above a load of 3×10^5 N/m at any surface velocity within the useful operating range. With Oil 2, secondary pressure peaks could be detected upto loads of 7.23×10^5 N/m.

The $\eta_o U$ value for traces 'a' and 'b' in Fig.6.6 are very similar and about double that of trace 'c'. However, traces recorded using Oil 3 at double the surface velocity of that of Fig.6.6 were broadly indistinguishable from that illustrated.

6.1.3 Effect of Load on Pressure Profiles

Oil 1

Two sets of pressure profiles are reproduced in Figs. 6.7 and 6.8, both sets being recorded using Oil 1. The set in Fig. 6.7 was recorded using the analogue oscilloscope and all three traces show a break in the profiles in the exit region. The active element of the device used for this set was about 50 μm wide and 1 mm long while the track width of the mating disc was 6 mm long. The surface velocities for the traces were close to 4.34 m/sec and the loading range covered was from 4.45×10^5 to 11.1×10^5 N/m. All three traces had to be individually calibrated as electrode wear was noticed during the test. Traces in Fig. 6.8 were recorded with a 10 μm wide active element and the track width used was 8 mm long. The surface velocities for all four traces were 7.2 m/sec and the loading range covered was 2.78×10^5 to 10×10^5 N/m.

A major difference between the traces in Figs. 6.7 and 6.8 can be seen on the exit side of the pressure profiles. Traces recorded with the finer devices always show a sharper transition of pressure from the secondary peak to the zero level, whereas a much gentler decay occurred with the traces in Fig. 6.7. A theoretical study of the effect of device width on pressure profiles in a later section confirms this observation. The gentle decay at the exit is believed to be the reason why pressure traces 'a' and 'b' shown in Fig. 6.7 show less conformity to the Hertzian pressure profile than other traces recorded with Oil 1 and using finer devices in this high load range. This is for the reason that the width of the transducer is, in effect,

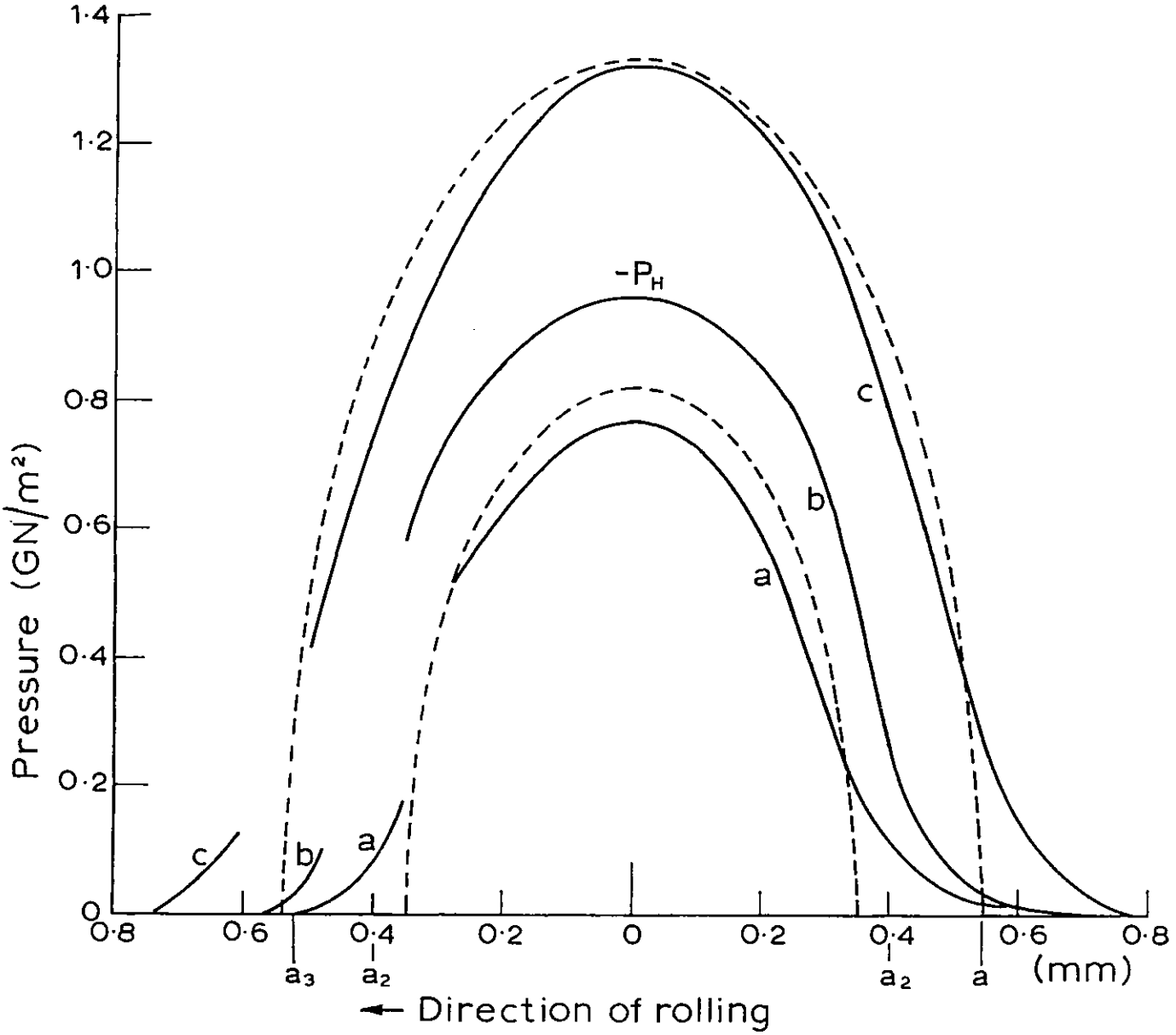

Fig. 6.7 Pressure profiles recorded with 50um device, using oil1, at a surface velocity of 4.34m/sec and loads of (a)0.445, (b)0.667, (c)1.11MN/m.

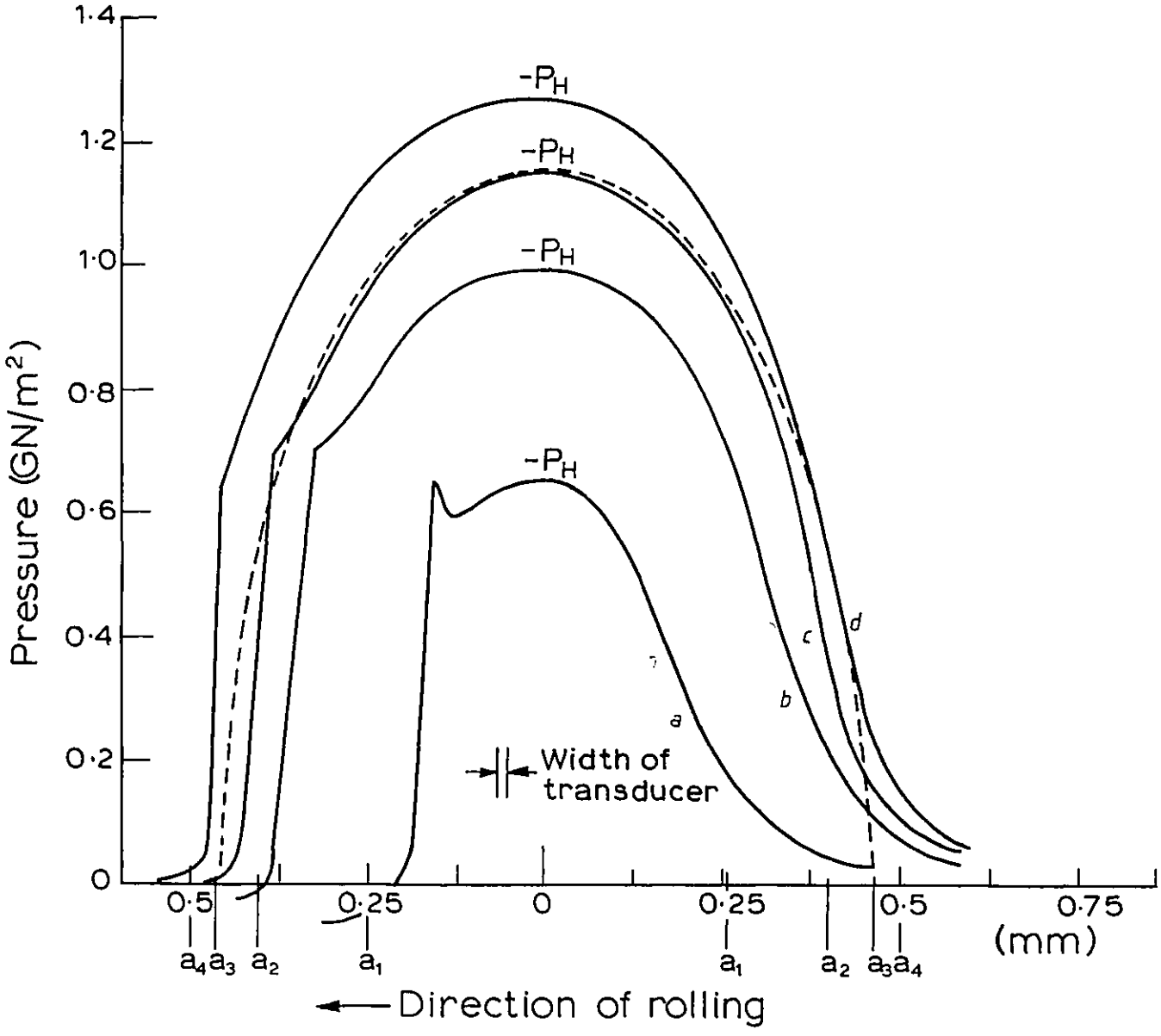

Fig. 6.8 Pressure profiles recorded wit h 10um device, using oil1, at a surface velocity of 7.2m/sec and loads of (a)0.278, (b)0.668, (c)0.83 & (d)1MN/m.

added to the Hertzian width. Since the area under the pressure profile depends only on load and speed it must be constant if these are fixed. Thus the effect of the apparently increased length of the Hertzian region will be an apparent drop in the peak Hertzian pressure recorded, as shown in Fig. 6.9.

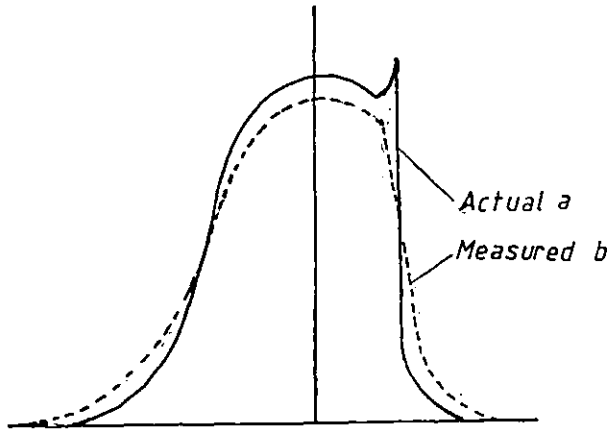

Figure 6.9 - Effect of Large Width Transducer on Pressure Profile: (a) Correct Profile, (b) Modified Profile due to Large Width Device.

The Hertzian pressure distribution for the conditions of trace 'c' in Fig. 6.7 is also shown (dotted line) in the figure. These two traces together show most of the typical characteristics of pressure distribution found at relatively high load in an EHL contact. The gradual development of pressure at the inlet starts beyond the Hertzian zone. The pressure profile then crosses the Hertzian distribution and remains confined within it until the secondary pressure peak region is reached. The end zone is better defined in trace 'c' in Fig.6.8 . The secondary pressure peak always occurs outside the Hertzian distribution; however, the rapid drop of pressure occurs within Hertzian contact width. This is in agreement with the theoretically derived curves by Dowson and Higginson (18).

Traces in Fig. 6.8 demonstrate the effect of loading on secondary pressure peak. At the low load of 2.78×10^5 N/m the secondary pressure peak shows up prominently. As the load is increased to 6.8×10^5 N/m, the peak disappears although a change of profile curvature can still be seen. At the highest load of 10^6 N/m the secondary peak zone can only be distinguished by the sudden change of slope of the pressure profile. Theoretically obtained pressure profiles show that the secondary pressure peak becomes narrower as the load is increased. A fixed width active element which can resolve the peak at low loads cannot do so at sufficiently high loads.

Oil 2

Three sets of pressure profiles are reproduced in Figs.6.10, 11 and 12. All these traces were generated by the same transducer with a 10 μm wide active element. Traces in Fig. 6.10 were at surface velocities of around 3.7 m/sec and the range of loading covered was from 1.67×10^5 to 5×10^5 N/m. Traces in Figs.6.11 and 12 are at surface velocities of 5.4 m/sec and 7.4 m/sec respectively and they cover the loading range between 1.67 to 6.67×10^5 N/m and 2.78×10^5 to 7.23×10^5 N/m respectively.

The primary peak pressures of the pressure profiles obtained with Oil 2 were found to differ from the peak Hertzian pressure by the largest amount for the three oils examined.

The three sets of traces together show the effect of load and surface velocity on the secondary pressure peak quite well. In Fig.6.10 the pressure peak gradually reduces with load and disappears at the load of 5×10^5 N/m; however, in Fig.6.11 with the increase of the surface velocity to 5.4 m/sec

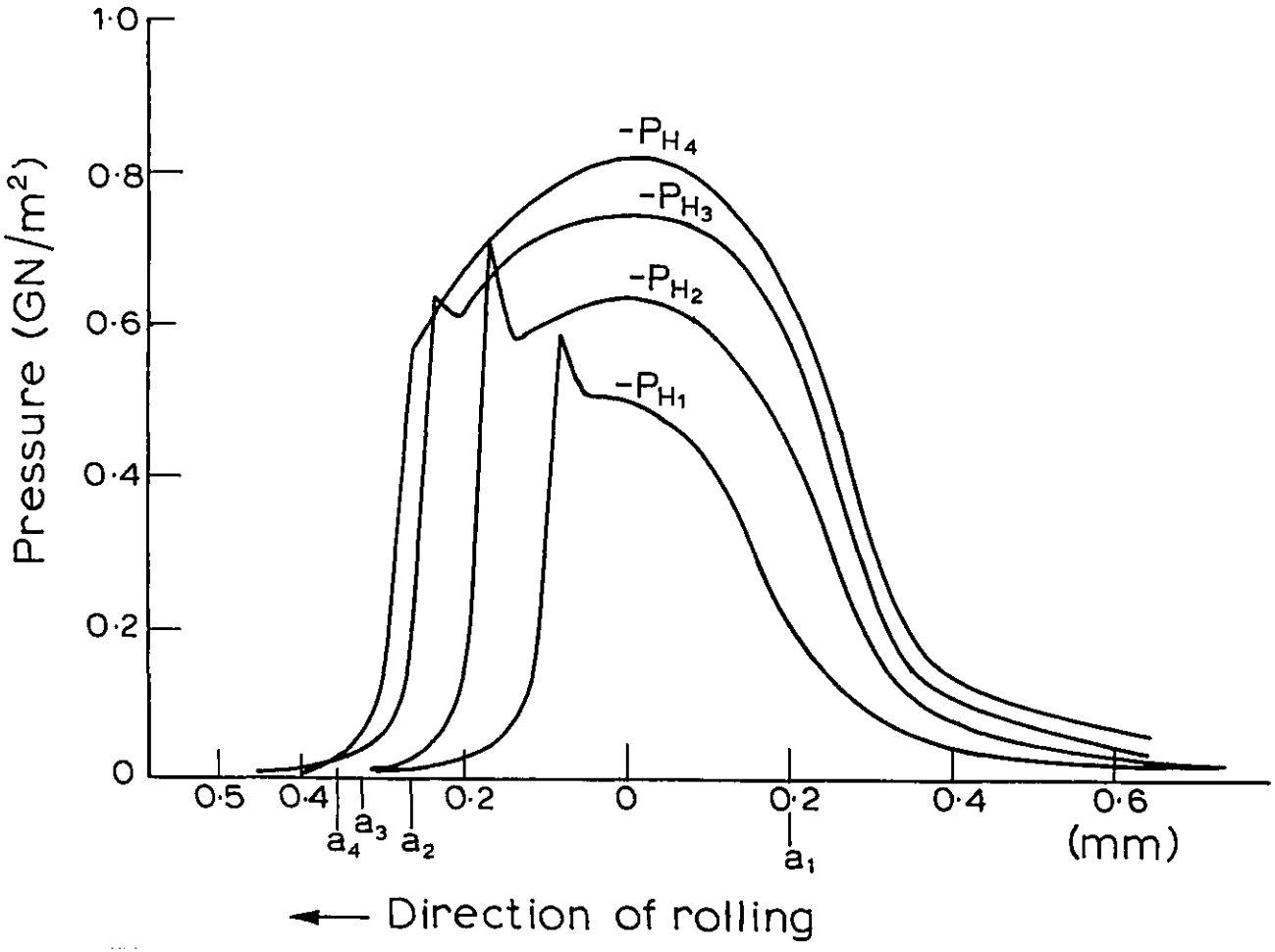

Fig. 6.10 Pressure profiles recorded with 10μm device, using oil2, at a surface velocity of 3.7m/sec and loads of (a) 0.167, (b)0.278, (c)0.417 & (d)0.5MN/m.

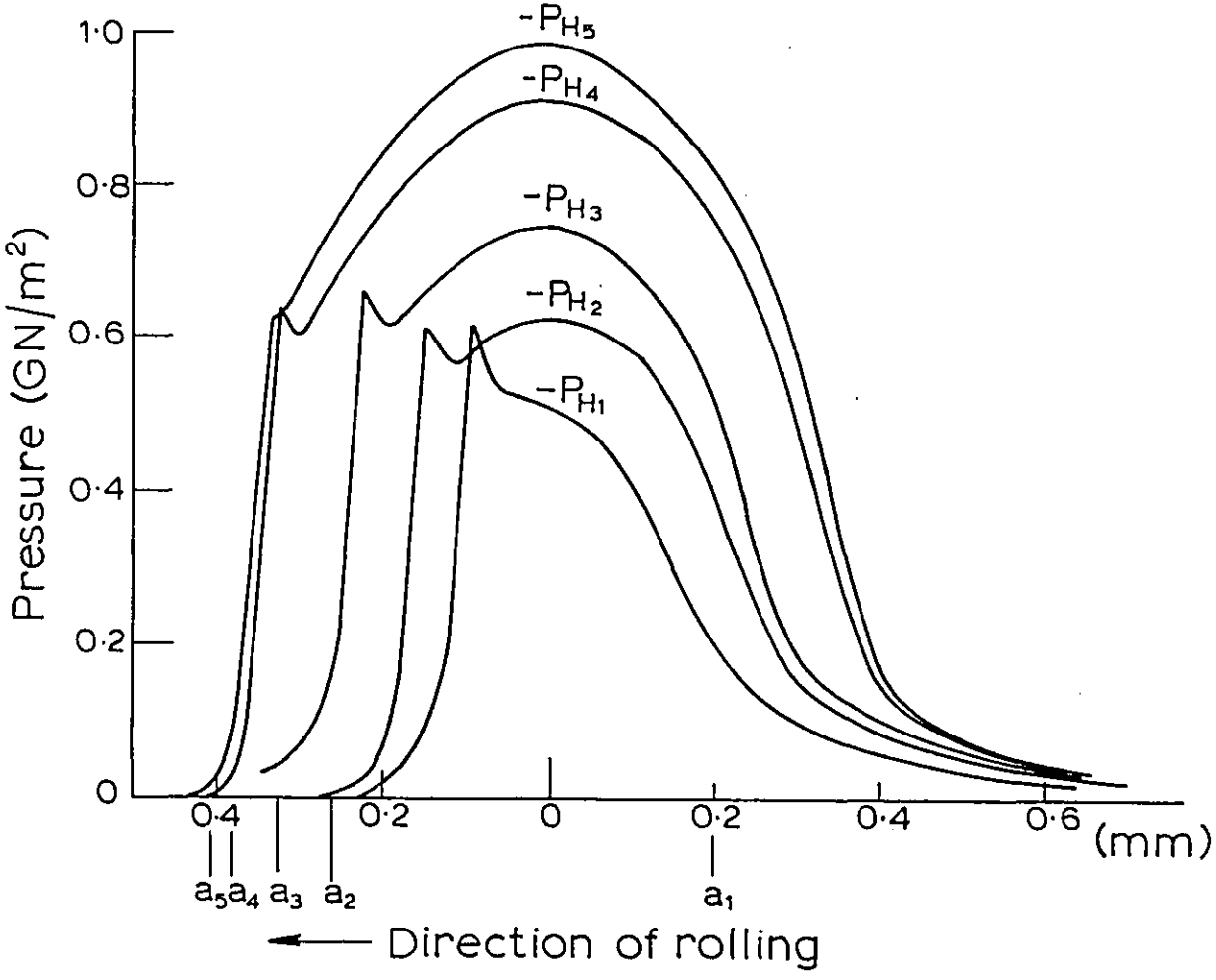

Fig. 6.11 Pressure profiles recorded with 10μm device, using oil2, fixed surface velocity of 5.4m/sec and loads of (a)0.167, (b)0.278, (c)0.417, (d)0.58, (e)0.667MN/m.

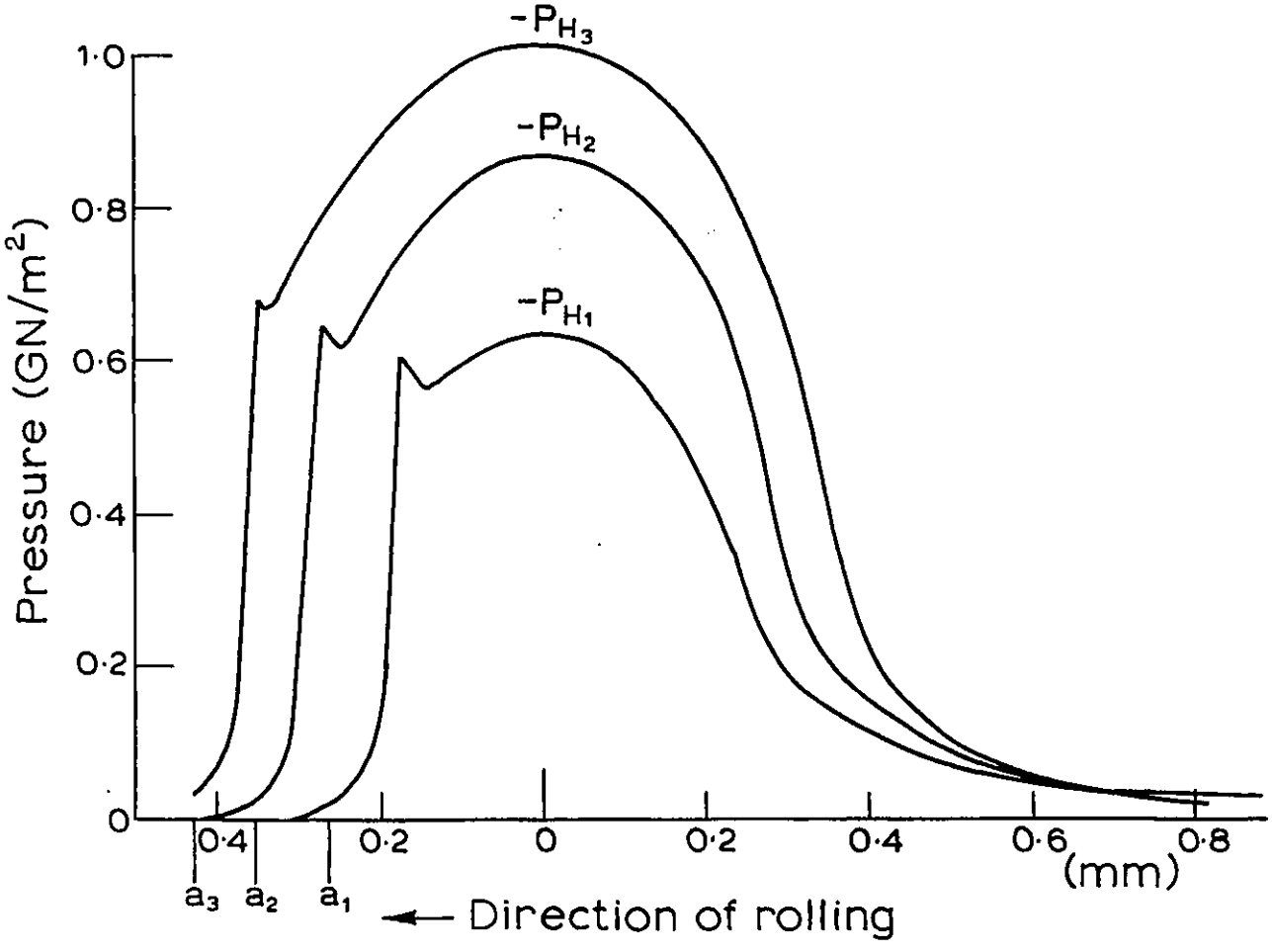

Fig. 6.12 Pressure profiles recorded with 10μm device, using oil2, at a surface velocity of 7.4m/sec and loads of (a)0.228, (b)0.5 & (d)0.723MN/m.

the secondary pressure peak shows up quite clearly even at a load of 5.84×10^5, but as the load goes up to 6.68×10^5 N/m in trace 5 the secondary pressure peak disappears again. The secondary peak reappears as the surface velocity is increased as can be seen in Fig.6.12c at a load of 7.23×10^5 N/m. The observations are consistent with the theoretical findings in that the theoretical pressure distribution shows the secondary pressure peak zone to become narrower with the increase of load and decrease of surface velocity.

For a constant surface velocity the effect of load on the development of pressure at the inlet zone is clearly demonstrated in Fig.6.11. The lowest pressure trace 'a' at a load of 1.67×10^5 N/m shows the gradual development of pressure even at a distance of 2a away from the Hertzian zone (where 2a is the width of the Hertzian contact), but as the load increases the ratio of this distance to the Hertzian width gradually gets lower and at the highest load trace 'e', at the load of 6.65×10^5 N/m, the development of pressure zone reaches only to 0.5a beyond the Hertzian zone.

The movement of the secondary pressure peak with load is also clearly demonstrated in Fig.6.11. At the lowest load the pressure peak occurs at a distance of about 0.4a away from the primary pressure peak. As the load increases the peak moves further away from the primary peak and at the highest load the secondary peak occurs at a distance of 0.8a from the primary peak.

Oil 3

Four traces are reproduced in Fig.6.13, which were also recorded using a device with a 10 μm wide active element.

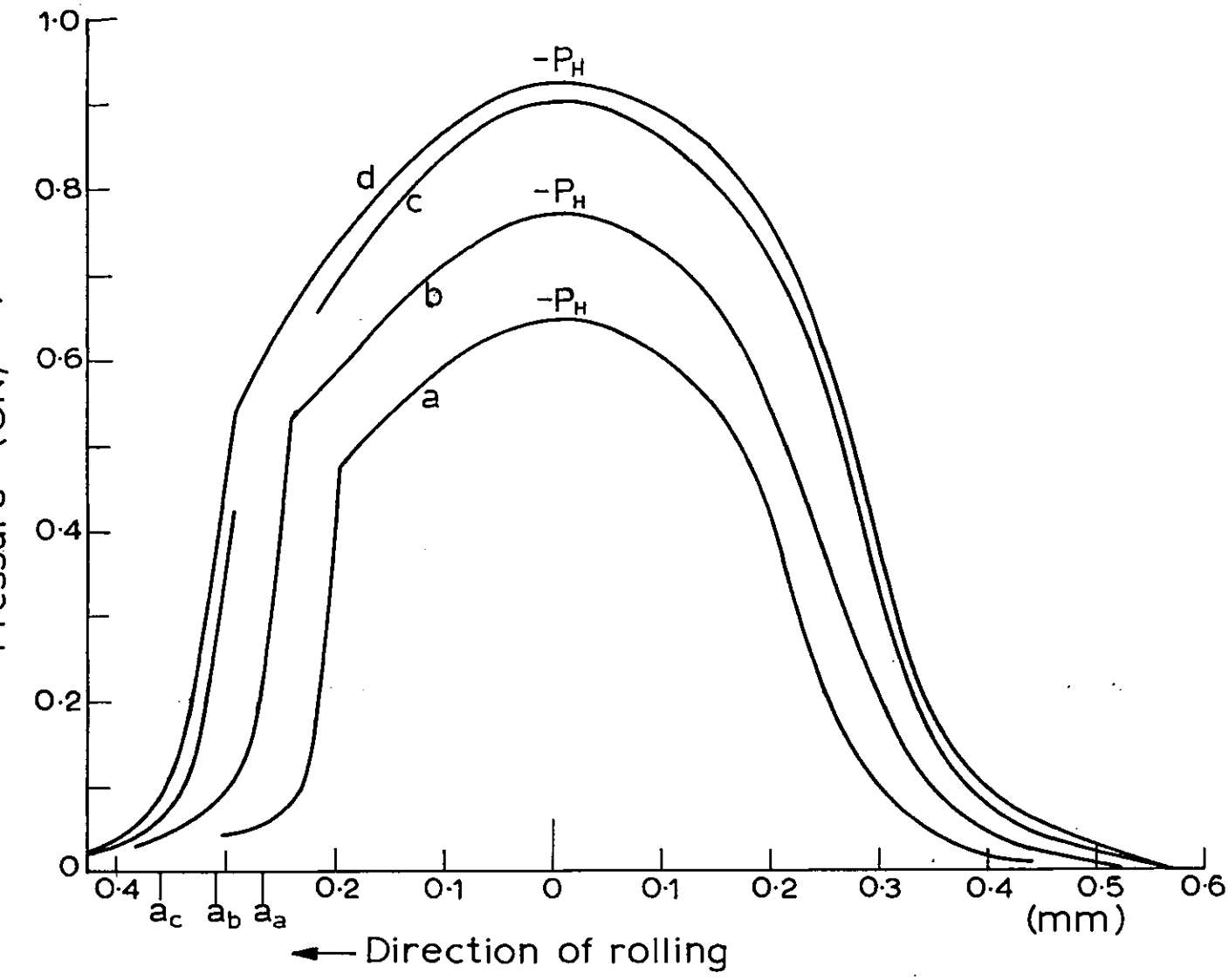

Fig. 6.13 Pressure profiles recorded with 10μm device, using oil3, at a surface velocity of 5.2m/sec for traces a to c and at 7.4m/sec for trace d and at loads of (a)0.278MN/m, (b)0.39, (c)0.556 & (d)0.565MN/m.

The surface velocities for the first three traces were 5.2 m/sec while the fourth trace was produced with a disc surface velocity of 7.4 m/sec. They cover the range of loading from 2.78 to 5.56×10^5 N/m. Electrical conduction through the oil film occurred where the film thickness was at a minimum, as the load was increased at a fixed surface velocity. However, increasing the surface velocity, and hence the film thickness, removed the short circuit.

Of the three oils used in this project, pressure profiles recorded with Oil 3, which has the lowest viscosity and α value, show the closest agreement between the primary peak pressure and the calculated peak Hertzian pressure. Most of the observations made of the pressure traces for Oils 1 and 2 were found to hold true for Oil 3 as well, with the exception of the secondary pressure peak, which never appeared using Oil 3. However, there was a limited range of operating conditions that could be covered with Oil 3.

6.1.4 Effect of Sliding on the Pressure Profiles

Very little sliding work was undertaken in this project, particularly with pressure transducers, as it was found to drastically reduce the life of the devices. However, a few devices with relatively wide active elements, were operated under sliding conditions. Usually sliding was introduced for a brief period, and careful checking of the reproducibility of a trace under a particular operating condition was not possible.

In Fig.6.14 two sets of pressure profiles are reproduced. In each set one trace was obtained under nominal rolling conditions and the other under some sliding. Both sets were

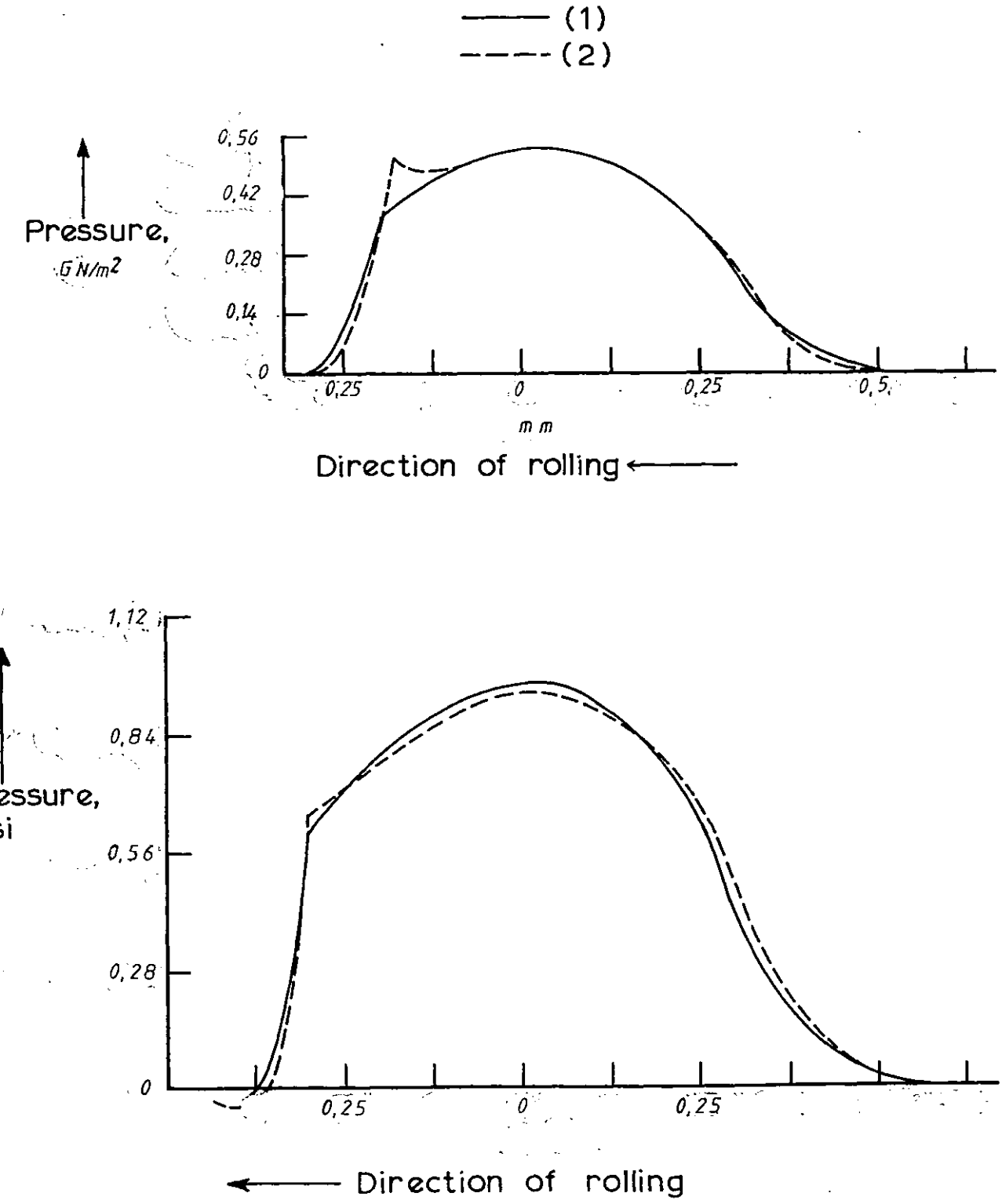

Fig. 6.14 Pressure profiles recorded under rolling and partial sliding conditions, using oil1; (a) fixed load of 0.222MN/m, surface velocity 4.1m/sec (i) rolling (ii)29% slip; (b) load of 0.52MN/m, surface velocity 4.76m/sec (i) rolling, (ii)17% slip.

obtained using Oil 1. None of the profiles recorded with this relatively wide device showed any sign of the secondary pressure peak under nominal rolling conditions. The set in Fig.6.14a was at the low load of 2.2×10^5 N/m while the set in Fig.6.14b was at a load of 5.2×10^5 N/m. In Fig.6.14a a 29% slip ratio at a mean rolling speed of 4.1 m/sec at the lower load produced a pressure profile almost identical to the profile produced under pure rolling except for the secondary pressure peak zone, which under sliding condition was found to change shape slightly to produce a vestigial secondary peak. The second set was recorded at a higher load and at 17% slip ratio at the mean rolling speed of 4.76 m/sec; very little change between the two profiles under rolling and sliding conditions could be detected.

In Fig.6.15 a set of three pressure profiles is reproduced, recorded using Oil 3. The change in loading is apparent, otherwise very little difference could be detected between trace'a', under pure rolling at 4.3 m/sec and trace 'b', where 4.7% sliding was introduced. However, with the introduction of this very low sliding, in trace 'b', breakdown of the oil film was found to occur near the oil outlet. With a further increase in sliding to 16%(trace c), breakdown occurred at the inlet zone as well.

6.1.5 Theoretical Study of the Effect of Transducer Width on the Pressure Profile

To study the effect of the width of an active element on a pressure profile, a theoretically obtained pressure profile was chosen from Dowson and Higginson's (18) work. The theoretical profile was then digitized into 250 random samples. A Fortran programme was developed which could

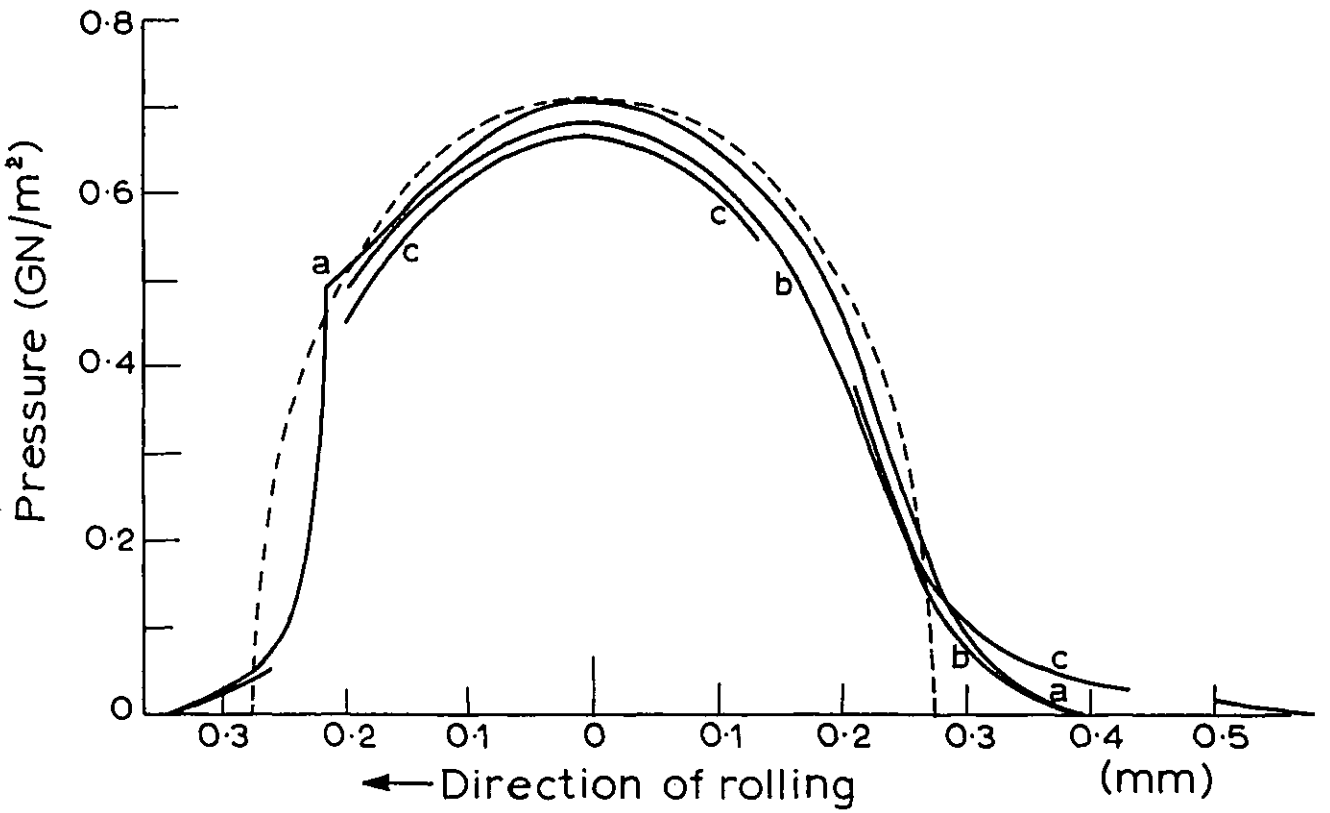

Fig. 6.15 Pressure profiles recorded using oil3, (a) rolling at surface velocity of 4.3m/sec, (b) slliding 4.7% slip (4.3:4.1), (c) sliding 16% slip(4.3:3.6).

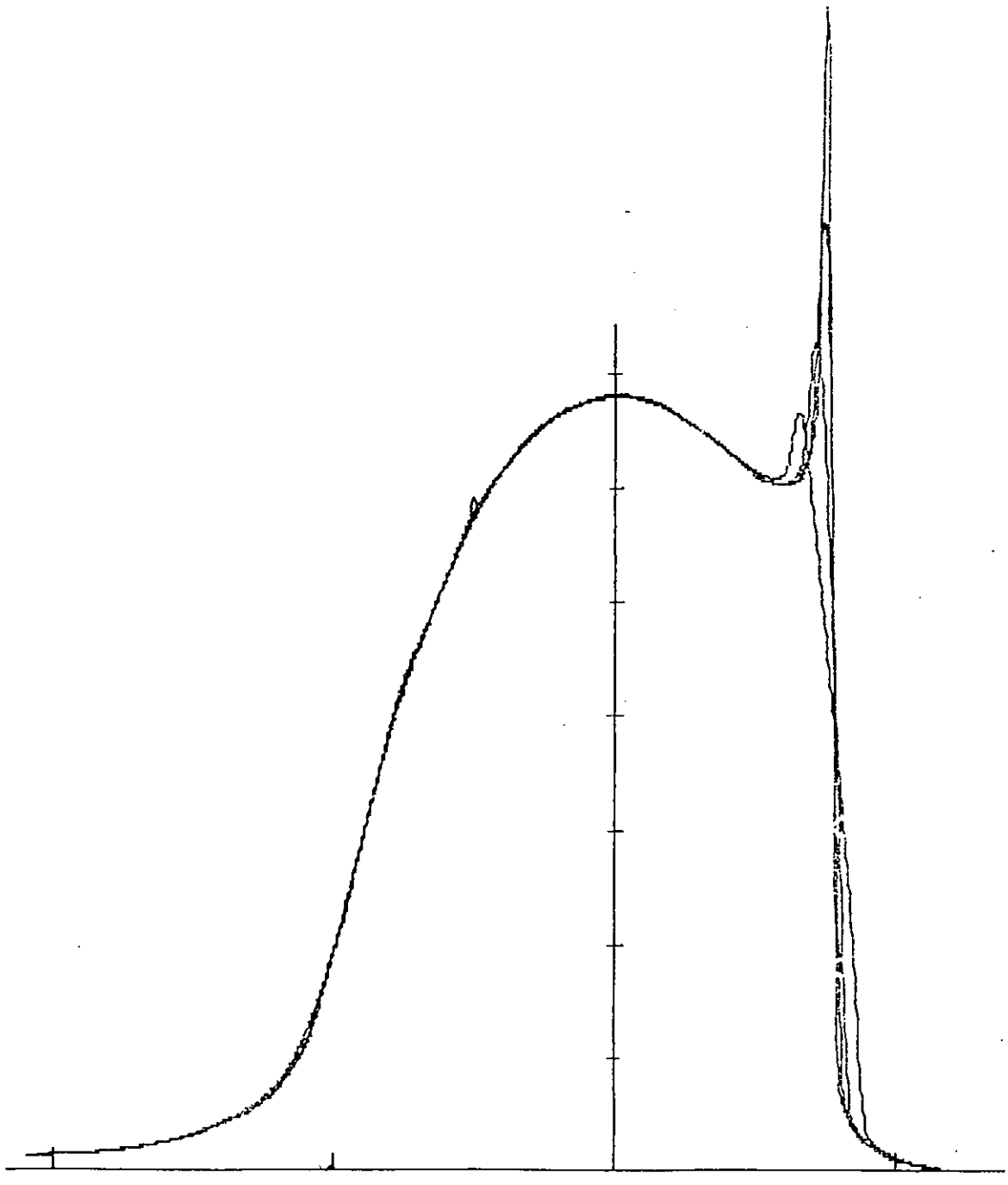

Fig. 6.16 Theoretical study of averaging effect of a finite width pressure transducer on a theoretical pressure profile.Width of transducer 3, 7.5, 15, 30μm.

transform these samples into 1000 points equally spaced along the distance axis. The overall width of the trace was taken as 1500 μm, as a result the distance between two consecutive points was 1.5 μm. Thus to study the effect of a 3 μm wide device, the sampled points were averaged using a sliding average of two points. The same method was followed for determining the effect of a 7.5 μm wide device, where a sliding average over five samples was performed. This method broadly simulates the effect of a finite width transducer moving at a steady speed through the contact. The result of such averaging for four different width devices is shown in Fig.6.16.

From Fig.6.16, it can be seen that the width of the device, used in this study, does not affect the pressure profile much at the inlet side, but major changes take place in the secondary pressure peak zone. The height of the secondary pressure peak reduces sharply as expected. In addition to this the slope of the pressure decay from the secondary pressure peak also decreases in magnitude as the device width increases. The secondary pressure peak moves towards the primary pressure peak and the point from which the secondary pressure peak starts to develop also moves towards the primary pressure peak.

6.1.6 Measurement of Maximum Shear Stress

In the process of digitising a transducer signal, the digital storage oscilloscope takes samples of the signal at very precise time intervals. There could be either 1024 or 512 samples over the overall sweep length of the screen. In either case the number of samples taken to construct the profile is so large that, when plotted by the

U.V. recorder, an apparently continuous profile was produced. However, in the region of rapid pressure transition from the secondary peak towards the zero pressure level, the sampling frequency becomes important. In Fig.6.17 four expanded pressure decay profiles are reproduced with correct spacing between the samples, for the sampling frequency used, the distance being determined from the disc surface velocity and oscilloscope sweep rate. Also shown is an original recording of one of the decay profiles.

It can be seen that in all four cases the curves flatten off at higher pressures. This is believed to be an experimental artefact arising from the finite width of the device and the limited frequency bandwidth available for the electrical signal. With an infinitely narrow device and an infinitely wide bandwidth the curves might conform with theory. The result of these limitations is that the maximum shear stress cannot be reliably obtained from the maximum slope of the curve. However the maximum estimated shear stresses are given in Table 6.1 , as determined from the two successive sample points where the largest pressure change occurred in the recorded pressure profile. The corresponding film thickness values were taken to be the minimum film thickness. This is thought to be a reasonable assumption as the exit constriction zone occurs immediately after the second pressure peak. From Table 6.1 it can be seen that the maximum absolute pressure gradient is generally higher at lower surface velocity, (which is also true for the overall pressure decay over the range from 600 MN/m^2 to 100 MN/m^2 as can be seen

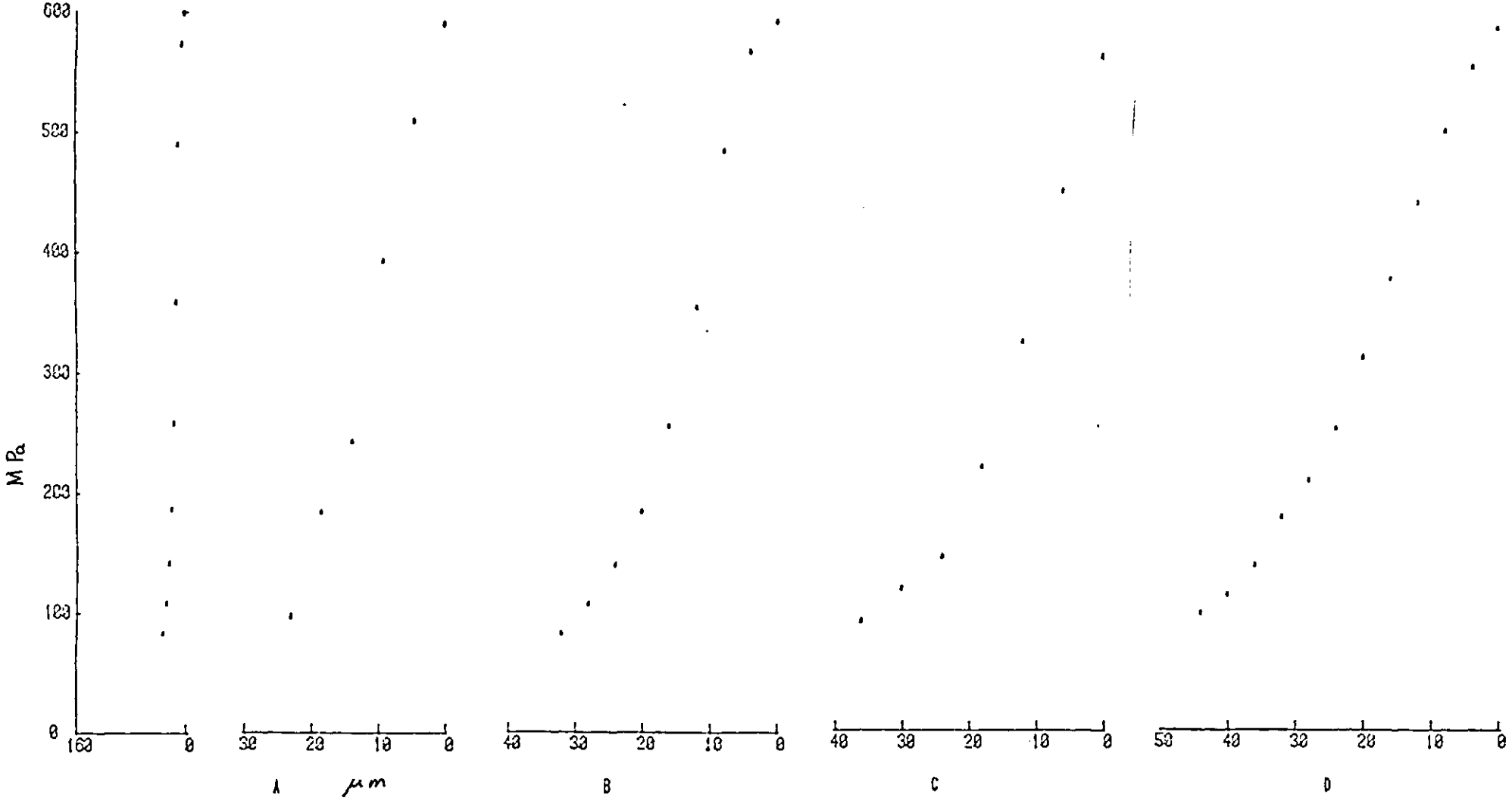

Fig. 6.17 Exit part of the pressure profiles, showing the pressure decay from the secondary peak pressure, pressure profiles reccorded at a fixed load of 0.275 MN/m and surface velocities of A)2.1, B)3.6, C)5.4, D)7.4m/sec, using oil1.

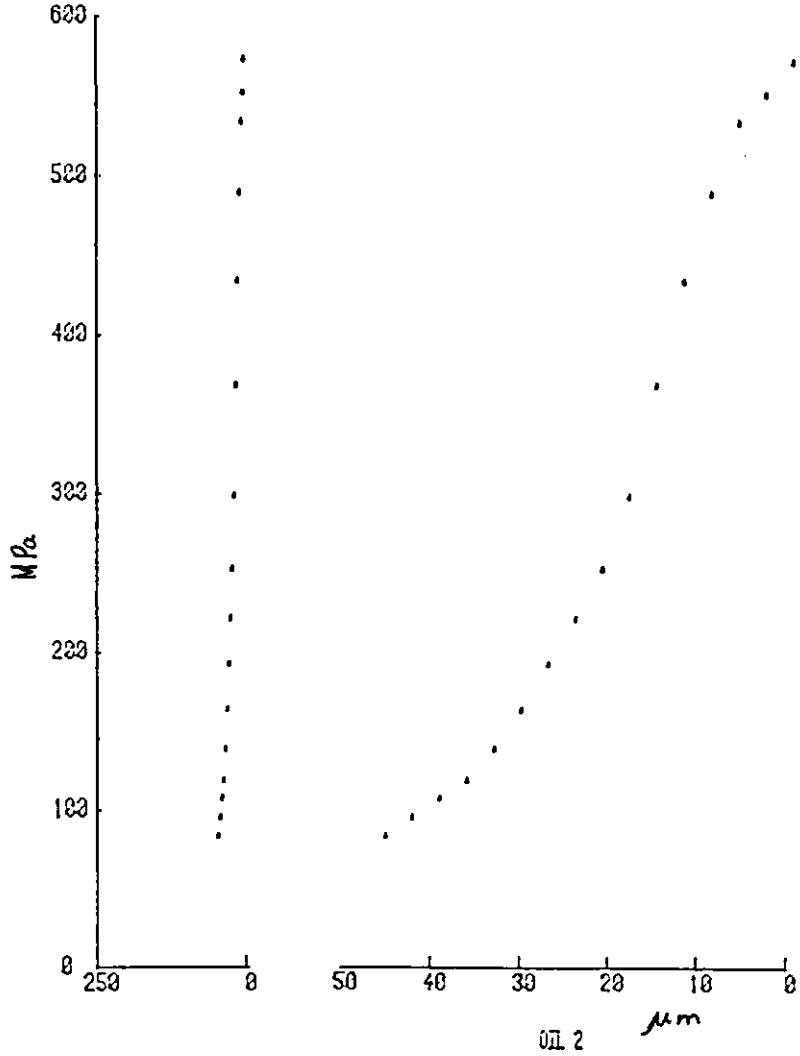

Fig. 6.18 Exit part of the pressure profile, showing the pressure decay from the secondary peak pressure, load 0.275MN/m, surface velocity 5.4m/sec, oil2.

in Fig.6.17). However, as the film thickness at higher surface velocity is also higher, the maximum shear stresses were found to be similar, and no systematic relation could be detected between surface velocity and shear stress.

In Fig.6.18,a similar expanded pressure decay profile is shown for Oil 2 and a set of maximum shear stress values are also calculated for Oil 2 in Table 6.1 . (The film thickness values for Oil 2 at load 0.417×10^6 N/m and 5×10^6 N/m are estimated).

Table 6.1

Oil	Load 10^6 N/m	Surface Velocity	Min. Film Thickness μm	$-\frac{dP}{dx}$ 10^{13} Nm^{-3}	$\frac{h_o}{2}\frac{dP}{dx}$ in M Pa.
		2.1	1	3.16	15.8
		3.6	1.28	3.3	21
1	0.278	5.4	1.56	2.1	16.4
		7.4	1.83	2.25	20
	0.278	3.6	1.6	3.5	28
		5.4	1.9	2.4	23
	0.417	3.6	1.18	3.1	18.3
		5.4	1.45	2.75	20
2		7.4	1.7	2.67	23
	0.5	5.4	1.45	2.93	21
		7.4	1.7	2.27	19

6.1.7 Effect of Non-dimensional Quantity g_3 on the Position of Secondary Peak

Following the assessments of theoretical solutions by Johnson (41) the relative positions of the secondary pressure peaks, $^{x}/_{a}$, were plotted against the logarithm of the non-dimensional parameter g_3. In determining the value of x, i.e. the distance along the disc surface between the secondary pressure peak and the maximum Hertzian pressure, measurements were made from the original traces and then converted into distance. In cases where the secondary pressure peak was not clearly defined, the break point where the change in slope of the pressure profiles took place was taken as the appropriate position. Occasionally it was found difficult to determine the position of the primary pressure peak due to the noise, in which case a smooth curve was drawn through the whole trace, keeping it as much as possible at the centre of the noise level and the point of the locus where the slope was zero was taken as the primary peak pressure.

In Figs.6.19, 6.20 and 6.21, the $^{x}/_{a}$ values for the various values of log g_3 are plotted along with Johnson's curve for oils 1, 2 and 3 respectively. Fig.6.19 shows the results from two experiments and Figs.6.20 and 6.21 were obtained from single experiments. Some scatter in results can be seen in all three figures. The main reason for this is believed to be the inaccuracies in the indicated load which would move both $^{x}/_{a}$ and g_3 values away from the curve.

The pressure profiles recorded in the experiment for

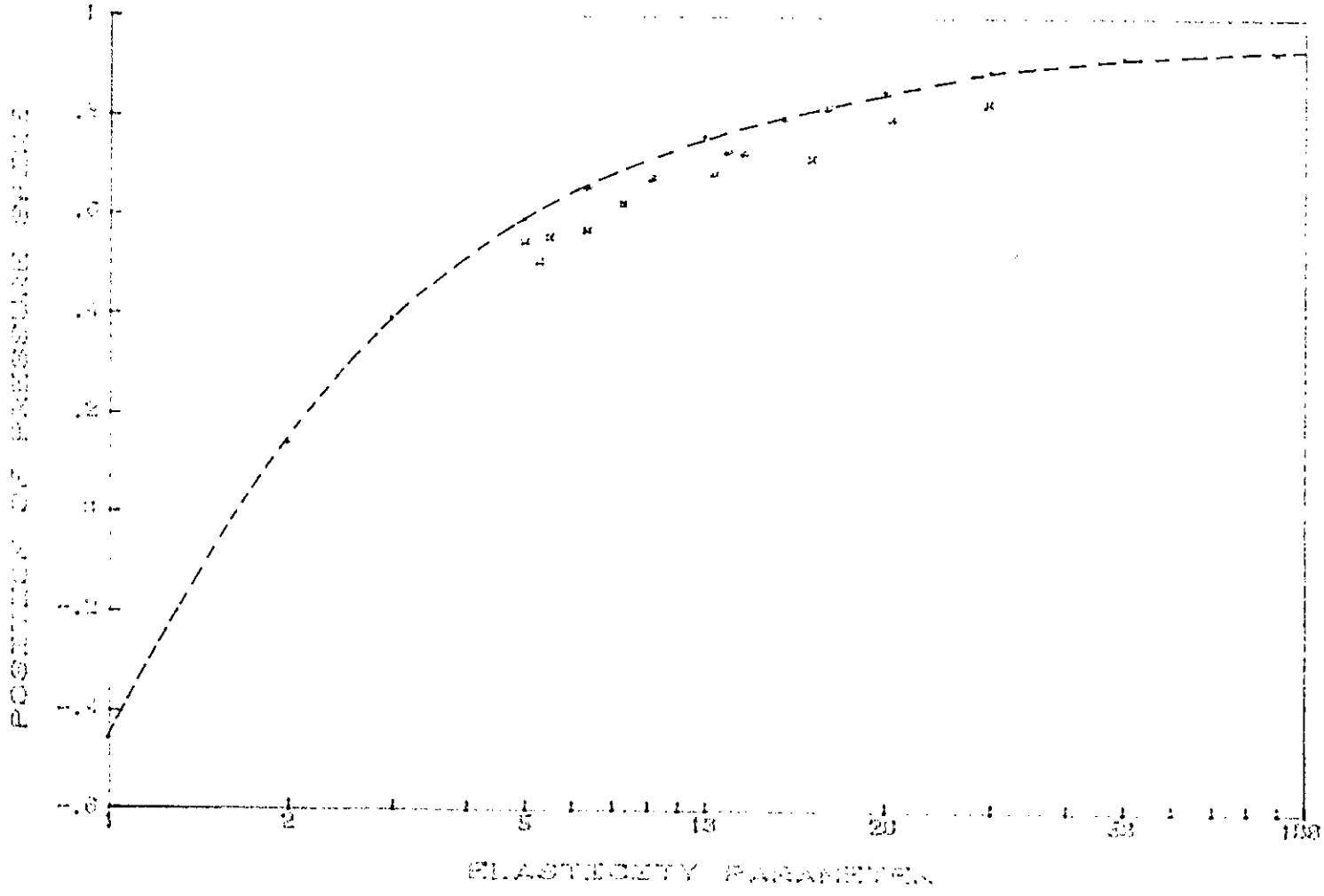

Fig. 6.19 Variation of the relative position of secondary pressure peak, x/a, with logarithm of non-dimensional quatity g_3, oil1. Johnson's prediction shown in broken line

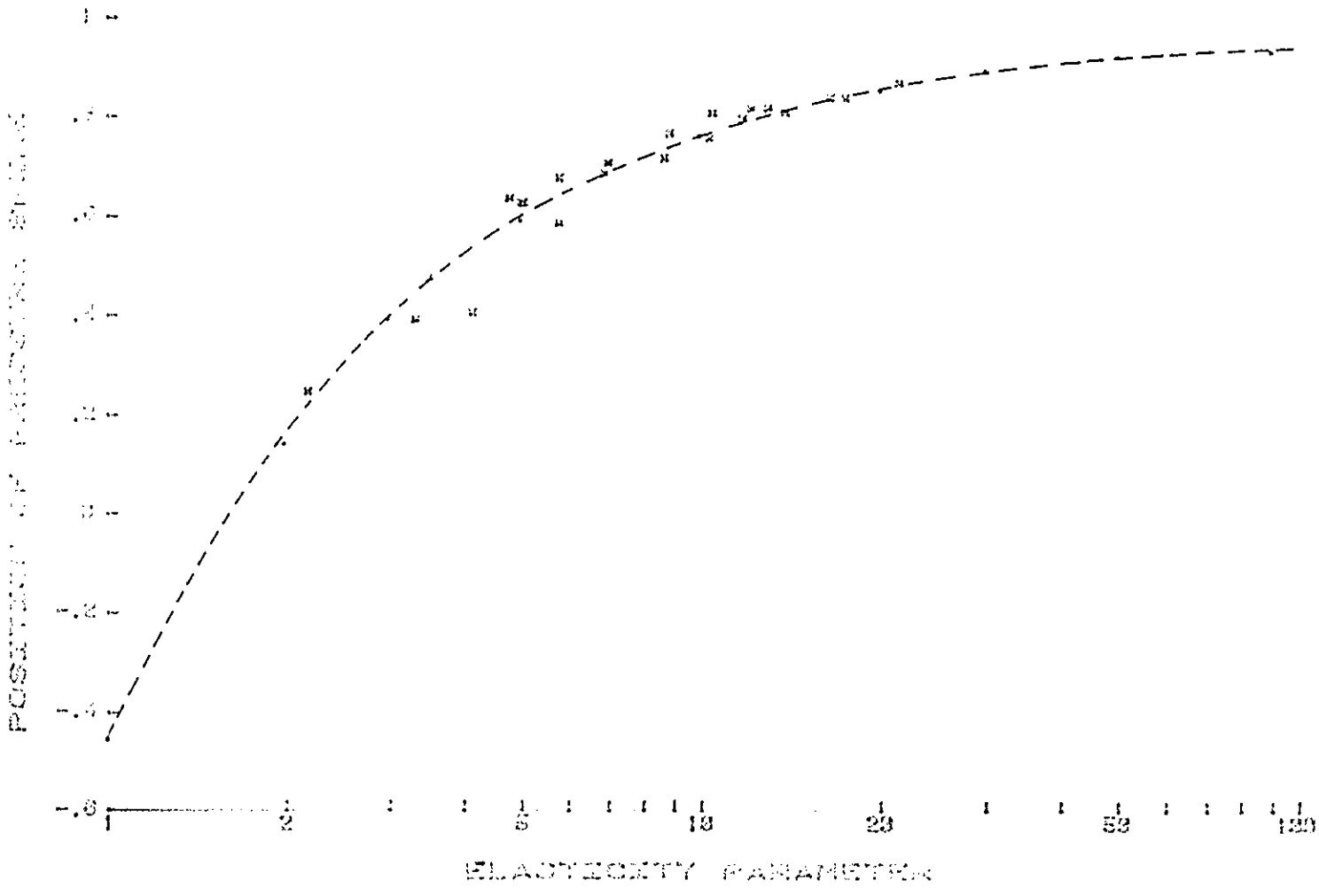

Fig. 6.20 Variation of the relative position of secondarypressure peak, x/a, with logarithm of non-dimensional quantity g_3, oil2.

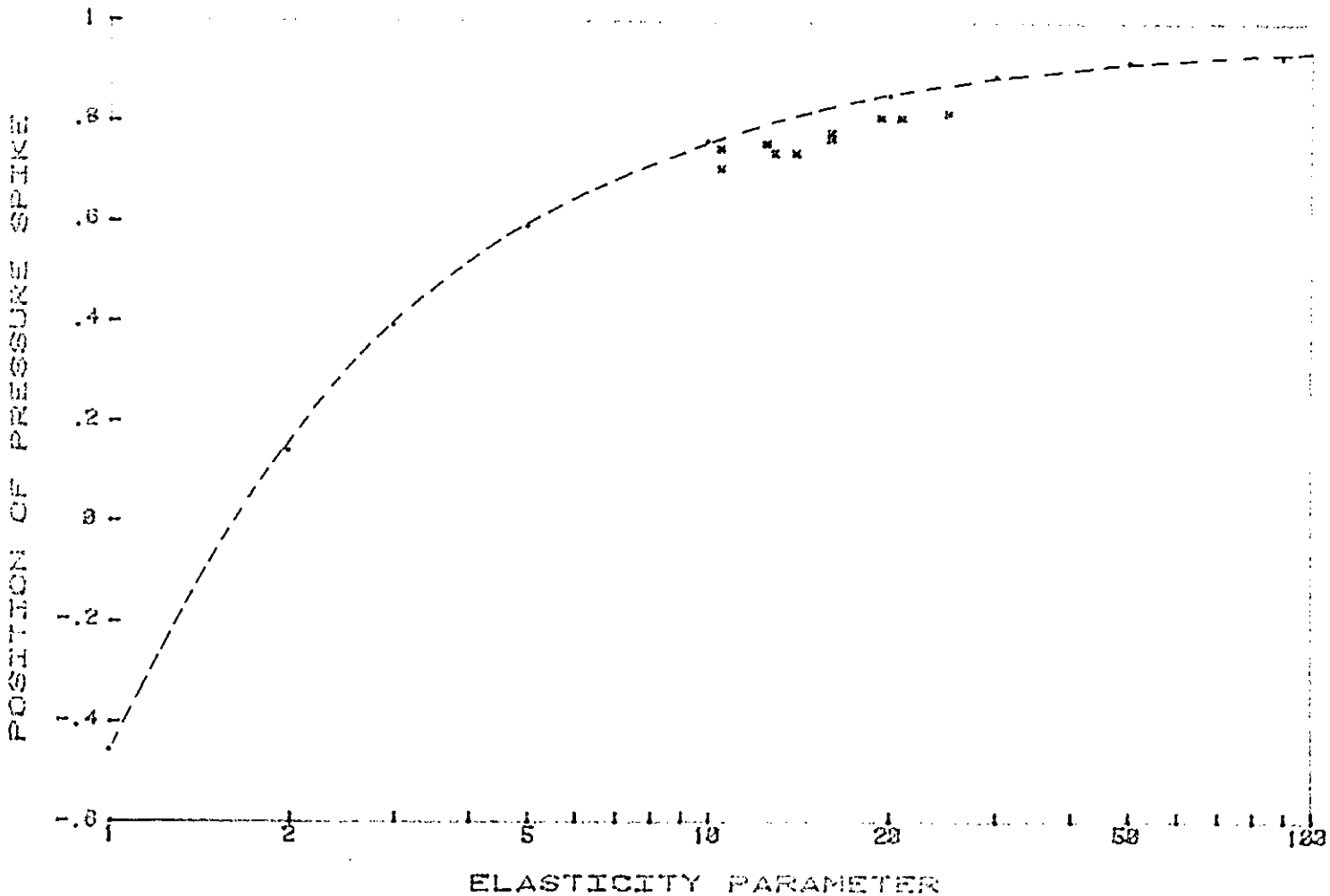

Fig. 6.21 Variation of the relative position of secondary pressure peak, x/a, with logarithm of non-dimensional quantity g_3, oil3.

in this project), follow the Hertzian profile very closely in this shoulder region. Experimentally obtained profiles consistently show slightly lower pressure than the Hertzian profiles in this region.

A very large pressure gradient at the exit is predicted by theory, but the experimentally obtained gradients were found to be much less. However, the large pressure gradient predicted by theory occurs immediately after the secondary pressure peak whereas the maximum pressure gradient measured in this work occurs slightly later due, as pointed out earlier, to the finite width of the device and the effects of bandwidth limitation. It is shown in Appendix 2 that a finite width transducer can read a maximum pressure gradient of $\frac{P}{a}$ where pressure is a step function of height P, and a is the width of the device; for a peak pressure of 6.9×10^8 Pa and a 10 μm wide device the maximum value of pressure gradient would be 6.9×10^{13} Pa/m. A step function would, of course, have an infinite gradient and the above calculation serves to illustrate that a finite transducer width will give a reduced reading for the pressure gradient. However, if a 1 um oil film thickness is assumed, the corresponding maximum shear stress is 34.5 MPa - a little larger than that measured.

6.2 Analysis of the Temperature Results

The pressure coefficienent of resistance of the thin film temperature transducer was sufficiently large to distort the temperature profiles substantially. Hence it was not possible to study the temperature variation within the EHL contact zone with these devices with a high degree of accuracy. The temperature sensors were used to study the inlet and exit zone where the pressure effects are negligible, the relative change of temperature due to different surface velocities at fixed load, and the relative change of temperature due to different amounts of sliding introduced between the two discs at a particular load.

To study the effect of surface velocity and sliding on temperature, the temperature profiles, like the pressure profiles were drawn on the same scale. However, unlike the pressure profiles, the centre of the contact can not be readily distingushed in the temperature profiles. Thus a somewhat roundabout method was followed for superimposing the temperature traces. It has been shown in section 5.9.2, with the use of synchronised pressure and temperature profiles, that the sharp spike that appears near the oil outlet in the temperature profiles was due to the rapid pressure drop that occurs after the secondary pressure peak. Hence the point where the rapid rise starts in the temperature profile coincides with the secondary pressure maximum. It has also been shown that for reasonably high loads the position of the secondary pressure Peak varies very little with the surface velocity for the range covered in this project. Hence in superimposing the temperature profiles the neck of the spike at the exit, as shown in fig 5.17

Fig.6.20 and one experiment in Fig.6.19 clearly exhibited secondary pressure peaks for a wide range of g_3 values and it was found that the plotted points were close to the predicted values. In cases where the secondary peaks did not appear, the plotted points generally remain below the predicted profile. This would be expected if the absence of a peak was caused by limited resolution of the transducer (which reduces the $^x/a$ value).

6.1.8 Comparison with Theory

The distribution of pressure, within an EHL contact, as determined experimentally by the thin-film pressure transducer, agrees well with theoretical predictions. Although the height of the secondary pressure peak could not be ascertained from the experiments, the presence of such peaks under some conditions is indisputable. Other properties associated with the secondary pressure peak initially shown by the theoretical solutions were also found to be valid. The secondary peak becomes narrower with increasing load and wider with increasing surface velocity. The movement of the peak with changing operating conditions was also found to be similar to the theoretical predictions.

The overall shape of the pressure distribution profiles matched the theoretical predictions reasonably well. The development of pressure in the inlet zone and the extension of pressure beyond the Hertzian region varied according to the operating conditions as theory predicts. However, slight differences in the theoretical profiles and the experimental ones were noticed in the inlet shoulder region of the pressure profiles. Theoretical profiles, under reasonably high load (the most common operating conditions

, was taken as the common reference.

6.2.1 Effect of Rolling Velocity on the Temperature Profiles

Figure 6.22 shows a set of redrawn temperature profiles recorded at fixed load of 0.22MN/m (1270lbf/in) with surface velocity varying between 1.8m/sec and 8.4m/sec in nominal rolling conditions. No attempt was made to correct the temperature profiles for the pressure effect, however, as the load was constant in all four cases, the relative change in temperature can only be caused by the change of surface velocity. The temperature at the primary peak can be seen to vary by only $4^{\circ}C$ for a change of surface velocity from 1.8 to 8.4 m/sec. The estimated temperature, determined from the pressure coefficient of reistivity of the temperature transducer, at 1.8m/sec is about $14^{\circ}C$ at the primary peak pressure zone.

Immediately after the secondary peak pressure zone, the temperature initially drops very rapidly then decays more slowly. This change in slope is more marked at higher surface speeds when the temperature rise within the contact is higher. The temperature rise at a distance of about 2a from the exit end of the Hertzian contact width remains about 5 times higher at a rolling speed of 8.2m/sec than at a speed of 1.8m/sec.

In figure 6.23 values of the temperature rises at 1.5a and 2a from the centre of the contact towards the inlet are plotted from figure 6.22. It is assumed that the pressure effect on the temperature profiles is small in these region and these two sets of temperature data are used later to study the effect of inlet temperature rise on the relation between film thickness and $\eta_o U$.

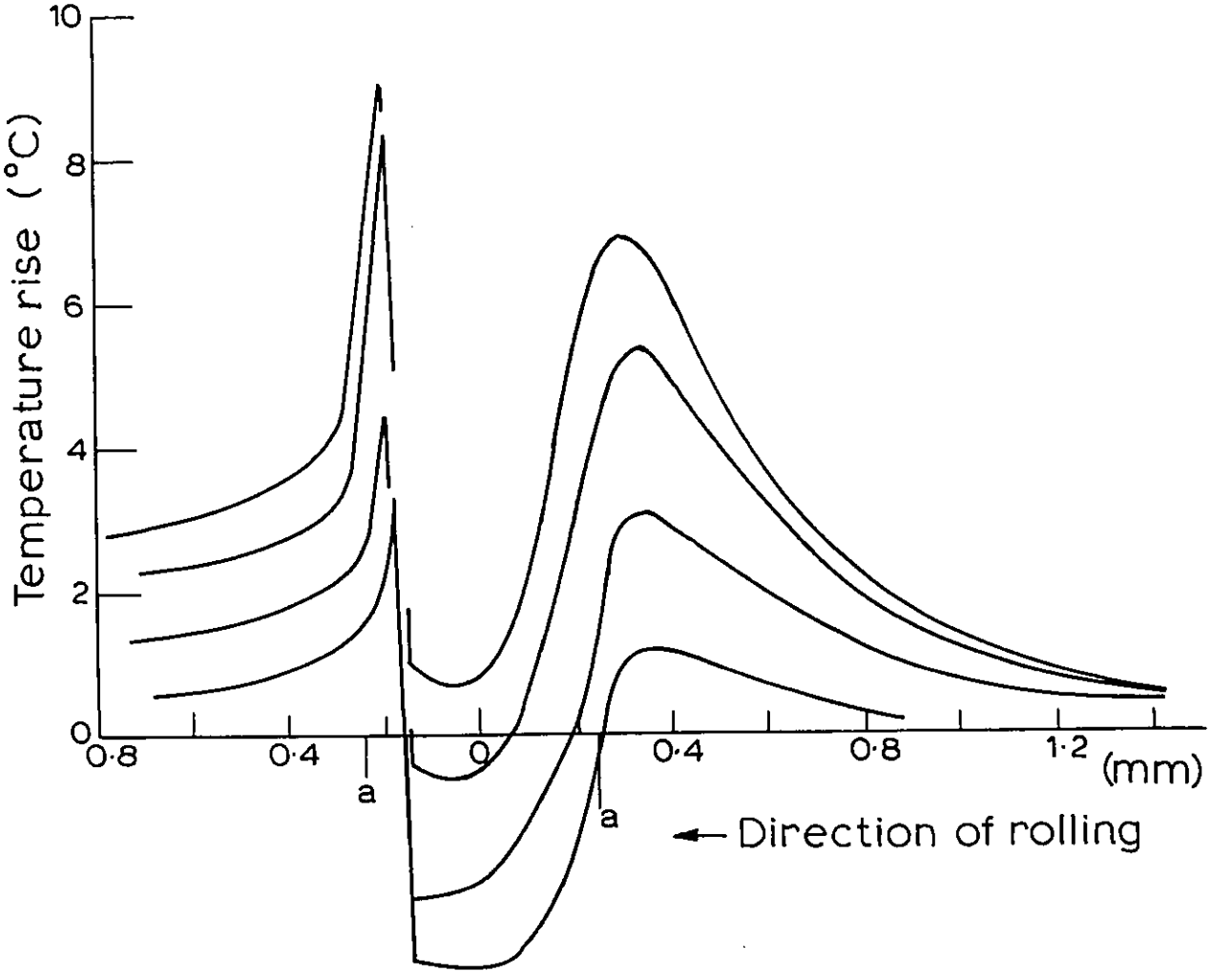

Fig. 6.22 Temperature profiles under pure rolling conditions, using oil2, at a fixed load of 0.222MN/m and surface velocities of (a) 1.8m/sec, (b) 3.56m/sec, (c) 6.5m/sec, (d) 8.4m/sec.

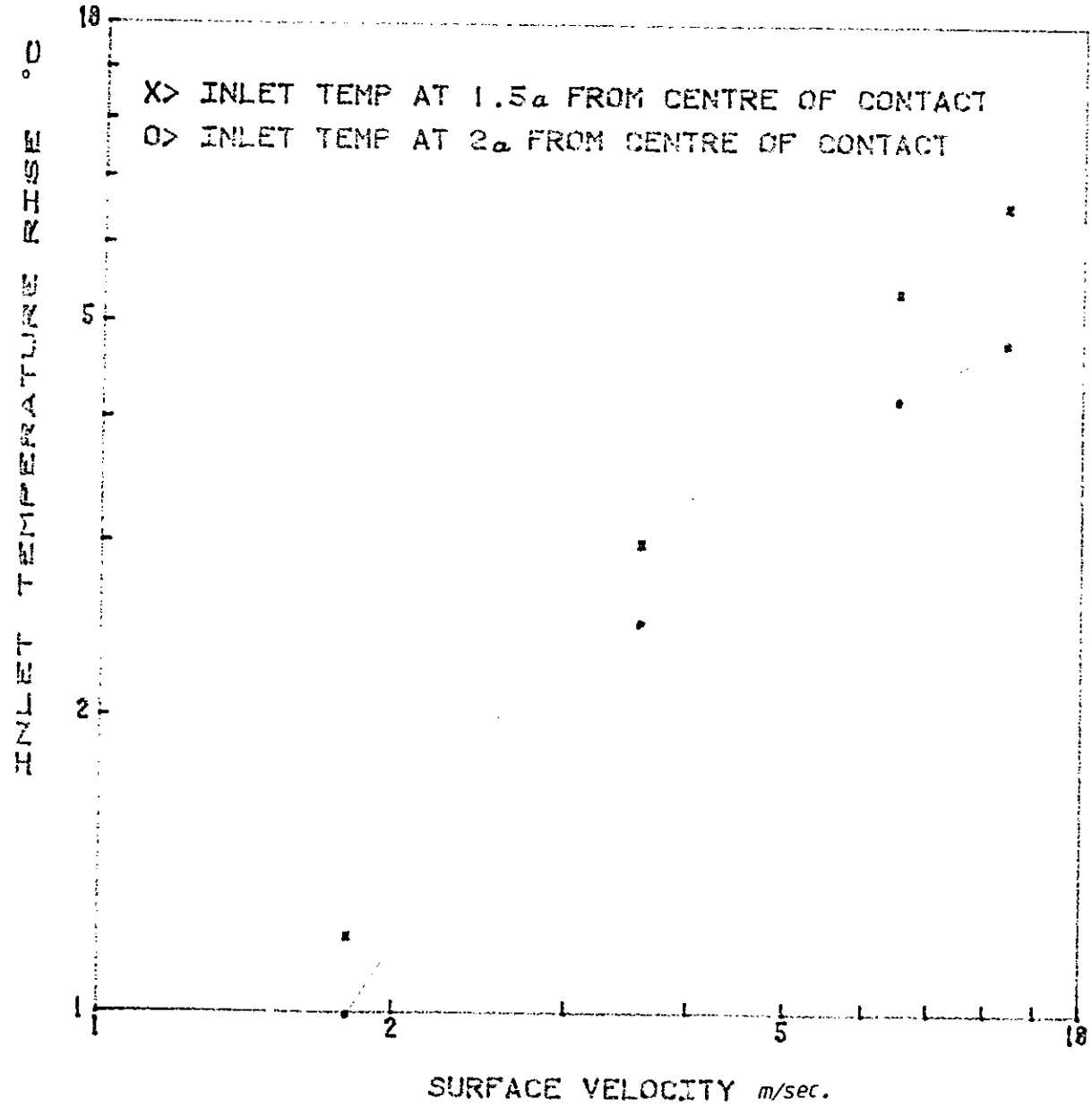

Fig. 6.23 Temperature rises at a distance of 1.5a and 2a, at the inlet side, from the centre of the contact measured from traces in fig. 6.22.

6.2.2 Effect of Sliding on the Temperature Profiles

Figure 6.24shows five temperature traces recorded under a fixed load of *0*.22 GN/m (12701bf/in) using oil 2. Trace a was under pure rolling condition with a surface velocity of 4m/sec and traces b to e were recorded with various amounts of sliding introduced between the two discs, by applying a brake on the driven disc.

The maximum temperature rise within the contact zone increases rapidly with sliding. For pure rolling, the corrected maximum temperature rise was estimated to be 14°C, whereas a temperature rise of about 100°C occurs at a slip ratio of 85%.

It is interesting to note that the temperature rise under sliding conditions remain the same as that for pure rolling conditions at the inlet. The temperature under sliding conditions, however, shows a rapid increase close to the Hertzian contact. The temperature decay at the exit show similar effect as the traces recorded under pure rolling conditions where the temperature rise outside the contact remain higher when the temperature rise within the conact was higher.

The maximum surface temperature rises are plotted in figure 6.25 against the slip ratio.

6.2.3 Comparison with Theory

Temperature results obtained in this project are compared with theoretically derived thermal EHD solutions by Cheng(22). Kannel in a discussion of the same work showed that his temperature results varied widely from those derived by Cheng. The reason was ascribed to the wide difference in inlet viscosity of the oils used by Cheng and Kannel respectively. To achieve a more sensible comparison, the results obtained with

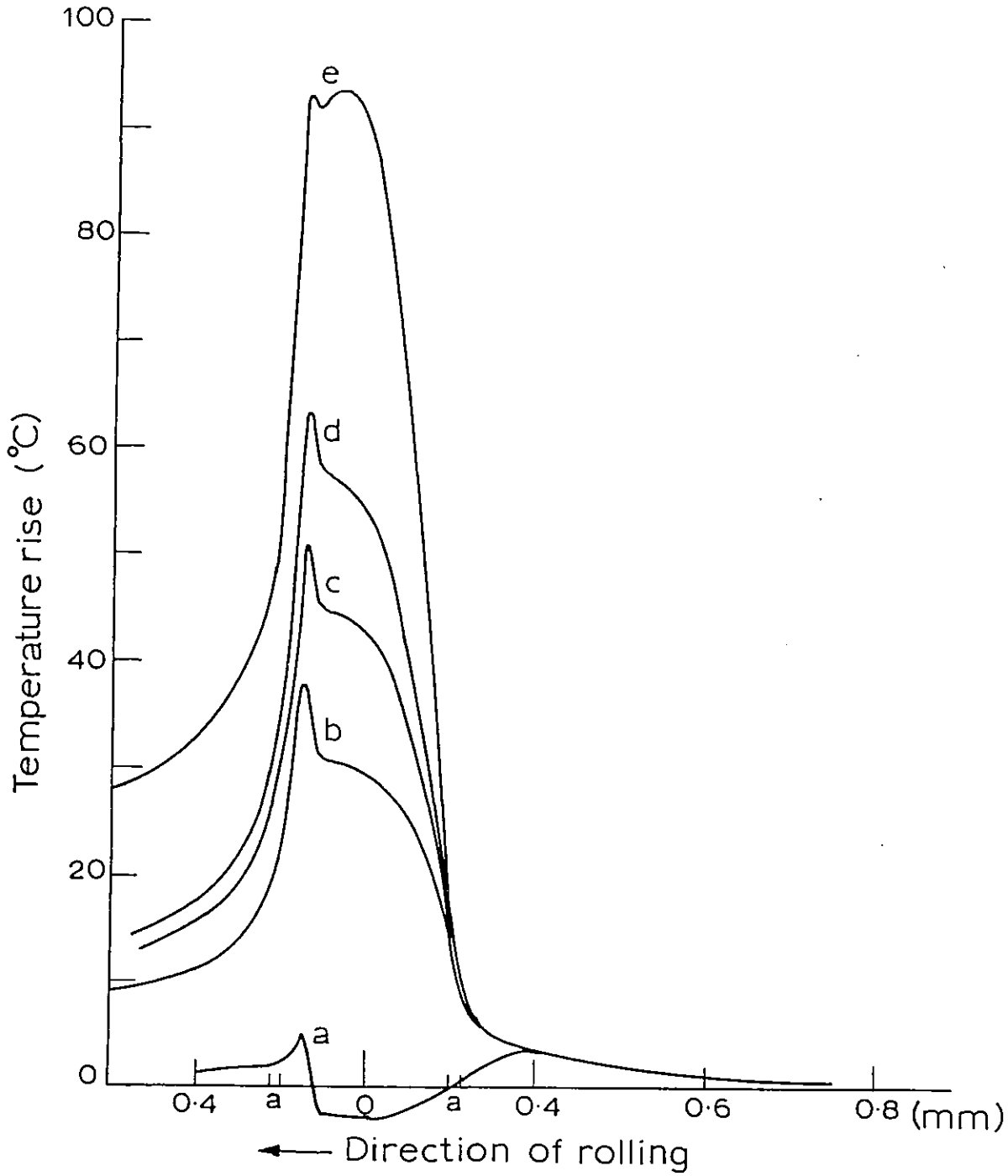

Fig. 6.24 Temperature profiles at a fixed load of 0.222MN/m (a) pure rolling at 4m/sec, (b) partial sliding 4:3.06m/sec, (c) partial sliding 4:2.5m/sec, (d) partial sliding 4:2m/sec, (e) partial sliding 4:0.62m/sec.

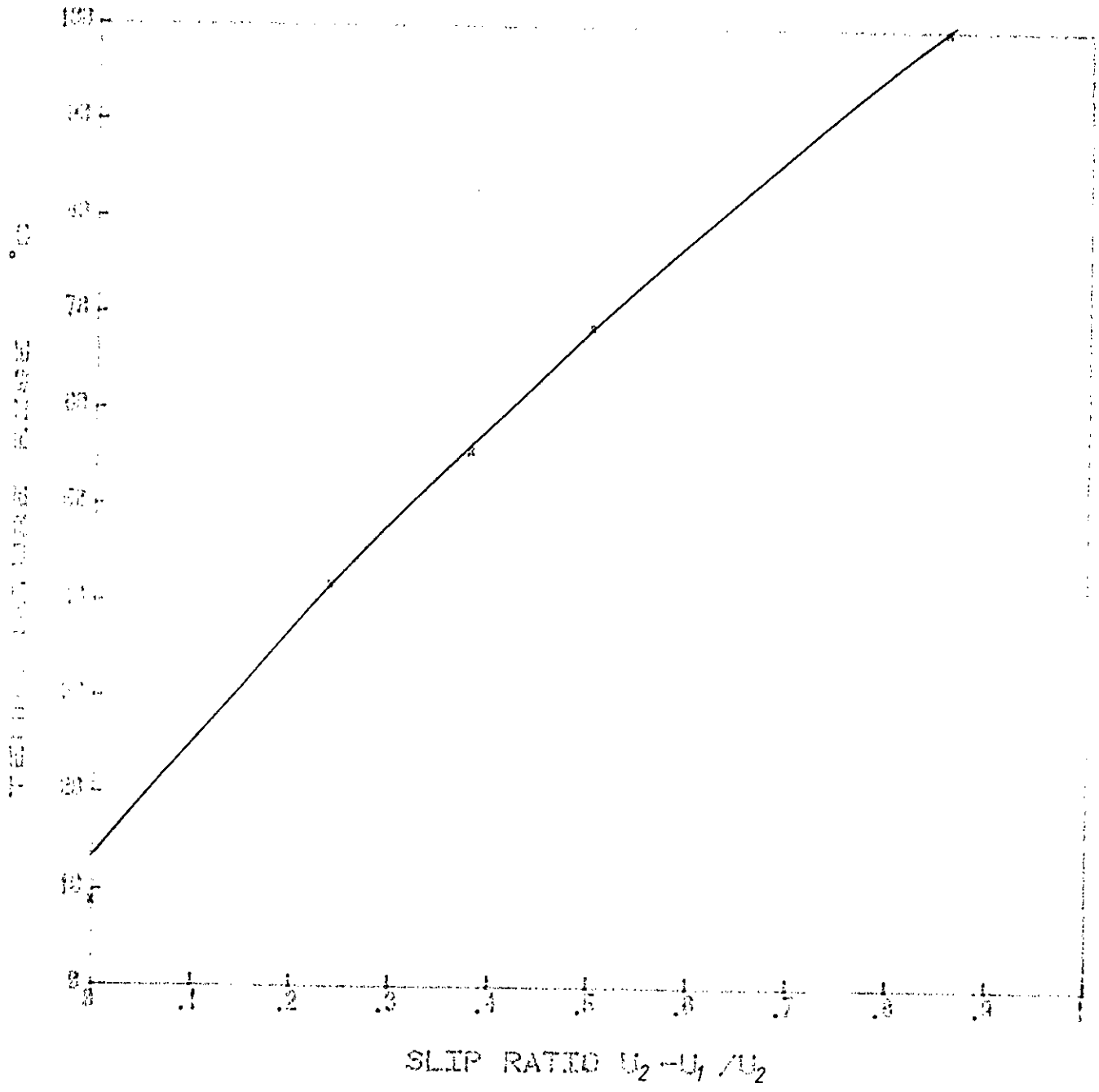

Fig. 6.25 Maximum temperature rises within the contact, at a load of 0.222MN/m and under pure rolling of 4m/sec and various amounts of sliding introduced between the discs.

oil 3, which has a viscosity of 0.039Pa.sec. at the operating temperature of 40° C, were used. Cheng also assumed the same viscosity value in his derivation. However, Cheng in his work kept the load constant at 0.125MN/m (715lbf/in) for the contact of two steel discs and the results, from this project, used for comparison were obtained at a load of 0.22MN/m. Hence there is a constant load discrepency in this comparison. Most of the results shown by Cheng were under partial sliding conditions, which was convenient for comparison with the experimental work, as under slliding conditions the temperature rise was larger and the error due to pressure effect was smaller.

Cheng calculated the maximum temperature rises both at the surface of the disc and in the oil film. For comparison the surface temperatures are used. In figure 6.26 three plots are shown, two of them are theoretiacally derived maximum temperature rise under different slip ratios within a metal-metal and metal-glass contact and the third one is the experimentally obtained maximum surface temperature plot. A wide difference can be seen between the theoretical metal-metal contact plot and the experimental plot. The experimentally obtained vallues are between 1.5 and 5 times higher than the theoretial values. One reason for this discrepency is no doubt the higher load used in the experiments, which will produce greater heating. The presence of the thin alumina layer under the temperature transducer could also contribute to the higher temperature rises measured. It is interesting to note that the shape of the experimental plot shows a closer similarity to the theoretical metal-glass contact. However, accurate comparison cannot be made between the two theoretical curves as the

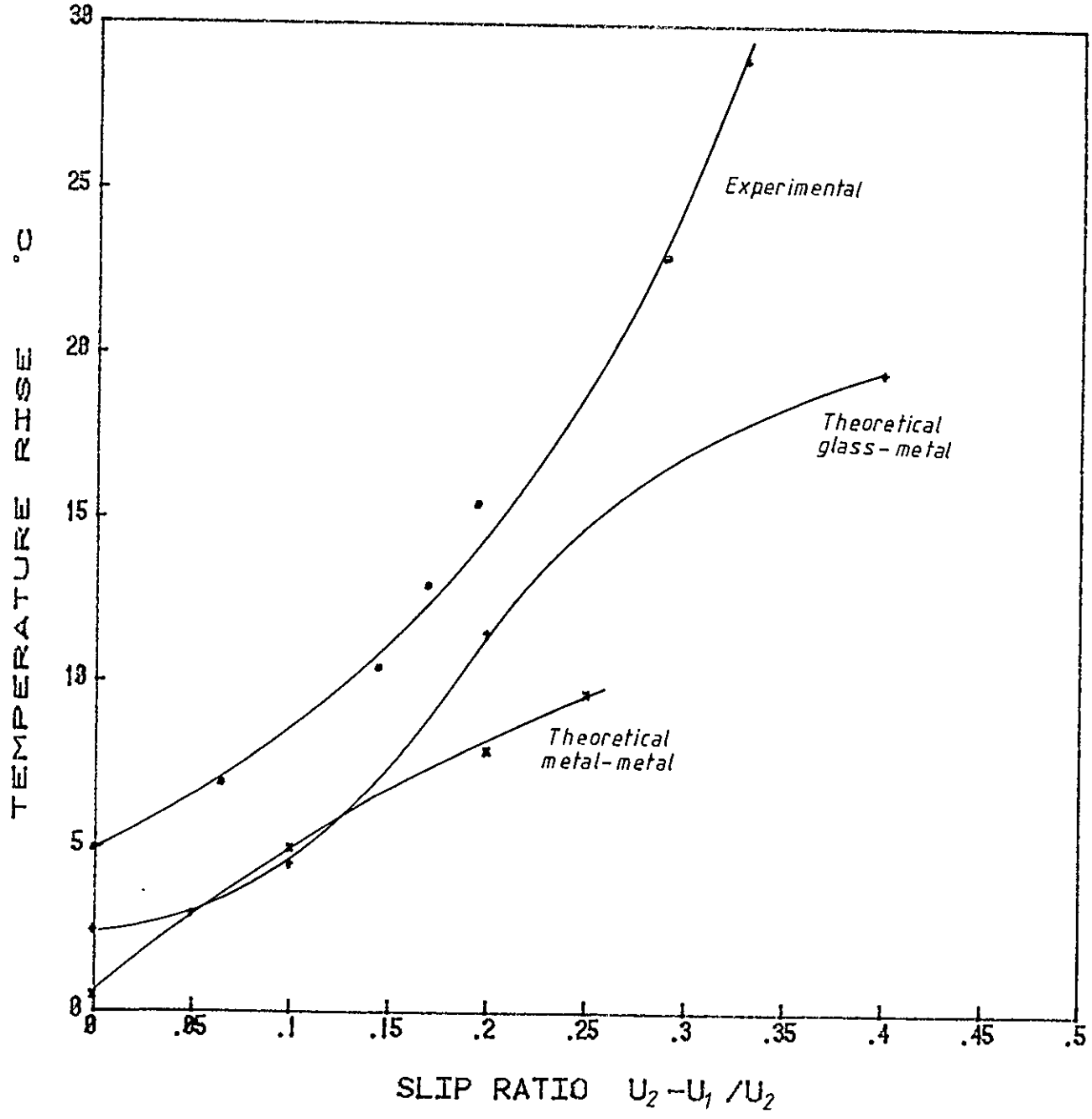

Fig. 6.26 Comparison with theory (after Cheng), maximum temperature rises on the surface of the disc under various slip ratios.

viscosity of the oil used in the calculation for metal-glass contact is about 3 times higher and the load assummed is about 2/3 the metal-metal contact value.

6.2.4 Comparison with Experimental Result

The temperature results obtained in this project are compared with the results published by Kannel and Dow(71) and Bertz and Ehlert(84). The results presented in the above publications suggest, in pure rolling, the maximum temperature rise changes little with the change of oils having a wide range of viscosity values. In the table below the temperature rises obtained by the different authors are presented.

Authors	Pressure GPa	Surface Velocity m/sec	Temperature Rise °C
Kannel & Dow	0.76	5.6-11.2	27-37
Bertz & Ehlert	0.75	5.6-7.55	11-15
Safa	0.55	1.8-8.4	14-18

Thus apparently, in rolling, the temperature rises obtained in this project is broadly similar to Bertz and Ehlert's results. However, the load used in this projet was lower, with increased load a higher temperature rise is expected, this would make the temperature readings lie somewhere between Kannel and Bertz's result.

Kannel and Dow (71) show that, in sliding, the temperature rise is a strong function of oil type and properties but they show that a mineral oil together with a 25% slip ratio, gives a maximum temperature rise of 30°C which compares reasonably well with the 40°C rise measured with the same slip ratio in this project.

6.3 Analysis of the Film Thicknes Results

In determining the film thickness profiles from the shape profiles recorded using the rate of change of capacitance method, the dielectric constant values measured in this project are used with necessary extrapolation to the higher pressure region of the contact. To study the effect of a particular operating parameter on the film thickness profiles, some of these profiles are superimposed, in most cases with the help of the associated synchronised pressure profiles. However, in some cases the pressure transducer could not withstand the severity of the condition, in which case the superimposed film thickness profiles show an assumed centre of contact which was chosen after studying several other film thickness profiles with the associated pressure profiles.

To compare the film thickness values obtained in this project with theoretical predictions, generally two readings were taken from each shape profile; one at the minimum film thickness at the exit constriction which is generally well defined and a second one at the point where the primary pressure peak occurs in the associated presure profile.

In calculating the value of the inlet viscosity, η_o, the measured oil temperature and the disc surface temperature under the operating conditions (as presented in section 5.6.4) were added together and used in the Walther-A.S.T.M formula. This, however, introduces some errors in the n value for oils 2 and 3 as the disc surface temperature could only be measured using oil 1.

The error bars shown in the h_o against $\eta_o U$ plots are estimated after considering two possible sources of error: (1) o

(1) the noise present in the film thickness profiles, which pevents the accurate measurement of the voltage and (2) the instrumental error in measuring and recording the voltage which is ~5% of the voltage recorded.

6.3.1 Effect of Load on Film Thickness Profiles

Figure 6.27 shows a set of synchronised pressure and film shape profiles obtained with oil 1 at a fixed surface velocity of 4.56m/sec. The shape profiles are converted to film thickness profiles and reproduced on the top of the figure. A fairly parallel oil film forms over most of the high pressure zone at relatively high load, but as the load decreases this parallel film slowly diverges. Because of the different scales of the two axes this angle appears fairly large. The angle from A to B in figure 6.27 is 0.08 relative to the distance axis.

The exit constriction in the film thickness profiles in figure 6.27 show up distinctly at higher load but slowly merges into the profile as the load is reduced. It is worthy of note that a slight increase in oil film thickness immediately before the end constriction exhibited by the theoretical solution of Dowson, Higginson and Whitaker (18) and later demonstrated experimentally by Crook, appears in the shape profiles for high loads in figure 6.27. We have seen in section 5.9.4 that the exit constriction in the film thickness profile occurs immediately after the secondary pressure peak and in figure 6.27 it can be seen that this constriction zone moves with the movement of the secondary pressure peak as expected.

6.3.2 Effect of Surface Velocity on Film Thickness Profiles

A general pattern was also noticed with the variation of the film thickness profiles in an EHL contact zone under

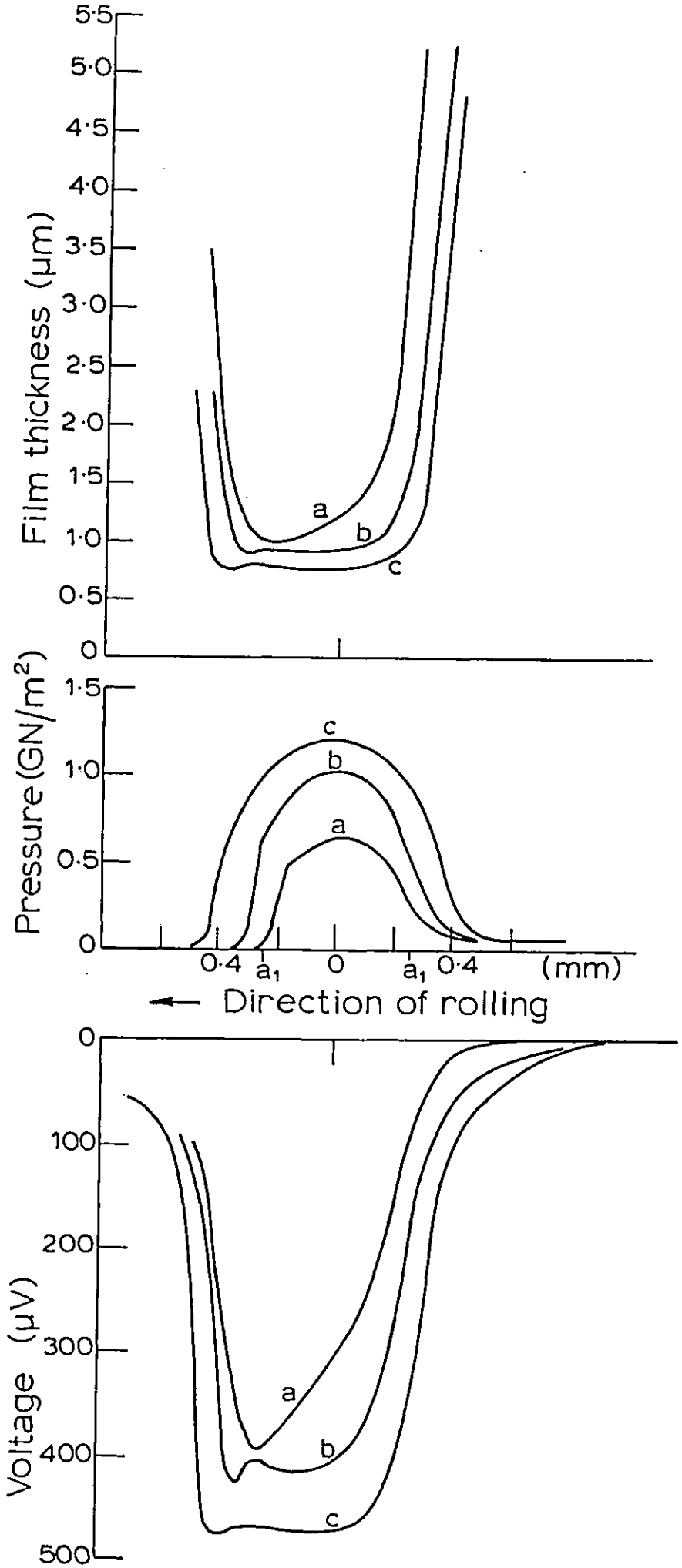

Fig. 6.27 Synchronised prssure and film thickness profiles at a fixed surface velocity of 4.56m/sec and loads of (a) 0.278, (b) 0.66, (c) 0·89 MN/

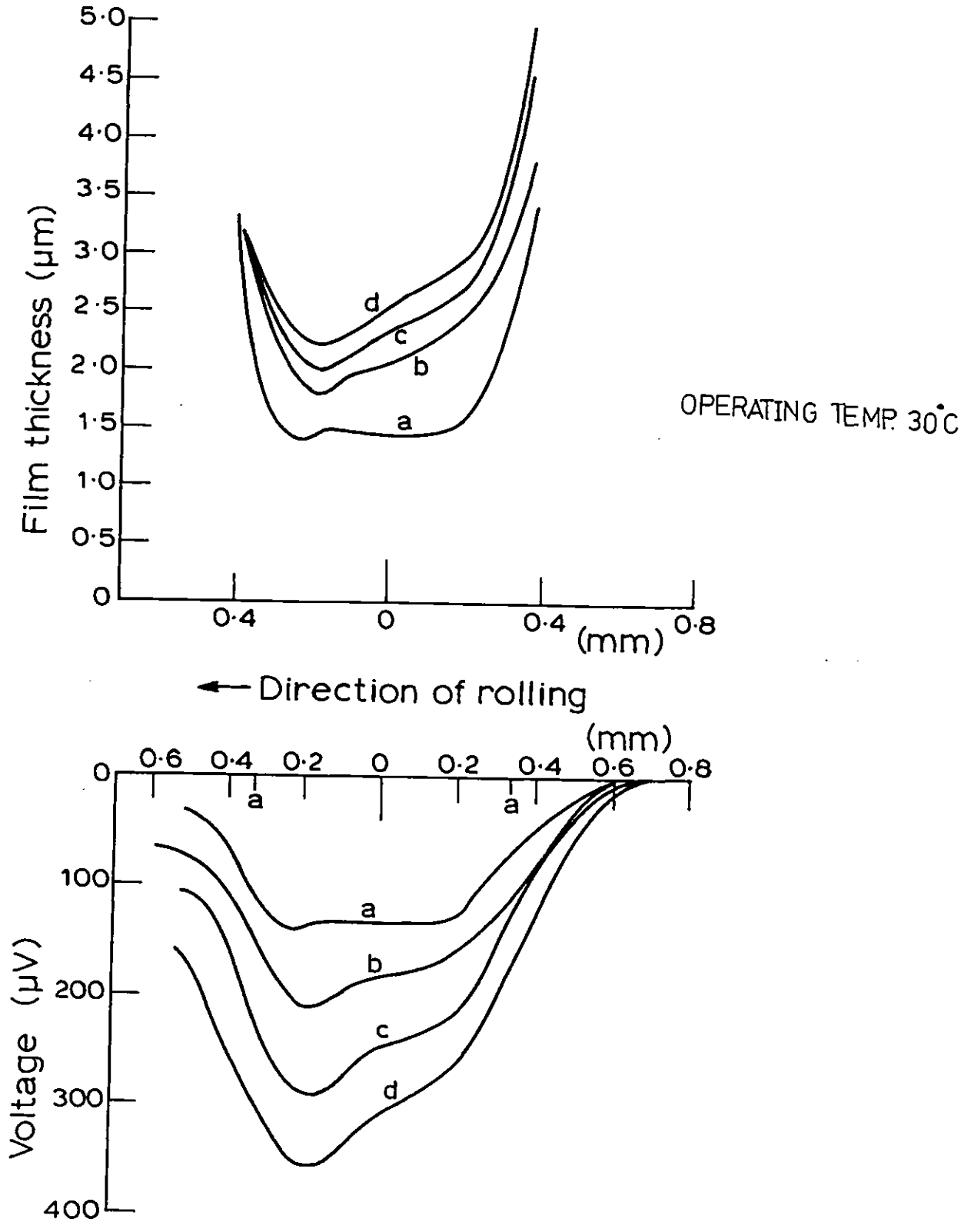

Fig. 6.28 Film thickness profiles at a fixed load of 0.445MN/m and surface velocities of (a) 2.3, (b)4.5, (c)6.9, (d)9 m/sec, using oil1.

constant load but variable surface velocity. Figure 6.28 shows a set of shape profiles converted into film thickness profiles. At low surface velocity a parallel film develops which end with the formation of the exit constriction. But as the surface velocity increses the parallel zone slowly diverges until the exit constriction can no longer be distinguished as a seperate feature. The value of the surface velocity at which the oil film forms a fairly parallel film varies with load. As the surface velocity increases, a higher load is required to remove the divergence of the two surfaces in the contact zone. A similar effect was observed with different oil viscosities, with low viscosity oil requiring less load to form a nearly parallel region. These observations are at least in qualitative agreement with EHL theory in that at low values of viscosity x speed the deformation of the surface is closer to that of the static contacts.

6.3.3 Effect of Sliding on the Oil Film Profiles

Figure 6.29 shows a set of shape profiles and the corresponding film thickness profiles obtained using oil 2 under fixed load with different amounts of sliding. This sliding was introduced by braking the driven disc, and increasing the speed of the driving disc. The transducer was on the driven disc which was made to rotate at a fixed velocity of 3.9m/sec. The results obtained is drastically different from that predicted by isothermal theory. The film thickness, instead of increasing with the increasing entrainment velocity actually reduces substantially under the sliding conditions.

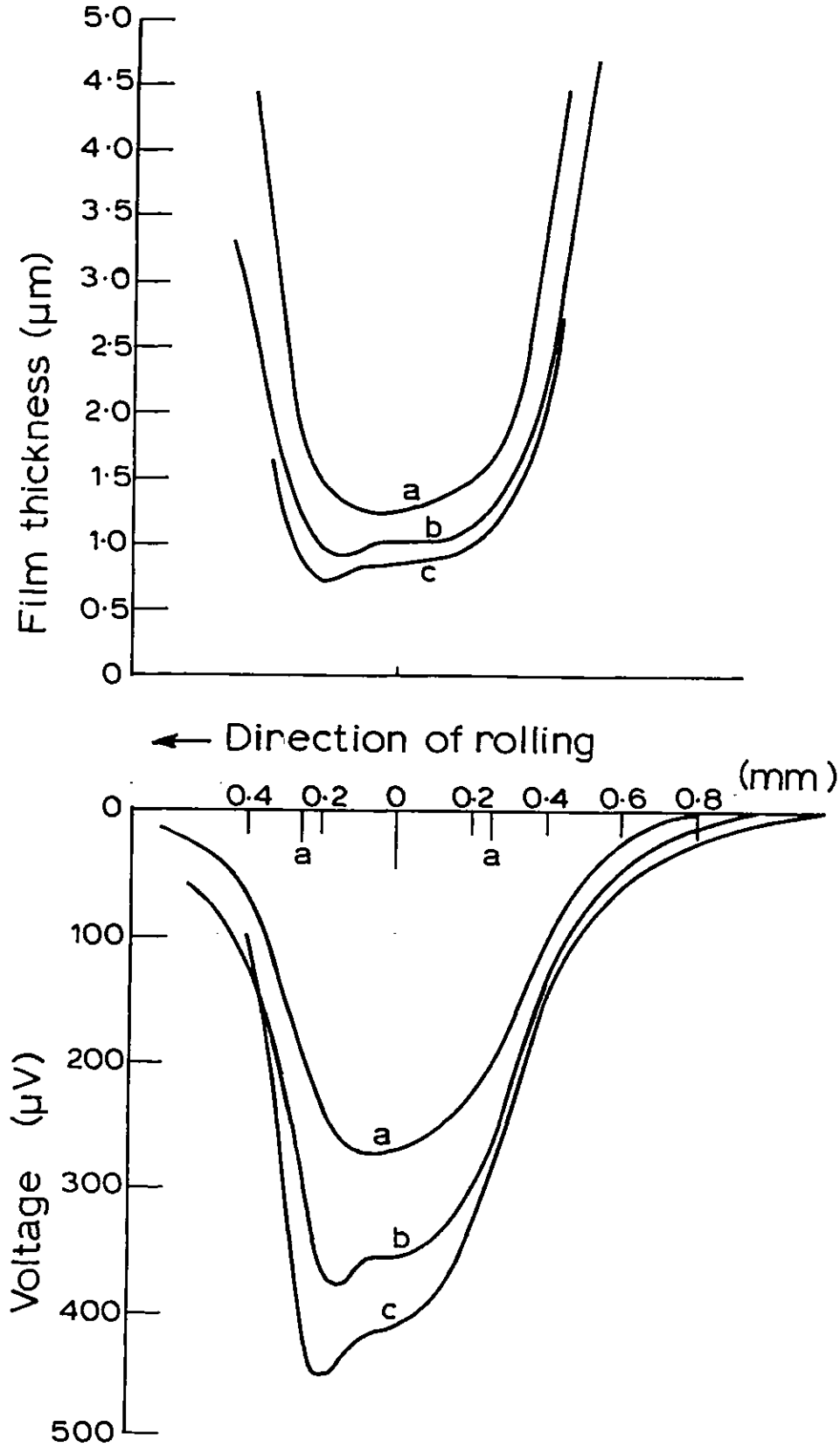

Fig. 6.29 Film thickness profiles at a fixed load of 0.222MN/m, (a) under pure rolling at 3.9m/sec, (b) partial sliding 3.9:5.9m/sec, (c) 3.9:6.3m/sec, using oil2.

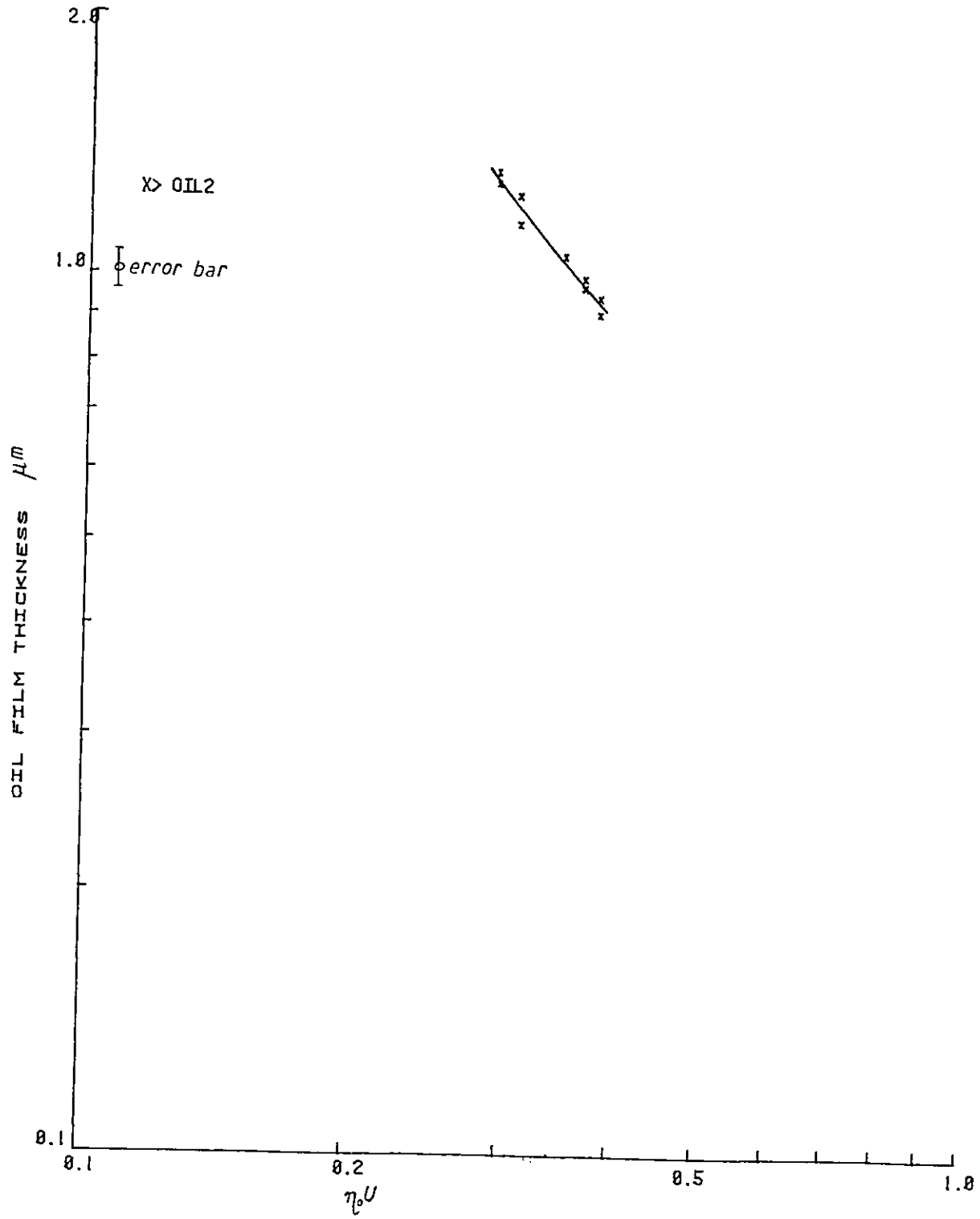

Fig. 6.30 Variations of minimum film thickness with nU under increased amounts of sliding between the discs. Broken line shows the isothermal prediction.

The exit constriction is another point of interest in these sets of results. In the pure rolling case shown in figure 6.29 no constriction region can be distinguished in the shape profile, as generally happens with high surface velocity or low load. With about 33% sliding introduced between the discs, the constriction zone show up quite prominently and a fairly Parallel oil film is also formed. With a further increase of sliding to 38% the constriction becomes wider and less distinct.

The above mentioned discrepency between isothermal theory and the change in shape profile with sliding can be explained if the viscosity of the oil at the inlet is reduced substantially due to a higher temperature rise under sliding conditions. The reduced oil viscosity would cause the film formed to be thinner for a given load and surface velocity and would also give rise to flattened profile in the centre of the zone as seen in figure 6.29.

In figure 6.30 a set of film thickness results obtained under sliding conditions using oil 2 is plotted against $\eta_o U$. This plot show the film thickness dependence on entrainment velocity to be in disagreement with theoretical predictions. If heating is regarded as the cause of this disagreement then a temperature rise in the region of 23°C would be required to bring the results at the highest slip ratio, with oil 2, in line with theory. Two heat sources can be considered, 1) the disc surface could heat up more under sliding than under pure rolling condition and 2) inlet shear heating.

Although the disc surface temperature could not be monoitored under controlled sliding conditions, it was thought unlikely that a temperature rise as high as 23°C could occur on

the entire disc surface under the above sliding conditions, particularly when careful monitoring of the disc surface temperature at the starting of the disc machine did not show any large temperature rise on the disc surface, even when a certain amount of uncontrolled sliding between the discs was achieved by starting the machine at lower than the usual starting load. The temperature rise within the contact under sliding conditions is high and in similar sliding conditions to those under discussion, a maximum temperature rise of 55°C was found within the contact. It would certainly be possible to find a location close to the conjunction where a temperature rise of 23°C occured. However, studying the temperature profiles in figure 6.24 it can be seen that this point would be somewhere near the Herzian contact boundary, which cannot be considered as the inlet zone of the contact. However the possibility of the summation of the effects of the two sources of heat discussed above could be expected to give rise to an increase in temperature of the required order.

6.3.4 Effect of Surface Velocity on Minimum and Central Film Thickness

The logarithms of minimum and central film thicknesses are plotted against $\log(\eta_0 U)$ in figures 6.31 and 6.32 for oils 1 and 2 respectively. From both these figures, it can be seen that the ratio of film thickness at the exit constriction to the centre of the contact gradually increases with the increasing surface velocity due to the change in the shape of the contact zone from near parallel to near cicular. As a result the slopes of the lines passing through the minimum and central film thickness show different values. These slopes yield the index n,

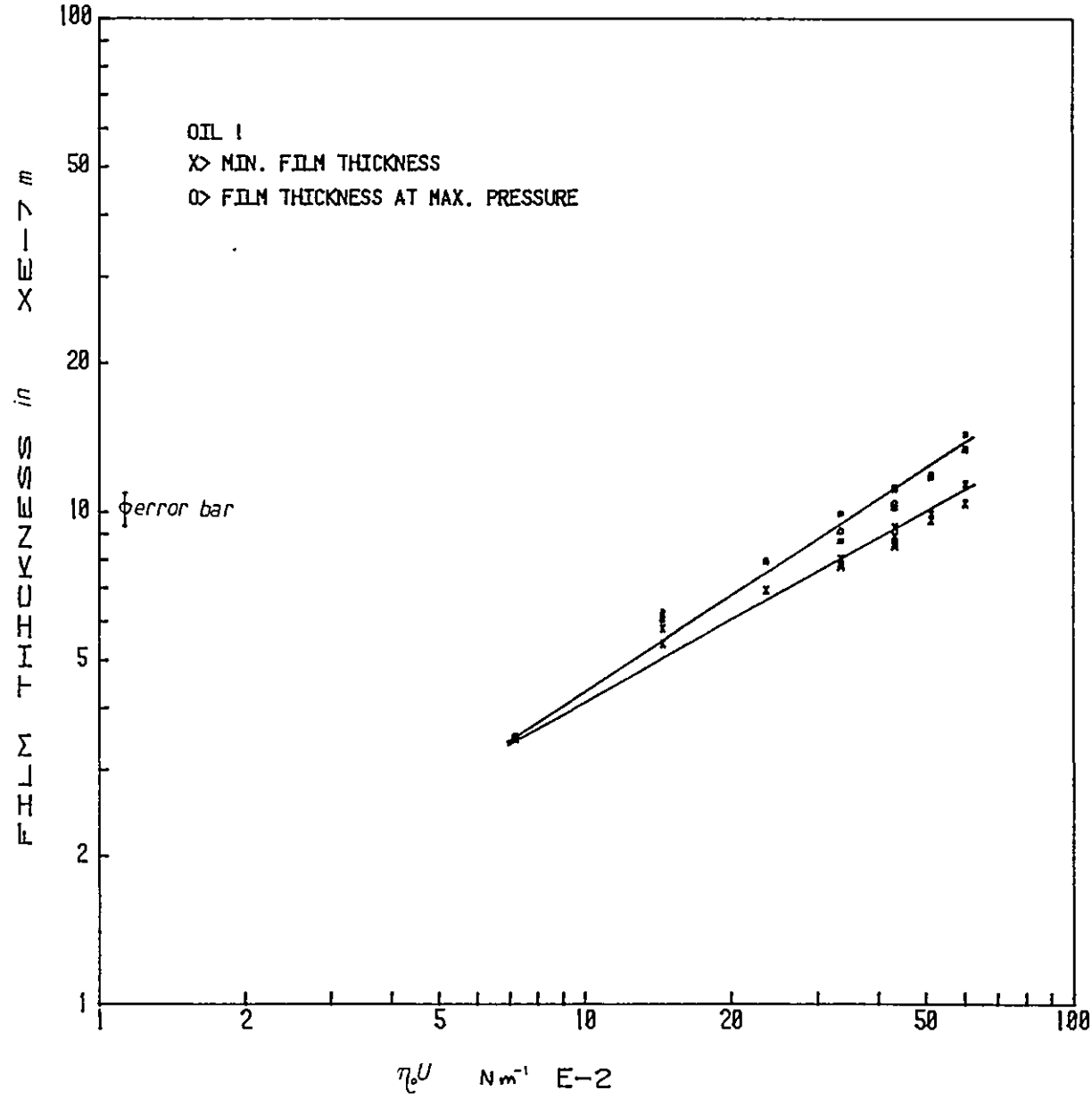

Fig. 6.31 Variation of minimum and central film thickness with η_o U, using oil1, under pure rolling conditions.

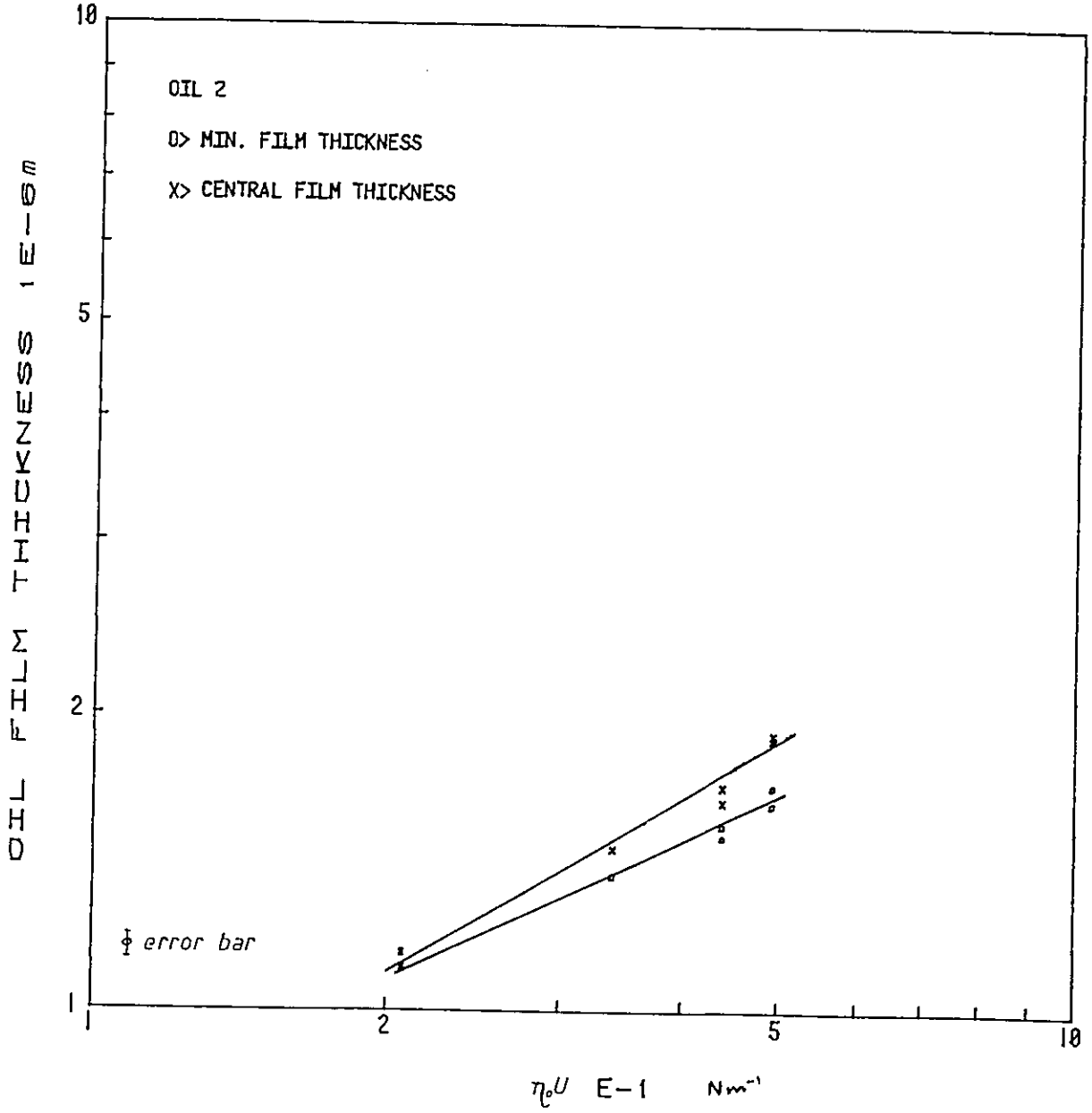

Fig. 6.32 Variation of minimum and central film thickness with $\eta_0 U$, using oil2, under pure rolling conditions.

in the relationship of $h_o \propto (\eta_o U)^n$. The isothermal theory predicts a value of about 0.7 for minimum film thickness whereas the slopes obtained from figures 6.31 & 6.32 are all about 0.5. The slopes of the lines through the central film thickness datas are about 0.55. This discrepency between the isothermal theory and the experimental observation was first noticed by Crook (57), whose measured index was 0.5 from three types of capacitance measurements. Recent work by Greenwood and Kauzlarich (30), March and Wilson (31), Hartrung (89) suggest the cause for this discrepency is the inlet shear heating of the oil. Possible ways of correlating the experimental results with the isothermal prediction are discussed further in section 1.1 .

6.3.5 Experimental Temperature Correction of Oil Viscosity

One cause of the discrepancy between the isothermal prediction and the experimentally obtained value of index n is inlet shear heating, which may occur so near the contact region that it is virtually impossible to measure the temperrature rise using any conventional temperature measuring technique. Thinfilm temperature transducer makes possible the recording of the change of temperature in the inlet region.

As the inlet region in an EHL contact is not well defined, the temperature rises at distances of 1.5a and 2a from the centre of the contact (shown in figure 6.23 for oil2) were used to obtain temperature corrections for oil viscosity. Figure 6.33 shows the effect of these corrections on the dependence of film thickness on $\eta_o U$. The index n in the proportionality $h_o \propto (\eta_o U)$ increases from 0.5 to 0.6 and 0.67 for the correction with the temperature readings taken at 2a and 1.5a respectively.

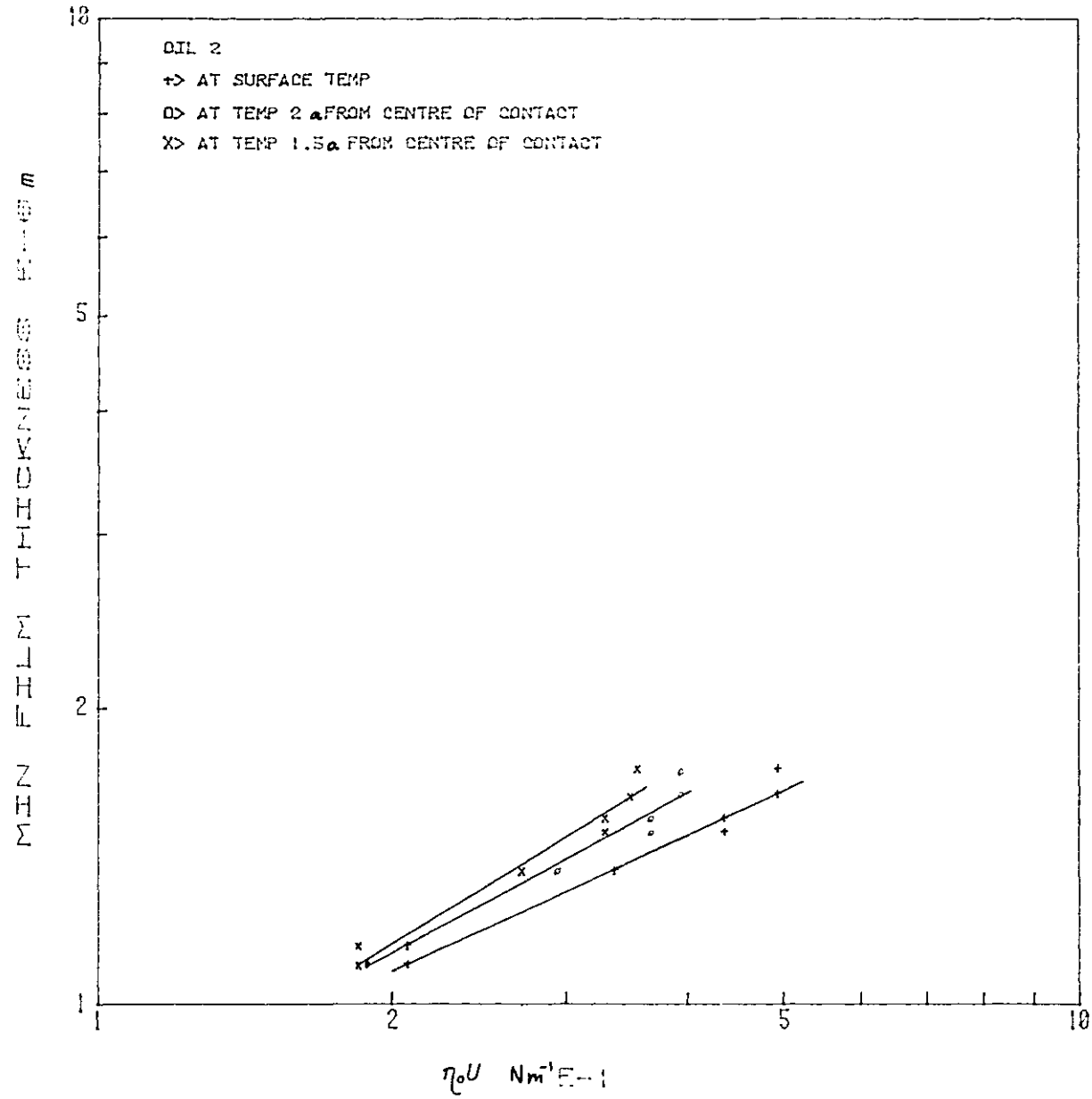

Fig. 6.33 Effect of correction of η_o values, using the temperature datas obtained in fig. 6.23, on the plot of minimum film thickness against $\eta_o U$.

6.3.6 Effect of Load on Film Thickness

Deviation from isothermal theory for minimum film thickness was also noticed in studying the effect of load on film thickness. In figures 6.34 and 6.35 the dependence of the minimum film thickness on $\eta_o U$ is shown for three different loads for oils 1 and 3 respectively. If isothermal predictions were valid, all three lines in figure 6.35 and the two higher load lines in figures 6.34 would have been much closer together since the index m, takes the value of 0.13 in the isothermal relation $h_o \propto (w)^m$. Below a load of about 0.44MN/m, it was found that the value of m is quite close to the isothermal prediction of 0.13 for both the oils, however, with the increase of load m was found to increase. For oil 3, the value of m was found to be approximately 0.27 between the loads of .44 and .66MN/m. Similarly, for oil 1, this value was found to increase from 0.3 to 0.47 between loads of .44 to .61MN/m and .61 to .83MN/m.

Similar deviation from isothermal theory were also detected by other researchers, for example Kannel and Bell (34) and Sibley and Orcutt (27) both using X-ray techniques and Lee et al (38) using an optical interferometry method. Sibley and Orcutt obtained a value for m of 0.365 and Kannel and Bell found a value of 0.71. Lee etal (38) also showed that the index m becomes much larger at higher load, reaching a value of 3.

6.3.7 Themal Correction Factors

The necessity for predicting the oil film thickness correctly in the design of machine elements, prompted several theoretical studies of the efffect of inlet shear heating on film thickness. Several correction factors were proposed which, when applied to isothermal film thickness predictions, produced

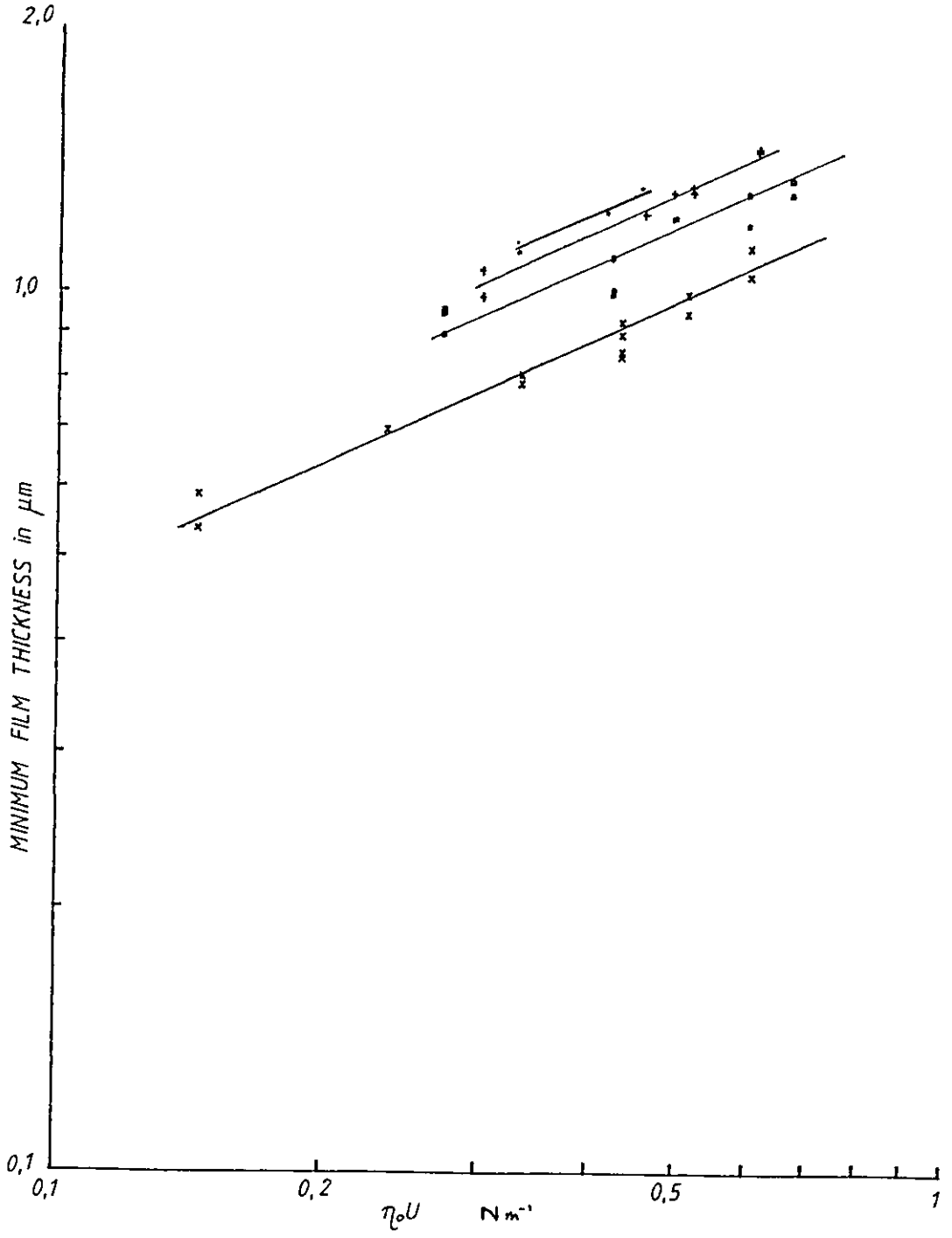

Fig. 6.34 Variations of minimum film thickness with $\eta_0 U$ for loads of (a)0.278, (b)0.446, (c)0.613 & (d)0.836MN/m, using oil1.

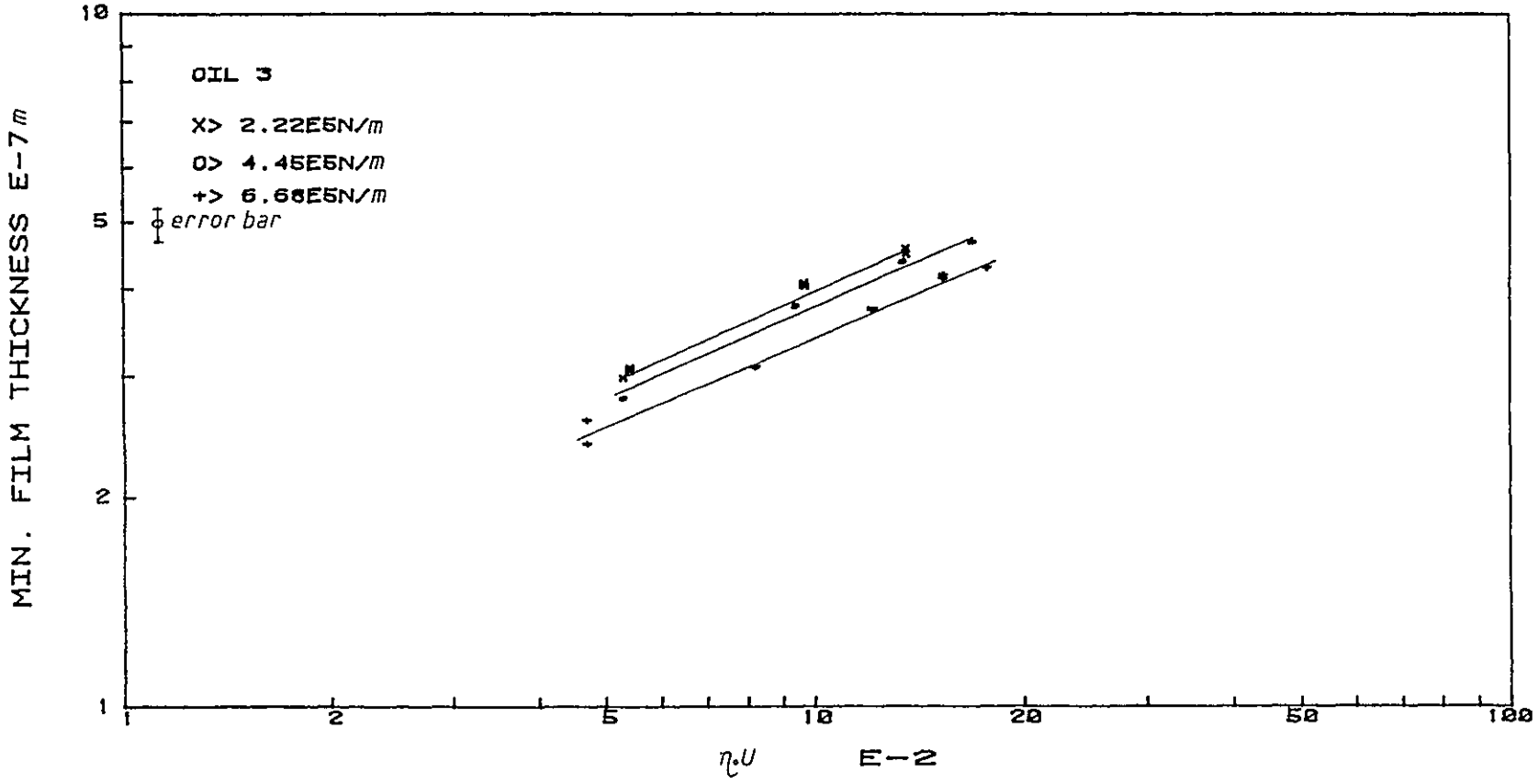

Fig. 6.35 Variations of minimum film thickness with $\eta_0 U$ for loads of (a)0.223, (b)0.445, & (c)0.667MN/m using oil3.

a more realistic value. All these correction factors use a thermal loading parameter defined as $X=\frac{\bar{U}^2}{k}\left(-\frac{d\eta_o}{d\theta}\right)$ Where $\bar{U}$ is the mean surface velocity, k is the thermal conductivity of the oil and $\frac{d\eta_o}{d\theta}$ is the temperature viscosity gradient at the operating temperature. Theoretical correction factor produced by March and Wilson (31), Goksem and Hargreaves (90), Greenwood and Kauzlarich (30), Dyson (52), as well as the experimentally derived correction factors by Wilson (33) were all plotted by Wilson (33) in a graph showing the ratio of real to isothermal film thickness against the logarithm of the thermal loading parameter, X. These plots are reproduced in section 1.1. Some of the film thickness results obtained experimentally in this Project are plotted along with March and Wilson's (31) theoretical prediction. The thermal conductivities of the oils were taken as 0.134N/(sec.deg.) at 0°C and 0.122N/(sec.deg.) at 100°C and a linear variation with temperature is assumed, following Wilson's work. The plot for oil 1 in figure 6.36 shows a dependence on load, upto a load of about 0.6MN/m, in which the data points remain close to the March and Wilson's predicted relation; however at a load 0.83MN/m a large deviation from the predicted plot is observed. This is to be expected since the film thicknesss results obtained in this project were found to be much more dependent on load than the isothermal theory predicts. In producing the above correction factors, these authors only tried to take into account of the inlet shear heating effect on film thickness. Although several authors have tried to explain this effect of high load dependence, as discussed in section 1.1, no well accepted explanation has yet been given. The plot for oil 3 in figure 6.35 shows that some

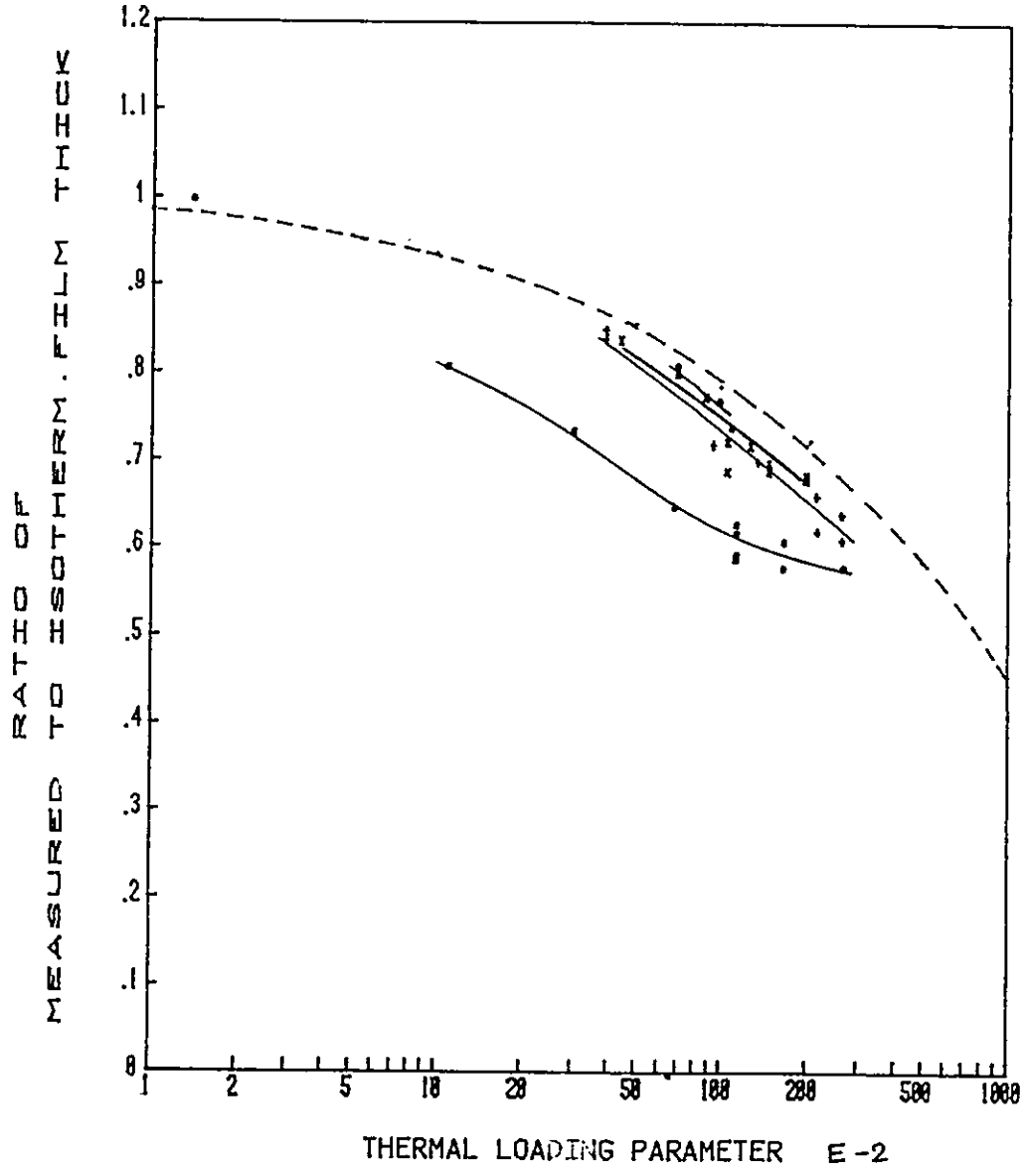

Fig. 6.36Variations of ratio of minimum to isothermal film thickness with logarithm of thermal loading parameters, using oil1, at loads of (a)0.278, (b)0.446, (c)0.613 & (d)0.836MN/m. Broken line shows the March and Wilson's prediction.

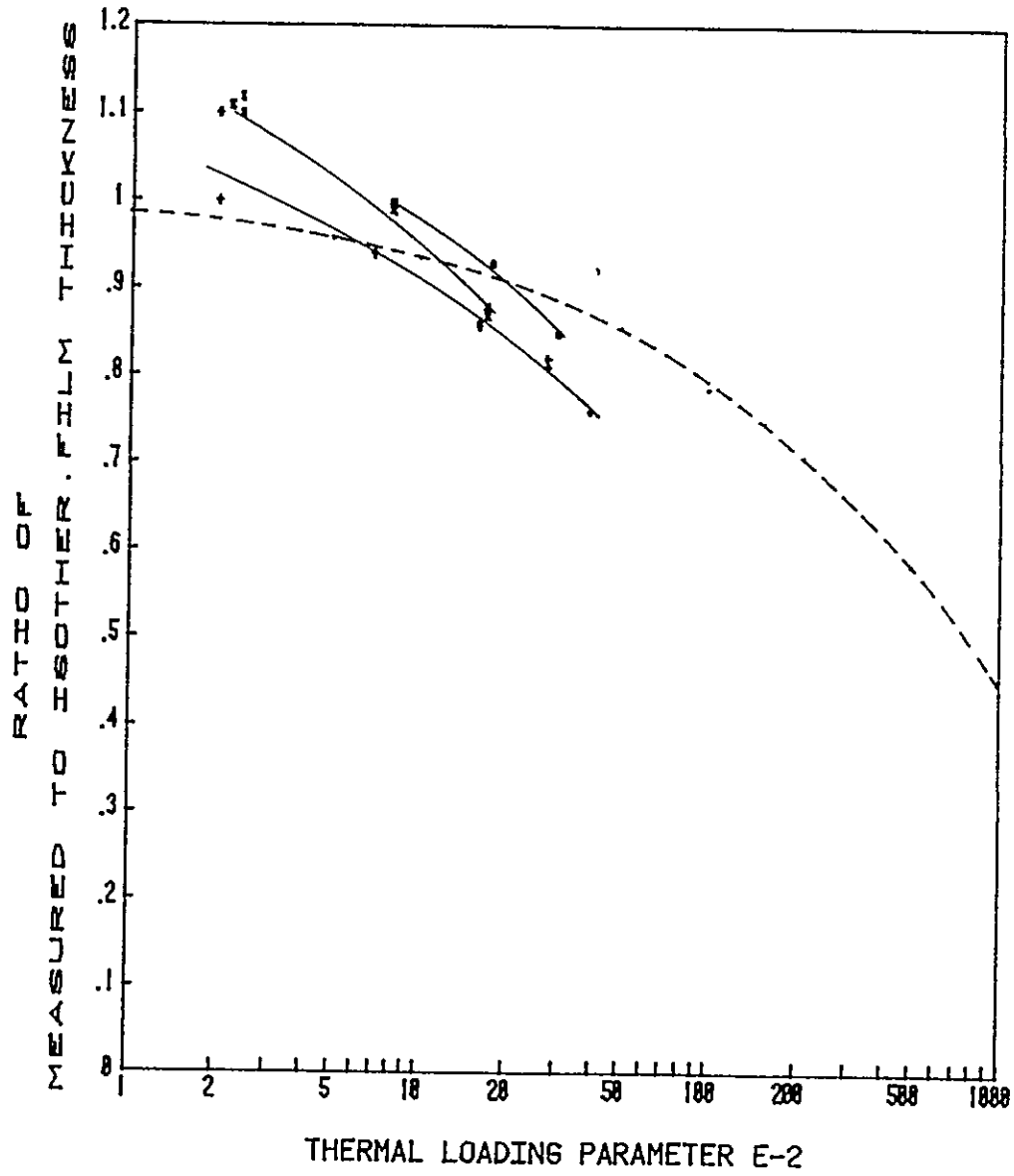

Fig. 6.37 Variations of ratio of minimum to isothermal film thickness with logartihm of thermal loading parameters, using oil3, at loads of (a)0.223, (b)0.445 & (c)0.667MN/m. Broken line shows March and Wilson's prediction.

data points at low surface velocities, thus the low thermal loading parameter values, have minimum film thickness larger than the predited film thickness. A similar effect was also detected by Wilson (33) and the possible explanation is the surface roughness which exerts an increasing effect on capacitance measurements as the oil film becomes thinner.

6.3.8 Conclusion

Film thickness profiles compare well with theory. The formation of the end constriction zone and its gradual merger with the rest of the profile with increasing surface velocity or reducing load is at least in qualitative agreement with theory. The formation of parallel films at high load or low surface velocity also match the theoretical findings.

Several deviations from the isothermal theory were detected once the dependence of the minimum film thickness on the various operating parameters was considered. The dependence on $\eta_o U$ produced an index n of 0.5. However, in formulating the isothermal prediction Dowson pointed out that the viscosity of the oil should be measured at the inlet temperature of the contact zone. It has been shown that a viscosity correction applied with a temperature measured at a distance of 1.5a from the centre of the Hertzin contact produces a value of index n of 0.67 which is quite close to isothermal prediction. The question remains as to whether this single measurement can be considered sufficient to characterise the inlet zone. Pressure and film thickness profiles recorded in this project indicate a very low pressure in this region , although the actual value would depend on the load and surface velocity. Likewise the film thickness profiles show that the separation between the discs at this

region is about 5 to 10 times the film thickness at the centre of the contact at reasonable load. On the other hand, the deviation from the isothermal prediction, found in this project, of the dependence of film thickness on $\eta_o U$ under sliding conditions would hardly be affected by a similar temperature correction. However, definite conclusions on the film thickness results under sliding conditions could not be made in the absence of accurate surface temperatures under sliding conditions. The substantial reduction in film thickness which occurs under sliding conditions gains support from the result of the pressure work, in which it was found that the oil film breaks down once sliding is introduced.

The large dependence of film thickness on load found in this project shows an interesting similarity with Sibley and Orcutt's (27) results. Three sets of their data are reproduced below at three different loads but fixed surface velocity of 13.2m/sec.

Oil	Load/Length MN/m	Velocity m/sec	Film Thickness μm
Mineral Oil	0.227	13.2	0.41
	0.341	13.2	0.41
	0.819	13.2	0.28

It can be seen that the film thicknesses do not change with the increase of load from 0.227 to 0.341 MN/m. However the change in film thickness becomes large once the load is increasd to 0.819MN/m and the index m comes to a value of 0.44. The same holds true for other surface velocities. In this project it was found that, upto a load of 0.44MN/m the value of the index m was low but with further increase of load, m increases at a similar

rate to that found by Sibley and Orcutt. This effect of higher load dependence was also found to limit the range of film thickness results which can be corrected reasonably well with the thermal correction formulas produced by various authors for low loads. Thus it is felt that a second term is needed in the the correction factor which can take into account of the higher load dependence of the minimum film thickness at higher loads.

CHAPTER 7

CONCLUSIONS AND FUTURE WORKS

7.1 Conclusions

Thin film transducers have been used to study the behaviour of nominal line contacts by several other researchers. However, the established techniques of fabricating such devices proved inadequate for satisfactory performance in the disc machine used in this project. Devices fabricated on a ceramic insulating layer deposited either by evaporation or sputtering could not withstand the first few revolutions in the hydrostatic disc machine where sliding between the discs under heavy load takes place initially. This problem was overcome by sputter etching the disc in specially designed equipment and by maintaining a high vacuum between deposition of the various layers until the device was completed. By gradual optimisation of the vacuum deposition parameters and by reduction in total number of operations performed under vacuum, the life of devices was improved from a few minutes to a few hours.

The devices fabricated and successfully used in this project were resistive pressure and temperature transducers and the capacitive device for monitoring oil film thickness. This rate of change of capacitance method has been used only with glass discs in previous works.

A method of fabricating masks was developed using laser milling with a computer controlled platform. Thus it became possible to make transducers with 10μm x 30μm active elements routinely. A few devices were made, using laser milled masks, with active elements of 6μm width. These pressure transducers revealed

a significant secondary pressure peak and the effect of the resolving power of this type of devices was clearly demonstrated. The above method of making masks also facilitated the fabrication of multiple devices on the same test specimen with high degree of alignment, thus making it possible to study the pressure, oil film thickness and temperature variation within the contact more accurately.

To support the high resolution devices, signal processing equipment was constructed with good frequency response and an accurate and fast permanent recording facility. Circuits were also designed to provide a wider contact zone monitoring facility.

A hydrostatic pressure vessel was designed, constructed and successfully used to study the pressure coefficient of resistivity of bulk and thin film manganin. Results obtained from these tests showed that both bulk and thin film manganin have linear pressure coefficient of resistivity, but in thin film form its magnitude is about three-quarters that of the bulk value. Films deposited on different substrate under the same vacuum show similar pressure coefficients.

Manganin alloys were made with varying composition and corresponding evapoarted thin films, within a limited range of composition, show little difference in eitherer linearity or magnitude of pressure coefficient of resistivity.

The dielectric constants of the three different oils were measured as a function of pressure using an apparatus built inside the hydrostatic pressure vessel.

Attempts to improve performance of pressure transducer by R.F.sputtering of manganin were unsuccessful and the probable reason was non-stoichiometry of the deposited film. However,

improvement in the performance of the evaporated manganin transducers was achieved by annealing the deposited films at elevated temperature. The reduction in temperature coefficient achieved this way made it possible to study the pressure variation within the contact under limited sliding conditions with reasonable accuracy.

A process for deposition of thin film thermocouples was developed and although these devices worked reasonably well under ordinary circumstances, their performance under EHL conditions was found unsatisfactory.

Various possible errors in the transducer signals, that might arise from a fault developing during tests, were investigated. Although the reason for one major fault, the zero level shift in the pressure transducer signal, could not be ascertained conclusively, an improved method of device fabrication effectively eleminated this fault.

Correction of the theoretical pressure distribution for transducer size and alignment effects showed variations in secondary pressure peak height and position that agreed well with the experimental observations. General agreement was also found with theory in the overall shape of the pressure profiles, the movement of the secondary pressure peak with the operating conditions and the height of the secondary pressure peak with oils of different pressure viscosity coefficients. At moderate load and high surface velocity, however, no pressure peak was observed but a constant pressure in the exit region developed instead.

Limited work on contacts undergoing some sliding showed similar pressure distributions to those obtained under comparable rolling conditions.

Calculation of maximum pressure gradient obtainable with transducers of given size agreed well with values found in experiments at low surface velocity.

Peak temperature rises of upto 18°C was found under nominal rolling conditions and upto 100°C were found under sliding conditions.

A model was developed for the interpretation of the capacitance measurement which showed that unambiguous interpretation of the minimum film thickness values were possible.

Film thickness results when corrected for thermal effect showed good agreement with theory as regards variation with speed but at high loads, film thickness was found to vary with load more strongly than theory predicts. Film thicknesses measured under sliding conditions were found to be less than predicted by theory.

7.2 Future Work

The pressure and the capacitive film thickness monitoring devices fabricated in this project produced satisfactory results. However, the formation of a constant pressure region on the exit side of the primary pressure peak under certain operating conditions needs further examination. The reduction of oil film thickness under sliding conditions should also be further studied.

Further work is necessary to improve temperature transducers in order to reduce their sensitivity to pressure. Thin film thermocouples performed well in static conditions but need further examination to ascertain the possible reasons for the behaviour found in this project under dynamic conditions.

The most obvious further uses of these devices are in EHL contact studies in more practical circumstances such as roller bearings and gears. Some work has already been done in this

(a)

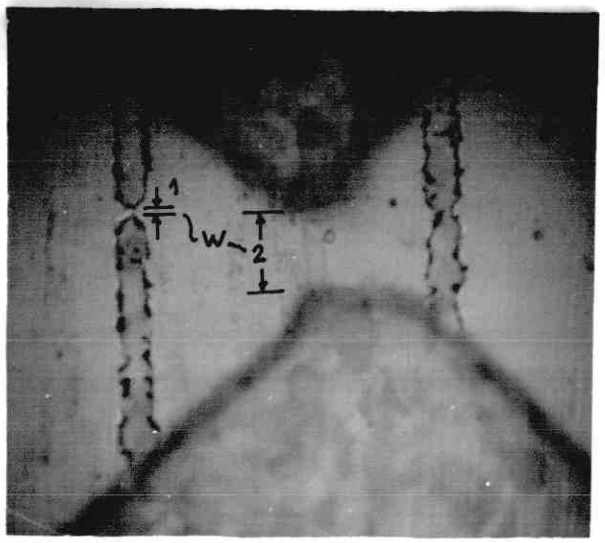

(b)

Fig. 7.1 (a) Active element of pressure transducer (1) direct cut, (2) deposited through metal mask. (b) Transducer fabricated for four point probe method.

respect as an extension of this project, where pressure and capacitive film thickness monitoring devices have been fabricated on the outer race of a roller bearing. These devices have been subjected to a maximum Hertzian pressure of 1.5GN/m^2. However, due to the small diameter of the rollers, the contact width in this case is much less than in the disc machine. To achieve a further reduction in the active element size, a new technique of fabricating these devices has been developed. Instead of depositing the pressure transducer through a metal mask with the electrode and the active element pattern on it, a single patch of material is deposited. Part of this material is cut away by the laser milling equipment so as to leave a small connecting bridge of material between two electrodes. It was found posible to remove the manganin film without damaging the alumina layer or the metal underneath. Figure 7.1a shows the two types of active elements for comparison. One, fabricated with a metal mask having a laser milled slit 10μm wide, has an active element 20μm wide extended by undercutting. The other has an active element about 3μm wide by 8μm long. Although these very fine devices can be used with the Wheatstone bridge circuits described in the text, their sensitivity will be limited by their low resistance compared with that of the electrodes. Better results will be obtained with the four point probe geometry, shown in figure 7.1b.

Another use of these very fine devices would be to study point contact.

APPENDIX 1

The interpretation of Capacitance Measurements

The equivalent circuits of the capacitance measuring system is shown in Fig.A.1 . A potential difference V_o is applied through a series resistor (of resistance R ohms) to the transducer.

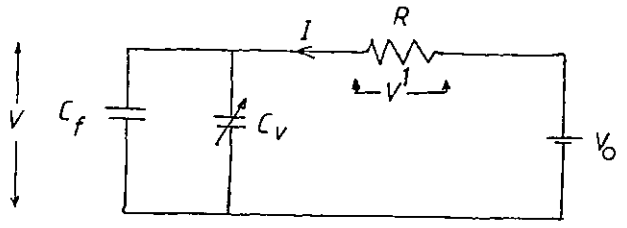

Fig. A.1 Equivalent circuit of capacitance measuring system.

The capacitance is split into a fixed capacitance C_f, and a variable capacitance C_v. C_f represents the capacitance between the electrode and the disc on which it is mounted and other stray capacitances. C_v is the opposing disc separated by the lubricant film . The total capacitance $C_f + C_v$ is C farads . When the system is disturbed from equilibrium a current, I , flows through the circuit. The potential V^1 across the resistor R is measured.

The equations governing the system are :

$$V_o = V^1 + V \qquad (1)$$

$$V^1 = IR \qquad (2)$$

$$Q = CV \qquad (3)$$

where Q is the charge stored in the capacitive elements. Both C and V are functions of time and differentiating equation (3) yields

$$I = \frac{dQ}{dt} = C\frac{dV}{dt} + V\frac{dC}{dt} \qquad (4)$$

And from (1), (2) and (4) :

$$V^1 = RV\frac{dC}{dt} - RC\frac{dV^1}{dt} \qquad (5)$$

Where $\frac{dV^1}{dt}$ is zero, i.e. at maxima and minima of the voltage time curve, then

$$V^1 = RV\frac{dC}{dt} = R\frac{dC}{dt}(V_o - V^1)$$

V^1 is three or four orders of magnitude less than V_o, thus to a good approximation

$$\frac{dC}{dt} = \frac{V^1}{V_o R} \qquad (6)$$

At points where $\frac{dV^1}{dt} \neq 0$ it may be necessary to include this term when deriving $\frac{dC}{dt}$:

i.e. $$\frac{dC}{dt} = \frac{V^1}{V_o R} + \frac{C}{V_o}\frac{dV^1}{dt} \qquad (7)$$

since $V_o \simeq V$.

As the electrode moves through the gap the rate of change of capacitance is given by

$$\frac{dC}{dx} = \frac{8.85\times10^{-8}\varepsilon_r\, l}{h} \quad F/m$$

where l is the leading edge of the electrode, ε_r is the relative dielectric constant of the oil under pressure, h is the film thickness. Then

$$\frac{dC}{dt} = \frac{8.85\times10^{-8}\varepsilon_r\, lv}{h} \quad F/sec$$

where v is the surface velocity of the disc on which the device is deposited. Using equation 6

$$h = \frac{8.85 \times 10^{-8} \varepsilon_r \, l v V_o R}{V^1} \quad m$$

APPENDIX 2

Measurement of $\frac{\partial p}{\partial x}$ from pressure traces

There is a maximum value of $\frac{\partial p}{\partial x}$ that can be measured because of integration by the transducer. The transducer is assumed to be perfectly homogeneous and of width a. If a pressure step of p' is encountered and the transducer is a distance x into the pressure step where $0 < x \leq a$ then the resistance of the device is given by

$$\frac{1}{R} = \frac{a-x}{a}\frac{1}{R_o}(1 - \alpha p_1) + \frac{x}{a}\frac{1}{R_o}(1 - \alpha p_1 - \alpha p^1)$$

where R_o is the resistance at ambient pressure.
(If $R = R_o(1 + \alpha p)$ we may write $\frac{1}{R} = \frac{1}{R}(1 - \alpha p)$ to a good approximation since αp is small).

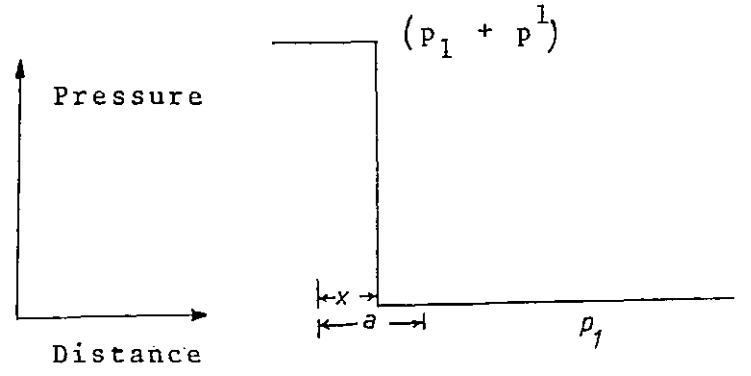

Now put $C = \frac{1}{R}$ $\qquad$ $C_o = \frac{1}{R_o}$

$$\frac{\partial C}{\partial x} = -\frac{C_o}{a}(1 - \alpha p_1) + \frac{C_o}{a}(1 - \alpha p_1 - \alpha p^1)$$

$$= -\frac{C_o}{a}\alpha p^1 \qquad . \qquad . \qquad . \quad (1)$$

We interpret this reading as that corresponding to a uniform pressure p over the whole device.

Thus $C = C_o (1 - \alpha p)$.

and $$\frac{\partial C}{\partial x} = - C_o \alpha \frac{\partial p}{\partial x} \qquad . \quad . \quad . \quad (2)$$

Thus identifying (1) and (2).

$$- \frac{C_o}{a} \alpha p^1 = - C_o \alpha \frac{\partial p}{\partial x}$$

i.e. $$\frac{\partial p}{\partial x} \text{ (measured)} = \frac{p^1}{a}$$

This is for an infinite slope pressure rise or drop.

Thus if $p^1 = 6.9 \times 10^8$ Pa (100,000 p.s.i.)

$a = 10^{-5}_m$ (10 μm).

Maximum measurable $\frac{\partial p}{\partial x} = 6.9 \times 10^{13} \frac{N}{M^3}$

In theory it should be possible to correct for this effect but requires a perfectly homogeneous transducer and accurately known dimensions.

LIST OF REFERENCES

1 Cameron,A. (1952) "Principles of Lubrication", Longmans, London

2 Martin,H.M. (1916) Engineering, London, 102

3 Peppler,W. (1936) V.D.I. Verlog, Berlin.

4 Peppler,W. (1938) V.D.I. Forschungsheft.

5 Meldahl,A. (1941) Brown Boveri Review, 28

6 Gatcombe,E.K. (1945) Trans. Amer. Soc. Mech. Engrs., 67

7 Blok,H. (1950) Ann. N.Y. Acad. Sci., 53

8 Cameron,A. (1952) J. Inst. Petrol., 38

9 Blok,H (1952) J. Inst. Petrol., 38

10 Grubin,A.N. Vinagrodova,I.E.,(1949) Central Scientific Research Institute for Technoloy & Mechanical Engineering, Book No. 30, Moscow.

11 Hertz,H. Translated by Jones,D.E.;Shott,G.A.(1896); Macmillan Co. Ltd., London.

12 Petrusevitch,A.I. (1951) Izo. Akad. Nauk. SSSR (OTN) 2.

13 Weber,C. & Saalfeld,K. (1954) Zeits. ang. Math. Mech., 34

14 Dowson,D. & Higginson,G.R. (1959) J. Mech. Engr. Sci., 1

15 Dowson,D. & Higginson,G.R. (1960) J. Mech. Engr. Sci., 2

16 Archard,G.D., Gair,F.C. & Hirst,W. (1961) Proc. Roy. Soc., A 262

17 Higginson,G.R. & Whittaker,A.V. (1962) J. Mech. Engr. Sc., 4

18 Dowson,D & Higginson,G.R. (1966) "Elastohydrodynamic Lubrication", Pargamon Press Ltd.

19 Archard,G.D., Gair,F.C. & Hirst,W, (1961); Proc. Roy. Soc. A 262

20 Sternlicht,B; Lewis,P & Flynn,p;(1961); Trans. Amer. Soc. Mech. Engrs., J. of Basic Engineering, 83, Series D, 2

21 Cheng,H.S. & Sternlicht,B.; (1964); ASME Paper No. 64, Lub11

22 Cheng,H.S.; (1965); Trans ASLE

23 Dowson,D. & Whitaker,A.V.; (1965); Proc. Instn. Mech. Engrs., 180 Part 3B

24 Dowson,D. & Higginson,G.R.; (1961); Engineering Lond, 192

25 Crook,A.W.; (1961); Phil. Transc. A, 254

26 Christensen,H.; (1964); ASLE Transaction 7

27 Sibley,L.B. & Orcutt,F.K., (1961); Trans. Amer. Soc. Lub. Engrs., 4

28 Dyson,A; Naylor,H. & Wilson,A.R. (1965) Proc. Instn. Mech. Engrs. 180 Part 3B

29 Cheng,H.S. (1972) J. of. Lub. Tech., Trans. ASME, Series F, 94

30 Greenwood,J.A. & Kauzlarich,J.J. (1973) J. of Lub. Tech., Trans. ASME, Series F, 95

31 March,L.E. & Wilson,W.R.D. (1975) J. Lub. Tech., Trans ASME, Ser F, 97

32 Wilson,W.R.D. & Wong,C.J. (1974) J. of Lub. Tech., Trans ASME, Ser F, 96

33 Wilson,A.R. (1979) 6th Leeds-Lyon Symposium on Tribology, Lyon

34 Kannel,J.W. & Bell,J.C. (1971) J. of Lub. Tech., Trans ASME, Ser G, 93

35 Bell,J.C. & Allen,J.W. (1971) J. of Lub. Tech., Trans ASME, Ser G, 93

36 Parker,R.J. & Allen,J.W. (1971) NASA TN D-6411, July

37 Parker,R.J. & Kannel,J.W. (1971) NASA TN D-6608, Dec.

38 Lee,D.; Sanborn,D.M. & Winer,W.O. (1973) J. of Lub. Tech., Trans ASME

39 Cheng,H.S. (1972) J. of Lub. Tech., Trans ASME, Ser G, 94

40 Archard,J.F. & Cowking,E.W. (1965) Lubrication And Wear Group Symposium On Elastohydrodynamic Lubrication, Paper3 (Instn. of Mech. Engr.,London)

41 Jonson,K.L. (1970) J. of Mech. Engr. Sci., 12

42 Theyse,F.H. (1966) Wear, 9

43 Archard,J.F. (1968) J. of Mech. Engr. Sci., 10

44 Higginson,G.R. (1962) Inst. J. Mech. Sci., 4

45 Dowson,D & Longfield,M.D. (1963) Inst. Mech. Engrs., Lubrication and Wear Convention

46 Lane,T.B. & Hughes,J.R. (1952) Brit. J. Appl. Phy., 3

47 Cameron,A (1954) J. Inst. Petrol., 40

48 Lewicki,N. (1955) Engineer, London 200, 176

49 Crook,A.W. (1958) Phil. Trans., A 250

50 El-Sisi,S.I. & Shawki,G.S.A. (1960) Trans. Amer. Soc. Mech. Engrs., J of Basic Engineering, 82

51 Mac Conochie,I.O. and Cameron,A. (1960) Trans. Amer. Soc. Mech. Engrs., J. of Basic Engineering, Ser D, 82

52 Dyson,A. (1966-7) Proc. Inst. Mech. Engrs., 181

53 Lewicki,W. (1955) Engineer, London, 197

54 Bondi,A. (1951) Physical Chemistry of Lubricating Oils, Reinhold, New York

55 Galvin,G.D.; Naylor,H. & Wilson,A.R. (1964) Inst. Mech Engrs., Lubrication and Wear Second Convention.

56 Archard,J.F. (1965) Proc. Instn. Mech. Engr., 180,3B

57 Crook,A.W. (1963) Phil. Trans., A, 255

58 Sibley,L.B., Bell,J.C. & Allen,C.M. (1960) WADD Technical Report, 60-189

59 Kannel,J.W.; Bell,J.C. & Allen,C.M. (1965) Trans ASLE, 8

60 Gohar,R & Cameron,A (1963) Nature, 200

61 Foord,C.A., Hamann,W.C. & Cameron,A (1968) Trans ASLE, 11

62 Wymer,D.G. (1972) Ph.D. Thesis, London University

63 Crook,A.W. (1961) Nature, 190

64 Crook,A.W. (1963) J. Inst. Petrol., 49, No 478

65 Kannel,J.W.; Bell,J.C. & Allen,C.M. (1965) Trans. ASLE, 8

66 Kannel,J.W. (1965) Proc. I. Mech. Engr., 180

68 Kannel,J.W. (1974) J. Lub. Tech., (Paper No. 74-Lub-D)

69 Kannel,J.W. & Dow,T.A. (1974) J. Lub. Tech. Trans. ASME

70 Kannel,J.W. and Zugaro,F.F. (1976) Annual Technical Summery Report, Battelle Coumbus Laboratories, Ohio

71 Kannel,J.W. & Dow,T.A. (1979) ASLE Transaction, 23

72 Orcutt,F.K. (1965) Trans. ASLE, 8

73 Cheng,H.S. & Orcutt,F.K. (1965-66) Proc. I. Mech. Engrs., 180

74 Hamilton,G.M. & Moore,S.L. (1967) Proc. I. Mech. Engrs., 182

75 Hamilton,G.M. & Moore,S.L. (1971) Proc. Roy. Soc., London A, 322

76 Johnson,K.L. (1970) J. of Mech. Engr. Sci., 12

77 Bridgeman,P.W. (1958) "The Physics of High Pressure", Bell, London

78 Adams,L.H., Goranson,R.W. & Gibson,R.E. (1937) Rev. of Sci. Instr., 8

79 Samara, & Giardini (1964) Rev. of Sci. Instr., 35

80 Lees,J. (1966) "Advances in High Pressure Research" ed R.S. Bradley, London & N.Y., Academic Press

81 Lees,J. (1969) High Temper. High Pressure, 1

82 Fujioka, ;Mishima & Kawai (1978) J. of Appl. Phy., 49

83 Schouton,M.J.W. (1973) Doctoral Thesis, Technical Univ., Eindhoven

84 Bartz,W.J. & Ehlert,J. (1976) J. Lub. Tech., Transc. ASME

85 Dowson,D (1965) Proc. J. of Mech. Engr. 180

86 De-Silva,S (1981) Ph.D. thesis, Univ. of London.

87 Alexander & Lengyl, (1971) "Hydrostatic Extrusion" Mills & Boons Ltd., London.

88 Mc Pherson,B.P., (1971) Ph.D. Thesis, Univ. of London.

89 Hartrung,H.A. ASME Paper No. 65

90 Hirst,W; Moore,A.J. (1974) Proc Roy Soc 337

91 HIrst,W; Moore,A.J. (1975) Proc Roy Soc 344

92 Hirst,W; Moore,A.J. (1978) Proc Roy Soc 360

93 Hirst,W; Moore,A.J. (1979) Proc Roy Soc 365

94 Hirst,W; Moore,A.J. (1980) Proc Roy Soc 298

95 Johnson,K.L; Trevaarwerk,J.L. (1977) Proc Roy Soc 356

96 Rohde & Oh (1974) Proc Roy Soc 343

97 Smith,F.W (1965) Trans ASME 870

98 Bair,S; Winer,W.O. (1979) Trans ASME 101

99 Bair,S; Winer,W.O. (1979) Trans ASME 101

100 Alsad,M; Bair,S; Sanborn,D.M; Winer,W.O. (1973) Trans ASME 100

101 Gecim,B; Winer,W.O. (1980) Trans ASME 102

102 Bair,S; Winer,W.O. (1980) Trans ASME 102

103 Trevaarwerk,J.L; Johnson,K.L. (1975) Wear 35

104 5th Leeds Lyon Symposium, (1978) Inst of Mech Engrs

105 2nd I Mech Engr Confer (1972)